SWASH ZONE DYNAMICS
IN A
RHYTHMIC 'BLACK-SAND' BEACH SYSTEM

by

J. J. MARRA

A dissertation

submitted to

the University of Canterbury

in partial fulfilment of the requirements

for the Degree of

Doctor of Philosophy

in Geology

University of Canterbury

1992

ABSTRACT

Patterns of physical change and the processes regulating change in the swash zone were examined at Nine Mile Beach, a heavy mineral-rich sand beach located on the west coast of the South Island, New Zealand. Concurrent observations of process and response parameters were made across scales ranging spatially from meters to millimeters and temporally from days to seconds. These observations indicate that a multi-scale system of process-response interactions governs swash zone dynamics.

At the *macroscale*, interactions between incident wave conditions and beach/ surf zone morphologies define a process-response network. At the *microscale*, interactions between swash/backwash flow characteristics, bedforms, sedimentary structures and sediment textures define a process-response network. Interactions between wave runup characteristics, beach water table characteristics, foreshore morphology, and foreshore stratigraphy define a *mesoscale* process-response network.

Interactions exist between, as well as within, each of these process-response networks. Specifically, a connection from incident wave condition-morphologic interactions occurring at the macroscale to flow-grain-bed interactions operating at the microscale, is established through their mutual relationship to the temporal and spatial variations in the relative dominance of swash versus backwash forces operating at the mesoscale.

Thus, while each network of process-response interaction may be viewed in isolation, it is in conglomeration that they define the larger network of interactions that constitutes swash zone dynamics.

"I do not know what I appear to the world, but to myself I seem to have been only like a boy playing on the sea-shore, and diverting myself now and then finding a smoother pebble or a prettier shell than ordinary, whilst the great ocean of truth lay all undiscovered before me."

Sir Isaac Newton

CONTENTS

TABLES

FIGURES

PHOTOGRAPHS

SYMBOLS

C_o	fractional volume concentration
D	sediment grain diameter
D_{al}	apparent long axis diameter
D_i	intermediate diameter
Do	distance of swell origin
Fr	Froude number
H_b	breaking wave height
H_s	significant wave height (= $H_{1/3}$)
H_o	deepwater wave height
K	wave number
L_b	beach length
L_e	edge wave wavelength
L_f	form wavelength
L_o	deep water wave length
R_v	maximum vertical runup height
R_h	maximum horizontal runup excursion
Re*	grain Reynolds number
T_e	edge wave period
T_i	incident wave period
T_r	runup or swash period
U	flow velocity
U*	shear velocity
U^*_d	critical dispersive shear velocity
U^*_e	critical entrainment shear velocity
W_s	sediment fall velocity
WT_h	maximum horizontal water table excursion

a_b	breaking wave amplitude
d	flow depth
f	frequency
g	acceleration due to gravity
k_s	boundary roughness height
m	longshore modal number
n	cross shore modal number
t	time
ß	beach gradient
$ß_e$	effective beach slope
Ω	Dean parameter
ε	surf scaling parameter
ξ	Iribarren number
ρ_f	fluid density
ρ_s	sediment density
κ	Von Karman's constant
τ_o	bottom shear stress
τ_e	critical entrainment stress
τ_d	critical dispersive stress
μ	viscosity
ν	kinematic viscosity
ω	wave radian frequency
δ'	viscous sublayer thickness
φ	static friction coefficient
Φ	dynamic friction coefficient

CHAPTER 1 INTRODUCTION

...It is astonishing and incredible to us, but not to Nature;
for she performs with utmost ease and simplicity
things which are even infinitely puzzling to our minds, ...

Galileo

1.1 SCOPE

Physical changes in the foreshore of sand beaches are manifest over a broad range of spatial and temporal scales. Theses changes involve mutual interactions between fluid motion, material properties, and surface forms. They accompany the movement of sediment that occurs in response to fluid flow.

This work is concerned principally with swash zone dynamics in a rhythmic 'black-sand' beach system. The scales of phenomena considered range spatially from local beach and surf zone morphologies down to grain-layer textural patterns; temporally from storm/recovery cycles down to turbulent burst/sweep cycles. Foreshore morphology, material properties, and fluid motions are described. Patterns of change and processes regulating change are examined. Individually as well as collectively, the chapters that follow illustrate the enmeshed nature of process-response interactions within sandy coastal systems.

1.2 CONCEPTUAL FRAMEWORK

An understanding of the behavior of sand beach systems has a variety of

applications. These range from the assessment of coastal stability for land management and planning purposes to paleoenvironmental reconstruction for oil and minerals exploration programs. As a result of these varied interests, sand beaches have been examined by a diverse group of workers that includes geographers, oceanographers, geologists, and engineers. Attempting to solve problems specific to their needs and taking different approaches, these workers have have tended to address in relative isolation different aspects of sand beach dynamics.

This tendency to examine natural phenomena in isolation from the whole, referred to as 'reductionism' (Capra 1982; Gleick, 1987), is not limited to coastal studies. The reductionist view forms the foundation of modern scientific thought. Its origins can be traced back to Descartes, Bacon, and Newton among others. That the reductionist view is characteristic of our general way of thinking is reflected in the compartmentalization of the scientific community (Capra 1982; Gleick, 1987).

Process-response hierarchies, such as those outlined by Allen (1967) for flow systems in general, Jackson (1975) for bedform dynamics in its fullest sense, Horikawa (1980) for coastal processes, and Slingerland and Smith (1986) for placer-concentration processes, typify the reductionist approach to analysis. Natural phenomena are described and explained at different levels in these hierarchies. Ideally, each level represents a coupled set of spatial and temporal interactions that are governed by causal-relationships between the parameters characteristic of that level.

Applying this segregated approach to analysis, it is possible to distinguish several levels of swash zone dynamics. A process-response hierarchy for swash zone dynamics is outlined in Figure 1.1. In this figure the microscale encompasses fluid-

---

Figure 1.1. Spatial and temporal levels of process-response interaction operating in the swash zone. The terms Macroscale, Mesoscale, and Microscale are used to subdivide this network of interactions into different levels. Each level, and the group of process-response interactions it encompasses - Nearshore dynamics, Foreshore dynamics, and Bed Dynamics respectively - corresponds to the topic of a chapter in this work. (OPPOSITE PAGE --->)

SPATIAL AND TEMPORAL LEVELS OF PROCESS/RESPONSE INTERACTION OPERATING IN THE SWASH ZONE

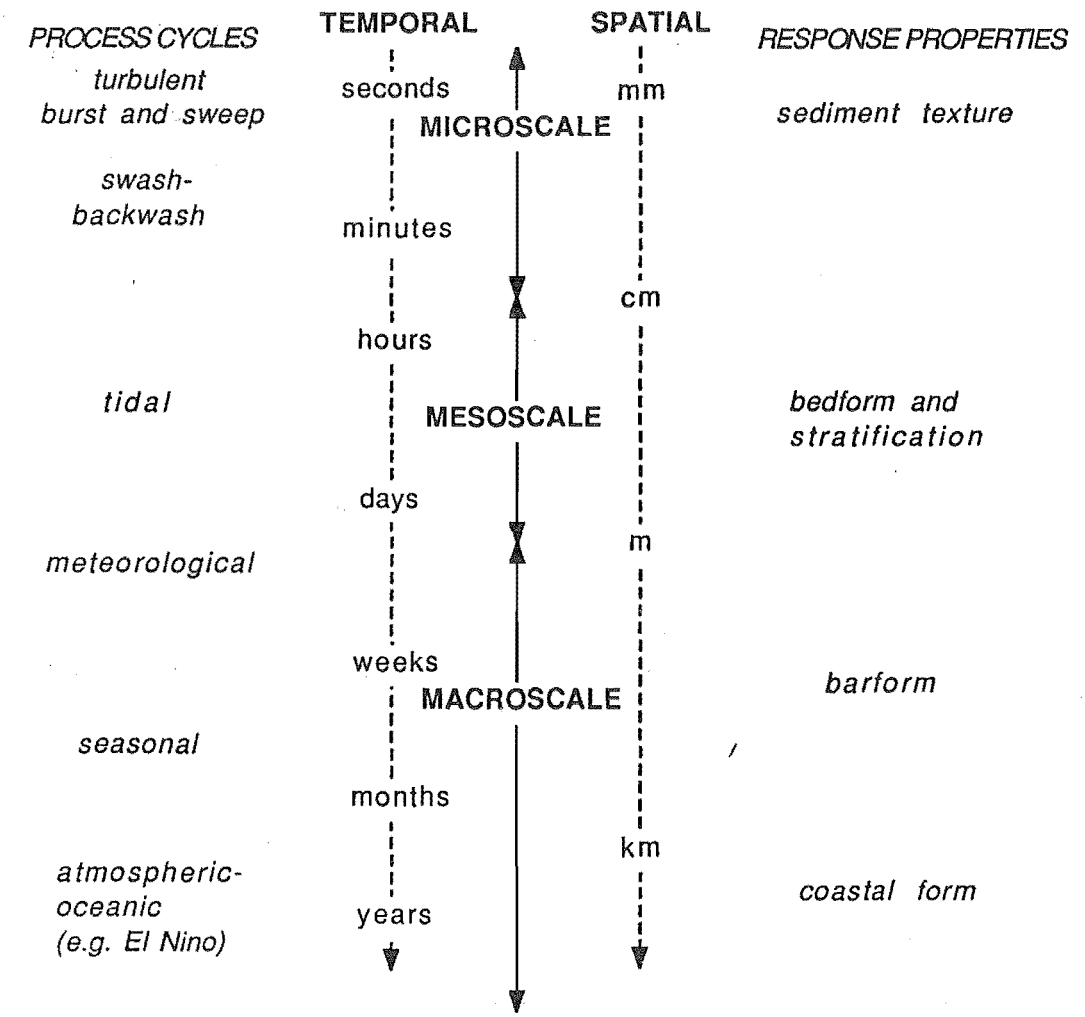

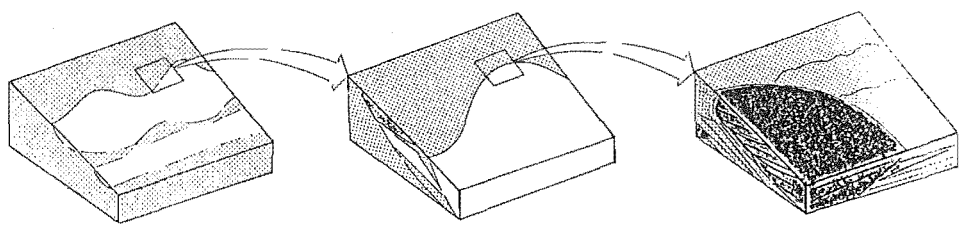

MACROSCALE
Nearshore Dynamics

MESOSCALE
Foreshore Dynamics

MICROSCALE
Bed Dynamics

grain-bed interactions that occur at fine scales - time scales of seconds to minutes and space scales of millimeters to centimeters. Similarly, the macroscale encompasses fluid-form interactions that occur at coarse scales - time scales of days to years and spatial scales of meters to kilometers. Finally, the mesoscale encompasses intermediate scales of fluid-form interactions - time scales of minutes to days and space scales of centimeters to meters.

Although it has proven to be extremely useful, the reductionist view has limitations. Following from conceptual revolutions made in physics around the turn of the century, it has become apparent that the enmeshed nature of many natural phenomena makes segregation unrealistic (Capra, 1982; Gleick, 1987; Carter, 1988). Rigorous application of reductionism results in a view that is too narrow and fragmented. Workers have begun to focus on more integrated approaches to analysis in order to obtain a broader, more unified understanding of natural phenomena.

The view of phenomena as an intricate web of relationships is referred to by Capra (1982) as 'systemic'. While maintaining the multileveled structure, the systemic view emphasizes the recognition of interconnection and interdependence both within and between levels. The concept of an ecosystem, where the individual organism, the population, and the community are distinct yet interrelated components, exemplifies the systemic view.

With respect to swash zone dynamics, application of this integrated view requires a conceptual modification of the process-response hierarchy given in Figure 1.1. In contrast to delineating separate levels of interaction, this figure now depicts components in a network of interactions that constitute swash zone dynamics. It is meant to illustrate the transmission of interactions across scales. For example, processes operating at tidal to seasonal scales combine to determine barform. Similarly, processes operating at turbulent to tidal cycles combine to determine bedform and stratification. The implication is that any response element is now regarded as the net effect of a spectrum of process-response interactions (Allen, 1967).

Although a specific process may be the dominant control on the given response element, superimposed higher and lower order effects represent additional influences that should be considered.

While the general aim of this work is to demonstrate the importance of recognizing the enmeshed nature of sandy coastal systems, the view taken here is that the reductionist and systemic views described above are complementary. Segregation is an efficient means for analysis of detailed mechanisms; integration is necessary to incorporate these mechanisms into the functioning of the whole system (Capra, 1982). Thus it is suggested that in order to gain a deeper understanding of sand beach dynamics, the system needs to be viewed both in its isolated parts and as an interconnected whole.

1.3 APPROACH

The combination of both segregated and integrated views can be described as 'bootstrapping', after the term in modern physics referring to the description and explanation of phenomena in terms of a mosaic of interlocking models (Capra, 1982; Hawking, 1988). It is this bootstrap approach that is taken throughout this work as a whole and within each of the individual chapters. The result is that following **Chapter 2**, which outlines the setting and methodology of this work, the ensuing three chapters effectively stand alone as separate treatments of different topics. They posses individual sets of background, results, discussion, and conclusions sections. Specifically, **Chapter 3: Nearshore Dynamics** examines macroscale interactions within the Nine Mile Beach system. **Chapter 4: Bed Dynamics** examines microscale interactions within the Nine Mile Beach system. **Chapter 5: Foreshore Dynamics** examines mesoscale interactions within the Nine Mile Beach system. **Chapter 6** summarizes the conclusions of the the previous three chapters in the context of the larger network of interactions that constitute swash zone dynamics within the Nine Mile Beach system.

CHAPTER 2 SETTING & METHODOLOGY

"Although nature begins with the cause and ends with the experience, we must follow the opposite course, namely, begin with the experience and by the means of it investigate the cause."

Leonardo Da Vinci

2.1 FIELD SITE

Field work was conducted on the northern portion of Nine Mile Beach (Figure 2.1). Nine Mile Beach (NMB) is a wide, gently sloping sand beach located near Westport, on the west coast of the South Island, New Zealand. Rocky headlands form northern and southern boundaries to the approximately 12 kilometer-long beach. Two tidal inlets dissect the central portion of NMB. A wide, shallow shelf extends seaward from the beach.

NMB is a post-glacial, prograded shoreline deposit. It is the most recent in a series which includes past interglacial shoreline deposits that exist as uplifted marine terraces in the Westport area (McPherson, 1978). NMB is composed mostly of fine quartz sand; however, a coarse sand component is also present, and heavy minerals (black sands) are abundant locally (McPherson, 1978; Marra, 1985). NMB sands are derived from a combination of sources. These sources include erosion of the small cliff of beach and dune sand deposits that backs the beach, longshore transport of river supplied sands derived from the rapidly eroding mountains along the west coast, and onshore transport of shelf sands that are former shoreline deposits stranded during the last transgression (McPherson, 1978; Marra, 1985).

At NMB tides are weakly diurnal and the tidal range is mesotidal according to the

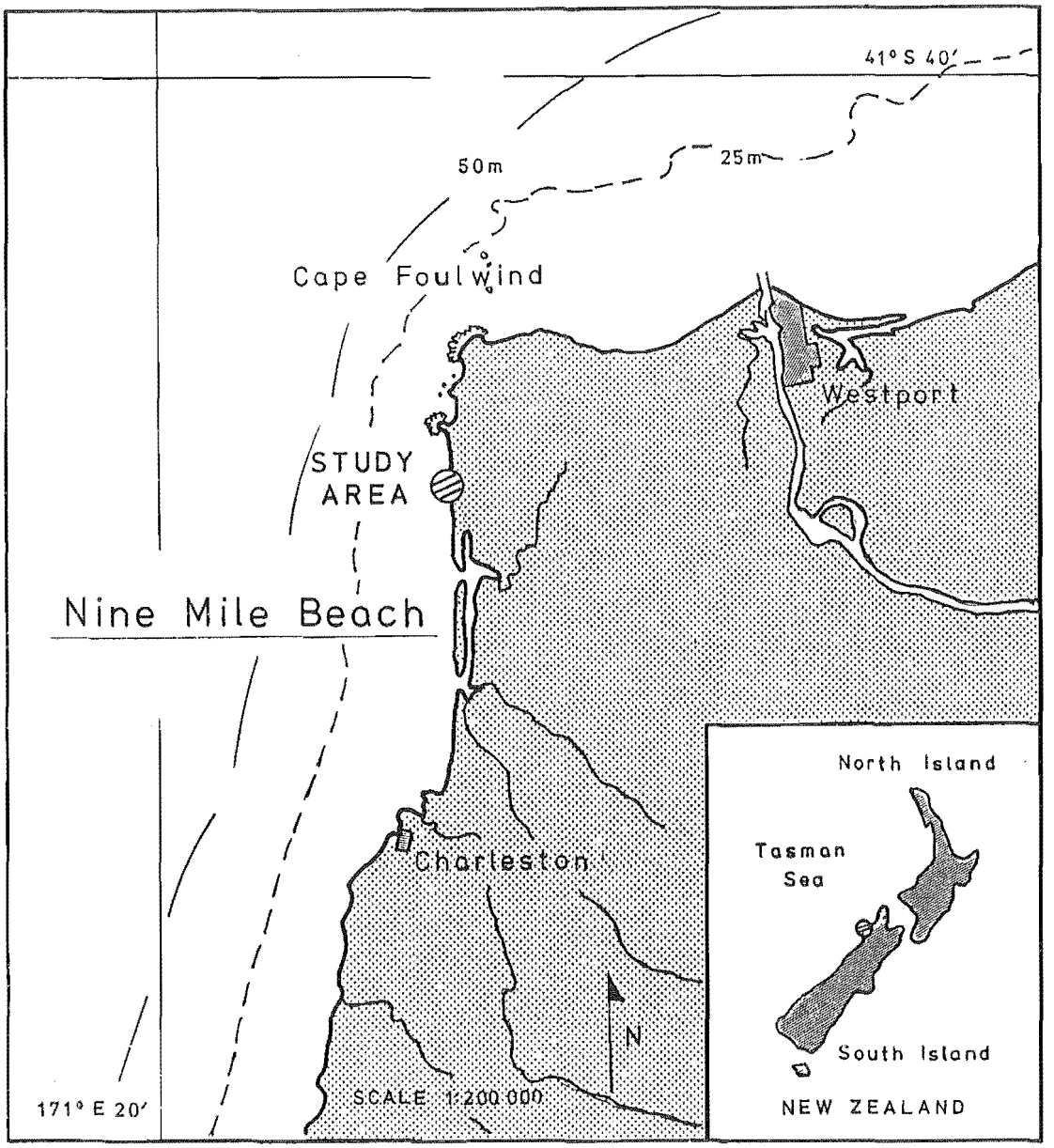

Figure 2.1. Map showing the location of Nine Mile Beach and the study area.

terminology of Davies (1964). Mean spring tidal range is 2.9 meters and mean neap tidal range is 1.7 meters. During a portion of the study period extending from December 28 , 1986 to January 4, 1987, extreme tidal ranges (3.4 + meters) occurred in association with the 18.6 year perigean signal (Westport Newspaper, 12/24/86 after

N.O.A.A.).

The regional weather pattern is characterized by the quasi-weekly passage of frontal systems associated with the prevailing westerlies (Davies, 1973; Pickrill and Mitchell, 1979; Valentine and Macky, 1984). The regional wave climate is characterized by highly variable, moderate energy swell (Davies, 1973; Pickrill and Mitchell, 1979; Valentine and Macky, 1984)). Weather patterns and the accompanying wave climate are considered at length in Chapter 3.

The northerly-flowing Westland Current is the principal feature of the regional oceanic circulation pattern (Carter, 1975). Although fluctuations in coastal currents, as well as other long-term variations in sea level, influence coastal form (Komar and Enfield, 1987), their effects on NMB are not considered in this work.

2.2 DATA COLLECTION

Essentially two different data collection plans were employed during this study to facilitate concurrent measurement of process-response parameters across a range of spatial and temporal scales. Below, data collection associated with large scale observations is described first. This is followed by a consideration of methodology associated with small scale observations.

LARGE SCALE DATA COLLECTION

Fieldwork on large scale observations was carried out through four storm/recovery cycles that occurred during an initial eight day and subsequent 27 day interval between November 1986 and January 1987. Additional observations were made in late June to early July of 1988 for a combined total of 43 days of observation.

Process Parameters

On a daily basis, at approximately two hours before the high tide, nearshore conditions were recorded. This recording time was chosen because work by Harrison

(1969) suggested that morphologic change shows the highest degree of sensitivity to the nearshore conditions that exist at this stage in the tidal cycle. All measurements made at this time were taken by the same observer. While not ideal, the shore-based visual observations made during this study proved to be a useful, cost-effective means of obtaining nearshore process data. The types of observations that were made are described below.

Wind and weather observations consisted of the measurement of local surface wind direction and magnitude at the field site with a compass and hand-held anemometer. A determination of incident wave height at the field site was made by making a visual estimate of the breaking wave height (H_b) at the outermost set of breakers (to within 0.25m). Incident wave period (T_i) was determined by recording with a stopwatch the time it took for 11 waves to break. This timing procedure was carried out at least three times during a recording interval and the results were averaged to the nearest 0.5 seconds. Observations on the direction of wave approach were made by watching wave trains seaward of the breakers. Visual estimates of surf zone width and character (type of breaking waves, number and distribution of breakers) were recorded. Finally, on a number of occasions, the location of the maximum shoreward excursion of runup and the location of the intersection of the beach water table with the foreshore surface were noted.

Surface floats and dye were both used to measure littoral currents at the field site. Longshore surface current velocity was obtained by timing the float or dye trace as it moved alongshore over a known distance. Information obtained using this technique was far from ideal. Wind effects on surface floats were significant. Also, the nature of the NMB surf zone is such that it is difficult to place either floats or dye an adequate distance out into the surf zone. When adequate placement was accomplished, both the floats and the dye were observed to move onshore or offshore, as well as alongshore, in response to local circulation patterns associated with rip cells. Nine measurements of surface currents using dye were deemed acceptable.

Observations of nearshore conditions made at the field site were augmented by

wind and wave data from several other sources. Information on regional atmospheric circulation patterns that existed during the study period was obtained from synoptic weather charts collected from the local newspaper. Thirteen months (from June 1986 to July 1987) of daily (9:00 am) readings of wind direction and speed recorded at the Westport Harbour meteorological station were obtained from the Westport Harbour Master. Mangin (1973) and Pfahlert (1984) reported shore-based visual observations of winds and waves from the Westport area and a location approximately 100 kilometers south of NMB respectively. Pickrill and Mitchell (1979) summarized oil rig records from off the west coast of the North Island that include the 17 month-long "Maui Waverider' record. A summary of wind and wave observations from ships in the Tasman Sea between 1957 and 1980 is provided by Reid and Collen (1983). Finally, Valentine and Macky (1984) reviewed roughly two years of data collected from 'Waverider' buoys located approximately two kilometers offshore at three locations near Westport.

These different data sets are not readily comparable. Pickrill and Mitchell (1979) provide a useful discussion of the sorts of difficulties encountered in attempting to compare different wave data sets. These include site variability - the effects of different local exposures and bathymmetries; length of wave records - most records are too short; measurement parameters - different definitions of different parameters; and method of data acquisition - shore-based visual versus offshore-instrumented records.

With respect to this last point, it has been generally assumed that shore-based observers estimate the height of the highest 30% of the breaking waves and that these values are comparable to significant wave height (H_S) obtained from offshore instrumented records (Munk, 1944; Pierson et al., 1955). A study by Bowman (1979) examining the validity of visually estimated wave parameters reached a similar conclusion. Bowman compared shore-based visual observations to those obtained from 'Waverider' buoys and found a good correlation between breaking wave height

and significant wave height. For experienced observers he reported the accuracy of visual observations to be within 20% of the instrumented observations. He also observed a tendency for visual overestimation, which became more pronounced with increasing wave heights. In a more recent study Balsillie and Carter (1984) also suggested that experienced observers can provide an estimate of breaking wave height to within 20% of instrumented observations. However, they suggested that visual observations of breaking wave height show a closer correspondence to the mean as opposed to significant wave height.

Bowman (1979) also examined the validity of visual estimates of wave period. He found correlation between a visual estimate of wave period and significant wave period to be poor. This result is not surprising considering the differences between timing and zero-upcrossing methodologies.

Morphology-plan

Inferences as to the nature of subaqueous morphology were based primarily upon visual observations of surf zone width and character. For example, breaker number corresponds to bar number, breaker distribution to bar type: 'regular' breaker zones represent linear topographic features, 'irregular' breaker zones represent more complex topographic features.

It would have been desirable to have obtained subaqueous bottom profiles to support the above interpretations of bar number and type from surf zone character. Neither was this possible, nor would it have been practical to attempt to do so considering the nature of the NMB surf zone. Taking into account these limitations, an experimental photographic technique was attempted on a limited basis as a means of obtaining additional evidence for the nature of subaqueous beach morphology. Based on the idea that waves break preferentially over topographic highs, a time lapse photograph was used to produce an 'image' of the offshore morphology. A long exposure (~4 minutes) was taken at night with a full moon from atop the rocky point north of the field site. The full moon at night highlights the contrast between the white

breaker zone (bars) and the black areas of non-breaking (troughs). The long exposure filters wave to wave variability. This technique is a variation on a more developed video technique recently employed by Lippman and Holman (1989). They provide an in-depth discussion of the basis, methodology, and applications of the technique within their paper. The technique employed here proved to be powerful, and was particularly well suited to a high energy surf zone like that of Nine Mile Beach.

Direct mapping of plan morphology was made at low tide when inner surf zone morphology was exposed. Plan sketches were made and photographs taken from the rocky point north of the field site on a number of occasions. On a regular basis, shoreline rhythms were paced-out on the lower foreshore to determine their extent.

Rhythmic topographies observed on NMB were categorized according to a classification scheme developed for this work. Table 2.1 summarizes the most commonly used nomenclature and defines the terminology used in this paper to describe rhythmic shoreline topographies.

Rhythmic shoreline topographies have been described in the literature by numerous workers, including Evans (1939), Bruun (1954), Russel and MacIntire (1965), Zenkovich (1967), Dolan and Ferm (1968), Hayes (1972), Sonu (1973), Vincent (1973), Dolan et al. (1974), Guza and Inman (1975), Komar (1976;1983a), Chappell and Eliot (1979), Hunter et al. (1979), Sallenger (1979), Short (1979), Wright et al. (1979), Inman and Guza (1982), Wright and Short (1983;1984), Seymour and Aubrey (1985), and Antia (1987).

As Komar (1983a) has pointed out, existing classifications of rhythmic topography have tended to be awkward and confusing. This is because a variety of terms have been applied by different workers to describe similar forms. In addition, most of the classification schemes have been based solely on the longshore dimension, or 'form length', of the rhythmic features. The morphogenetic classification scheme used in this work and given in Table 2.1 is an attempt to remedy this situation.

Following from the terminology of Inman and Guza (1982), the primary distinction

TABLE 2.1 MORPHOGENETIC CLASSIFICATION OF RHYTHMIC TOPOGRAPHIES

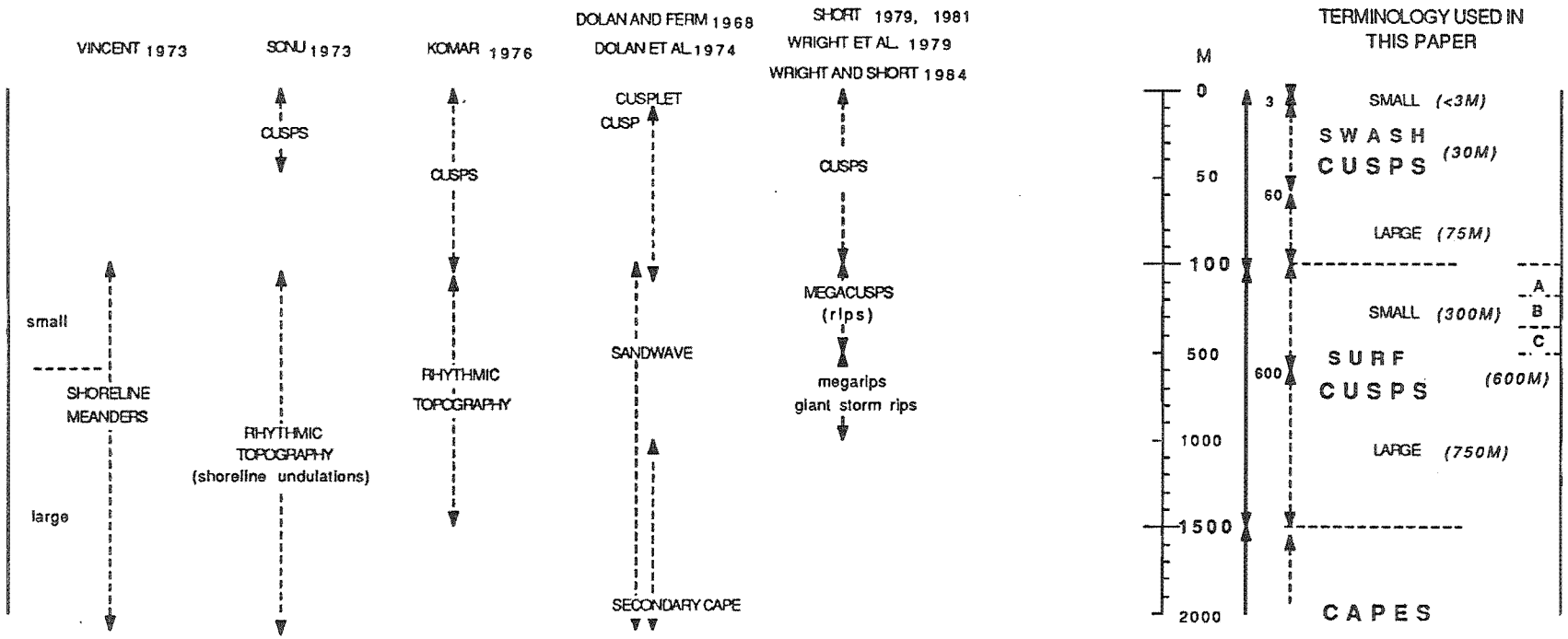

made here is between *swash cusps* (≤100m) and *surf cusps* (100-1500m). Aside from being smaller in scale, swash cusps are essentially subaerial features. The larger scale surf cusps, in contrast, are subaerial features that are coupled with the subaqueous morphology (Sonu 1973; Komar, 1976,1983a; Inman and Guza, 1982). Another important distinction made here is between *small* (100-600m) and *large* (600-1500m) surf cusps. Small surf cusps tend to be associated with the inner bar system, large surf cusps with the outer bar system (Vincent,1973). Finally, in this work the small surf cusps are in turn subdivided into three size classes - *A*(100-150m), *B*(250-300m), and *C*(400-500m) - as the observed spacings tended to cluster around these values.

In addition to form length, form *amplitude*, *symmetry*, *mobility*, and *nature of occurrence* were also noted. Form amplitude refers to the extent of cross shore relief. Form symmetry refers to the orientation of the rhythm with respect to the general trend of the shoreline, ie. *normal* versus *skewed or oblique* rhythms (Vincent,1973; Sonu,1973; Hunter et al. ,1979; Wright and Short,1983, 1984; Antia,1987). Mobility refers to wether forms are *migratory* or *nonmigratory*. Finally, the nature of occurrence refers to the degree of form summation (Dolan and Ferm,1968; Komar, 1983a), where here, rhythmic shoreline topographies are referred to as an irregular, *nested* set (multiple superimposed forms), or as a regular, *isolated* set of forms.

Morphology-profile

The location of a primary profile line was established on the NMB foreshore. On a daily basis, during low tide, the beach profile at this location was surveyed. From a fixed position above the base of the dune scarp seaward to the position of low water, the beach elevation was recorded (to within 0.5cm) at five meter cross-shore intervals. Additional profile surveys were also carried out at two other locations 100 meters to the north and south of the primary profile line on several occasions.

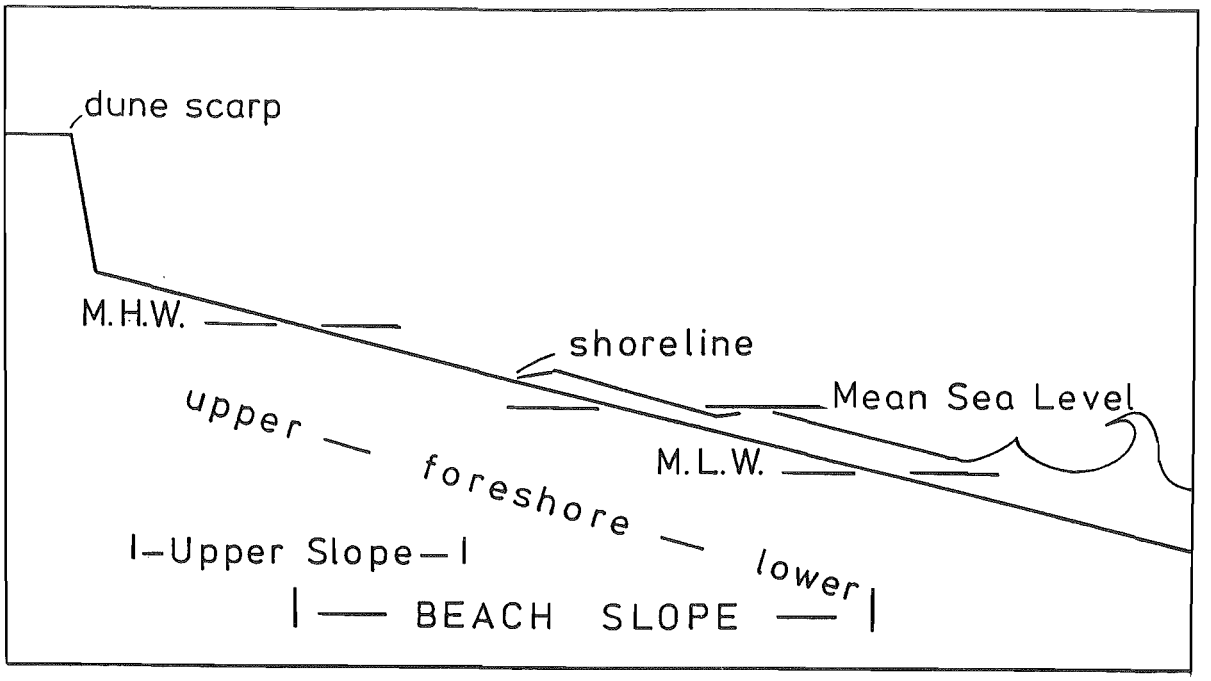

Figure 2.2. Profile definition sketch.

The beach profiles were used in combination with published tide tables to establish a mean sea level (M.S.L.) datum by extrapolation of the sea level position recorded at the time of profiling. The average value of the location of M.S.L. obtained from this procedure was taken as the position of M.S.L. This position was used together with the profiles to determine beach slope, width, and volume. Specifically, beach slope is taken as the mid-tide slope of the subaerial beach, essentially from below mean high water to above mean low water through the position of mean sea level (Figure 2.2). Similarly, upper beach slope is the foreshore slope through the position of mean high water. Beach width and volume are that of the subaerial beach extending from the shoreward backshore limit (base of dune scarp) to the position of mean sea level (as opposed to the position of mean low water). Thus beach volumes given in later chapters do not include the lower beach volume. The reasons for this apparent neglect are two-fold. First, the primary area of interest in this study is the upper foreshore. Second, owing to the high energy nature of the NMB surf zone, profiling in the lower foreshore was

difficult and at times dangerous. Even when data was obtained, it was often of questionable accuracy.

In addition to the standard profile parameters described above, several other profile parameters were determined from the beach profiles. They included: volume exchange, defined by Short (1981) as the standard deviation of beach volume; beach mobility, the standard deviation of beach width; and backshore mobility, the coefficient of variation (mean beach width / standard deviation of beach width) (Dolan et al., 1974; Short, 1981). Ratios that express profile form in terms of the degree of profile concavity or convexity were also calculated. These parameters, referred to as *profile shape indices*, are defined here as the ratio of high-tide beach slope to mid-tide beach slope (*RBS*) and the ratio of mid-tide beach width to high-tide beach width (*RBW*).

Stratigraphy and Sedimentology

In order to carry out grain size analyses of NMB sands, bulk sediment samples were collected on two different occasions during the study period. A sample consisted of handfuls of sand collected, at approximately ten meter increments from the dune scarp seawards to the location of mean low water, at two locations located approximately 100 meters apart alonghsore, and grouped together. In the laboratory heavy mineral-separation, as well as sieving and settling tube analyses, were preformed on the samples using standard procedures as outlined in Lewis (1982).

Descriptions of sedimentary structures and textures were taken from trenches excavated in the NMB foreshore (Plate 2.1). The trenches were one to two meters in cross-shore length, and were located at five meter increments down the upper foreshore (Figure 2.3a). Trenching in close proximity to the primary profile line was carried out on a regular basis. Trenching along the northern and southern profile lines was carried out less frequently. In addition to descriptions made in the field, the trenches were sketched, photographed, and videotaped for further examination at a

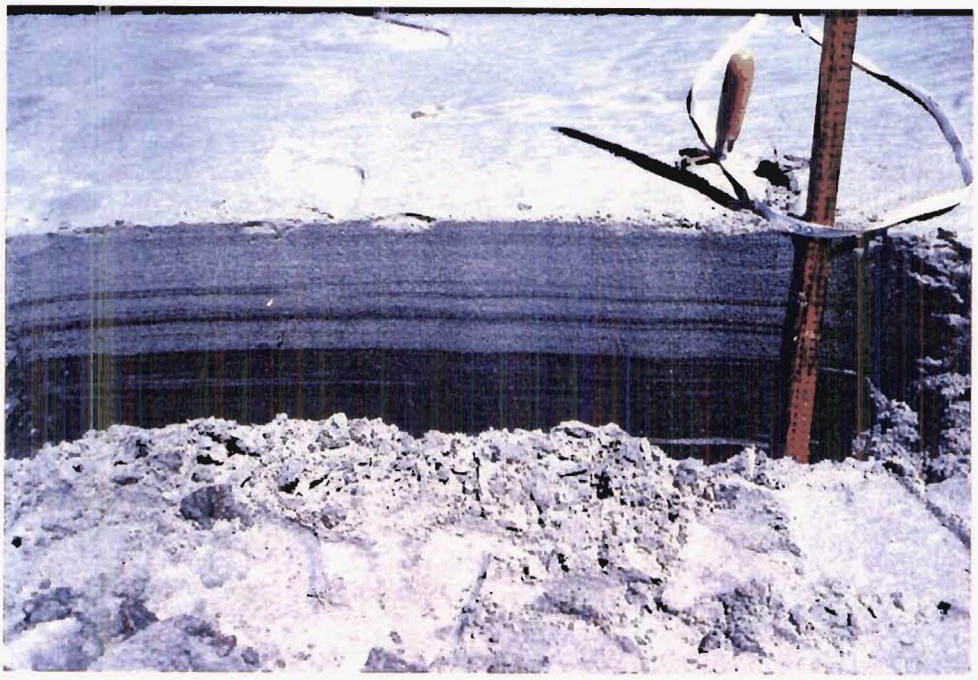

Plate 2.1. Representative example of a trench excavated in the upper foreshore.

later date.

Bedforms present on the upper foreshore were measured on several occasions during the study period. The height, wavelength, and symmetry of the bedforms were measured with a tape-measure in a manner similar to that described in Broome and Komar (1979).

SMALL SCALE DATA COLLECTION

In conjunction with the large scale data collection described above, small scale data collection was carried out on 10 occasions during the 27 day interval between December 1986 and January 1987. Small scale data collection involved the deployment of an equipment array (Figure 2.3a, Plate 2.2) and the recording of a variety of measurements through the tidal cycle (Figure 2.3b).

The Data Collection Run

At low tide the beach profile was surveyed. Poles were placed along the profile line at five meter increments between the zero to 40 meter mark (upper poles) and at 10

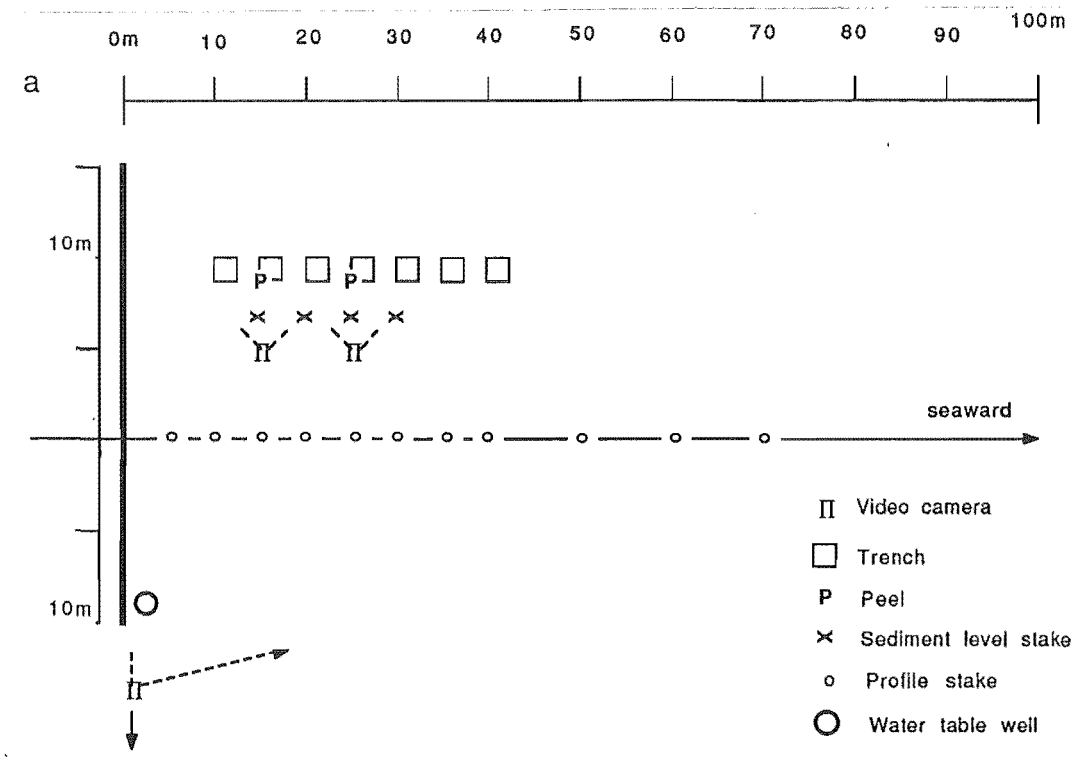

b

LOW TIDE

Survey Profile and Stake-out Profile Line
Deploy Data Collection Array
Deploy Depth-of-Activity Rods
Excavate Water Table Well

Record Nearshore Conditions,
Runup and Water-Table Excursion

HIGH TIDE

Simultaneous Flow Videos and
Sediment Level Recordings

Record Nearshore Conditions, and
Runup and Water Table Excursion

LOW TIDE

Resurvey Profile
Disassemble Data Collection Array
Record Depth-of-Activity
Excavate and Describe Trenches
Take Box Cores and Make Peels
Describe Bedforms

Figure 2.3. Data collection on NMB. (a) Schematic representation of the data collection array; b) Various aspects of data collection carried out through the tidal cycle.

Plate 2.2. A low tide view of the data collection array deployed on the NMB foreshore. In this photo red flagged poles mark 10 m increments along the survey line; V8 Video camera show up as the two yellow squares to the left of the profile line; and the four rods used for bed elevation measurements show up as white lines at the left of the video camera. (See also Figure 2.3a.)

meter increments from the 40 to 70 meter mark (lower poles). Depth-of-activity rods (Clifton, 1969; Greenwood and Mittler, 1984) were placed on the upper poles at this time. A water table well (Emery and Foster, 1948; Lanyon et al., 1982) was excavated in the uppermost portion of the foreshore and the measurement of the water table elevation every 15 minutes was commenced. The remainder of the data collection array, described in greater detail below, was deployed at this time.

In conjunction with the recording of nearshore conditions before the high tide, the location of the maximum runup excursion and the location of the intersection of the beach watertable with the foreshore surface were noted. Over a one-half to three hour period during the high tide, video recordings of runup and measurement of the bed elevation were made simultaneously. The location of the maximum runup excursion and the location of the intersection of the beach watertable with the foreshore surface were again noted at approximately three hours after the high tide.

At the subsequent low tide, the beach profile was resurveyed. Readings from the

the depth-of-activity rods were recorded. Trenches were excavated and small box cores (Bouma, 1969) were taken at this time. The data collection array was then disassembled.

Of the ten data collection runs that were carried out, only five of the sets of runup video recordings, bed elevation measurements, and sediment peels were used in this study for further analyses. (These five runs constituted two run sets - one of set of three runs and one set of two runs.) There were several reasons why this was done. Desirable contrasts in both morphology and nearshore processes were exhibited - The sets of observations were taken at horn and bay locations under both storm and swell conditions. Effects due to variations in the tidal level were at a minimum - The same high tide level existed for each run set. Complete runs were obtained- Good video recordings were made at the same fixed location for each run set.

Video Recordings of Runup

In the swash zone, where the beach is periodically inundated by shallow, rapid, sediment-laden flows, obtaining process measurements can present difficulties. During this study, video techniques were successfully employed to measure runup excursions, and runup depths and surface velocities on the upper foreshore. Although the film techniques were inexpensive and the logistics were simple, the data acquisition was time consuming. Film techniques similar to those described below have been used previously by others [e.g. 'close-up' films of runup made by Miller and Zeigler (1958), Wright (1976), and Bradshaw (1982); 'wide-angle' films of runup made by Holman and Guza (1984), Holman and Sallenger (1985), Holman (1986)]. Additional descriptions and discussions of filming methodology are provided by these workers.

The filming of runup carried out for this study involved a combination of 'close-up' (two V8) and 'wide-angle' (VHS) video recordings (Plate 2.2, Figure 2.3a). The wide-angle video recordings consisted of the filming of runup with a single camera

located approximately 100 meters to the north of the profile line at an elevation of approximately three meters. The close-up video recordings involved the following procedure: After the low tide profile survey, two thin metal rods, spaced one meter apart and separated by a central rod marked with 2.5cm gradations, were placed in the sand. This rod setup was emplaced at two different locations spaced ten meters apart on the upper foreshore (Figure 2.3b). A "SONY V8 'Handycam'" video camera was positioned near each location to view each rod setup and an area approximately 2.5 meters on either side of the central rod. During high tide synchronous video recordings were made of the water as it flowed up and back, through each rod setup.

Results obtained from the close-up video were those principally used in this study. In the process of dubbing a clock onto them, five V8 video recordings were transferred to a VHS format. (Thus only one of the pair of V8 video recordings taken during each data collection run was used.) Water depth was measured directly from the video recording to within 1.25cm. Velocities were obtained by timing the leading swash edge and/or pieces of surface foam as they traversed the one meter section. When viewed frame by frame, individual pieces of foam could be tracked on the video player to within 0.04 seconds - the time interval between frames. A total of 241 individual swash/backwash events were sampled, approximately every 1.5 seconds on average, using this method. Employing a similar cine-camera technique, Wright (1976) suggested that the margin of error on the velocity measurements is on the order of ±5%.

In the manner just described, complete videos were digitized to yield a time series of runup flow depth and velocity at a given location (Figure 2.4a,b). By integrating the surface velocity and depth values over an individual swash/backwash event, an average swash and backwash surface velocity and depth for each runup event was obtained.

In addition to the surface velocity and depth measurements, the time (in seconds) and location (to within 2.5 meters) of individual runup excursions that entered the viewing area were noted. This data, corroborated and supplemented by runup data

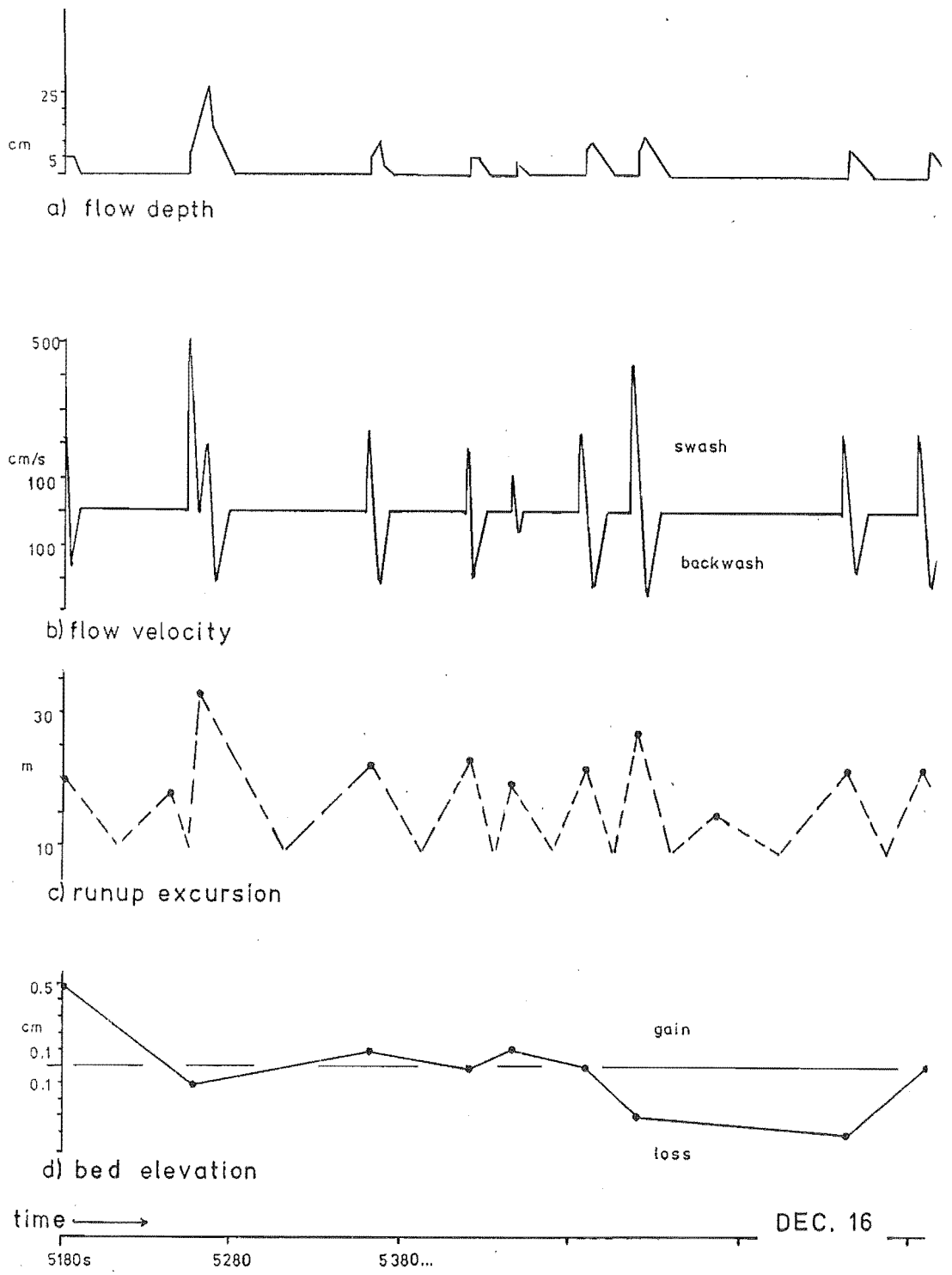

Figure 2.4. Representative portions of time series collected during the high tide recording interval. (a) time series of runup depth; b) time series of runup -swash and backwash- velocity; c) time series of runup excursion width - dashed line indicates interpolation between runup maxima [see Chapter 5];d) time series of bed elevation.)

obtained from the wide-angle video, was used to construct a runup excursion width time series (Figure 2.4c).

Originally it was intended to use only the wide-angle video to track runup excursions. However, the wide-angle video suffered from several limitations. The low slope of NMB beach and the wide tidal range resulted in a zone of runup that exceeded 100 meters on several locations. Therefore, the distance the wide-angle camera needed to be located away from the profile line in order to view the entire swash zone severely limited the precision of the measurements. Also, wind-induced flutter of the camera during video recording added to the difficulty in locating the position of the runup line accurately. Thus, while it would have been desirable to capture the entire swash zone, the decision was made to obtain a more precise, albeit truncated, record of runup on the upper foreshore.

Measurement of Bed Elevation

Measurements of the bed elevation were recorded in conjunction with the runup video recordings. To facilitate measurement of the bed elevation in the upper foreshore, thin rods were placed at four cross-shore locations spaced five meters apart in the uppermost foreshore, during the low tide (Plate 2.2, Figure 2.3a). (Two of these locations corresponded to those where the flow video recordings were made.) At a given location, the change in bed elevation was recorded following each runup event by using a meter stick with a hinged base plate to measure the change in sediment level relative to the height of the rod at that location. Time series of the bed elevation at the four locations were obtained from these measurements (Figure 2.4d).

Sallenger and Richmond (1984) and Howd and Holman (1984a) provide detailed descriptions of this methodology. These workers reported the accuracy of the bed elevation measurements to be on the order of ±1.5mm.

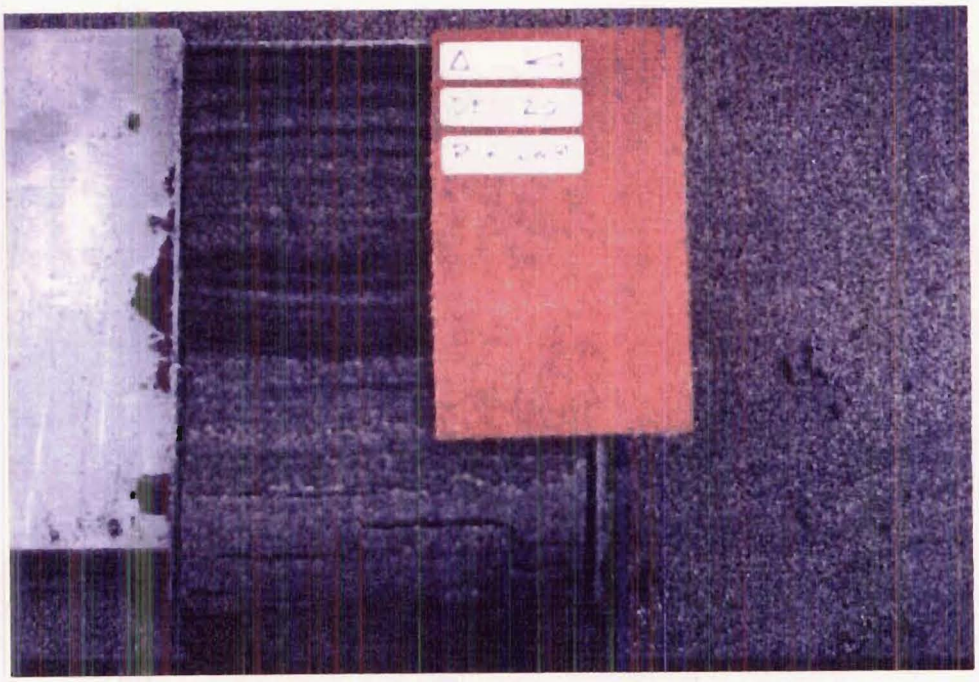

Plate 2.3 A box core prior to making a peel

Textural Analysis of Sediment Peels

Sediment peels were made from the small box cores using a rapid field technique described by Yasso and Hartman (1972) (Plate 2.3, Figure 2.3a). (The last step in their process, application of lacquer to the face of the peels, was not carried out. It was not required to maintain the peel surface and was found to coat the surface such that microscopic examination of the peels was severely limited.)

Sediment peels were made at the two locations where synchronous bed elevation and flow measurements were made during the recording interval. The five peels that were chosen for analysis were those that corresponded to the five close-up runup video recordings that had also been chosen for analysis. For each peel, a grid pattern was laid out, the peel was magnified to a predetermined scale, and the peel was photographed in overlapping rows and columns. The width of peel photographed was determined by the peel size (~10cm). The depth of peel photographed represented the 'active' sediment depth at that location. This depth was determined for each location by comparing the maximum depth of disturbance with the net elevation change observed at the given location over the tidal cycle. This depth ranged from 1.1-7.1cm.

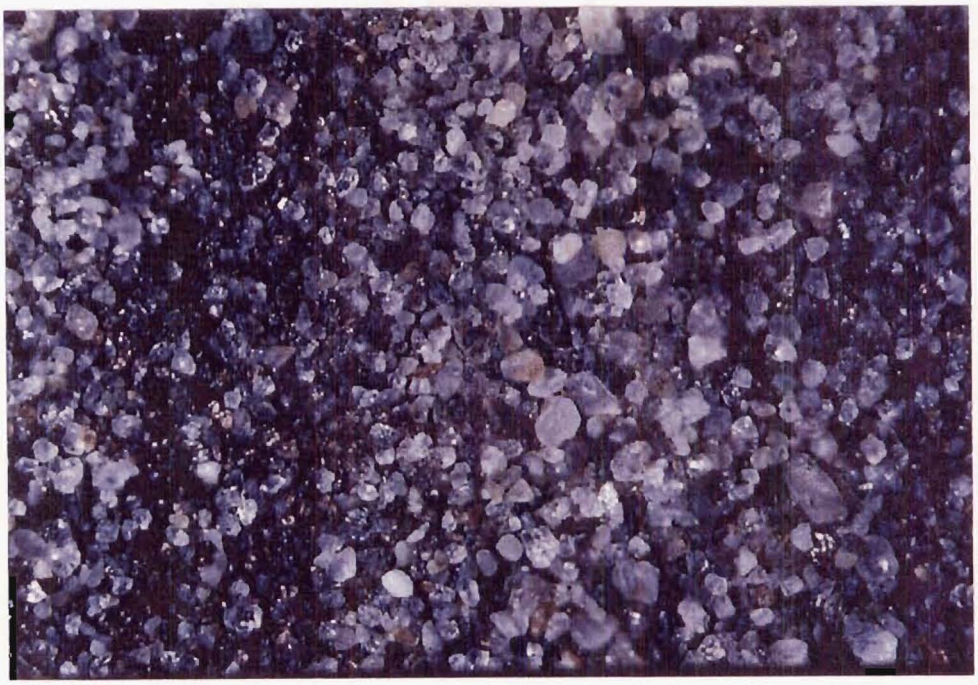

Plate 2.4 Representative example of a slide made from a peel.

Sets of color slides obtained from the above procedure were used for grain counts. Each slide was projected back onto a grid pattern (Plate 2.4). To avoid sampling across grain layers, care was taken to align the grid normal to bedding. Individual grain layers were sampled at one millimeter vertical increments down the slide by counting (i.e. its outline traced and its mineralogy identified) any grain that fell within or came into contact with equally spaced areas marked horizontally along each grain layer.

Only grains identified as quartz, garnet, or ilmenite were counted. Restriction of sampling to these these three minerals was deemed appropriate. In addition to covering a desirable range in density, and being easy to identify, these three grain types accounted for the bulk (~86%; [quartz 43%, garnet 29%, and ilmenite 14%]) of all mineral species found in NMB sands: The next most abundant minerals (zircon and epidote) each account for less than 3% of observed mineral species (Marra, 1985). Densities of 2.65 g/cm^3, 4.0 g/cm^3, 4.8 g/cm^3, were assigned to quartz, garnet, and ilmenite grains, respectively, for use in later calculations (Lewis, 1982).

The counting procedurewas repeated for each slide, moving across columns and down rows until the whole section of peel was sampled. A total of 170 individual grain layers were sampled from the five peels. The average sample size was 168 grains, and ranged from 62 to 300 grains, per grain layer. In contrast to a similar micro-scale sampling technique described by Cheel and Middleton (1986a), this technique yielded significantly larger sample sizes, and avoided mixing of grain layers (Cheel and Middleton counted 20-30 grains per 2-3 grain layer thick sample).

The validity of this measurement technique is supported by the good correspondence between textural parameters obtained from the peels and those from other more standard techniques. Assuming that the mean of the measurements of the apparent long axes of grains (D_{al}) from their outlines approximates the mean sample intermediate grain diameter (D_i) (Ibbeken and Schleyer, 1986), a total population mean grain size of 0.238mm (±0.004) was determined from the peels. Although slightly higher, as expected, this value compares favorably with the values of mean grain size obtained from standard sieving (0.19mm) and settling tube analyses (0.22mm) of NMB bulk sediment samples. Similarly, the mean settling velocity 2.97cm/s calculated from the peels is also comparable to the mean settling velocity of 2.70 cm/s measured from settling tube analysis of bulk samples.

Grain size distribution summary statistics were calculated using the method of moments (Lewis, 1982), both for the whole sample, and for each of the three mineral species within each grain layer sample. The grain layer sample means were used to determine mean settling velocities and mean grain dispersive pressures for each of the mineral species in the grain layers. Settling velocities were calculated by first employing Gibbs et al. (1971) empirical equation for the evaluation of spherical grains of approximately quartz density in water. An empirical density correction factor given by Komar (1981) was then applied to the Gibbs settling velocity values. Finally, these corrected values for spherical grains were in turn converted to settling velocities for natural grains using empirical equations provided in Baba and Komar (1981) for quartz,

and Komar and Wang (1984) for the two heavy mineral species. Grain dispersive presure was claculated as $\rho_s D^2$ (Komar and Wang, 1984).

CHAPTER 3 NEARSHORE DYNAMICS: MACROSCALE

"The mentioned idealization of continuous natural transitions by discrete values is, of course, more due to the desire for practical classification rather than a scientific necessity."
M.S. Yalin

This chapter describes Nine Mile Beach nearshore morphologies and processes. Based upon a comparison to the Australian morphodynamic model, NMB macroscale process-form assemblages are identified and a NMB macrodynamic model outlined. Also, by attempting to apply it to NMB, the universality of the Australian model is explored.

3.1 BACKGROUND: SAND BEACH MORPHODYNAMICS AND THE AUSTRALIAN MODEL

Early investigators focused considerable attention on describing the effect that changes in wave height have on the beach profile. They found that during periods of large waves, sand moved offshore and barred, 'storm', profiles developed: During periods of small waves, sand moved onshore and bermed, 'swell', profiles developed (Bagnold, 1940; Johnson, 1949; Shephard 1950; Bascom, 1954; Hayes and Boothroyd, 1969; Zenkovich, 1967; King, 1972; Komar, 1976a).

Although this two-dimensional model remains as the framework for investigations of sand beach morphodynamics, a greater appreciation has developed for the diversity of forms and processes in sandy coastal systems. As a result, recent workers have focused

their attention on the description of three-dimensional patterns of beach change and the identification of a group of governing processes. In this vein, the Australian model of coastal morphodynamics outlined by Wright and Short (1983, 1984) represents an attempt to provide a more comprehensive framework for the investigation of sand beach dynamics.

MORPHODYNAMIC STATES

Wright, Short, and their coworkers carried out fieldwork on the open-coast sand beaches of Australia (Wright and Thom, 1977; Wright et al., 1979; Short, 1979, 1981; Wright, 1981, 1982; Wright et al., 1982; Wright and Short, 1983,1984). These beach systems are predominantly microtidal (Mean Spring Range=1.5m), are characterized by highly variable/high energy wave climates, and have weak to negligible longshore drift. Based on morphologic and hydrodynamic observations carried out over long time periods at these different beaches, Wright and Short suggested that variations in depositional form and coupled wave-generated fluid motions are "quasi-systematic". They identified a sequence of *morphodynamic states* that occurred through storm/recovery cycles. Each state represented a specific assemblage of beach and surf zone morphologies, incident wave energy levels, resonant frequencies, and nearshore circulation patterns.

Synthesizing morphologic classification schemes presented in earlier papers (i.e. Short, 1979, 1981; Wright et al., 1979), Wright and Short (1983, 1984) described a "Reflective" end member state, a series of four intermediate states ("Low Tide Terrace", "Transverse Bar and Rip", "Rhythmic Bar and Beach", "Longshore Bar and Trough"), and a "Dissipative" end member state.

Although this terminology is used in all their subsequent work, Wright et al. (1985) provided a coarsened version of the original six state classification. In this classification scheme, similar to the one described in Short (1981), adjacent states are combined. The Reflective end member and the Low Tide Terrace states are merged into a *Reflective* state; the Transverse Bar and Rip state is merged with the Rhythmic Bar and Beach state to form an *Intermediate or Rhythmic* state; and the Longshore Bar and Trough, and Dissipative end member are merged into a *Dissipative* state. This simplified three state classification

is favored and is the one adopted in this work.

The process-form assemblages that characterize each of the three morphodynamic states are summarized in Table 3.1 and described below. Additional aspects of the Australian model are also reviewed.

AUSTRALIAN MODEL MORPHOLOGIES

Beach and surf zone morphology is the primary element in Wright and Short's beach classification scheme. Specific morphologic criteria considered in the Australian model includes surf zone width, number and types of nearshore bars, and subaerial beach profile shape. Based on these criteria, distinct plan and profile configurations are recognized for each state (Figure 3.1).

Reflective Morphologies. Reflective morphologies correspond to the accreted 'convex', 'swell', 'summer', or 'berm-step' profiles described in the coastal literature (e.g. Hayes, 1972; King, 1972; Komar, 1976a; Wright and Short, 1983; CERC, 1984). Characteristic features are a steep, linear beach face capped to shoreward by a high, straight berm, and terminated to seaward by a pronounced step. The surf zone is narrow or absent.

Under the lowest energy conditions the shoreline is straight. Greater morphologic complexity is observed at increased energy levels: Beach cusps are often present in the swash zone and a relatively narrow low tide terrace may occur below the steep beach face. The terrace may be dissected by narrow rip channels that separate extensive inshore shoals.

Dissipative Morphologies. Dissipative morphologies correspond to the eroded, 'concave', 'storm', 'winter', or 'barred' profiles described in the coastal literature (e.g. Hayes, 1972; King, 1972; Komar, 1976a; Wright and Short, 1983; CERC, 1984). A wide featureless low gradient subaerial beach, often scarped at its inner margin, is characteristic of dissipative morphologies. At the highest wave energy levels, multiple longshore bars and broad shallow troughs underlie wide surf zones. In plan, dissipative beaches generally lack longshore rhythmicity.

At decreased wave energy levels longshore bars are fewer in number and closer to shore.

TABLE 3.1 THE AUSTRALIAN MORPHODYNAMIC MODEL (after Wright and Short, 1983;1984)

MORPHOLOGY	BEACH STATE	SIMILARITY PARAMETERS
"BAR and TROUGH" Wide, flat subaerial beach with a linear shoreline fronts a wide surf zone with multiple linear bars and broad troughs	**DISSIPATIVE** DISSIPATIVE + LONGSHORE BAR AND TROUGH	ε_b > ~30 Ω > ~4.50
"RHYTHMIC" Steep 'bays' and flat 'horns' on the sub-aerial beach coupled to transverse or crescentic bars in the surf zone define a rhythmic shoreline	**RHYTHMIC** RHYTHMIC BAR AND BEACH + TRANSVERSE BAR AND RIP	Ω ~3.0-4.0
"BERM and STEP" Linear or cusped berm caps a narrow, steep subaerial beach with plunge step and narrow or absent surf zone	**REFLECTIVE** LOW TIDE TERRACE + REFLECTIVE	ε_b < ~3 Ω < ~2.50

Table 3.1.- The Australian Morphodynamic Model (after Wright and Short, 1983, 1984). Column 1 is a descriptive summary of the beach state morphologies; Column 2 summarizes the beach state nomenclature; Column 3 presents similarity parameter threshold values for each state (ε is the surf similarity parameter; Ω is Dean's parameter);

PROCESSES Wave Height	Resonant Periods	Currents	"Process Signature"
HIGH ≥2.5 M	BROADBAND INFRAGRAVITY (T > 30 sec)	VERTICALLY STRATIFIED - bottom return flow -'surfbeat' dominated runup	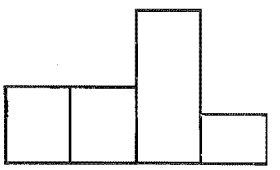
MODERATE 1.0-2.5 M	MULTIPLE (T, 2T, 4T) (T>30S)	HORIZONTALLY SEGREGATED -'rip' cells with offshore flow at bays and onshore flow at horns	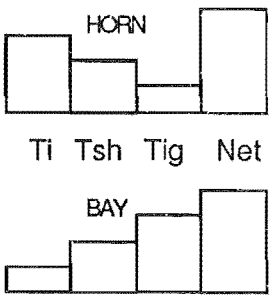
LOW ≤ 1.0 M	INCIDENT-SUBHARMONIC (T, 2T)	GENERALLY ABSENT -'drift' confined to swash zone -'swash' dominated runup	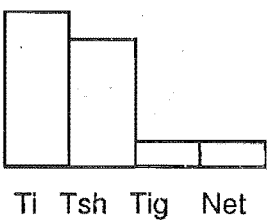

Columns 4-7 summarize process elements within the model - column 4 wave energy level, column 5 relatively dominant oscillatory motions, column 6 net circulation patterns, and column 7 schematic *process signatures*, where 'Ti', 'Tsh', and 'Tig' refer to incident, subharmonic, and incident frequencies respectively, and 'Net' to net circulations.

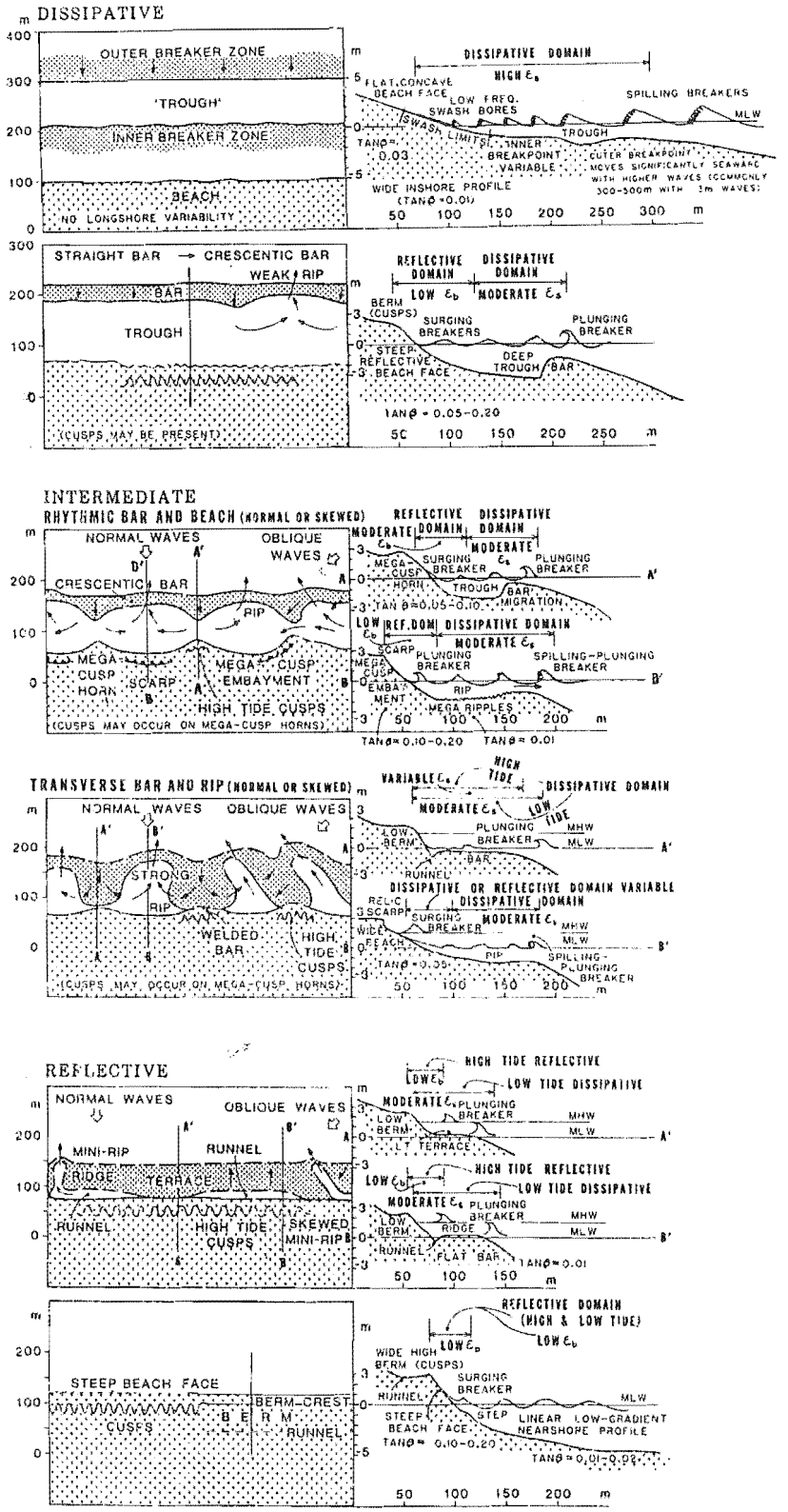

Figure 3.1. Plan and profile configuration of the six morphodynamic beach states recognized within the Australian model' (from Wright and Short, 1983). Note that Wright and Short's (1983, 1984) six states are grouped into three states in Table 3.1 and throughout this work.

The troughs are narrower and deeper. Weak rhythmicity may exist in the form of widely spaced broad rip channels and cusped berms atop a steepened beach face.

Rhythmic Morphologies. Characteristics of rhythmic morphologies were considered in Chapter 2 in the context of their classification. Rhythmic morphologies consist of large scale longshore undulations of the subaerial beach and/or submarine bar. A variety of forms fall within this general definition.

Rhythm wavelength ranges in scale from large rhythms during periods of large waves to small rhythms during periods of small waves. The inner bar may be crescentic and separated from the beach by a trough, or transverse and shore-attached. The foreshore may exhibit pronounced horns and bays or only slight protrusions. With oblique incident waves, horns and bays may be deflected in the direction of littoral drift. Commonly rhythmic morphologies are a composite of these various forms.

These complex morphologies are intermediate between the reflective and dissipative end members. As a result they posses both reflective and dissipative morphologic elements. Swash bars and berms are common on the relatively steeply sloping, reflective horns. The relatively gently sloping, dissipative bays may posses well developed swash cusps.

AUSTRALIAN MODEL PROCESS SIGNATURES

Wright and Short suggested that at different wave energy levels, different combinations of fluid motions exist. The different hydrodynamic process assemblages, or *process signatures*, indicate the relative contribution of different modes of fluid motion to sediment transport. They accompany the different beach state morphologies described above. The process signatures associated with the three morphodynamic states of the Australian model are described briefly below (see also Table 3.1).

Modes of fluid motion that are considered important in the Australian model are summarized in Table 3.2. They include a variety of wave generated mean and oscillatory flows, as well non-wave generated currents. (e.g. Longshore currents, rip currents and associated net drift patterns that are driven by gradients in wave energy dissipation [Wright

TABLE 3.2 MODES of FLUID MOTION in the NEARSHORE

(after Wright and Short, 1983, 1984)

WAVE GENERATED CURRENTS

Oscillatory Flows

-Progressive wave motions directly associated with the incident waves at incident frequencies (T)

-Standing wave motions in the form of 'leaky' mode standing waves and/or 'trapped' edge waves at a range of frequencies

-edge wave motions confined to the immediate vicinity of the beachface at incident and subharmonic frequencies (T-2T)

-edge wave motions trapped inshore between the beachface and bar at subharmonic frequencies (2T-4T)

-standing wave motions extending across the entire width of the surf zone at high infragravity and low infragravity ('surf beat') frequencies (T=50-100sec., T>100sec.)

Mean Flows

-Onshore-offshore currents

-Vertically stratified 'drifts'

-Horizontally segregated 'rips'

-Longshore currents

NON-WAVE GENERATED CURRENTS

Tidal

Shelf (barotropic/baroclinic)

Local Wind Shear (storm surge)

and Thom, 1977; Komar, 1983b]; Standing waves that develop as a result of wave reflection at the shoreline, and produce local fluid motions that are superimposed upon the net drift patterns [Bowen, 1980].)

Reflective Processes. The low energy Reflective states are dominated by swash as opposed to surf processes. Waves undergo little dissipation as they traverse the narrow barless surf zone. Reaching the beach face, they collapse on the plunge step or surge up the beach face without breaking. As a result, reflection is strong and the existence of relatively high frequency, edge waves at synchronous and subharmonic frequencies is favored. Swash cusps are a morphologic response to these standing motions. High

frequency, swash dominated runup is a characteristic expression of the dominant standing motions. Infragravity oscillations and mean currents are generally negligible in reflective process signatures. Nearshore circulation is principally confined to the narrow swash zone and net cross-shore drift is shoreward.

Dissipative Processes. The high energy Dissipative states are dominated by surf processes. Waves break by spilling and plunging, and then cross the surf zone as bores while continuing to loose energy. The dissipation of wave energy in breaking suppresses subharmonic and synchronous resonance, and instead favors the existence of motions at infragravity frequencies. These low frequency motions produce oscillatory currents that dominate over incident wave motions and mean currents in the control of sediment transport. Low frequency, setup dominated runup is a characteristic expression of these standing motions. Although weak relative to surf beat motions, net cross-shore drift is characterized by seaward bottom return flow. Cell circulation is in general weak, the exception being headland bounded beaches where strong large-scale rips frequently accompany storms.

Rhythmic Processes. Rhythmic states exhibit complex process signatures. Like their associated beach and surf zone morphologies, process signatures vary spatially and posses both reflective and dissipative elements. Incident frequencies dominate surf zone spectra. Resonance at subharmonic frequencies, in the form of relatively low frequency/long wavelength edge waves, prevails along the length of the beach. Infragravity motions, of relatively high frequency, are most pronounced in the vicinity of rip embayments.

Mean flows are strong relative to oscillatory motions. Persistent rip cells, with shoreward flow at the horns and seaward flow in the bays, are a characteristic feature of rhythmic states. Longshore currents may also influence the circulation pattern.

DYNAMIC SIMILARITY

Wright and Short have attempted to quantify the process-form associations noted above in terms of *dynamic similarity parameters*. Several different forms of dynamic similarity

parameters are used within the coastal literature (Galvin, 1972; Battjes, 1974; Guza and Inman, 1975; Horikawa, 1980; Wright and Short, 1983, 1984). As well as morphology, a number of surf properties including breaker type, reflectivity, and runup height, have been shown to covary with these parameters- effectively as a function of wave height, wave period, and beach slope/sediment size.

Short (1979, 1981) observed a correspondence between wave height and morphologic state. Based on almost 1200 observations at a particular beach system, and augmented by observations at other sites, threshold values of breaker height were recognized. Each state was associated with a specific range of breaker heights (Table 3.1).

Wright et al. (1979) emphasized the connection between the surf scaling parameter, ε, and the reflective and dissipative states. After Guza and Inman (1975)

$$\varepsilon = a_b \omega^2 / (g \tan^2\beta) \qquad (3.1)$$

where a_b is breaker amplitude, ω is incident wave radian frequency ($2\pi / T_i$), g is acceleration due to gravity, and ß is beach (ε_b) or surf zone (ε_s) gradient. Based on their large data sets (up to 6 years of daily observations, at over 25 different beaches) Wright and Short (1983, 1984) proposed dissipative and reflective threshold ε values: ε_s < 1-3 and ε_s > 30-100 accompanied reflective and dissipative morphologies respectively (Table 3.1). For the rhythmic states, ε_b varies alongshore, being higher (more dissipative) in the bays and lower (more reflective) on the horns. ε also varies with tide level, typically being higher at low tide and lower at high tide.

Wright and Short (1984), and Wright in later work (Wright et al., 1985; Wright et al., 1986; Wright et al., 1987) examined the relationship between Dean's (1973) parameter, Ω, and morphodynamic state, where

$$\Omega = H_b / (W_s T_i), \qquad (3.2)$$

and W_S is sediment fall velocity. Laboratory based threshold values of $\Omega<1$ and $\Omega>6$ were reported for reflective and dissipative states respectively, though threshold values determined from natural beaches are less well defined (Dalrymple and Thompson, 1977; Wright and Short, 1984). Based on different sized data sets (ranging form 586 to 1842 observations) at a single beach location, several different sets of Ω value/beach state combinations were presented. The 'equilibrium' values (Ω_e) of Wright et al. (1985) are those given in Table 3.1.

RESPONSE ASYMMETRY AND TEMPORAL ENERGY VARIABILITY

Wright, Short and coworkers recognized that process-form feedbacks act to complicate the simple correspondence between existing wave energy level and beach morphology implied by the dynamic similarity parameters. In the progression from dissipative to reflective states the ability of incident wave energy to change morphology decreases relative to the ability of morphologic inheritance to force fluid motions (Sonu and James, 1973; Chappell and Eliot, 1979; Wright et al. 1979, Wright and Short, 1983, 1984). As a result of this *response asymmetry*, contrasting patterns of morphologic change occur. Beach recovery associated with decreasing wave heights is a relatively slow process. The pattern of change is sequential; Morphologies evolve through the down-state sequence. With increasing wave energy levels morphologic change may be effectively instantaneous. The pattern of change is discontinuous; steps in the up-state sequence are skipped (Short, 1981; Lippman and Holman, 1990).

Together with response asymmetry, *temporal energy variability* may act to dictate patterns of morphologic change. This is because the rate at which wave energy levels change controls the range over which morphology may vary (Sonu and James, 1973; Wright and Short, 1983, 1984). At least two scenarios, here termed *seasonal* and *storm* models, are possible (Sonu and Van Beek, 1966; Carter, 1988). The seasonal model refers to a situation where the dominant variation in wave height is a low frequency cycle. In this situation, although response asymmetry occurs, its effect is minimized: There is sufficient time between changes in wave energy level for the full dissipative to reflective spectrum of morphologic configurations to develop. The storm model applies to a situation where the

dominant variation in wave height is a high frequency cycle. In this situation the effect of response asymmetry is maximized: Although wave energy levels may vary widely, morphologies are confined to a narrow range of configurations because there is insufficient time for the projected range of morphologies to develop.

Seasonal variations in wave height and beach morphology are characteristic of the west coast beaches of North America, and are well documented within the coastal literature (King 1972; Komar, 1976a). Wright and Short suggested that storm variations in wave height are the dominant cycle in the Australian and many other coastal systems characterized by moderate energy, temporally variable wave climates.

Having briefly reviewed the principal components of the Australian model, it is used as a basis for comparison in the description and classification of NMB nearshore dynamics that follows.

3.2 RESULTS: NMB NEARSHORE MORPHOLOGY, WAVE CLIMATE, AND DYNAMIC SIMILARITY

3.2.1 NINE MILE BEACH NEARSHORE MORPHOLOGY

SUBAQUEOUS BEACH MORPHOLOGY

A histogram of surf zone widths plus representative photographs of various surf zone characteristics at NMB are presented in Figure 3.2 and Plate 3.1. Surf zone widths ranged from 50-1000m, but were generally within the 100-500m range (79%). Inferred bar number and type ranged from multiple (2+) linear, shore-parallel bars with widely spaced rips to a single irregular, poorly developed bar. Most commonly, the surf zone exhibited two well developed breaker zones characterized by an outer more linear bar and an inner more irregular bar. The inner bar is inferred to be predominantly crescentic in shape, but it may range in character from a linear bar separated from the shoreline by a well developed trough, to a transverse bar attached to the shoreline. It was not uncommon for wave

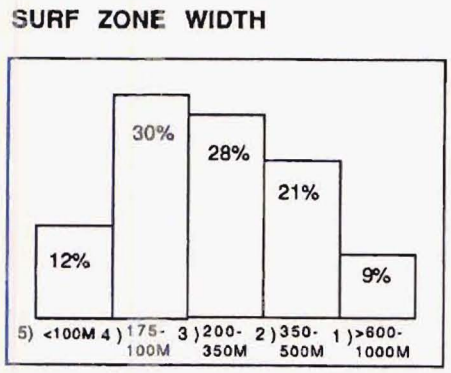

Figure 3.2. Distribution of observed surf zone width estimates. Surf zone width range for each class is given at base of figure. The percentage of occurrence for each class is also indicated in this figure.

Plate 3.1. Representative photographs of surf zone character. The numbers next to each photograph correspond to the surf zone width classes given in the accompanying figure.

breaking to be visible only over the highly variable inner bar.

The above interpretation of bar morphology from surf zone characteristics is generally supported by the results of the time lapse photographic technique described in Chapter 2. In Plate 3.2 the upper photograph is a 'normal' exposure taken of the surf zone during relatively high energy wave conditions. The pattern of wave breaking in this photo suggests the presence of an irregular inner bar and a more regular outer bar. The lower photograph is a time-lapse image of the surf zone at the subsequent high tide, under essentially the same wave conditions. The time-lapse image highlights particularly well the presence of the irregular, possibly crescentic, inner bar. The presence of an outer bar is less obvious in the time lapse image.

The surf zone morphologies just described place NMB primarily within the rhythmic to lower dissipative end of the Australian model spectrum (Table 3.3). The variable bar and trough topographies of the Nine Mile Beach surf zone correspond to 'Longshore Bar and Trough' (LBT), 'Rhythmic Bar and Beach' (RBB), and 'Transverse Bar and Rip' (TBR) states of Wright and Short (1983, 1984). However, in comparison to Australian model surf zone morphologies, analogous NMB bar and trough topographies generally exhibit larger width scales.

SUBAERIAL BEACH MORPHOLOGY - Plan

Figure 3.3 presents representative plan sketches showing the different rhythm length classes together with a histogram giving their frequency of occurrence. Longshore spacings ranged from 60-1000m, with an average wavelength of 250-300 meters. Small surf cusps were the predominant rhythmic shoreline topography, occurring 76% of the time. Class A, B, and C surf cusps occurred 17%, 33%, and 26% of the time, respectively. Large surf cusps were present 15% of the time and swash cusps 9% of the time.

Rhythm amplitude on NMB ranged from weakly sinuous, with subdued horns and bays, through sinuous, with distinct horns and bays, to strongly sinuous shorelines expressed as transverse bars. Weaker sinuosity was associated with the larger rhythm classes. Only the smallest form length classes exhibited what could be termed transverse bars (high

Plate 3.2. Nine Mile Beach subaqueous surf zone morphology. -1) normal exposure (f16 @1/125), 2) time lapse exposure (f16 @~4min.).

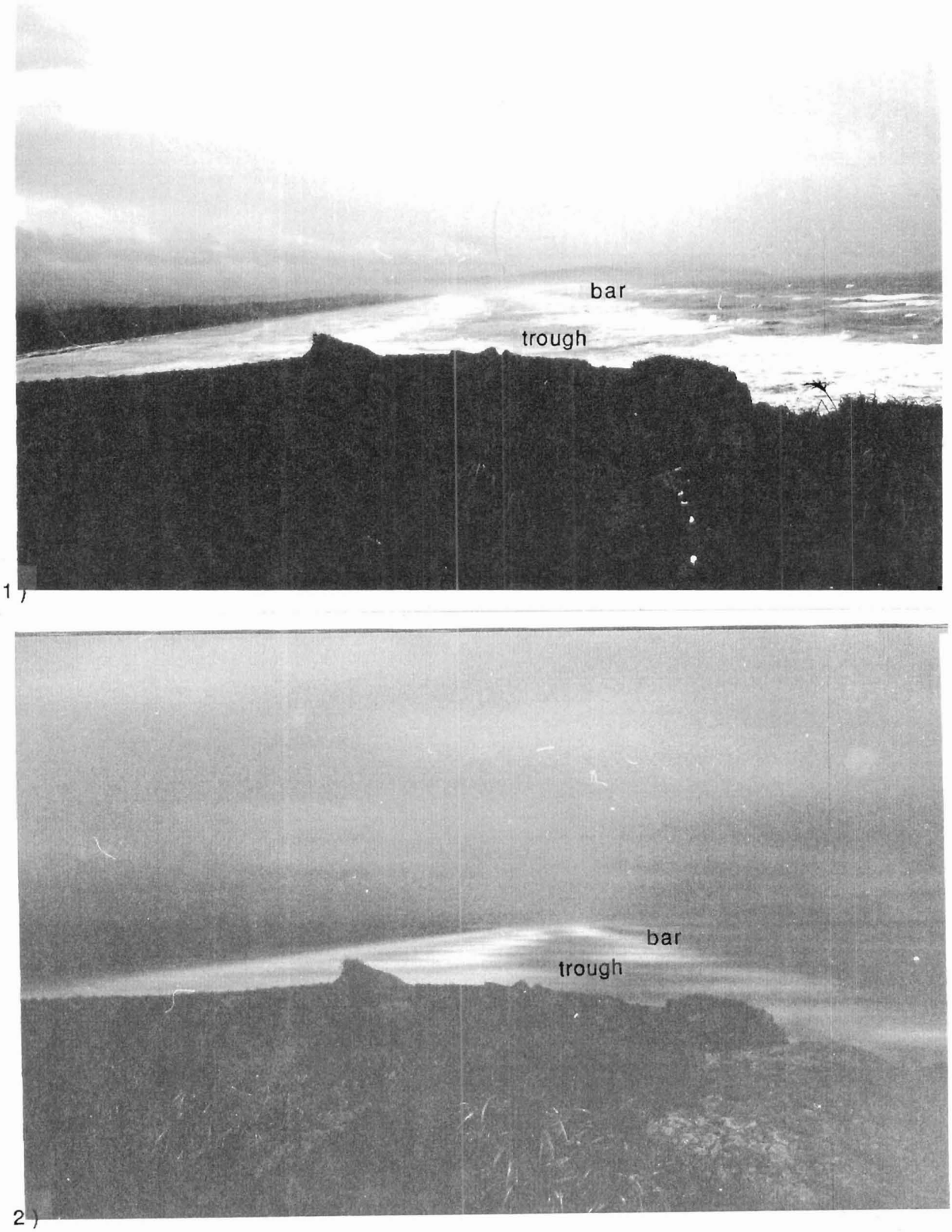

Plate 3.2. Nine Mile Beach subaqueous surf zone morphology. -1) normal exposure (f16 @1/125), 2) time lapse exposure (f16 @~4min.).

TABLE 3.3 AUSTRALIAN MODEL MORPHOLOGIC CRITERIA

STATE	Dissipative	Rhythmic	Reflective
SURF ZONE width	Wide ~500m (<1000-250m)	Intermediate ~150m (250-50m)	Narrow ~20m (<50m)
BARS number type	Multiple <2 "regular" linear, parallel +/-wide rips	Bar - trough 1-2 "irregular" crescentic - transverse	Barless 0 narrow rips and shoals
NINE MILE BEACH	◄———	———	———►
BEACH -plan Form -amplitude -spacing	Linear shoreline	Rhythmic shoreline (150-400m) weak | strong (500-200) | (200-100)	Linear-cusped shoreline
NINE MILE BEACH	◄———	———	———►
BEACH -profile slope width volume spatial variability	Gentle <2° Wide Small Uniform	Variable 2-4° Variable Variable Variable	Steep >4° Narrow Large Uniform
NINE MILE BEACH	◄———	———	———►

Arrows below sections indicate the range of occurrence of comparable Nine Mile Beach morphologies.

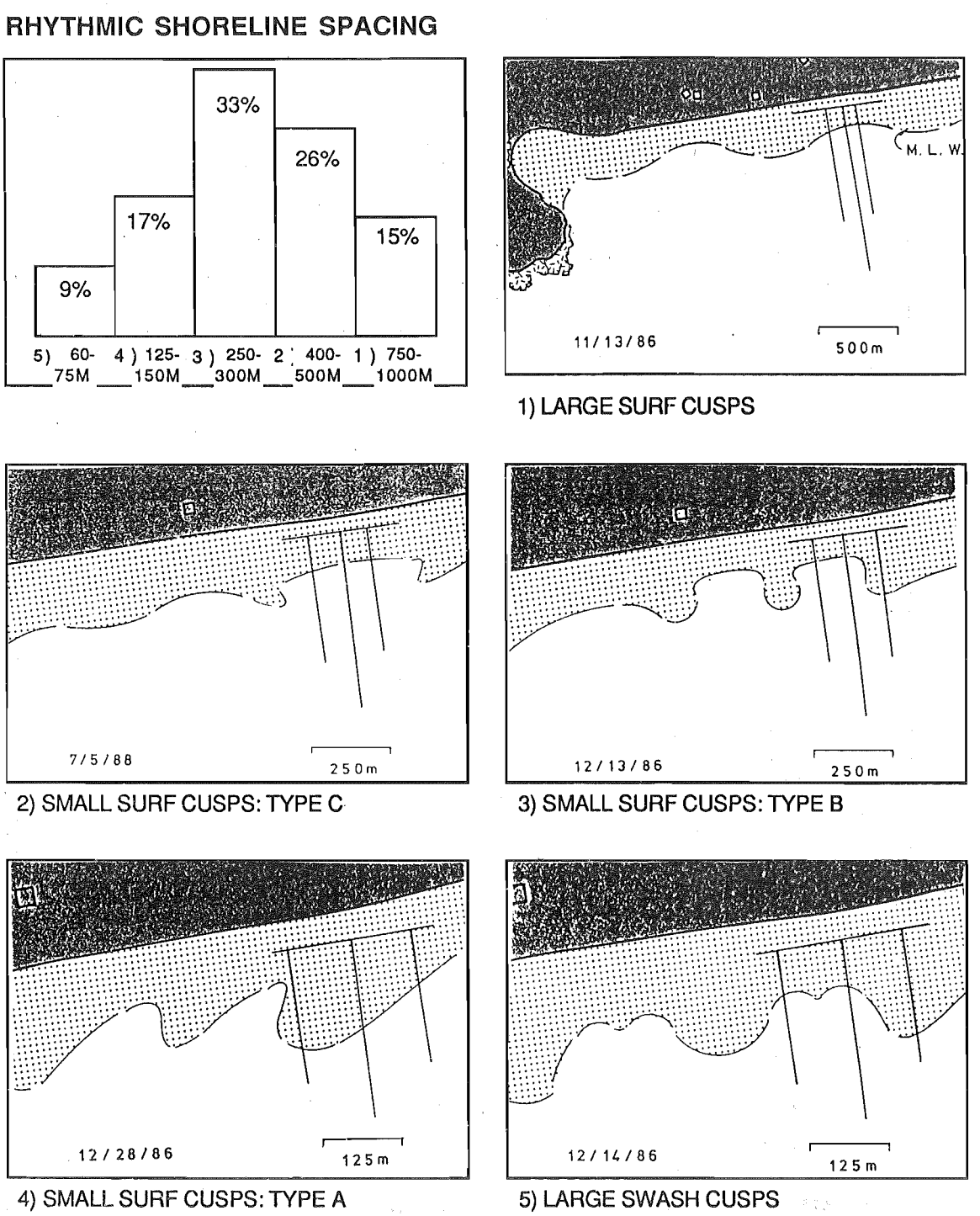

Figure 3.3. Representative plan sketches and frequency of occurrence of the rhythm classes observed at Nine Mile Beach.

amplitudes).

Figure 3.4 provides representative examples of nested and isolated rhythmic topographies, plus histograms showing the frequency of occurrence of rhythm classes associated with these topographies. Nested rhythms were common, while single forms occurred only 35% of the time. Vincent (1973) suggested that small surf cusps tend to occur in ensembles and larger surf cusps in isolation. At Nine Mile Beach the large surf cusps did occupy a relatively greater proportion of isolated rhythm occurrences than did the nested rhythm occurrences. However, in contrast to Vincent's observations, large surf cusps occurred as frequently in isolation as in nested sets. Also, although nested small surf cusps were the most common forms, the larger (class C) surf cusps dominated nested rhythm occurrences (39%), whereas the smaller (class B) surf cusps dominated isolated rhythm occurrences (40%).

Representative occurrences and size class histograms of skewed and normally oriented rhythmic topographies observed on Nine Mile Beach are given in Figure 3.5. Skewed shoreline rhythms were common (30%), but their occurrence was subordinate to that of the normally oriented shoreline rhythms (70%). When skewed rhythms were observed, they were associated with only the smallest rhythm classes. (i.e. All skewed rhythm occurrences were in class B and A surf cusps, and all class A surf cusps were skewed.) All asymmetries in rhythms showed deflections towards the north. In contrast to the fixed location of the normally oriented rhythmic forms, skewed forms generally migrated alongshore towards the north. A migration rate on the order of 5m/tidal cycle was obtained from contour maps and profiles made during two five day periods. The periods of longshore migration and skewed topography were specifically associated with a shift from class B to class A surf cusps.

Based on the description of rhythmic topographies given above, two end member rhythm types are recognized. Type 1 rhythms are nested, normally oriented, non-migratory class C small surf cusps: Type 2 rhythms are isolated, skewed, migratory class A small surf cusps. These two NMB rhythm types are comparable to the two rhythmic morphologies described by Wright and Short (1983,1984). Specifically, Type 1 rhythms correspond to the

NESTED RHYTHMS (65%)

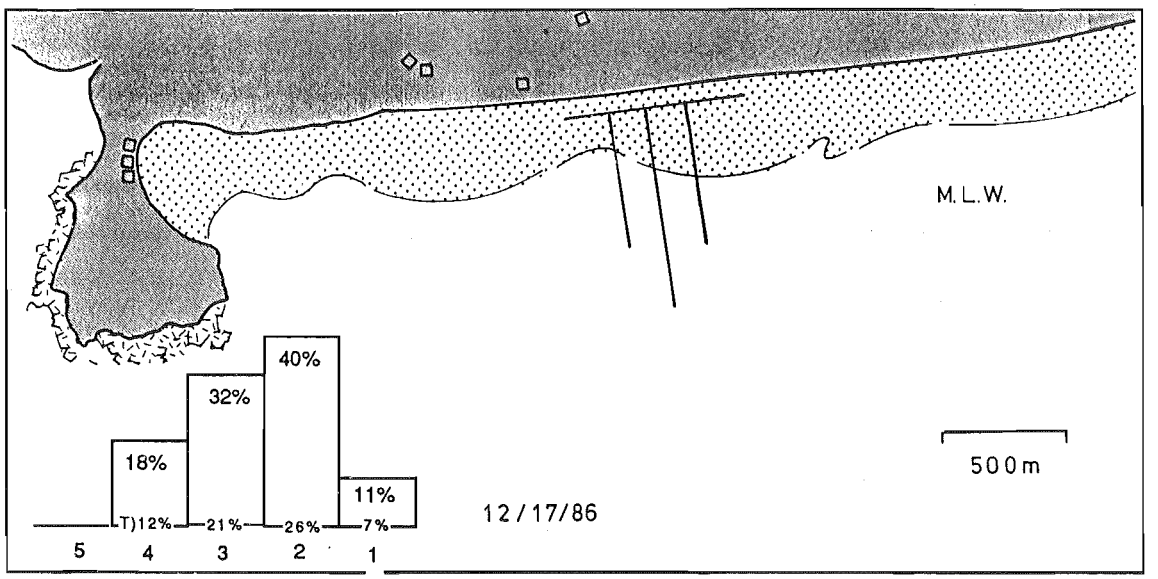

ISOLATED RHYTHMS (35%)

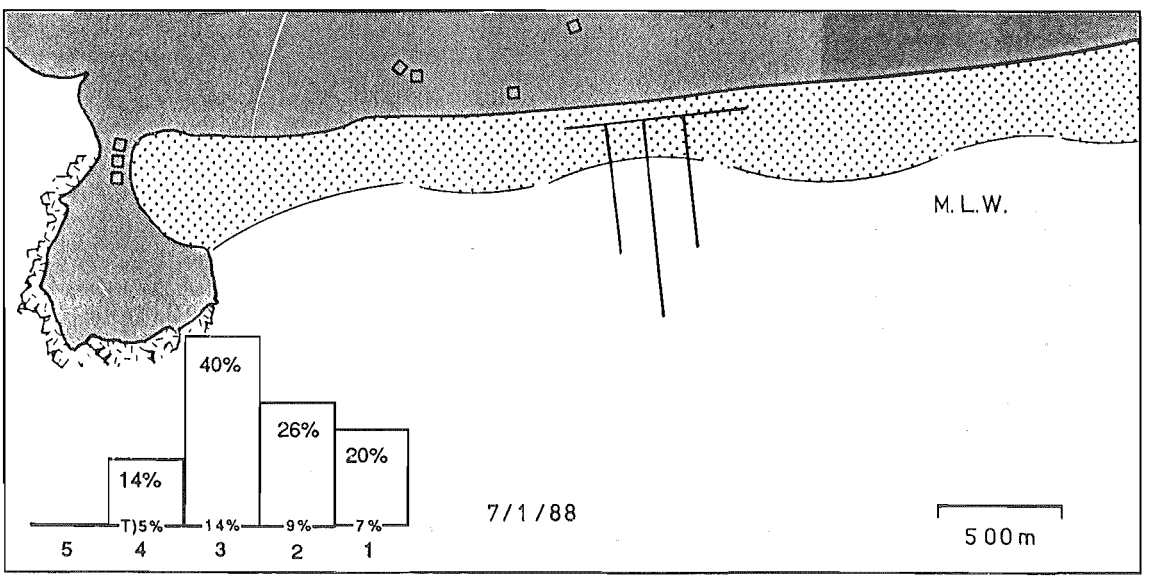

Figure 3.4. Representative examples of nested and isolated rhythms observed at Nine Mile Beach and the distribution of rhythm classes associated with these topographies.

NORMAL RHYTHMS (70%)

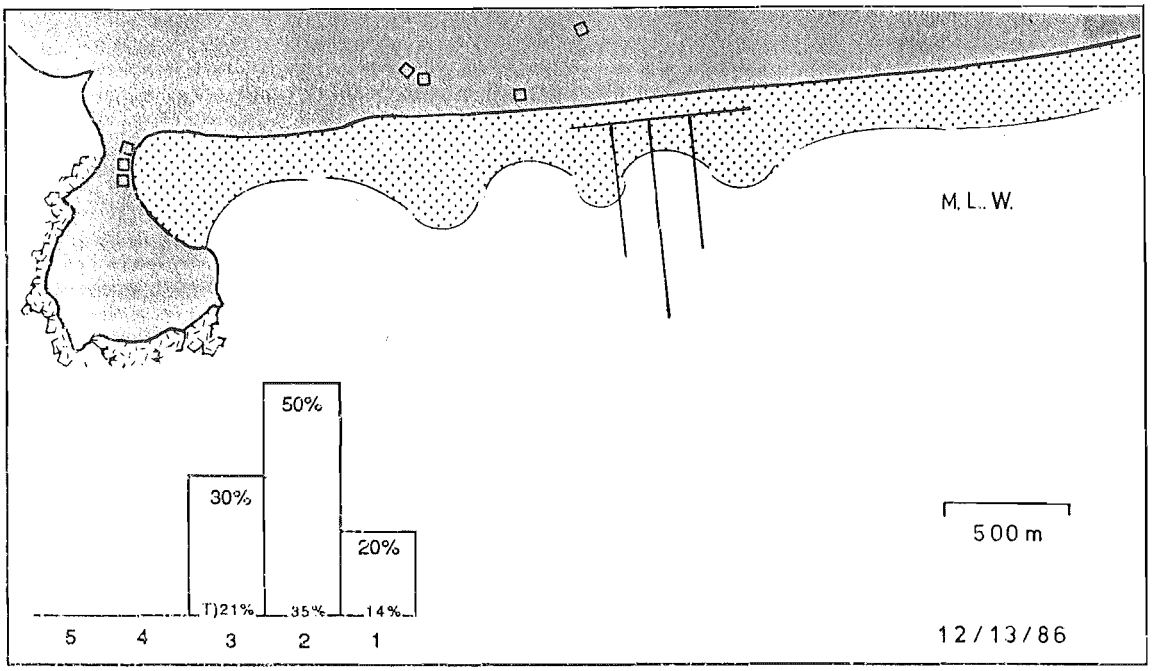

SKEWED RHYTHMS (30%)

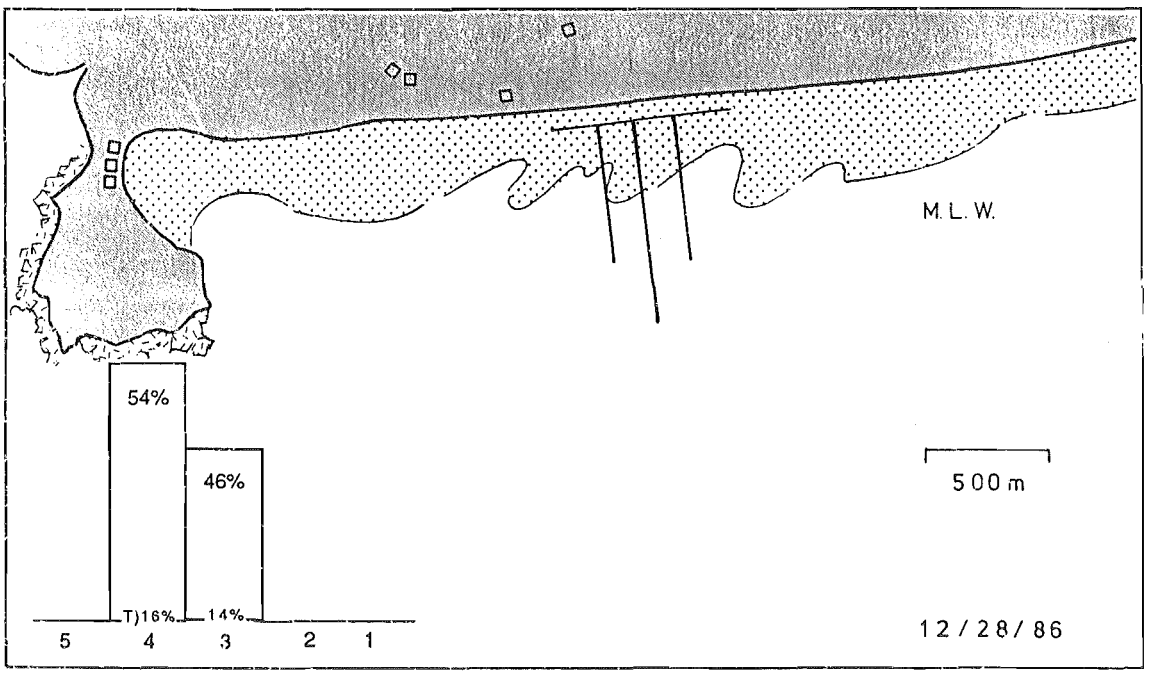

Figure 3.5. Representative examples of normal and skewed rhythms observed at Nine Mile Beach and the distribution of rhythm classes associated with these topographies.

'Rhythmic Bar and Beach' morphologies and Type 2 rhythms correspond to the 'Transverse Bar and Rip' morphologies of the Australian model (Table 3.3). However, the skewed forms that migrate alongshore (NMB Type 2 rhythms) are not a common feature of the Australian beach systems described by Wright and Short.

SUBAERIAL BEACH MORPHOLOGY - Profile

Representative NMB profiles and summary statistics of profile variation through time are presented in Figure 3.6.

The NMB foreshore can be described as wide and gently sloping. It averaged approximately 90m in width at mid-tide and commonly extended over 120m at low tide. Beach mobility and backshore mobility indices (defined in Chapter 2) for Nine Mile Beach are 6.2m and 14.4 respectively. The high-tide beach, averaged 44m in width, and was particularly stable, with a mobility index of 2.9m. Similarly, beach slopes varied little. Mid-tide beach slopes fall within the 1-2^{o} range, with a mean slope 1.36^{o}. High-tide slopes fall in the 2.0-2.5^{o} range, with an average slope of 2.3^{o}.

Although the absolute values are affected by the use of mean sea level as the datum (Chapter 2), in general NMB did posses a relatively small subaerial beach volume (115 m^3/m) and low subaerial volume exchange ($8m^3/m$). The total observed range in beach volume accounted for only about 25% of total subaerial beach volume. The profiles in Figure 3.6 suggest that the uppermost portion of the foreshore exhibits the least volume exchange. In contrast, the lower portion of the foreshore exhibits the most volume exchange. Thus, the beach width, slope, and volume exchange parameters all suggest that the subaerial beach is relatively stable.

The profile shape indices RBS and RBW (defined in Chapter 2) suggest that a relatively steep narrow high tide beach and a relatively flat wide mid-tide beach are the general case for Nine Mile Beach. However, within the narrow absolute range of beach slopes and widths, there was a relatively wide range of internal variability that represents the horns and bays described in the previous section on plan morphology. On average, the high-tide slope was steeper than the mid-tide slope (mean RBS = 1.75), but the high-tide

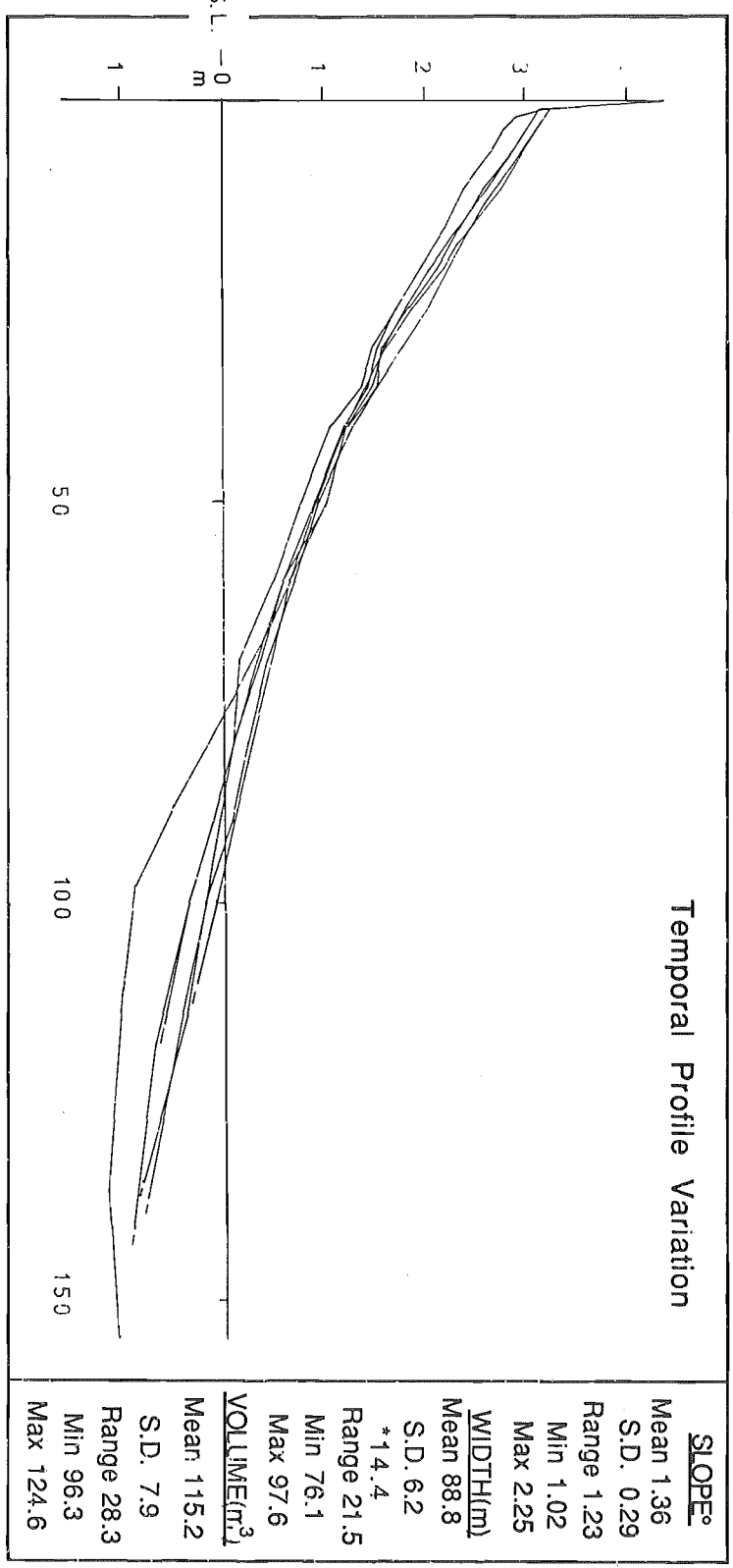

Figure 3.6. Summary statistics of temporal profile variation and representative profiles over time (*=backshore mobility index).

beach may be either flatter or steeper than the mid-tide beach (range RBS = 0.93-2.39). Also, the high-tide beach was generally narrower than the mid-tide beach (mean RBW = 2.02 ±0.03) but again, a wide range of width variability did occur (range RBW = 1.58-2.30).

At first glance NMB profiles appeared featureless in the field, but on closer inspection they exhibited subtle profile variations. These subtle profile shape variations represent long, low berms and swash bars. Specifically, the flat-topped berms were 15-30m wide and .05-.15m high. The swash bars were 30-60m wide and .05-.10m high, with relatively narrow, steep fronts, and shoreward migration rates on the order of 30m/day.

A representative set of profiles distributed alongshore and spatial profile variation summary statistics are presented in Figure 3.7. The spatial profile envelopes are qualitatively similar to the temporal profile envelopes described above (Figure 3.6). Profile size, shape, and variability are quantitatively comparable as well. Mean spatial versus temporal volume, width, and slope are 124:115m^3, 89:89m, and 1.67:1.36° respectively. Volume exchange and beach mobility indices show somewhat larger longshore variation, suggesting greater spatial profile variability. Thus, within the NMB system there was generally equivalent or less profile variation at one location over a period of days then there was in the longshore on any given day. This high spatial profile variability is an expression of the shoreline rhythmicity described earlier.

According to the Australian model criteria, the profile characteristics described above suggest that absolute profile morphologies on NMB are dissipative (Table 3.3). Wide, flat, stable profiles are associated with dissipative beach states (Wright and Short, 1983, 1984). However, if relative profile morphologies are considered, they strongly suggest that NMB profiles are characteristic of rhythmic states. This is in agreement with the plan morphologies described earlier. The tendency for spatial profile variation to be on the same order as temporal profile variation is a feature unique to rhythmic beach systems (Sonu, 1973; Short, 1981; Wright and Short, 1983, 1984). The high stability of the uppermost portion of the beach, and the relatively high mobility of the lowermost portion of the beach are also characteristics associated with rhythmic morphologic states (Short,

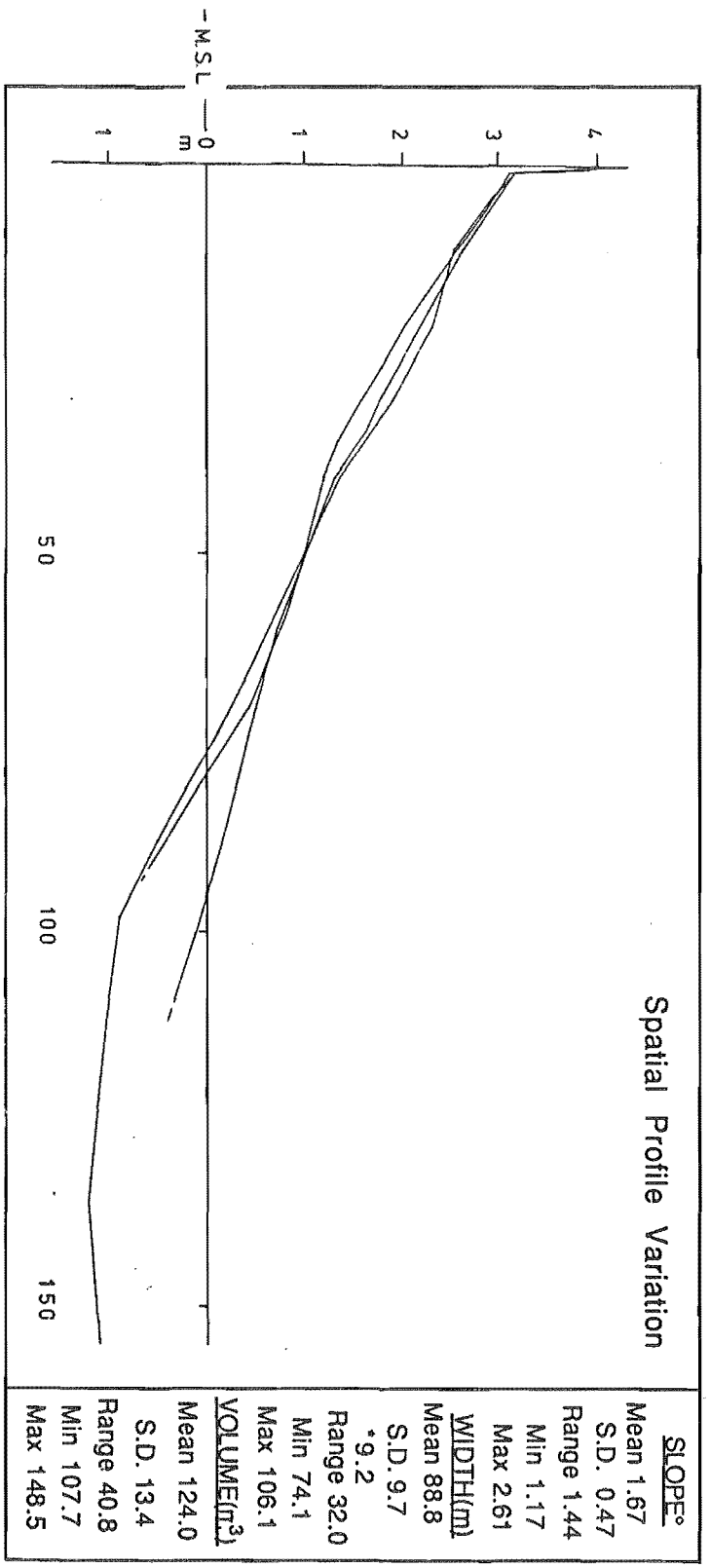

Figure 3.7. Summary statistics of spatial profile variation and representative profiles alongshore (*=backshore mobility index) Note: Although the spatial profile statistics are for a particular morphologic state, they are a good representation of spatial profile variation.

1981, Wright and Short, 1983, 1984, Wright et al., 1986). Finally, although markedly more subtle (longer and lower) in appearance than analogous features described within the literature, the swash bars and berms that occur on NMB are morphologic features generally not associated with dissipative morphologies (Wright and Short, 1983, 1984).

NINE MILE BEACH MORPHOLOGIC STATES

Based on the plan and profile observations presented above, four NMB morphologic states are identified. The morphologic criteria that distinguishes each state is described below and summarized in Table 3.4. The four morphologic states are schematically illustrated in Figure 3.8. The frequency of occurrence of the particular beach states - the NMB beach stage curve - is also given in this figure.

The **Low Tide Terrace** (LTT) state is characterized at high tide by a narrow, poorly developed surf zone (75m wide) with irregular skewed shoals. At low tide these shoals are expressed as a similarly irregular terrace that represents coalesced and in-filled smaller rhythms (i.e. small surf/large swash cusps (100-150m) of moderate amplitude). Possessing subtle berms and swash bars, the reflective profile is more convex in shape. It has a narrower, steeper sloping mid-beach, and a wider, gentler sloping upper beach. Profile volumes are relatively large, are moderately stable, and are relatively uniform alongshore. This reflective end member, which represents a 'fully accreted' beach state for the NMB system existed rarely, occurring only 4% of the time. This LTT state corresponds to the 'Low Tide Terrace' state of the Australian model.

The **Multiple Bar and Trough** (MBT) state exhibits a wide (750m), linear, multiple (2+) barred surf zone, with broad, widely spaced rip current channels. Large surf cusps (1000-500m) with bays that correspond to the locations of rip currents characterize shoreline morphology. The large surf cusps exhibit weak sinuosity, are not skewed, tend to occur in isolation, and are non-migratory. The dissipative profile is more concave in shape. It has a wider, gentler sloping mid-tide beach, with a narrower and steeper sloping upper beach. Profile volumes are relatively small, and exhibit little variation alongshore.

TABLE 3.4 NINE MILE BEACH MORPHOLOGIC CRITERIA

STATE	DISSIPATIVE	RHYTHMIC		REFLECTIVE
		RBB	STBR	
SURF ZONE width	Wide ~750m	Variable ~300m	~150m	Narrow ~75m
BARS number	Multiple 2+	Bar - trough 1-2		Single 1
type	"regular" linear, parallel with wide rips	"irregular" crescentic inner-linear outer bar	crescentic-transverse bar	"irregular" skewed shoals
BEACH -plan Form	Weak	Strong		Moderate
-amplitude	low amplitude	high amplitude		medium amplitude
-spacing	Large surf cusps (1000-500m)	Small surf cusps(500-100m) 500-200m	300-125m	Small surf cusps-large swash cusps (150-100m)
-symmetry	Normal Persistent	Normal Persistent	Skewed Migratory	Skewed
-nesting	Larger rhythms isolated	Strong nesting	Isolated	Nested-isolated
BEACH -profile	Concave	Variable		Convex
slope (upper/middle)	Steep/Gentle	Variable		Gentle/Steep
width	Narrow	Variable		Wide
volume	Small			Large
spatial variability	Uniform	Variable		Uniform

This dissipative end member, which represents a 'fully eroded' beach state for the NMB system, was common, occurring 26% of the time. This MBT state corresponds to 'Dissipative' and 'Longshore Bar and Trough' states of the Australian Model.

The **Rhythmic Bar and Beach** (RBB) state is characterized by a ~300m wide surf zone with a crescentic inner bar, that appears with or without an outer linear bar. Small

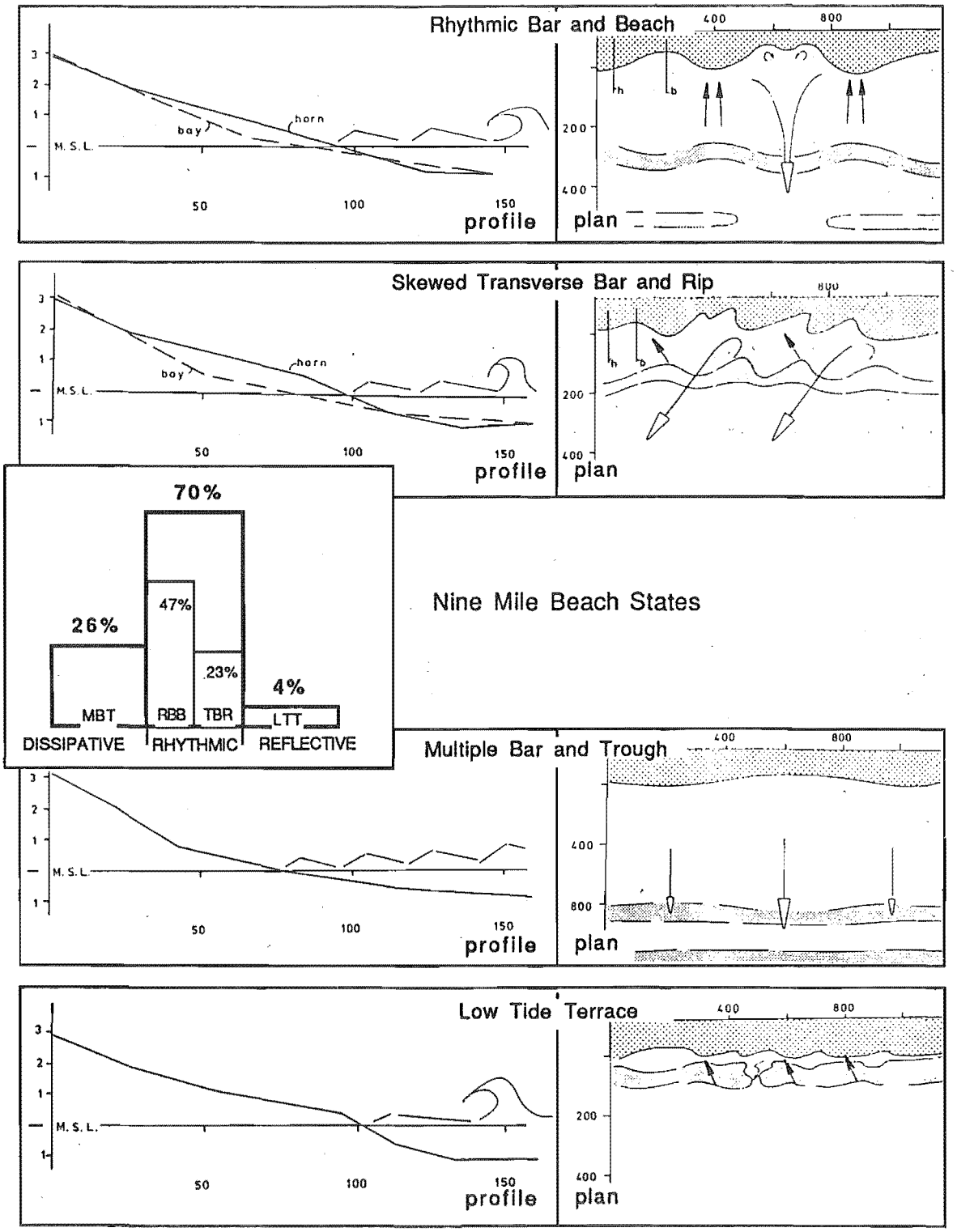

Figure 3.8. Plan and profile configurations of the four Nine Mile Beach states and the Nine Mile Beach beach stage curve. Arrows are inferred direction of sediment transport. All dimensions are in meters. (Note differences in plan scales.)

surf cusps occur in nested sets, have a 200-500m length range, and appear as well developed, normally oriented, horns and bays that tend to remain in a fixed location. Large swash cusps may be present in bays. Beach profiles are smaller in volume, gentler in slope, less spatially variable, and tend toward a more concave, 'eroded' shape
in this the more dissipative of the two rhythmic states.

The **Skewed Transverse Bar and Rip** (STBR) state is characterized by a ~150m wide surf zone with an attached crescentic-transverse inner bar. Small shoreline rhythms occur in isolation, have a 125-300m length range, are strongly sinuous and tend to migrate alongshore in the direction of littoral drift. Beach profiles are larger in volume, steeper in slope, more spatially variable, and tend toward a more convex, 'accreted' shape, in this the more reflective of the two rhythmic states.

These two rhythmic states (RBB,STBR) were the most common morphologic states observed on NMB, representing 70% of all occurrences. The Rhythmic Bar and Beach state was the modal beach state for NMB. This beach state, which corresponds to the 'Rhythmic Bar and Beach' state of the Australian Model, existed 47% of the time. The Skewed Transverse Bar and Rip state, which is comparable to the 'Transverse Bar and Rip' state of the Australian model, existed 23% of the time.

PATTERNS OF MORPHOLOGIC EVOLUTION OBSERVED ON NMB

In general the patterns of morphologic evolution observed at NMB, and described below, are comparable to the evolutionary sequence described for the Australian model by Short (1979, 1981) and Wright et al. (1979).

At NMB the Multiple Bar and Trough state develops 'over-night' from the previous state as sand moves offshore to the outer surf zone where a series of broad multiple linear bars are developed. Once established, the dissipative state is short lived, existing for only two to three days. This time period compares favorably with observations of Lippman and Holman (1990) who reported a mean residence time of 2 days for their high energy bar

morphologies.

The onset of the NMB down-state transition sequence is marked by the the movement of the inner bar, which becomes more irregular as it begins to migrate shoreward. The outer bar may migrate shoreward and develop weak rhythmicity, but is less dynamic than the inner bar. The inception of rip current cells corresponds with the appearance of subtle, widely spaced horns and bays on the subaerial beach. These changes represent the initial development of rhythmic topographies and mark the onset of a gradual progression through a sequence of rhythmic morphologies that develop in association with the onshore migration of sediment.

Sediment accumulation on the subaerial beach is initially confined to the horns, as swash bars move out of the inner surf zone and weld onto the foreshore. Seaward transport and erosion occur in the bays, which are normally oriented and relatively large in scale. Swash bars begin to move alongshore as well as onshore through the narrowing surf zone, and continue to weld onto the subaerial beach. As the horns widen due to the accumulation of sediment, rip spacing shifts down in size. The nested sets of the normally oriented, stationary, larger surf cusps of the Rhythmic Bar and Beach state give way to the isolated sets of the skewed, migratory smaller surf cusps of the Skewed Transverse Bar and Rip state. These changes characterize the latter stages of the NMB down-state evolutionary sequence. Although generally similar to the Australian model progression, it as it this latter stage that the principal differences between the NMB and Australian model progressions are manifest (i.e. skewing and migration of forms).

Finally, sediment moves onshore along the entire length of the beach and the small rip channels are filled as swash bars move into and up the bays. With the bulk of sediment transport now confined to the swash zone, the down state transition sequence culminates in the development of a continuous berm/terrace characteristic of the Low Tide Terrace state.

This ideal progression through the complete MBT-LTT down state evolutionary sequence occurred at NMB over a time period as short as 6-7 days. This is in contrast to Wright and Short (1984), who noted that the transition through the complete reflective to dissipative sequence in the Australian systems occurred over periods of weeks or even

months. This difference between NMB and the Australian beach systems, in the time required for a progression through a complete evolutionary sequence, may however simply be due to the fact that NMB moves through a narrower range of morphologies than do the Australian systems.

Although the complete evolutionary sequence was approached on two occasions during the study period at NMB, the progression from the MBT-LTT state was generally interrupted. Therefore, most morphologic change observed within the NMB system involved oscillations back and forth between the dissipative end member and/or the two rhythmic states.

'Internal' transitions between the two rhythmic states were the more common occurrence. The predominance of internal transitions accounts for the persistence of the rhythmic states at NMB for periods of 5-14 days. These values also compare favorably with those given by Lippman and Holman (1990), who reported a mean residence time of 11 days and a range of 5-16 days for their attached rhythmic bar morphologies.

Internal transitions involve the same morphologic changes as those described above for the intermediate phase of the complete transition sequence. The cutting back of horns and widening of bays takes place as the rip cells become more active movers of sediment offshore. Conversely, the welding of swash bars on to horns and the narrowing of bays occurs when sediment migrates onshore. Both the offshore and onshore migration of the inner bar accompanies these morphologic changes.

3.2.2 NINE MILE BEACH WAVE CLIMATE

WEATHER

Wind

Observations of surface wind direction and magnitude for the NMB area are summarized in Figure 3.9. Summary statistics from the Westport Harbour Board data set (see Chapter 2) are used in the following description of NMB area wind characteristics. Calm days

HARBOUR BOARD WIND DATA

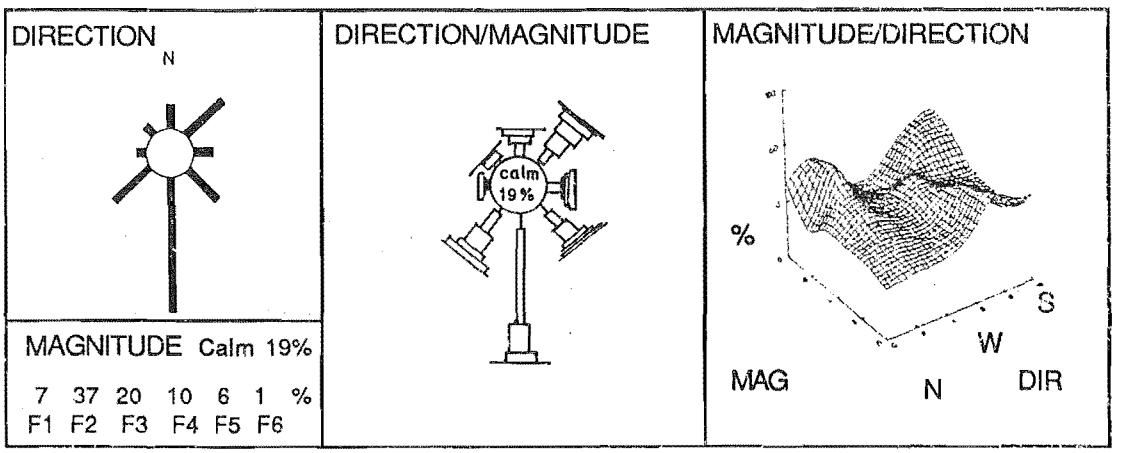

STUDY PERIOD WIND DATA

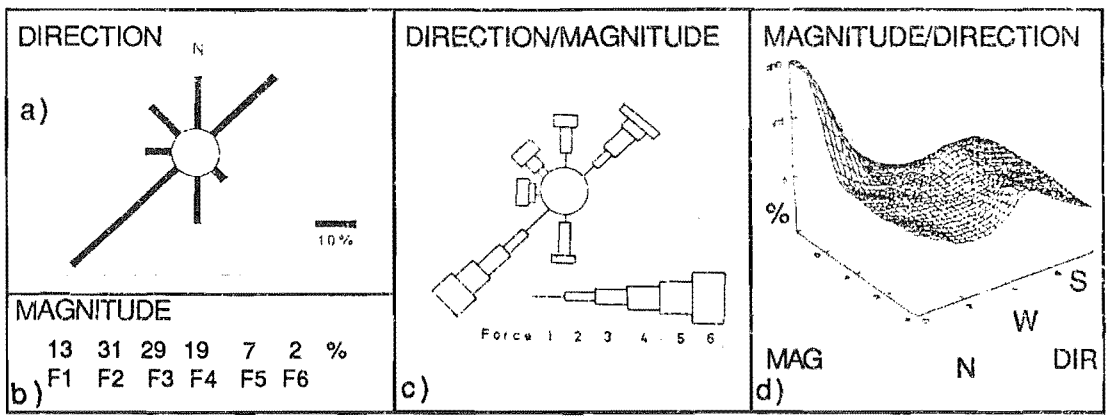

Figure 3.9. Summary statistics of surface wind direction and magnitude for the NMB area. Upper portion of the figure is Westport Harbour Board data, lower portion of the figure is Nine Mile Beach data. (a) Wind Direction Rose, b) Wind Speed Class Frequencies, c) Wind Direction/Magnitude Rose, d) Three-dimensional Plot of Wind Magnitude/Direction.)

accounted for 19%, modal wind speeds of 5 knots (Force 2) accounted for 37%, and wind speeds of ≤10 knots (Force 3) accounted for 83% of all observations. Winds ≥17 knots (Force 5), capable of generating waves larger than 1.5m in height, accounted for only 7% of all observations. The most frequent winds were south-southwesterlies (43%). However,

a secondary north-northeasterly component (17%) was also present. This bimodality in wind direction is more marked if magnitudes for individual directions are considered: for winds ≥17 knots southwesterlies comprised 36%, northeasterlies comprised 32%. Northeasterlies accounted for 60% of all occurrences ≥22 knots (Force 6).

These observations suggest that, in terms of wind direction and magnitude, three principal regimes exist within the NMB system: 1) Calm to low energy south-southwest winds - the most common, 2) high energy south-southwesterlies, 3) high energy northeasterlies. These conclusions are consistent with the few published reports of wind conditions that exist for this isolated section of coast (Reid, 1981; Reid and Collen, 1983; Valentine and Macky, 1984; Pfahlert, 1984).

Weather Patterns

A coherent picture of NMB weather patterns emerges when the wind observations are considered in conjunction with atmospheric circulation patterns. Valentine and Macky (1984) described elements of the atmospheric circulation around New Zealand; their classification was slightly modified after Davies (1973). Atmospheric circulation on the west coast of the South Island is characterized by sporadic 'local' depressions superimposed upon a continuous 'regional' pattern of east-northeast migrating anticyclones and front sequences. These circulation patterns are illustrated in synoptic weather charts representative of the study period (Figure 3.10).

The anticyclones and front sequences, which migrate east-northeast, are associated with the belt of prevailing westerlies and high energy storm centers located south of New Zealand (Pickrill and Mitchell, 1979). Davies (1973) refers to the 'Southern Storm Belt' as the "most important and clearly definable wave generating area in the world". This zone is characterized by extremely consistent high energy westerly winds. Davies suggests gale force winds occur there on the order of 20% of the time. Reid and Collen's (1983) observations in the southernmost New Zealand quadrant bear this out; gale force winds (Force 8) occur 16% of the time, mean wind speeds are 21 knots (Force 6).

In contrast to this regional pattern, depressions of local origin represent a combination

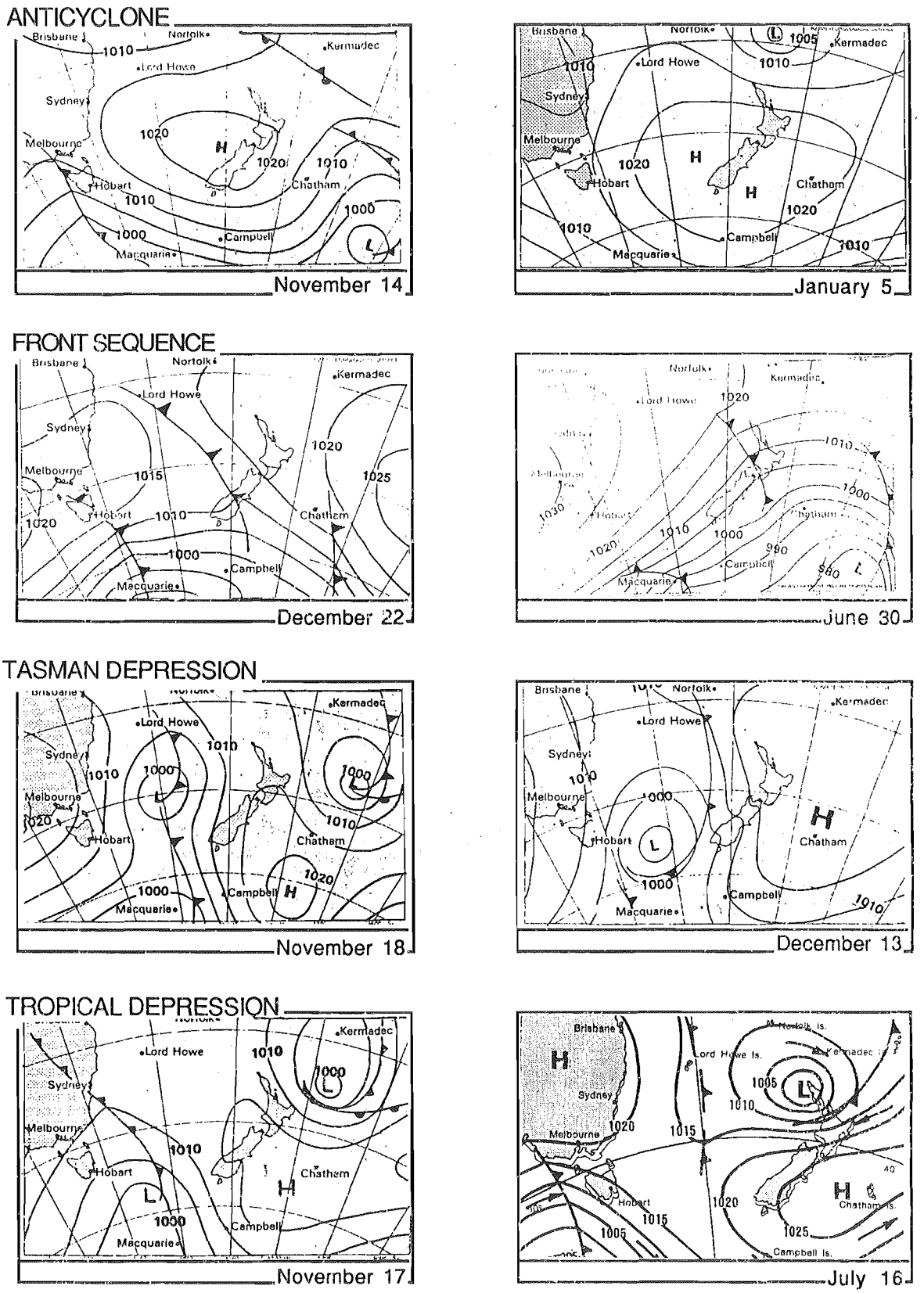

Figure 3.10. Synoptic weather charts illustrating the characteristic atmospheric circulation patterns of New Zealand area.

of those that develop within the Tasman Sea- 'Tasman depressions', and those that develop in tropical regions and migrate towards New Zealand- 'tropical cyclones' (Valentine and Macky, 1984).

The three NMB surface wind regimes noted earlier correlate with the atmospheric circulation elements described above. The high frequency south-southwesterly winds are associated with the passage of the anticyclone and front sequences. The calm to low energy south-southwest winds reflect the anti-clockwise-rotating high pressure systems. The high energy southwesterlies reflect the front sequences. The clockwise-spinning Tasman depressions and tropical cyclones generate the high energy northeasterly winds observed at NMB.

WAVES

Magnitude and Range

Incident wave conditions observed during the study periods at NMB (see Chapter 2) are summarized in Figure 3.11. Breaker heights ranged from 0.75 - 3.5m, with a mean breaker height of 1.75 m. Wave heights were highly variable; no markedly modal wave height was present. The majority (54%) were of moderate height (1.0m < H_b <2.5 m). The distribution is skewed towards lower wave heights, low waves (≤1.0m) comprised

---

Figure 3.11. Summary of incident wave conditions observed at NMB and elsewhere around the central west coast of New Zealand. NMB Shore based visual (sv) observations include breaking wave height (H_b), wave period (T_i), and wave approach direction. Pfahlert (1984) gives similar parameters. Reid and Collen (1983) give offshore ship-based visual (ov) records of significant wave height (H_s). Both Pickrill and Mitchell (1979) and Valentine and Macky (1984) give offshore instrumented (oi) records of significant wave height (H_s) and zero-upcrossing wave period (T_z). Unrefracted wave breaker height (given as H_b in each box) was calculated for each of these records using an empirical equation from Komar and Gaughan (1972). The dominant direction of wave approach reported by these workers is located in the lower right-hand corner of each box. Note that the arrows indicate an approximate location of the recording sites with respect to the study area. (OPPOSITE PAGE -->)

H_s (oi)	Mean 2.5m Range 1-3m	
T_z	6.7-8.3 sec	
H_b	2.2m	SW

Pickrill and Mitchell (1979)

H_s (ov)	Range 1-3m	
T_s	6-7 sec	
H_b	1.0-2.6m	W-SW

Reid and Collen (1983)

H_s (oi)	Mean 1.2/1.5m Range 0.5-4.5m	
T_z	7.5/9.0 sec	
H_b	1.3/1.7m	

Valentine and Macky (1984)

Nine Mile Beach Wave Climate

Wave Height (Hb)

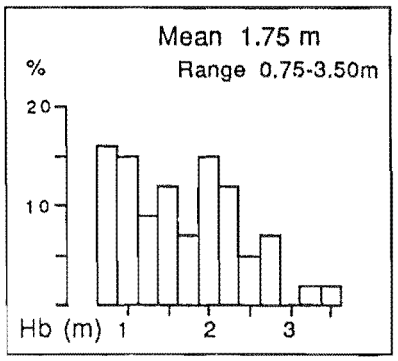

Wave Period (T)

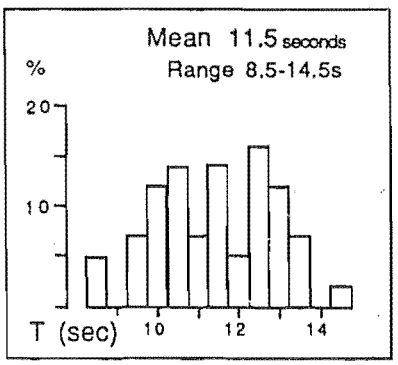

Wave Approach Direction

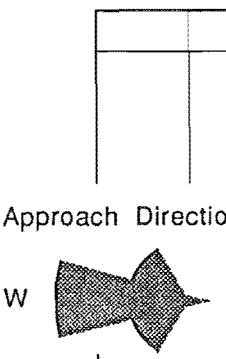

H_b (sv)	Mean 1.75m Range 0.25-4.25m	
T_s	Mean 10.5 sec Range 6-18s	W

Pfahelert (1984)

30% and high waves (≥2.5m) comprised 16% of the distribution.

Wave period ranged from 8.5s to 14.5s at NMB. The average wave period was 11.5 seconds. Incident wave period is distributed symmetrically; most waves fall within the 10-13s range (74%), and ≤10.5s and ≥12.5s periods each occupy 37% of the distribution.

It was noted in Chapter 2 that the published wave climate observations from elsewhere on the west coast are not ideal. Nonetheless, they do provide a basis for comparison. To facilitate such a comparison, wave statistics from the published records were converted to unrefracted breaking wave heights using an empirical equation given in Komar and Gaughan (1972). The results are summarized in Figure 3.11. Mean breaker heights are moderate (1.25-2.25m), although a wide range is reported (0.25-4.5m). The agreement between observed wave periods is not as good as that between wave heights, with wave periods ranging from 6-12 seconds. Considering inherent limitations, the wave data of other workers elsewhere on the west coast generally compare favorably with that obtained from Nine Mile Beach and suggest that NMB is part of a relatively well defined central west coast wave climate

Direction of Wave Approach and Longshore Currents

Most (56%) waves were observed to approach normal to the shore (Figure 3.11). However, slightly oblique approach angles from both the southwest and northwest were also common and were equally as likely to occur (21% and 23% respectively). Considering the dominance of southwesterly winds in the area, southwesterly approach angles would be expected to be more common at NMB. West-southwest is the dominant approach direction in the published reports given in Figure 3.11. This discrepancy may be attributable in part to strong refraction across the wide shelf, and in part to the difficulty in making an accurate determination of approach direction using visual observations (see Chapter 2).

Qualitative observations of littoral drift, and the drift alignment of morphologic features suggest a northerly littoral drift in the NMB area. This is confirmed by local residents. Also, of the nine acceptable measurements of longshore currents at NMB made during this

study (see Chapter 2), flow was to the north on all but one occasion. The three best measurements, obtained from dye traces on days of low to moderate wave height, gave north-flowing surface current velocities of 10cm/s, 27cm/s, and 40cm/s.

The few observations that have been made previously suggest that north-flowing longshore currents are a significant component of nearshore circulation within the NMB system. As early as 1947, Furkert estimated rates of longshore drift for the Westport area and noted that a strong north moving drift affects the whole coastline. Recently, Lumsden, Kirk, and Hastie (1985) produced refraction diagrams for the Westport area in order to estimate rates of longshore drift. Their calculated net transport to the east (at rate of 1.1×10^6 m3/yr) for the Westport area would correspond to northward drift at NMB. Pfahlert (1984) used surface floats and determined a northerly versus southerly flowing current direction ratio of 2:1. This ratio is effectively identical to the swell approach ratio reported by Reid and Collen (1983) and used by Lumsden et al. (1985) in their drift calculations.

WAVE CLIMATE COMPONENTS

An improved understanding of the NMB wave climate is obtained by considering the characteristics of natural wave trains. According to Thompson (1972), the typical property of swell generated by storms is the continuous decrease of period with time from the initial appearance of long periods. This decrease in wave period is commonly accompanied by an increase in wave height. In contrast to distant swell, local waves are characterized by the initial appearance of short periods, which increase with time as the sea grows until the wave height peak is reached (Thompson, 1972). Following the passage of the peak waves, the wave period values decrease with time and become more swell-like in appearance.

Thompson (1972) presented a method to calculate the distance (Do) and time of origin for a swell train from the time rate of change of wave frequency using the equation

$$Do = \frac{1.515}{df/dt} \qquad (3.3)$$

where Do is in nautical miles (NM), f is wave frequency in Hertz, and t is time in hours. The slope of a wave period time series line (converted to frequency) thus reflects the distance from the wave-generating area. Lower slopes correspond to more distant source areas.

Assuming that the visually recorded wave period is comparable to the peak spectral period, and prominent maxima in the spectra represent individual wave trains, then wave period patterns represent individual wave trains, each generated by a synoptic weather event (Thompson, 1972, Siemelink, 1984). Based on this assumption, wave height and wave period time series were used to distinguish 'local waves' from 'swell' wave trains (Figure 3.12). Approximate source distances, calculated for the swell trains from equation 3.3, were used to segregate 'local' as opposed to 'regional' swell. Synoptic weather charts and winds observed at the study site were examined in conjunction with these wave records. Consistent patterns emerged from this analysis, and three components of the NMB wave climate were recognized; 1) Regional swell, 2) Local swell, and 3) Local waves. Each wave climate component is an expression of the weather patterns in terms of wave train characteristics. The classification and the frequency of occurrence of the three NMB wave climate components is described below and summarized in Table 3.5.

Regional swell is the dominant component of the NMB wave climate (60%). Characterized by a relatively gradual decrease in wave period over time, it travels distances greater than ~1500 nautical miles (generally on the order 3500NM) to the recording site, and is associated with the occurrence of southwesterly winds. The weather patterns and apparent distance of travel suggest that this component originates in the 'Southern Storm Belt'. On average, this component accounts for the longer period, and both the highest and lowest waves observed at the beach. Most wave heights greater than 2.0 m (93%) and wave periods of 12 seconds or longer (79%) are associated with this

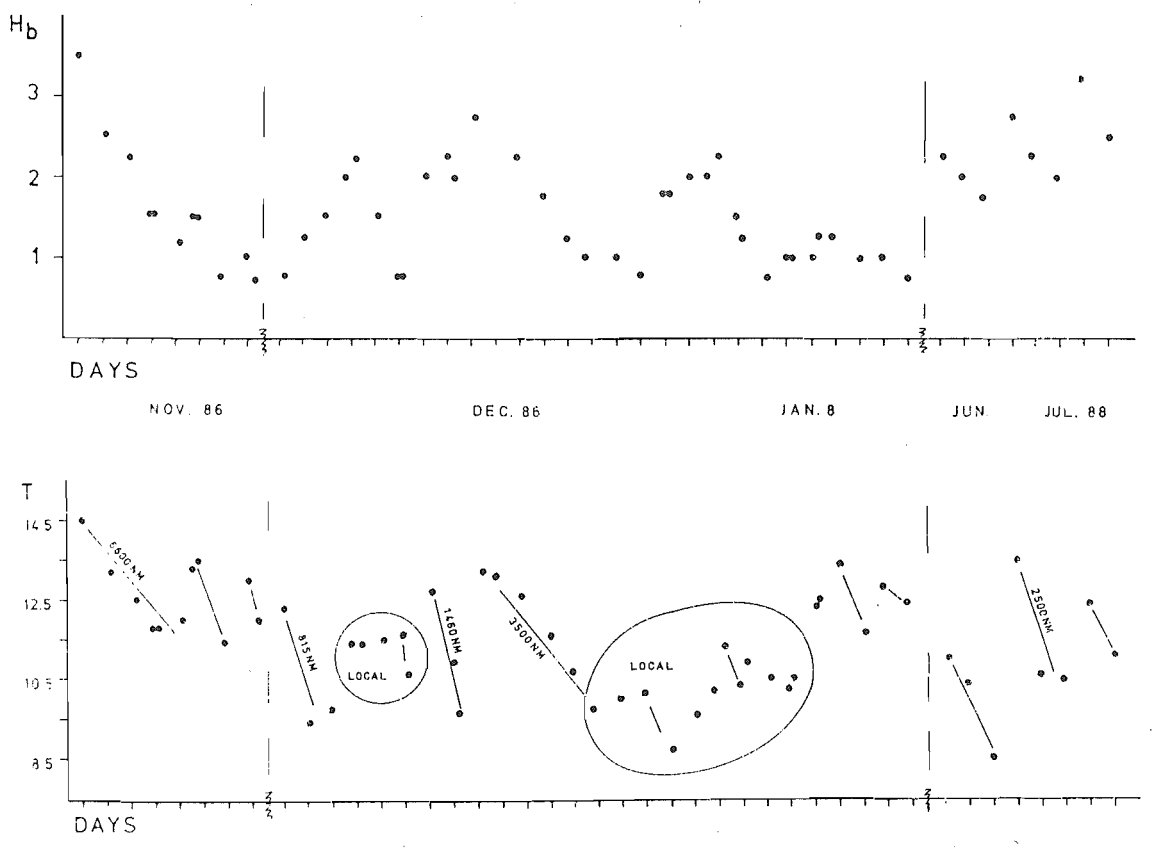

Figure 3.12. Time-series of wave height and wave period observed during the study periods at NMB. Upper figure is wave breaker height (H_b), lower figure wave period (T_j). In the lower figure, wave trains have been identified and classified as 'swell' or 'local' waves using criteria outlined by Thompson (1972; See text for details). On swell wave trains calculated source distances are given in nautical miles.

component. Also, it is the obliquely incident waves associated with this wave climate component that are responsible for generation of the north-flowing longshore currents that are an important element of nearshore circulation in the NMB system.

Local swell is a relatively minor component within the NMB wave climate (12%). It is characterized by travel distances less than ~1500NM; generally on the order of 1000 nautical miles. This component is associated with northerly winds. These properties suggest that this component originates from storms that occur within outer portions of

TABLE 3.5 NINE MILE BEACH WAVE CLIMATE COMPONENTS

"REGIONAL" SWELL	"LOCAL" SWELL	LOCAL WAVES
60%	12%	28%
Distance ~3500NM 7000-1500NM	Distance ~1000NM >1500-500NM	Distance On Site
Direction Southwesterly	Direction Northerly	Direction North-->South
Source Southern Storm Belt	Source Tasman and Tropical Cyclones	Source Tasman and Tropical Cyclones
Waves	Waves	Waves
Mean Height 2.0m Range 3.5-0.75m	Mean Height 1.5m Range 2.25-0.75m	Mean Height1.5m Range 2.0-0.75m
Mean Period 12.0s Range 14.5-8.5seconds	Mean Period 11.5s Range 13.0-9.5seconds	Mean Period 10.5s Range 11.5-8.5seconds
Mean Steepness 0.0014 Range .0005-.0025	Mean Steepness 0.0011 Range .0005-.0019	Mean Steepness 0.0014 Range .0006-.0024

the Tasman Sea in association with tropical and possibly Tasman depressions. Moderate wave heights and intermediate wave periods characterize the local swell component.

Local waves are a significant component of the NMB wave climate, not only in terms of frequency of occurrence (28%), but in terms of potential influence upon morphology. This component exhibits distinct wave period patterns through time, ideally characterized by the occurrence of short wave periods that build and then slowly taper-off. This pattern is accompanied by a progressive shift in local winds from northerly to southerly directions, suggesting that this component originates from Tasman and tropical depressions that occur close to the recording site and impinge upon the New Zealand land mass. On average, these local waves are of moderate height and relatively short period, exhibiting wave

steepness values that are equivalent to those of the high waves of the distant swell component.

3.2.3 NINE MILE BEACH DYNAMIC SIMILARITY

BREAKER HEIGHT (H_b)

Within the NMB system, mean wave heights (1.75m) correspond to modal rhythmic morphologies (Table 3.6a). Mean wave heights for the individual morphologic states are 2.75m for the dissipative (MBT) state, 1.5m for the rhythmic states, and 0.75m for the reflective (LTT) state. The individual RBB and STBR morphologic states correspond to mean wave heights of 1.5m and 1.0m respectively.

Based on the correspondence between mean wave heights and the individual beach states, and the spread of the wave height distributions associated with each state, breaker height threshold values are assigned. Dissipative morphologies exist in conjunction with waves $\geq$ 2.25m; reflective morphologies with wave heights below 1.0m. When the beach is rhythmic, wave heights between 1.0 and 2.0m are most common. These NMB breaker height threshold values are in close agreement with the threshold values reported by Short (1981; Table 3.6a).

Wave heights associated with the rhythmic states occur over a range that crosses the ideal threshold boundaries (Figure 3.13a). This overlap is most marked for the 'rhythmic-reflective end member' threshold. As a result, although all reflective morphologies are associated with low wave heights, the percentage correspondence is low (14%; Table 3.7). The poor correspondence is further illustrated in the frequency distributions of morphologic state and wave height: Wave heights occur evenly over a broad range. However, beach morphologies tend to remain within a relatively narrow range in terms of the possible spectrum of morphologies - the distribution being skewed toward the occurrence of the more dissipative morphologies.

In contrast, the 'rhythmic-dissipative end member' threshold exhibits strong segregation

of beach type on the basis of wave height, and the correspondence between existing wave height and beach state is high. The dissipative end member occurs 92% of the time when wave height is ≥ 2.25m. When wave height falls below this value, rhythmic morphologies exist 91% of the time if the lower threshold is neglected altogether.

With respect to segregation of the two rhythmic morphologies (RBB and STBR), the wave height distribution of the two rhythmic states does appear weakly bimodal, and a threshold wave height of ~1.25m could be considered. Using this value, the RBB state exists on all occasions if wave height is between 1.25 and 2.25 meters (Figure 3.13a). However, the STBR state exists only 60% of the time when wave height falls below the 1.25m wave height threshold value. Thus, as was the case above for the 'rhythmic-reflective end member' threshold, correspondence to beach state is worse for lower wave heights.

THE SURF SCALING PARAMETER (ε_b)

Reflective and dissipative end member morphologies show good segregation on the basis of surf scaling parameter values (Table 3.6b). Within a wide range of ε_b values (7.5-128.8), mean ε_b for the dissipative state is 54, the reflective state 23. Also, the standard deviation of ε_b values for the end member states is low. A threshold value of ε_b=~30 segregates the two end member NMB states.

TABLE 3.6. SUMMARY STATISTICS AND CORRESPONDING EXISTENCE FIELDS DIAGRAM OF THE DYNAMIC SIMILARITY PARAMETERS FOR BEACH STATES In existence fields diagrams the horizontal arrows indicate standard deviation of distributions; x, o represent the mean values. Vertical lines indicate proposed thresholds. (a) Wave breaker height (H_b) - Existence fields and thresholds of Short (1981) are presented in the lower diagram b)Surf scaling parameter (ε_b) - Existence fields and thresholds of - Wright et al. (1979) are presented in the lower diagram; c) Dean parameter (Ω) - Existence fields and thresholds of Wright et al. (1985) are presented in the lower diagram. (OPPOSITE PAGE --->)

a) H_b (m)

STATE	n	Mean	S.D.	Range
DISS	11	2.75	0.4	2.25-3.50
RHY	30	1.50	0.5	0.75-2.25
rbb	20	1.50	0.4	0.75-2.25
tbr	10	1.00	0.2	0.75-1.25
REF	2	0.75	0.2	0.75-1.00
Total	43	1.75	0.75	0.75-3.50

b) ε_b

STATE	n	Mean	S.D.	Range
DISS	5	53.7	5.4	46.1-59.8
RHY	21	44.6	27.9	7.5-128.7
rbb	12	55.1	31.1	28.2-128.7
tbr	9	30.7	15.4	7.5-59.6
REF	2	22.7	5.0	19.2-26.3
Total	28	44.7	25.2	7.5-128.7

c) Ω

STATE	n	Mean	S.D.	Range
DISS	11	7.85	0.94	6.66-9.78
RHY	30	4.81	1.87	2.15-7.77
rbb	20	5.60	1.75	2.15-7.77
tbr	10	3.23	0.79	2.28-4.96
REF	2	2.59	0.47	2.26-2.92
Total	43	5.48	2.20	2.15-9.78

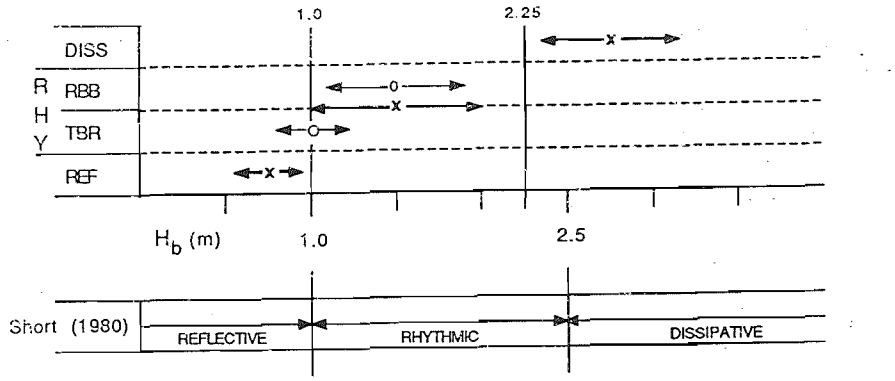

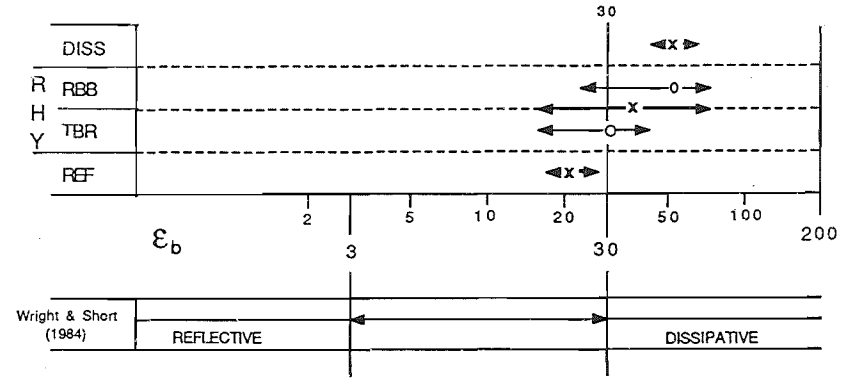

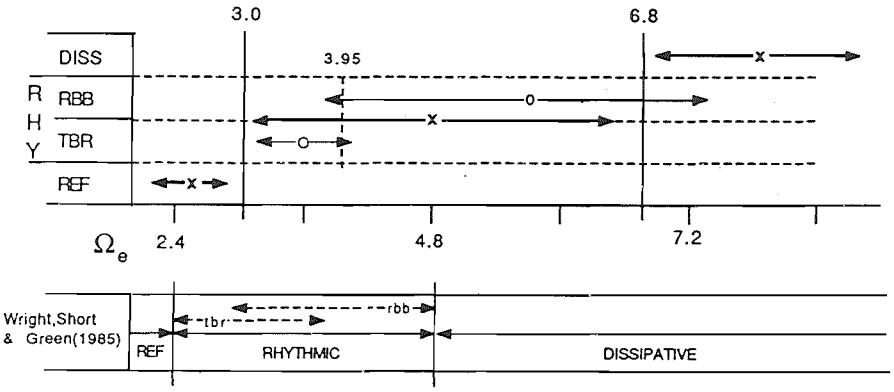

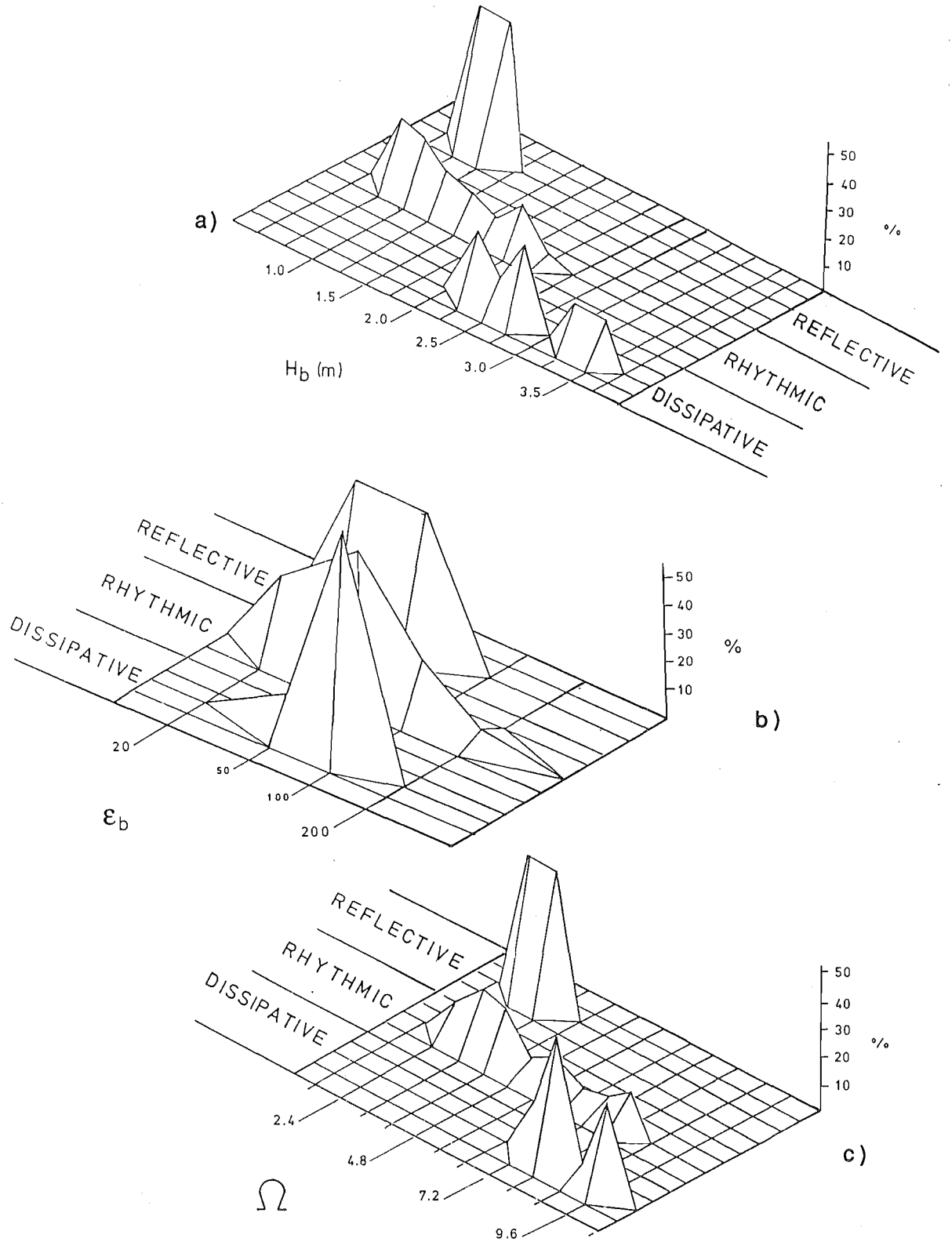

Figure 3.13. Frequency distributions of the various dynamic similarity parameters for each morphologic state. (a) distributions of wave breaker height; b) distributions of surf scaling parameter (ε_b); c) distributions of Dean parameter (Ω).

TABLE 3.7. PAIRED BEACH STATE HISTOGRAM / DYNAMIC SIMILARITY PARAMETER DISTRIBUTION AND PERCENT CORRESPONDENCE BETWEEN BEACH STATE AND DYNAMIC SIMILARITY PARAMETER THRESHOLD VALUES.

SIMILARITY PARAMETER	BEACH STATE: MBT	RHYTHMIC: RBB	RHYTHMIC: STBR	LTT
WAVE HEIGHT(H_b)				
≥2.25m	92%		8%	0%
1.0 - 2.5m	0%		96%	4%
<1.0m	0%		86%	14%
1.25-2.0m		100%	0%	
1.0-1.25m		30%	60%	10%
SURF SCALING(ε_b)				
> 30	75%		25%	
< 30	14%		86%	
DEAN(Ω)				
> 6.8	56%		44%	0%
3.0 - 6.8	0%		100%	0%
< 3.0	0%		75%	25%
3.95-6.8	17%	75%	8%	
3.0-3.95		29%	71%	

Surf similarity parameter values for the rhythmic states cover the entire range of values (Figure 3.13b). Thus the surf scaling parameter is a poor discriminator of rhythmic morphologies. However, the ε_b=~30 value does provide a reasonable segregation between the two rhythmic morphologies. By using the ε_b=30 threshold, and pairing the individual rhythmic morphologies with their respective reflective and dissipative end member morphologies, the 'dissipative pair' is found to occur 75% of the time when ε_b is greater than 30 and the 'reflective pair' to occur 86% of the time when ε_b is less than 30 (Table 3.7).

The ε_b=30 threshold value used here does agree with the upper bounds of Wright and Short's (1983, 1984) dissipative-reflective ε threshold values (Table 3.6b). However, in comparison to the Australian model values, for similar morphologic states the average surf scaling parameter values are high at NMB (Mean ε_b=45). According to the Australian model, the bulk (75%) of ε_b values on NMB correspond to dissipative morphologies.

THE DEAN PARAMETER (Ω)

In terms of the individual NMB states, there is good segregation on the basis of both the mean and standard deviation of Ω values (Table 3.6c). The dissipative state corresponds to Ω values in excess of ~6.8, the mean value being 7.85. Rhythmic states are associated with Ω values between ~3.0 and ~6.8 and a mean value of 4.81. The reflective state corresponds to Ω values below ~3.0, the mean value being 2.59. For the individual rhythmic states, mean values of the Dean parameter are 5.60 for the RBB state and 3.23 for the STBR state. A value of Ω=~3.95 segregates these two states.

As has been pointed out previously for the other two similarity parameters under consideration, Dean parameter values associated with the rhythmic states occur over a range that crosses the ideal threshold boundaries (Figure 3.13c). As a result, using immediate Ω values imposes similar constraints on predictability. The reflective state occurs only 25% of the time when Ω falls below ~3.0 (Table 3.7). The dissipative state

occurs 56% of the time when Ω exceeds ~6.8. However, rhythmic states occur on all occasions when the Dean parameter falls between these values, and 88% of the time when it falls below the upper threshold. Also, the RBB and STBR states are correctly predicted 75% and 71% of the time respectively on the basis of the rhythmic threshold value of Ω=~3.95.

In general the Dean parameter values associated with the particular morphologic states are high (Mean=5.5) in comparison to those reported in Wright et al. (1985) (Table 3.6c). However, while the values associated with the more dissipative morphologies are high, the Ω values associated with the more reflective morphologies are in close agreement with Australian model values. Still, as was the case with ε_b, the use of the Australian model Ω values would in general over-predict the occurrence of dissipative morphologies.

3.3 INTERPRETATION AND DISCUSSION: NMB NEARSHORE DYNAMICS

In the following section, the NMB beach state morphologies are related to the NMB wave climate components, based on the correspondence between beach state morphology and the similarity parameters. The combined NMB morphology-wave climate associations described below and summarized in Table 3.8 represent the framework of the NMB nearshore/macrodynamic model. Additional aspects of this model are outlined in the ensuing sections.

NINE MILE BEACH MORPHODYNAMIC STATES

The Low Tide Terrace (LTT) state. The narrow irregular surf zone and shoreline that characterize reflective end member morphologies within the NMB system existed only in conjunction with the lowest wave heights. A further requirement of low wave steepness for this state is suggested by low Dean parameter values (< 3.0). Also, surf scaling parameter values (ε_b) were consistently below 30 for the LTT state.

TABLE 3.8 THE NINE MILE BEACH MACRODYNAMIC MODEL

BEACH STATE	MORPHOLOGY	DYNAMIC SIMILARITY	PROCESSES
DISSIPATIVE	MULTIPLE BAR AND TROUGH	$\varepsilon_b > 30$ $\Omega > 6.8$	$H_b \geq 2.25m$ Southwesterly Regional Swell
RHYTHMIC	RHYTHMIC BAR AND BEACH	$\Omega = 3.95 - 6.8$	MIXED ?Local Waves?
		$\Omega - = 3.0 - 6.8$	$H_b = 1.0\text{-}2.25m$
	SKEWED TRANSVERSE BAR AND RIP	$\Omega = 3.0 - 3.95$	?Southwesterly Regional Swell? MIXED
REFLECTIVE	LOW TIDE TERRACE	$\varepsilon_b < 30$ $\Omega < 3.0$	$H_b < 1.00m$ Southwesterly Regional Swell

The low wave heights and, in particular, long periods needed to produce the low steepness values associated with the reflective end member rule out a local wave origin for this state. The low wave heights and periods, together with the tendency for morphologies to be skewed in the direction of northerly drift, suggest a low energy regional or local southwesterly swell origin for this state. That this state was observed to have existed only during conditions of southwesterly regional swell (Table 3.9), suggests that it is principally this wave climate component that develops the Low Tide Terrace state observed on NMB.

TABLE 3.9 COUNT OF BEACH MORPHOLOGIES THAT EXISTED IN CONJUNCTION WITH THE WAVE CLIMATE COMPONENTS.

WAVE CLIMATE COMPONENT	BEACH STATE			
	MBT	RBB	TBR	LTT
REGIONAL SWELL	11	10	3	2
LOCAL SWELL		3	2	
LOCAL WAVES		7	5	

The Multiple Bar and Trough (MBT) state. The wide, multiple barred surf zone and wide, weakly sinuous subaerial beach that characterize dissipative end member morphologies within NMB system occurred only during periods of high waves: Wave heights greater than or equal 2.25m consistently existed with this state. As a result, ε_b was always greater than 30, and Ω was consistently above 6.8.

The high waves, apparently required to develop dissipative morphologies, preclude all but high energy regional southwesterly swell conditions in the formation of this state. That the MBT state was observed to have existed only during conditions of southwesterly regional swell, supports this suggestion (Table 3.9) .

The Rhythmic Bar and Beach (RBB), and Skewed Transverse Bar and Rip (STBR) states. The irregular barred surf zone and sinuous subaerial beach characteristic of the modal rhythmic morphologies existed in conjunction with a range of incident wave conditions. The wide range in wave heights (1-2.25m), Dean parameter values (3.0-6.8), and surf scaling parameter values (7.5-128.7) suggest that any of the wave climate components have the potential to develop rhythmic morphologies: Both regional and local swell, as well as local waves, posses the attributes of moderate wave height and period

that are associated with the occurrence of rhythmic morphologies.

As a result, it is difficult to assign either of the two rhythmic states to a specific wave climate component. The high wave steepness values required to generate the high Dean parameter values (3.95-6.8) of the RBB state, suggest that a principal role is played by short period, moderately high local waves. Similarly, long wave periods required to generate low Dean parameter values (<3.95) and topography skewed in the direction of longshore drift, together strongly suggest that regional southwesterly swell is the primary influence on development of the STBR state. However, the correspondence of these states to observed wave climate occurrences does not confirm these suggestions (Table 3.9) .

INFERENCES ON NMB PROCESS SIGNATURES: PERIODS OF RESONANCE AND OBLIQUE WAVE INCIDENCE

Based upon the Australian model process signatures, it is possible to make some inferences about the relative dominance of particular wave generated mean and oscillatory flows in each of the NMB states.

The suggestion that inshore resonance has a primary influence upon the scale of beach and surf zone morphologies is a central aspect of the Australian model (Wright et al, 1989; Wright and Short 1983:1984). This suggestion is based upon reported agreement between the observed wavelengths of rhythmic morphologies and those predicted from standing wave and edge wave dispersion relationships using observed periods of resonance (e.g. swash cusps have been linked to edge waves at synchronous and subharmonic frequencies [Guza and Inman, 1975; Sallenger, 1979a; Guza and Bowen, 1981; Wright, 1982]; surf cusps have been linked to standing waves and standing edgewaves at infragravity frequencies [Bowen and Inman, 1971; Short, 1975; Wright 1982; Holman and Bowen, 1982]. From the edge wave dispersion equation, Komar (1983) gives the relationship between the wavelength (L_e) and period (T_e) of a standing edgewave as

$$L_e = \frac{g}{2\pi} T_e^2 \sin[(2n+1)\beta]. \qquad (3.4)$$

A set of solutions to this equation is given in Table 3.10a.

Along the lines of the Australian model , it is suggested that the decrease in rhythm spacings that is characteristic of the NMB pattern of morphologic evolution represents a shift downward in the dominant period of resonance from low infragravity periods (>100s) for the MBT state, through high infragravity (100-50s) and subharmonic ($4T_i$) periods for the modal rhythmic states, to subharmonic periods ($2T_i$) for the LTT state (Table 3.8).

The results given in Table 3.10a show that zero mode standing edge waves with periods on the order of 100 to 200 seconds (low infragravity) have wavelengths in the 500-1000m range. From this it can be inferred that the large surf cusps that exist at NMB in conjunction with the MBT state are generated by such long period, large scale oscillatory motions[3.1]. Mean flows, in the form of broad, widely spaced rip cells that cut across the surf zone, coexist with these inferred oscillatory motions. Although seaward return flows are concentrated in the rip channels, in the MBT state, seaward bottom return flows may dominate along the entire length of the shore.

According to Table 3.10a, edge waves with periods on the order of 50 to 100 seconds (high infragravity to subharmonic) have wavelengths in the 500-100m range. From this it can be inferred that the small surf cusps that exist at NMB in conjunction with the two rhythmic states are generated by such motions. (It will be shown in Chapter 5 that NMB runup spectra obtained during moderate energy conditions do exhibit significant peaks within a range of comparable periods [~40-80 seconds]). For the two rhythmic states, rip cells also exist in conjunction with these inferred oscillatory motions. In contrast to the MBT state, however, the rip cells of the rhythmic states are not only more closely spaced, but are also narrower and only extend shoreward past the inner bar. In this instance net seaward flows appear to be concentrated in the rip channel bays and shoreward flows on the horns.

Finally, according to Table 3.10a, edge waves with periods on the order of 25 to 50 seconds (subharmonic) have wave lengths in the 100-150m range. Again, it can be

TABLE 3.10

a) EDGE WAVE LENGTHS (after Komar 1983) $L_e = \frac{g}{2\pi} T_e^2 \sin[(2n+1)ß]$.

	for ß=0.01	for ß=0.03	for ß=0.05
T_e(s)	L_e(m)	L_e(m)	L_e(m)
25	10	29	49
50	39	117	195
75	88	263	439
100	156	468	781
150	351	1053	1755
200	625	1872	3100

b) FORM LENGTHS AND CURRENT VELOCITIES $K = (g/U^2)\, ß$

L_f(m)	Velocity (m/s)
125	1.4
250	2.0
300	2.2
500	2.8
1000	3.9

inferred that similarly spaced small surf cusps and swash cusps of the the LTT state are generated by such motions. In this instance, the rip cells are poorly developed, and net shoreward flow may dominate along the entire length of the shore.

A simple standing edge wave model appears to provide a reasonable explanation for the generation of rhythmic morphologies on NMB. While such a model seems particularly applicable to the generation of the larger-scale, normally-oriented, stationary, rhythmic forms observed on NMB (MBT and RBB states), a variant on the standing edge wave model may in fact be required to explain the occurrence of the smaller-scale, skewed, migratory rhythmic forms that develop on NMB at the late stages of recovery (STBR

state).

Holman and Bowen (1982) have outlined a 'phase-locking' model where the superposition of different modes of progressive edge waves interact to yield a complex standing pattern. Although this model does provide a mechanism to generate skewed, apparently nested/irregular morphologies such as those observed on NMB, it does not allow for form migration.

Another alternative to the simple standing edge wave model, one that does involve form migration and leads to the generation of skewed forms, is a model for a wave standing on a current. Although such a model was suggested by Sonu (1973) and outlined by Barcilon and Lau (1973), it has received little attention. In this model the rhythmic morphologies represent bedform fields that result from the instability of the longshore current and wave perturbed surf zone bed. Following from the relationship derived for unidirectional flow in alluvial channels by Kennedy (1961) (used later in Chapter 4), Barcilon and Lau (1973) give the relationship between form wavelength (L_f) and current velocity (U) on a sloping beach as

$$K = (g / U^2) \beta \qquad (3.5)$$

where K = wave number $2\pi / L_f$ and ß is beach slope in radians (taken here as .01). Longshore current velocities predicted from this relationship for a range of rhythm wavelengths observed at NMB are given in Table 3.10b.

The results of this analysis predict that longshore currents with velocities in the 1-2m/s range would be required to generate the smaller-scale rhythms observed at NMB. Although these longshore current velocities are higher than the few current velocities measured during this study, velocities in this range are not unreasonable. (P.A. Howd [pers. comm., 1990] reports that longshore currents during storms at Duck, North Carolina exhibited eight hour average velocities of 2m/s with peak velocities of 3m/s that lasted for 10-15 seconds. Howd also reports that with highly oblique angles of wave approach, low

(1m) waves generated longshore currents with velocities of 1 m/s.) According to the values given in Table 3.10b, the larger-scale, stationary rhythms (which are not of particular interest in this case) require current velocities greater that ~3m/s. Velocities in this range, although possible, may not be so reasonable. This is in contrast to the apparent viability of the 'wave on current' model for the generation of the smaller-scale, migratory forms that are of interest.

Aside from representing another possible mechanism for the generation of rhythmic morphologies, what this model and these results suggest is that longshore currents may be an important process component in the NMB system - particularly during the later stages of recovery and in conjunction with the development of the STBR morphologies (Table 3.8). The prevalence of southwesterly approaching winds and waves, and associated northerly flowing longshore currents in the NMB area would support this suggestion. Also, the closer affinities of the STBR morphologies to those described elsewhere and interpreted to represent the influence of obliquely incident waves and longshore currents, than to the TBR morphologies of the Australian model, supports this suggestion (e.g. The skewed, longshore migration of forms at late stages of recovery together with the appearance of 'meandering longshore currents' within the surf zone observed on Outer Banks of North Carolina by Sonu [1973]; The highly skewed bar and rip systems developed during recovery and associated with oblique winds and waves on the southeast coast of Australian described by Chappel and Eliot, [1979]; The oblique bar and rip channel systems of the Oregon coast described by Hunter et al. [1979])

The potential influence of oblique wave incidence/longshore currents upon nearshore morphology has not been excluded from the Australian model. Wright and Short (1983, 1984) did attribute the occurrence of skewed morphologies to the presence of longshore currents. However, probably because it is not an important process component in the beach systems studied by Wright and Short, little attention has been given to oblique wave incidence/longshore currents in the Australian model.

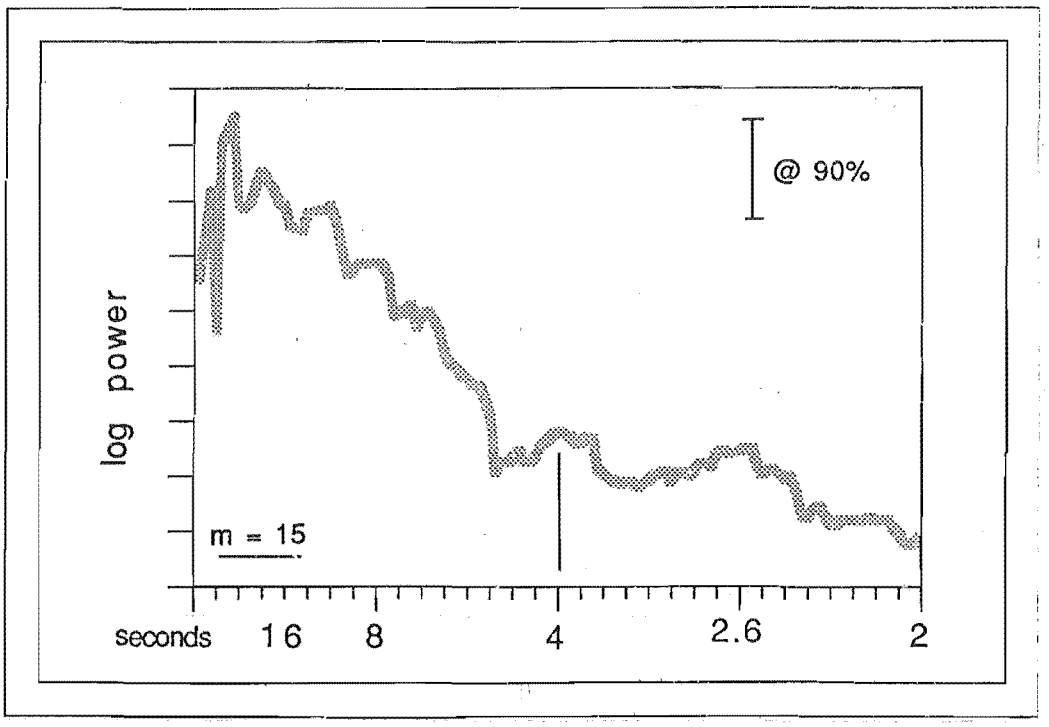

Figure 3.14. Log plot of the smoothed power spectrum of Pfahlert's (1984) wave height estimates. Pfahlert's year long time-series was demeaned, detrended, and tapered prior to fourier analysis. Following these transformations the resulting time series was, smoothed (with a moving average) and the log plot of the smoothed power spectrum produced. The confidence interval (90%) is given in the upper right hand corner of the figure. The smoothing bandwidth (m=15) is given in the lower left hand corner of the figure.

MORPHOLOGIC RESPONSE TO MULTIPLE SCALES OF UNSTEADINESS

Storm/Recovery Cycles

Observations made during this study and by others suggest that high frequency storm/recovery events are a characteristic feature of the central west coast wave climate. In the wave height and period time series introduced earlier (Figure 3.12), wave height variations could be seen to occur approximately every 3-8 days and individual wave trains to have arrived at approximately 2-5 day intervals. A fourier analysis of Pfahlert's (1984) year long daily record of wave height (Section 2.2 of Chapter 2) carried out during this

study revealed an ~4 day cycle of wave height variation (Figure 3.14). This time period is comparable to that given by Pickrill and Mitchell (1979), who based upon a fourier analysis of a wave height time series obtained from oil rigs off the North Island west coast, reported that wave height variations exhibited a 5 day cycle. Finally, R.M. Kirk (pers. comm., 1990), during an investigation recently carried out near the study site at Cape Foulwind, has also found that depending upon the weather conditions, distinctive patterns of waves and currents persist in the area for periods of ~4-14 days.

Based on these observations it is suggested that the the storm model applies to NMB: At NMB rhythmic morphologies prevail primarily because there is insufficient time for more reflective morphologies to develop. This interpretation would explain why morphologic patterns of evolution at NMB are characterized by oscillations between the dissipative end member and/or the two rhythmic states, although incident wave conditions vary over a broad range. It would account for the poor correspondence between morphologic state and incident wave conditions that was observed at low wave energy levels. Thus the combined effects of response asymmetry and high frequency temporal energy variability, as outlined in the Australian model, are an important aspect of NMB nearshore dynamics.

Higher Frequency Cycles

Wave height variations at even higher frequencies also have an influence upon NMB beach and surf zone morphology. Wright et al. (1987) considered the effect that variations in tidal range have upon morphology. They suggested that nearshore topographies are more pronounced when tidal ranges are low, more subdued when tidal ranges are high. The comparison of the Australian model to NMB morphologies made earlier supports this suggestion. NMB posses a higher tidal range than the Australian systems and correspondingly, analogous NMB morphologies are more subtly expressed than their Australian counterparts : NMB surf zones are wider, bar forms are more widely spaced and are wider and lower in relief. Thus, within the NMB system the principal effect of tidally-induced variations in surf zone width and breaker position on morphologic development

appears to be a modifying influence upon existing forms.

Wright et al. (1987) also considered the effects that wave groupiness may have on morphologic development. They suggested that for the same incident wave height, higher groupiness can lead to the development of a higher energy state. Contrasts in wave groupiness are implicit in the swell versus local wave climate components proposed for NMB, and as a result groupiness effects would be expected to be an important aspect of NMB nearshore dynamics. However, it is beyond the scope of this work to address them.

COMPARABILITY OF DYNAMIC SIMILARITY PARAMETERS

In this study differences were observed in the correspondence of the three similarity parameters (H_b, ε, Ω) to beach state, both within the NMB system, and between the NMB and Australian beach systems.

The NMB morphologic states showed the strongest dependence upon the breaking wave height parameter. The Dean parameter was also useful, being a particularly good discriminator of the two rhythmic morphologies. Although a useful discriminator of reflective and dissipative morphologies, the surf scaling parameter had the lowest overall discriminating power.

Wright and Short (1983;1984) did not directly compare the predictive capability of the three parameters used in this study (H_b, ε, Ω). However, Lippman and Holman (1990) did make such a comparison. In agreement with the observations made during this study, they found that their bar types showed the the strongest dependence upon a simple wave height parameter.

What these observations suggest is that at a fixed location within a particular beach system, where slope and grain settling velocity variables are effectively constant, morphology exhibits a direct dependence upon incident wave conditions, in particular wave height. This would explain why the surf scaling parameter was a poor discriminator of the two rhythmic states: Scatter is induced by the inclusion of beach slope in the

similarity parameter in a rhythmic system such a NMB, because within the same state there is a wide range in beach slopes between horns and bays.

When NMB similarity parameter values were compared to those given in the Australian model (Wright and Short, 1983,1984; Wright et al.,1985), both surf scaling parameter and Dean parameter values were higher (more dissipative) at NMB than would be predicted from the Australian model. Differences in methodology, specifically visually estimated versus instrument recorded wave heights, could explain the discrepancies between NMB and Australian model similarity parameter values. However, the close agreement between NMB and Australian model wave height values suggest other causes for the discrepancies.

With respect to the the surf scaling parameter, the dissipative values at NMB may in part be attributable to the higher tidal range at NMB than in the Australian systems: The attenuating effect of the tide, resulting in lower beach slopes for comparable states, would push surf scaling parameter towards more dissipative values. Also, differences in exactly what slope is being used may also influence the surf scaling parameter values. This last point may also provide an explanation for the discrepancy between NMB and Australian model Dean parameter values.

Dean (1973) originally suggested that the mean grain settling velocity at the bar crest is to be used. In this study, the mean grain settling velocity over a 100m cross-shore by 200m longshore area was used. It is unclear what settling velocity value was used by Wright et al. (1985). In fact, noting that mean grain settling velocities vary from the surf zone to the beach face, there is a reference to having adjusted the settling velocity used to calculate the Dean parameter on the basis of the observed surf zone width; lower values were chosen for wider surf zones in order to improve predictability. Perhaps this explains why at NMB the Dean parameter values showed close agreement to Australian model values at the reflective end of the spectrum, but poor agreement to those at the dissipative end of the spectrum. It should also be noted with respect to differences between NMB and Australian model Dean parameter values, that the Australian model values were obtained from a single beach system, and therefore difference are to be expected.

Despite the discrepancies between NMB and Australian model similarity parameter

values described above, and in contrast to the case for intracomparisons, similarity parameters that include slope, or better yet grain settling velocity, should be used when comparisons are being made between different beach systems.

3.4 CONCLUSIONS

Based on a comparison with the Australian morphodynamic model, four NMB macroscale process-form assemblages were recognized in this study. The Rhythmic Bar and Beach and Skewed Transverse Bar and Rip states were modal states within NMB system. The range of rhythmic topographies associated with these two states existed in conjunction with all wave climate components (ie. southwesterly regional and local swell, and local storm waves). The broad surf zones and multiple bars of the Multiple Bar and Trough state developed at the onset of high energy southwesterly wave conditions. The narrow surf zones and irregular shoals of the Low Tide Terrace state developed only after extended periods of low energy southwesterly swell.

In general NMB nearshore morphologies are comparable to those described in the Australian model. However, differences exist between NMB and Australian model morphologies at the late stages of post-storm recovery: The migratory, oblique bar and rip channel morphologies of Nine Mile Beach STBR state are not a prominent feature of the Australian model. This difference, suggested to result from the greater influence of oblique wave incidence and accompanying longshore currents on morphology in the NMB system than in the Australian systems described by Wright and Short (1983;1984), highlights an area where further refinement of the Australian model framework is required. As Chappel and Eliot (1979) have suggested previously, oblique bar and rip channel states may not simply be asymmetric counterparts of the rhythmic bar and beach or transverse bar and rip states.

Differences were also observed between NMB and Australian model morphologies in terms of morphologic expression: Comparable morphologies are more subtly expressed in the NMB than the Australian beach systems. In this instance these differences, attributed

to a higher tidal range in the NMB than the Australian systems, are accounted for within the present framework of the Australian model.

The present framework of the Australian model, which encompasses the combined effects of response asymmetry and temporal energy variability, is also able to account for the prevalence of rhythmic morphologies within the NMB system. NMB morphologies remained within a narrow but dynamic morphologic range, characterized by the onshore-offshore migration of the inner bar. This is because, although a broad range of incident wave conditions existed (ie. wave breaker heights 0.5-4.0m; wave periods 8-14 seconds), incident wave conditions varied over short periods of time (~5 days). As a result there was insufficient time for the full spectrum of morphologic configurations described in the Australian model to be developed at NMB.

Thus, for the most part, the current framework of the Australian model was able to account for the patterns of three dimensional morphologic response to changes in wave energy level that were observed at NMB. Qualitatively at least, it provides a useful beach and surf zone classification scheme that is applicable to a range of environmental conditions. Quantitatively, some care should be taken in the application of the dynamic similarity parameters.

Finally, the central theme of this work - the enmeshed nature of process-response interactions in sandy coastal systems- is well illustrated by the nature of macroscale process-response interactions described in this chapter. Here it was shown that nearshore morphologies represent a response to a variety of influences operating simultaneously across a range of scales.

3.1 The possibility that large scale edge waves are forced by reflections off the two headlands that bound NMB beach was investigated using another form of the edgewave dispersion relationship that gives the standing edgewave frequency for a given combination of edge wave cross (n) and longshore (m) modal numbers (edge wave lengths) on a plane sloping beach within a basin of a given dimensions as

$$f^2 = \frac{g\, m\, (2n+1)\, \beta_e}{4\, L_b\, \pi} \qquad (3.6)$$

after Culley (1986), where β_e is effective beach slope (Holman and Bowen, 1979 [taken here to be 0.01]), and L_b is beach length (taken here as 12,000m). The frequency and cross-shore dimensions of a basin trapped standing edge wave predicted by this relationship for a range of longshore wavelengths observed on NMB are given in Table 3.11. The results of this analysis suggest that it is unlikely that the headlands that bound the NMB compartment act as reflectors for edge waves of longshore dimensions being considered (500-1000m). This is because the longshore mode numbers are too high (m=24 for 100m and m=48 for 500m): Only the lower modes of both m and n edgewaves would be expected to be excited (Holman, pers. comm, 1990). It is possible that the inlet deltas act as reflectors, as the the largest scale rhythms (1000-2000m) observed would have lower modal numbers (m=4 and 8 respectively). If this is the case then it is only the lowest cross-shore mode numbers (n=0,1) that would hug the shore.

Also, it is interesting that the fit of a mode (6, 0) edge wave within the NMB beach compartment has longshore length scales that match the location of the two inlets that dissect NMB. In the cross-shore this edge wave has dimensions that correspond to those of the offshore extent of the headlands. The period of such a wave would be on the order of 10 minutes. Extremely regular runup highs at periods of ~9-10 minutes were noted during fieldwork, although no quantitative measurements exist to support this observation.

EDGE WAVE DIMENSIONS $f^2 = \frac{g\, m\, (2n+1)\, \beta_e}{4\, L_b\, \pi}$

Ly (meters)	(m,n)	T(s)	Lx(meters)
12000	(2, 0)	877	4775
	(2, 1)	506	6367
4000	(6, 0)	506	1592
	(6, 1)	292	2122
2000	(12, 0), (4, 0)*	358	760
	(12, 1)	207	1061
1000	(24, 0), (8, 0)*	253	398
	(24, 1), (8, 1)*	146	530
500	(48, 0), (16, 1)*	179	199

* Modal numbers when delta lobes act as reflectors.

CHAPTER 4 BED DYNAMICS: MICROSCALE

"What cannot be seen is called evanescent;
What cannot be heard is called rarefied;
What cannot be touched is called minute.
These three cannot be fathomed
And so they are confused and looked upon as one"
Lao Tzu

The nature of interactions that take place between grains, fluid, and bed within the swash zone of NMB are examined in the context of the microdynamic framework outlined in this chapter. Bedforms, stratification, sediment textures, and flow characteristics observed in the upper foreshore of NMB are described. Microscale process-form assemblages are recognized. The implications of these observations and interpretations to models for the formation of near-horizontal lamination in the swash zone are briefly explored.

4.1 BACKGROUND: GRAIN-FLUID-BED INTERACTIONS AND THE MICRODYNAMIC FRAMEWORK

Based on detailed measurements of the bed surface and video recordings of the near-bed layer during upper flow regime conditions in a flume, Paola et al. (1989) suggested that near-horizontal lamination results from the superposition of two processes. High frequency, 'turbulent scour and fill' controls the vertical sorting within the lamination.

TABLE 4.1 THE MICRODYNAMIC FRAMEWORK

DEPOSIT CHARACTERISTICS
- EXTERNAL CHARACTERISTICS (geometry)
  - Bedforms
  - Stratification

BEDFORM DYNAMICS

TRANSPORT DYNAMICS

- INTERNAL CHARACTERISTICS (texture and composition)
  - Intergrain-layer patterns
  - Intragrain-layer patterns

FLOW REGIME
- Lower Regime
- Upper Regime

FLOW CHARACTER
- Smooth, *Viscous* Boundary Layer
- Transitional Boundary Layer
- Fully Rough, *Turbulent* Boundary Layer

TRANSPORT STAGE
- Lower Stage, *Bare-bed* Transport
- Upper Stage, *Rheologic* Transport

DEPOSITION MECHANICS
- Progressive Deposition
- Instantaneous Deposition

Low frequency, 'subturbulent bedform migration' determines the position of lamination boundaries.

Viewing this distinction in a broader context, a microdynamic framework is outlined below to describe the network of grain-fluid-bed interactions that occur during the sedimentation process. As it forms the basis for the investigation of microscale dynamics within the swash zone of NMB, a particular emphasis is placed upon aspects of the framework that are most relevant to swash zone bed dynamics.

The components of the microdynamic framework are summarized in Table 4.1 and detailed below. Along the lines of the suggestion made by Paola et al. (1989), the principal distinction made within the microdynamic framework is between 'external deposit characteristics and bedform dynamics' and 'internal deposit characteristics and transport dynamics'. External deposit characteristics refer to the geometric properties of bedforms and stratification - height/thickness, length, and other spatial descriptors. Within the microdynamic framework, external characteristics are regarded as a response to larger-flow thickness-scale processes (i.e. *bedform dynamics*). Internal deposit characteristics refer to the material properties of the deposit - grain size, sorting, grading and other textural descriptors. Internal characteristics are regarded as a response to smaller-near bed-scale processes (i.e. *transport dynamics*). Although these two aspects of microdynamics are treated separately, it is acknowledged that only when considered in combination do they completely describe deposit characteristics and the sedimentation process.

BEDFORM DYNAMICS

A standard method of relating bedforms to hydraulic conditions is through diagrams of bedform existence fields (Simons et al., 1965; Allen, 1968; Znamenskaya, 1969; Blatt et al., 1980; Leeder, 1982; Allen, 1983, 1985). In these diagrams the occurrence of different types of bedforms are associated with different combinations of flow and

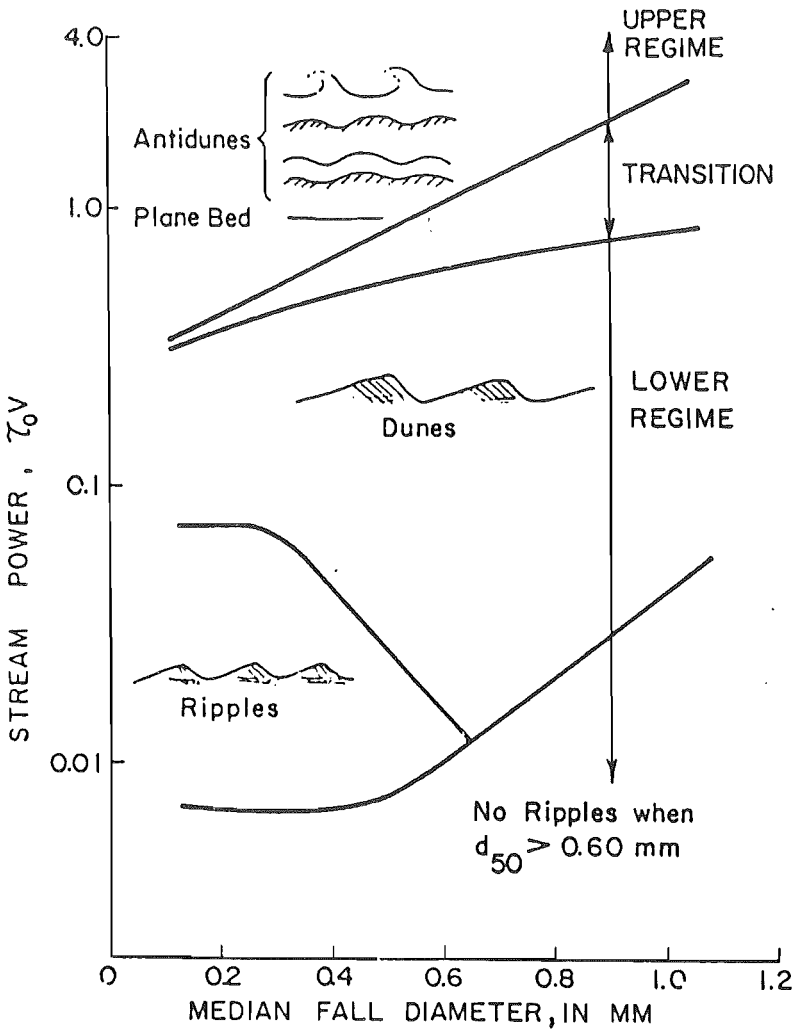

Figure 4.1. Relation of stream power and median fall diameter to bedform (from Simons et al., 1965).

sediment parameters. A typical form of these diagrams is given in Figure 4.1.

Common to all these diagrams is a division between *upper* and *lower* flow regimes. In addition to bedform type, phase relations between the bed and water surface, and the nature of sediment transport, is different in these two regimes (Bagnold, 1956, 1966; McBride et al., 1975; Allen and Leeder, 1980). In the lower flow regime the bed surface is out of phase with, and is not determined by, the form of the water surface (Yalin, 1972; Jackson, 1975; Leeder, 1979; Allen and Leeder, 1980). Sediment transport is relatively discontinuous. In the upper flow regime, where sediment transport is

relatively continuous, the bed surface is in phase with the water surface and is dependent on the form of the free surface (Yalin, 1972; Jackson, 1975; Leeder, 1979; Allen and Leeder, 1980).

Although a transitional boundary separates the two regimes, a Froude number of one, ($Fr = U^2/gd$, where U is mean velocity and d is flow depth), is often used as a boundary between them (Kennedy, 1961; Moss 1972; Reineck and Singh 1980; Middleton and Southard, 1984). When $Fr < 1$ (subcritical/tranquil flow), lower flow regime bedforms are stable; when $Fr > 1$ (supercritical/rapid flow), upper regime bedforms are stable.

Ripples and dunes are the characteristic bedforms of the lower flow regime (Simons et al., 1965; Reineck and Singh, 1980; Leeder, 1982; Allen, 1983, 1985). As these forms migrate, downstream-dipping ripple and dune cross stratification is developed through grain avalanching and foreset accretion (Blatt et al., 1980).

In comparison to the lower flow regime, upper flow regime bedforms and stratification have received little attention (Cheel, 1990). Plane beds and antidunes are the most commonly recognized bedforms in the upper flow regime (Simons et al., 1965; Reineck and Singh, 1980; Leeder, 1982; Allen, 1983, 1985). The association of antidune forms with upstream dipping cross stratification is well established (Blatt et al., 1980; Reineck and Singh, 1980; Langford and Bracken, 1987). Plane beds are generally associated with horizontal lamination (Bridge, 1978; Reineck and Singh, 1980; Blatt et al., 1980; Leeder, 1982; Allen 1983, 1985; Cheel and Middleton, 1986b; Bridge and Best, 1988; Paola et al., 1989; Cheel, 1990).

Recently, increased attention has been given to long wavelength, low relief 'bedwave' forms, detected during upper flow regime conditions in flumes (Smith, 1971; McBride et al., 1975; Cheel, 1984; Bridge and Best, 1988; Paola et al., 1989; Cheel, 1990) These bedwaves are interpreted to result from local perturbations caused by water surface waves (Kennedy, 1961; Allen, 1985). The perturbation velocities, when coupled with 'net' drift velocities, cause local periodic stream-wise variations in the transport rate and thus alternating patches of erosion and deposition that are represented as bed undulations. The bed undulations that result from this process occur on the same scale

as the water surface undulations. Kennedy (1961) gives the relationship between flow velocity and the preferred wavelength of in phase bed and water surface undulations, L_f, as

$$L_f = (2\pi/g)U^2 \qquad (4.1).$$

In his observations of upper flow regime bedforms in flumes, Kennedy found good agreement with this relation derived from theory. Cheel (1984) and Bridge and Best (1988) have also reported correspondence between flow velocity and bedwave wavelength as predicted by Kennedy's relationship.

Cheel (1990) incorporated Kennedy's (1961) observations with those of more recent workers and proposed a succession of bedform-stratification type associations, or 'bed phases', for the upper flow regime (Table 4.2; Figure 4.2). Cheel identified a succession from plane bed, to downstream-migrating in-phase bedwaves, to stationary bedwaves, to upstream-migrating in-phase bedwaves (antidunes), that occurs with increasing flow strength for a given flow depth. Accompanying this succession of bedforms is a succession from horizontal lamination, to downstream-dipping (foreset) cross-lamination, to wavy bedding, to upstream-dipping (backset) cross-lamination respectively.

TABLE 4.2. TERMINOLOGY USED FOR UPPER FLOW REGIME BED PHASES
(from Cheel, 1990)

Bed phase	Description
Plane bed	Plane bed with no regular relief greater than a few grain diameters
In-phase waves	Trains of sinusoidal bed waves which are approximately in phase with the water surface. Bed waves are most commonly straight-crested (2-D) but short-crested (3-D) forms are also known
Downstream-migrating	2-D in-phase waves which migrate in the downstream direction
Standing	2-D in-phase waves which do not migrate upstream or downstream
Antidune	2-D in-phase waves which migrate in the upstream direction, water surface waves may break periodically
3-D	Short-crested in-phase waves which are not well known. Some forms may be stationary (J. Shaw, pers. comm.) while others may migrate up and/or downstream

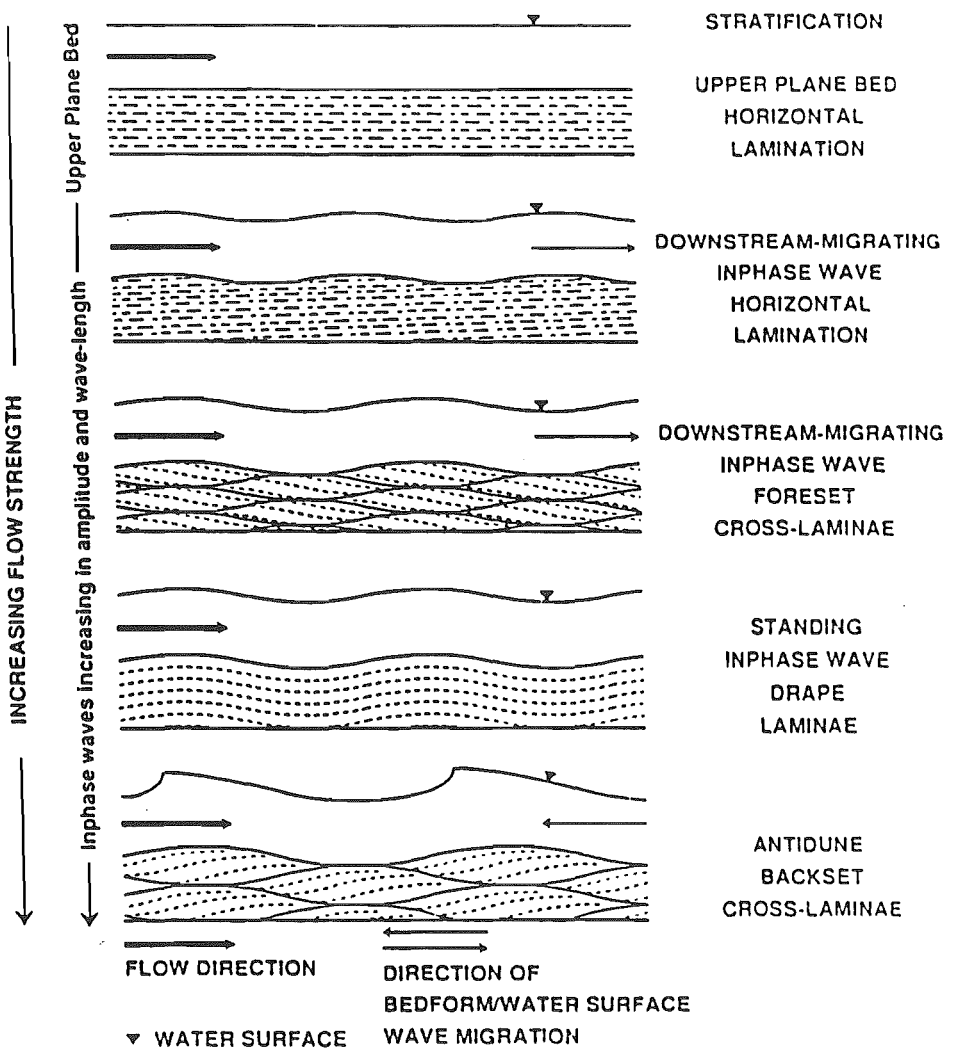

Figure 4.2. Schematic illustration of upper flow regime bed phases and stratification (from Cheel, 1990). Terms on the right denote the idealized stratification type produced by each bed phase.

Sediment Textures

Emery and Gale (1978) and Grace et al. (1978) observed marked textural variations between grain layers within laminae. They suggested that the mixing of individual grain layers, that occurs during the collection of a bulk sediment sample, obscures what may be valuable process information present at the microscale because this is precisely the scale at which hydraulic fractionation occurs. Thus the predominance of bulk sampling procedures has resulted in information loss, and may in part account for what has been rather limited success in relating sediment textures to formative processes.

The few exceptions to the bulk sampling rule include Clifton (1969), Sallenger (1979), and Cheel and Middleton (1986a,b), who have obtained microscale textural samples. While these workers have been relatively successful in making process inferences from sediment textural patterns, even they have taken a rather narrow view of microscale textural patterns. Consideration of textural patterns both within and between grain layers in combination might result in a broader basis for interpretation. In this respect, a distinction between *intragrain-layer* and *intergrain-layer* textural patterns is made here and applied later in this work (Table 4.1).

Standard descriptions of sediment textures are generally centered around, and limited to, grain size; other grain properties such as density and shape are excluded. As was the case for bulk sampling, this standardized procedure has also resulted in the loss of process sensitive information (Winkelmolen, 1982). Parameters that have the potential to represent the complex grain-bed-flow interactions that occur during the sedimentation process would be more appropriate choices as textural parameters.

Recent investigations by Slingerland (1977, 1984) and Komar and Wang (1984) have met with some success in relating sediment textures to formative processes by considering hydraulic grain parameters and equivalence relationships. Hydraulic grain parameters employed by these workers include a grain's settling velocity, its critical entrainment stress, and its dispersive pressure. These hydraulic grain parameters can be

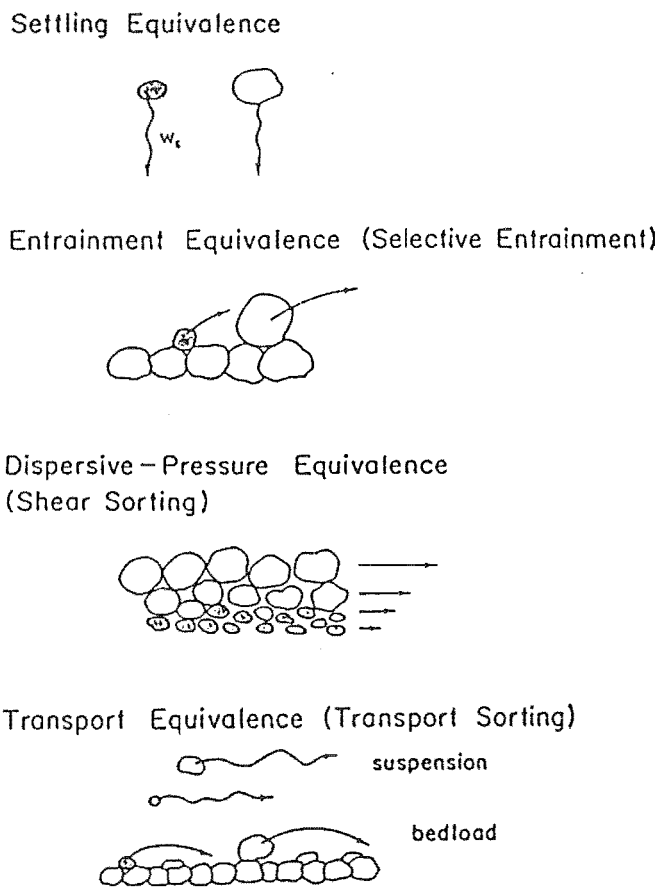

Figure 4.3. Types of Dynamic Equivalence (from Komar, 1989). The term 'dynamic equivalence' follows from Ruby's (1933) concept of 'hydraulic equivalence' which is limited to equivalent settling rates. The types of dynamic equivalence are: settling equivalence (grains that settle together in a clear fluid), entrainment equivalence (grains that require the same bottom stress to be moved off the bed), dispersive equivalence (grains that require the same force to be maintained within a concentrated granular dispersion), and transport equivalence (grains that are transported at the same rate).

framed within the context of 'dynamic equivalence', a term which Komar (1989) has recently employed to encompass, in the broadest sense, the grouping together of sediment grains that respond similarly in different conditions (Figure 4.3).

Flow Character

As fluid flows past a rigid boundary, the velocity decreases from its value at the free surface to zero at the boundary itself. The fluid velocity, depth, density (ρ_f) and viscosity (μ), and boundary roughness (k_s) determine the shape of the velocity profile.

For *fully rough*, steady, uniform flows of clear fluids over a rigid boundary, with a logarithmic velocity profile

$$U = (U^* / \kappa) \ln (30d / k_s). \qquad (4.2)$$

U^* is shear velocity (cm/s), where $U^* = (\tau_o / \rho_f)^{1/2}$ and τ_o is bottom shear stress; κ is von Karman's constant, taken as ~0.4 for clear flows; and k_s is taken as D_{i50} (after Komar, 1976b[Figure 4.4a]). The onset of fully rough conditions is defined by $Re^* \geq 70$, where $Re^* = U^* k_s / \nu$ is a dimensionless grain Reynolds number and $\nu = \mu/\rho_f$ is kinematic viscosity (Komar, 1976b; Middleton and Southard, 1984). In fully rough flows, turbulence extends all the way to the boundary and the bed receives the full effect of fluid turbulence (Komar, 1976b): Near-bed turbulence is distributed over a relatively wide range about the mean (Yalin, 1972 [Figure 4.4a]).

In contrast to fully rough boundary flows, *smooth* boundary flows are characterized by the presence of a thin basal viscous sublayer that has a linear velocity profile and is separated by a buffer layer from the fully turbulent zone with its logarithmic velocity profile (Komar, 1976[Figure 4.4b]). Smooth boundary flows are defined by $Re^* \leq 5$, and $k_s/\delta' < 1$, where $\delta' = 5 \nu / U^*$ is the thickness of the viscous sublayer (Komar, 1976b; Middleton and Southard, 1984). In smooth flows the grains lie within the viscous sublayer and are sheltered from the full effects of fluid turbulence (Komar, 1976b): Near-bed turbulence is distributed over a relatively narrow range about the mean (Yalin, 1972[Figure 4.4b]).

Transitional flows are said to exist when $5 < Re^* < 70$ (Komar, 1976b; Middleton and Southard, 1984). In transitional flows, the larger grains protrude through the viscous sublayer so that the bed no longer receives the full sheltering effects of the viscous

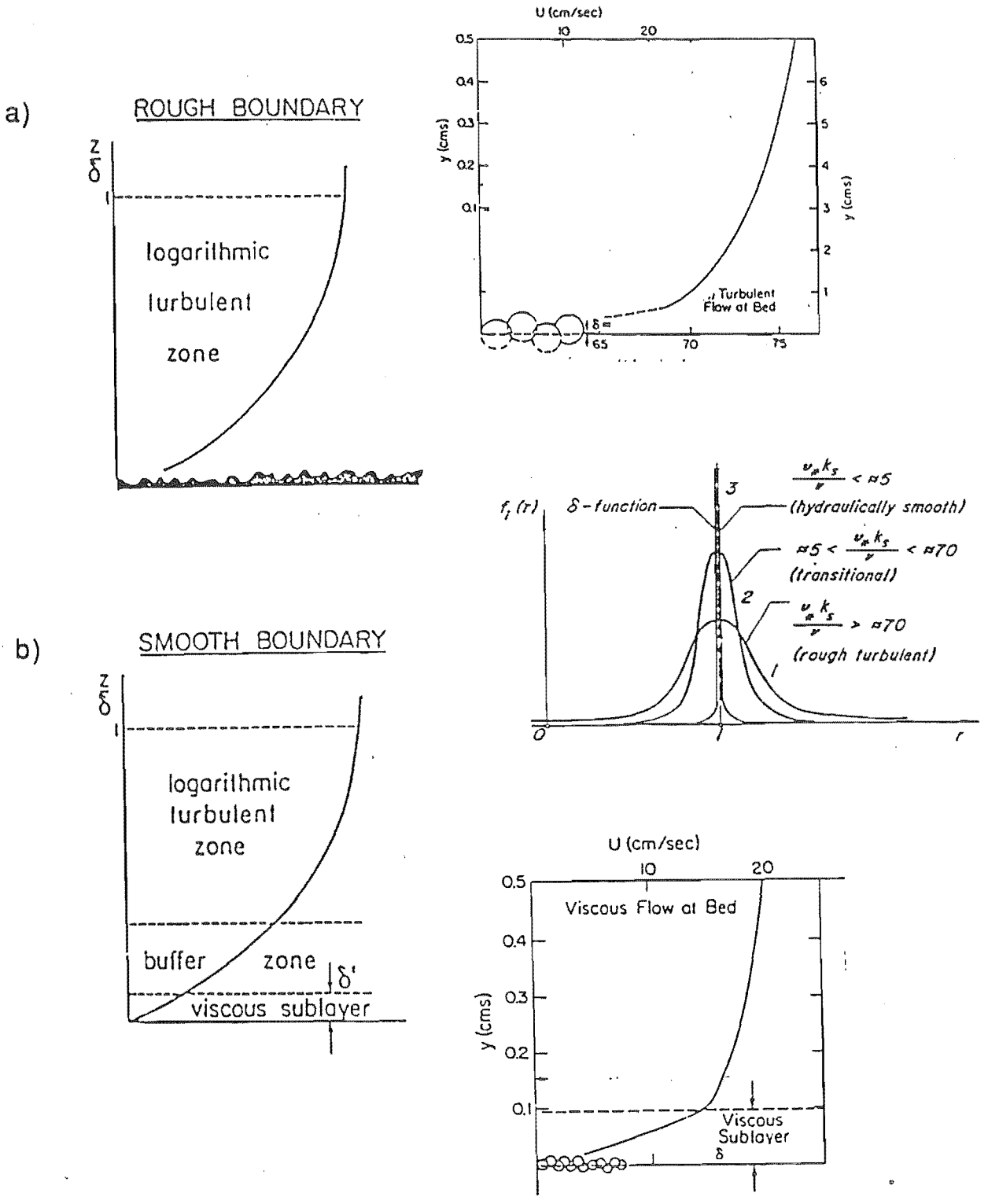

Figure 4.4. Schematic representation of velocity profiles in clear, smooth, steady unidirectional flows: a) Fully rough velocity profile b) Smooth velocity profile (from Komar, 1976b; Blatt et al., 1980). Also shown in this figure is a representation of the distributions of bottom shear stress for rough, transitional, and smooth flows (from Yalin, 1972).

sublayer (Komar, 1976b). Komar (1976b) gives a relationship to describe the velocity profile in transitional flows. Based on the work of Nikuradse (1933), it contains an empirical correction factor that is dependent upon the ratio of roughness height to sublayer thickness (k_s/δ').

As fluid flows past a loose boundary, a condition of entrainment arises when the weight force of the grains on the bed is offset by the drag and lift forces of the fluid exerted on the bed (Middleton and Southard, 1984). Komar and Wang (1984) provide an empirical relationship to predict the mean bed shear stress required to entrain grains from a bed of mixed sizes and densities. For $D_i < 0.1$ cm they give

$$\tau_e = 0.00515\,(\rho_s - \rho_f)\,g\,D_i\;\;0.568\;\;\tan\Phi \qquad (4.3)$$

where ρ_s is sediment density and Φ is the pivoting angle given as $\Phi = 61.5\,(D_i / k_s)^{-0.3}$. This relationship predicts that coarser, light mineral grains tend to be more easily removed from the bed than finer, heavy mineral grains. This is because the coarse light grains protrude higher into the flow and posses smaller pivoting angles (Slingerland, 1977; Komar and Wang, 1984).

Transport Stage

Once sediment transport begins, two ideal modes of grain motion are distinguished within a continuum of grain motions (Yalin, 1972; Leeder, 1979; Middleton and Southard, 1984). During initial stages of *bed load* transport the grain is moved intermittently within the flow by fluid drag and lift (Middleton and Southard, 1984). In *suspended load* transport the grain is maintained within the flow by the vertical component of fluid turbulence (Middleton and Southard, 1984).

As fluid shear increases and appreciable amounts of sediment begin to be transported, concentration effects become important. The nature of bedload transport changes. Bedload is now characterized as a dense grain layer, or traction carpet, supported by an upward acting dispersive pressure that results from grain to grain interactions in the

shearing near-bed layer (Bagnold 1954, 1956, 1966; Leeder, 1979; Middleton and Southard, 1984; Allen 1985). A relationship for the critical stress required to maintain this bedload is given by Bagnold (1966) as

$$\tau_d = (\rho_s - \rho_f)\, g\, D_i\, C_o \tan \phi \qquad (4.4)$$

where tan ϕ is a static friction coefficient, and C_o is the fractional volume concentration in the static bed.

Thus an important distinction can be made between *lower stage*, or *bare-bed* transport and *upper stage*, or *rheologic* transport (Moss, 1972 [Table 4.1]). During lower stage transport the free flow interacts directly with the grains forming the bed surface and sediment transport is dominated by the influence of fluid turbulence (Bagnold, 1956, 1966; Moss, 1972; Leeder, 1979, 1983; Hanes and Bowen, 1985; Hicks et al., 1988). In contrast, during upper stage transport the free flow interacts with the bed through an intervening high concentration buffer layer and sediment transport is dominated by granular-fluid mechanics (Bagnold, 1956, 1966; Moss, 1972; Leeder, 1979; Allen and Leeder, 1980; Leeder, 1983; Hanes and Bowen, 1985; Hicks et al., 1988).

Leeder (1979) has used the transport stage parameter (U^*/U^*_e) of Francis (1973) to segregate upper from lower stage transport. For the transport of coarse sands over plane beds in water flows, upper stage transport should occur at transport stage values of about two. For the transport of fine sands, as is the case at NMB, upper stage transport is expected to occur at somewhat lower transport stage values (Leeder, 1979).

Unlike lower stage transport, where the well known equations describing velocity profiles in a clear flow might apply, no well defined relationships exist to describe the flow structure during upper stage transport. Hanes and Bowen (1985) outlined a theoretical model for the flow structure and mechanics of upper stage transport. In Hanes and Bowen's model, a basal layer dominated by grain-grain collisions and granular fluid mechanics is separated from the clear flow layer by an intervening

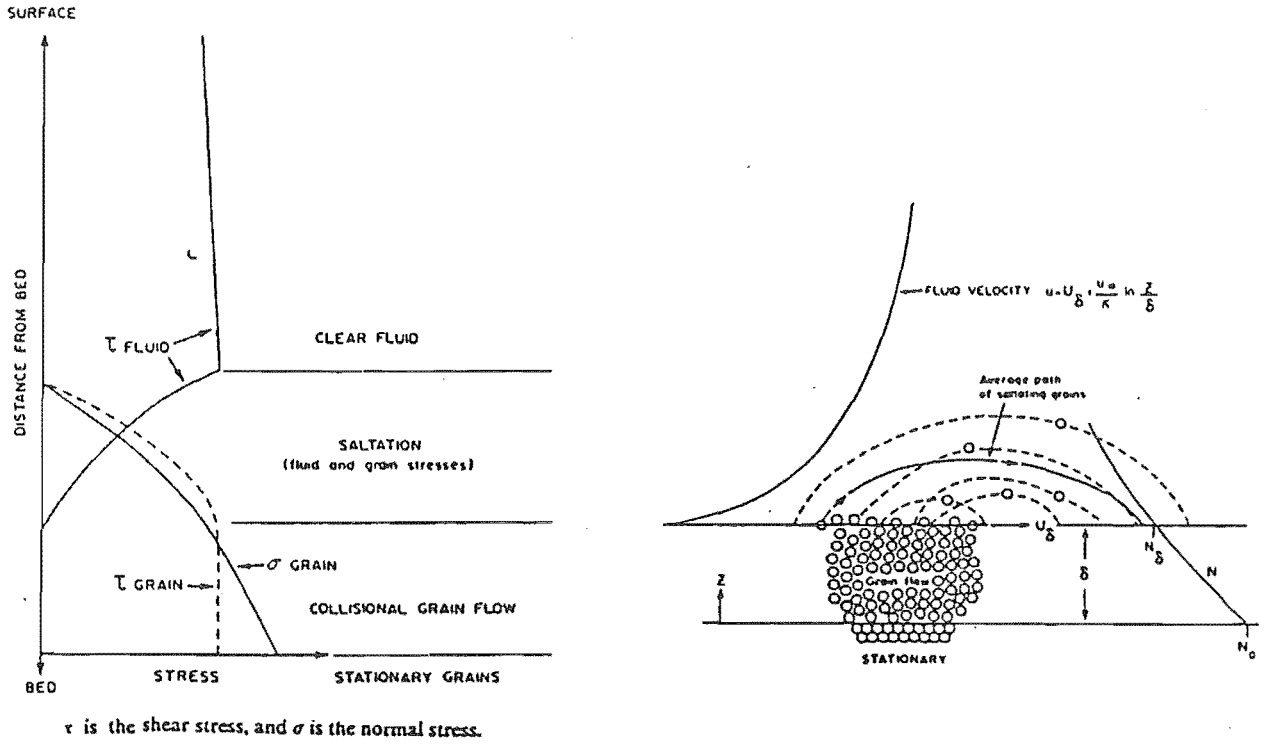

Figure 4.5. Schematic representation of velocity profile and layered flow structure in upper stage flow (from Hanes and Bowen, 1985).

saltation layer (Figure 4.5). The saltation layer, in which individual particles do not interact with one another, is dominated by turbulent fluid mechanics. Hanes and Bowen found that upper stage sediment transport rates predicted by their model compared favorably with transport rates determined empirically.

Hanes and Bowen's model for the flow structure and mechanics of upper stage transport is not unlike a mixed 'traction carpet/suspension cloud' model described by Lowe (1982, 1988) for the flow structure in turbidity currents. In Lowe's model, a traction carpet layer exists at the base of the grain dispersion. In this layer sediment concentration is high and as a result near-bed fluid turbulence is damped (Walker, 1978; Allen and Leeder, 1980; Bridge and Best, 1988; Lowe, 1982, 1988). A turbulent suspension cloud layer exists at the top of the grain dispersion.

The possibility of comparisons between the flow structure of turbidity currents and unidirectional flows at high transport stages has also been suggested by Clifton (1969),

among others. If the assumption that upper stage unidirectional flows are comparable to turbidity currents is accepted, then the affinities between the Hanes and Bowen (1985) and Lowe (1982, 1988) models described above provide the basis for a general conceptual model of the mechanical structure of flow during intense transport conditions. The central component of these models, and therefore of a general model, is the existence of a two layer flow structure; a lower traction carpet layer dominated by granular fluid mechanics and an upper suspension cloud layer dominated by turbulence.

Although generally not considered in the context of upper stage transport, an extension of the basic analogy to encompass all types of sediment gravity flows would allow for the full spectrum of concentration related effects associated with sediment gravity flows to potentially be operative in upper stage transport, and thus be included in the general model. This suggestion seems reasonable, as the general process being considered is essentially the maintenance and movement of a concentrated granular dispersion (Leeder, 1982; Lowe, 1982).

Four types of sediment gravity flow are commonly distinguished (Middleton and Hampton, 1976; Lowe,1979; Leeder, 1982; Middleton and Southard 1984 [Table 4.3]). Ideally, each flow type is characterized by a particular sediment support mechanism. In turbidity currents the dense sediment cloud is supported by fluid turbulence; escaping pore fluid maintains the sediment dispersion in fluidized or liquefied flows; collision generated dispersive pressure is the support mechanism in grain flows; in debris flows grains are supported by matrix strength. More realistically, however, in each flow type these support mechanisms act in conjunction with each other and concentration related buoyancy and hindered settling effects to maintain the dispersion (Middleton and Hampton, 1976; Lewis, 1982).

Deposition Mechanics

Lowe (1988), and more recently Arnott and Hand (1989), have given some consideration to how variations in the suspended load fallout rate influence the nature of deposition, and as a result the character of the deposit. Lowe made a distinction between

TABLE 4.3 GRAVITY DRIVEN FLOWS AND SEDIMENT SUPPORT MECHANISMS
(after Middleton and Hampton, 1976; Lowe, 1979)

TYPE	SUPPORT MECHANISM
FLUID GRAVITY FLOWS	Fluid Turbulence
SEDIMENT GRAVITY FLOWS	
FLUIDAL FLOW	
Turbidity Current	Fluid Turbulence
Fluidized Flow	Escaping Pore Fluid
DEBRIS FLOW	
Grain Flow	Dispersive Pressure
Debris flow	Matrix Strength

'net' accelerating and decelerating flows. He suggested that in contrast to accelerating flows, where the bedload layer is generated by active erosion of the underlying substrate, the bedload layer in decelerating flows is derived from collapse of the overlying suspension cloud.

Lowe's (1982, 1988) turbidity current model summarized above, included a description of the envisioned process of deposition in a decelerating flow. During sediment cloud collapse, traction carpet sedimentation is followed by suspension cloud sedimentation in a process of sequential deposition. At the base of the flow, where dispersive pressure is important, deposition occurs immediately in response to a drop in the driving force below that needed to support the grain layer (Middleton and Hampton 1976; Lowe, 1979, 1982). This process has been observed by Moss (1972) and Paola et al. (1989), during conditions of upper stage flow in flumes, as the instantaneous appearance of patches of grains on the bed surface. Whereas deposition of the lower

layer of the flow is *instantaneous*, deposition of the upper layers of the flow is *progressive*, occurring from the base upward as grains are laid down particle by particle upon the bed (Middleton and Hampton 1976; Lowe, 1979, 1982).

Ideally this process preserves the entire flow structure, resulting in a deposit with a basal inversely graded layer, representing the traction carpet layer that passes upward into a normally graded layer representing the suspension cloud layer. Commonly, however, more complex grading patterns exist as prior to complete suspension cloud collapse, pulses of traction carpet deposition may occur in order to keep the flow moving (Lowe, 1979, 1982). In addition to different grading patterns, the different layers in the deposit should be occupied by grain populations having different textures. These textural differences are expected to exist because different combinations of support mechanisms operated during the transport process.

SWASH ZONE FLOWS AND THE MICRODYNAMIC FRAMEWORK

Although the above discussion is concerned principally with upper flow regime bedform dynamics and upper stage transport dynamics in unidirectional stream flows, these concepts should also apply to swash zone flows. This suggestion is supported by theory and empirical observations.

Analytical treatments of bore propagation and conversion to runup are reviewed by Miller (1968), Meyer and Taylor (1972), Waddell (1973), Nelson and Miller (1974), and Bradshaw (1978) among others. The final phase of the runup process, following bore collapse, is described by equations governing the motion of a frictionless unit mass moving up an inclined plane with some starting velocity (swash), or started from rest moving down slope under the influence of gravity (backwash). These workers have pointed out that if friction is included in the analysis, this motion is analogous to that of unsteady stream flow.

Using criteria applied to unidirectional flows, Wright (1976) and Tanner (1977) have described the swash and backwash as shallow, rapid, supercritical flows (ie. upper

regime flows). In agreement with these observations, bedforms and stratification types generally associated with upper flow regime conditions are commonly found on sandy foreshores. Plane beds and horizontal lamination on the foreshore have been described by numerous workers (Thompson, 1937; Andrews and Van Der Lingen, 1969; Walker, 1979; Blatt et al., 1980; Reineck and Singh, 1980; McCubbin, 1982). The occurrence of antidune forms and backset cross-lamination on sandy foreshores has also been reported (Panin and Panin, 1967; McCubbin, 1982). It is particularly noteworthy that the presence of features exhibiting affinities to the bedwaves described in flumes have recently been observed on apparently planar foreshores. Waddell (1973, 1976) described bedforms that appeared to move downslope in the backwash. Sallenger and Richmond (1984) and Howd and Holman (1984a,b) described very long (~10-15m), low relief (1.0-6.0cm) bedforms that appeared to migrate shoreward in the swash.

Nelson and Miller (1974) studied the interaction of fluid and sediment in idealized swash cycles, through glass walls of a specially designed flume. Based on similarities in flow character and modes of sediment transport, they concluded that over short intervals swash and backwash flows could be regarded as decelerating or accelerating unidirectional flows. However, they did note that while this assumption is quite reasonable for backwash, it may be less so for swash. They divided swash into two parts; a highly turbulent, sediment-laden leading portion, and a less turbulent trailing portion, and suggested that if the vortex-like motion of the swash tip was excluded, it is reasonable to compare swash flows to unidirectional flows. As for the leading edge of the swash, similarities exist between its structure, as described by Nelson and Miller (1974), and that of the structure of a turbidity current head as described by Middleton and Southard (1984), among others (Figure 4.6). Both are highly turbulent, high concentration-density layered, decelerating flows.

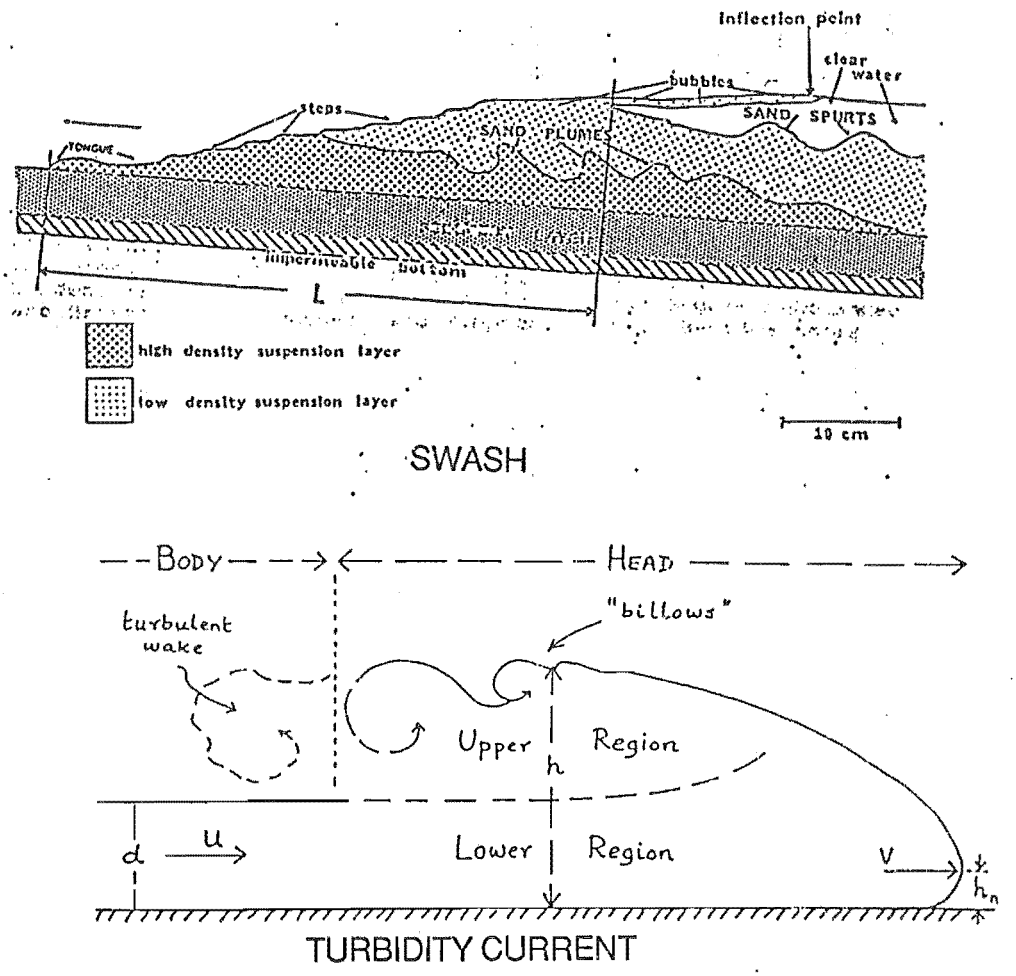

Figure 4.6. Schematic representations of the flow structure in a swash flow (Nelson and Miller, 1974) and a turbidity current (from Middleton and Southard, 1984). Note that both flows have a highly turbulent, sediment-laden leading portion, and have a lower - high concentration/low turbulence - layer and and upper - low concentration/high turbulence - layer.

4.2 RESULTS: NMB SWASH ZONE BEDFORMS, STRATIFICATION, SEDIMENT TEXTURES, AND FLOW CHARACTERISTICS

Having introduced the microdynamic framework and reviewed the key aspects of bedform and transport dynamics that are contained in it, this section describes bedforms, stratification, sediment textures, and flow characteristics observed in the upper foreshore of NMB.

4.2.1 BEDFORMS AND STRATIFICATION

Visual observation of the upper foreshore surface and analysis of the bed elevation time series (see Chapter 2) revealed that long wavelength, low relief features are the characteristic swash zone bedforms observed on NMB. Near-horizontal lamination was the stratification type most commonly observed in the upper foreshore trenches (see Chapter 2) at NMB. Low and high-angle, shoreward-dipping cross-stratification were also observed. These bedform and stratification types are described in greater detail below.

Bedforms

On the usually planar upper foreshore surface, antidune forms were occasionally visible. The antidune forms generally occurred in sets of 8-10 bedforms that migrated shoreward in the seaward flowing backwash. Their dimensions varied over a considerable range, but they were consistently characterized as long (mean wavelength=81cm), low (mean height=1.5cm) asymmetrical forms (Table 4.4).

TABLE 4.4 ANTIDUNE GEOMETRY

HEIGHT	Min. - Max.	
Complete Range	0.4 - 4.5 cm	
Mean Range	1.0 - 2.8 cm	Mean 1.5 cm
WAVELENGTH		
Complete Range	32 - 210 cm	
Mean Range	67 -102 cm	Mean 81 cm
SYMMETRY (shoreward : seaward)		
Range 1 : 4 - 1 : 1		Mean 1 : 2

(n=81, from 8 sets)

Although indiscernible visually, examination of the bed elevation time series suggests that other long, low bedwave forms also existed on the foreshore surface. The height, wavelength, and direction of migration of these forms was determined from the bed elevation times series referred to in Chapter 2 (Table 4.5; Figure 4.7a-f). Form wavelengths were found to be on the order of 10-20m. Form heights ranged from from 0.10-2.60cm. On two occasions (December 16 and 20), and in agreement with observations made by Howd and Holman (1984a,b), form height decreased continuously towards the shoreward-most location. However, on the other two occasions, such a trend was not evident. On one occasion (December 20[Figure 4.7b]), and again in agreement with the observations of Howd and Holman (1984a,b), form migration was principally towards the shore. On all other occasions, however, form migration was found to be shorewards lower on the foreshore, and seawards higher on the foreshore. Although not reported in their paper, similar patterns of bi-directional form migration were observed by Howd and Holman (P.A. Howd, pers. comm., 1990).

TABLE 4.5 BEDWAVE CHARACTRISTICS

DATE	HEIGHT (cm)			WAVELENGTH	MIGRATION
DEC. 16	a	0.2		10-20m	Shoreward
(n=60)	b	0.6			and
	c	0.7			Seaward
	d	2.1			
DEC. 20	a	0.2		" "	Shoreward
(n=26)	b	0.3			
	c	0.5			
	d	1.2			
DEC. 31	a	1.7	2.6	" "	Shoreward
(n=48)	b	1.1	1.6		and
	c	2.4	1.9		Seaward
JAN. 4	a	0.7	0.1	" "	Shoreward
(n=23)	b	2.2	2.2		and
	c	1.7	1.0		Seaward
	d	2.5	1.5		

Bedwave height for each location was calculated as twice the standard deviation of a demeaned and detrended bed elevation time series (Howd and Holman, 1984a); 'a' of Table 4.5 is the shoreward location, and 'b', 'c', and 'd' are located 5m seaward of this location consecutively. Form wavelength was determined from visual inspection of cross-shore plots of the bed elevation time series taken at different time intervals (Sallenger and Richmond, 1984). The direction of form migration was determined through cross-correlation analysis of the bed elevation time series (Davis, 1973; Howd and Holman, 1984a[see also Figure 4.7]).

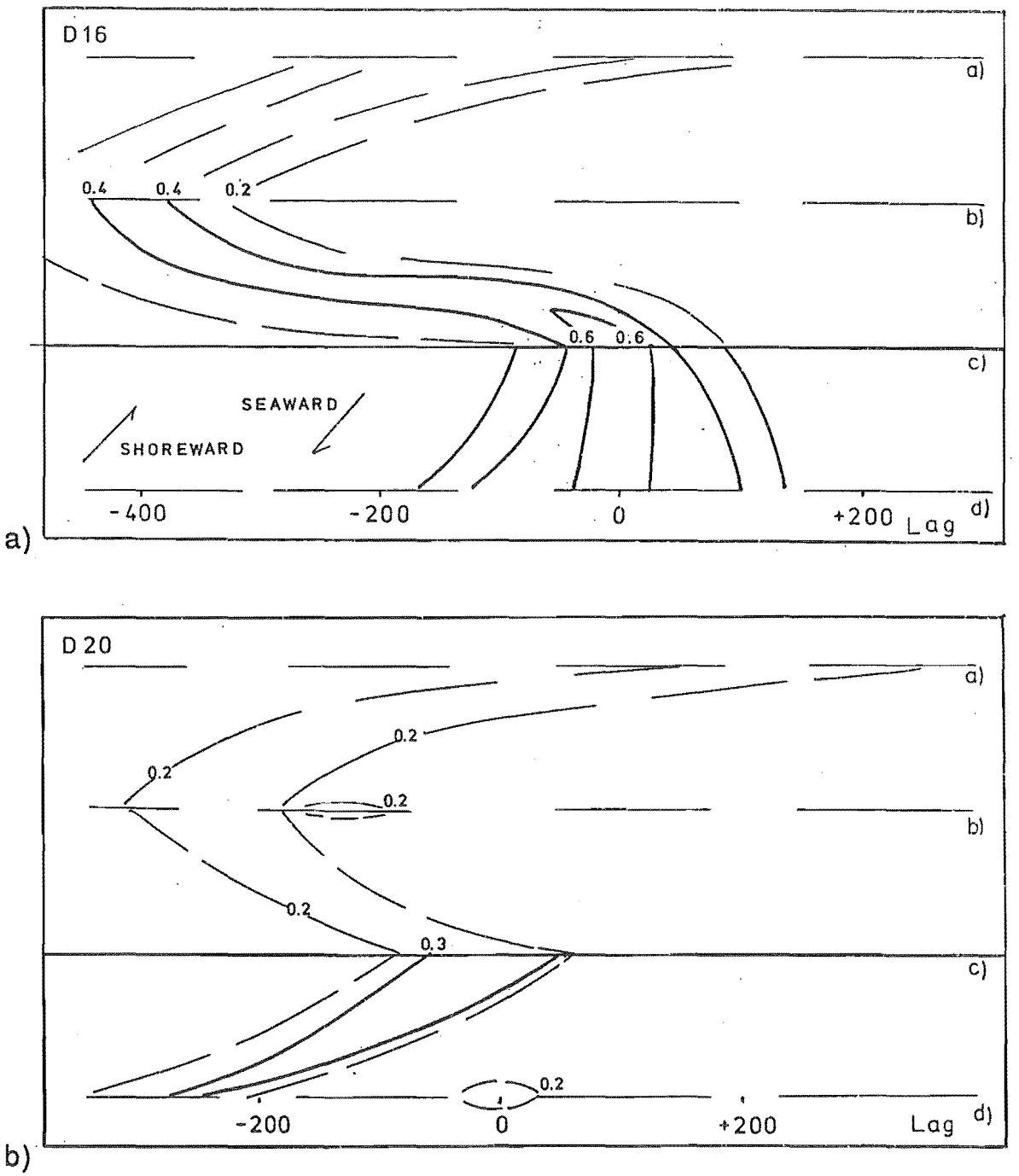

Figure 4.7a-f. Contour plots of cross-correlation to the reference time series ('c') versus lag distance (after the procedure outlined in Davis, 1973; Howd and Holman, 1984a). In these plots, positive or negative trends correspond to seaward or shoreward migration of the forms respectively: Solid lines represent significant correlation at or above the 90% level.

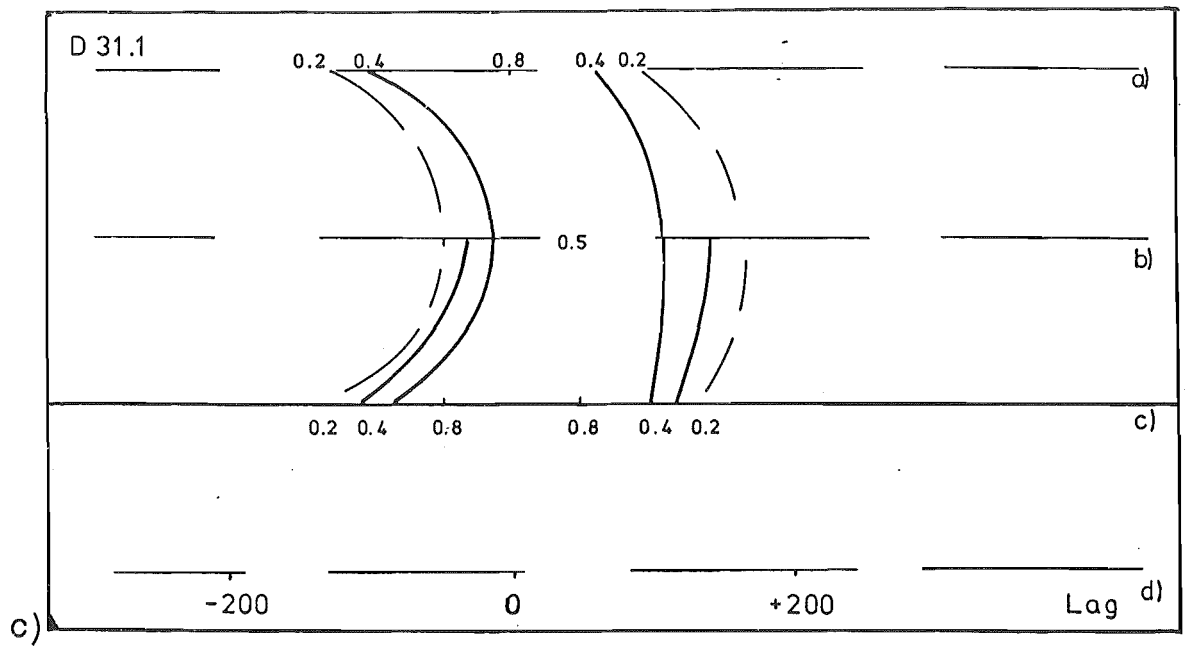
D 31.1
0.2 0.4 0.8
0.4 0.2
a)
0.5
b)
0.2 0.4 0.8
0.8 0.4 0.2
c)
-200
0
+200
Lag
d)

c)

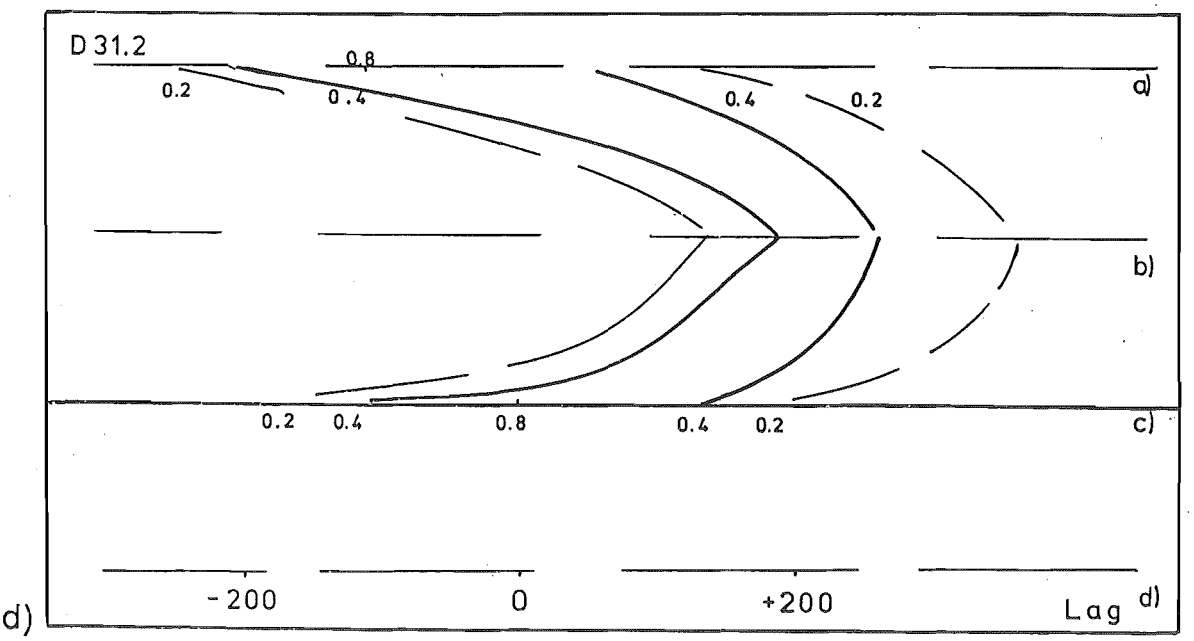
D 31.2
0.8
0.2
0.4
0.4
0.2
a)
b)
0.2 0.4 0.8
0.4 0.2
c)
-200
0
+200
Lag
d)

d)

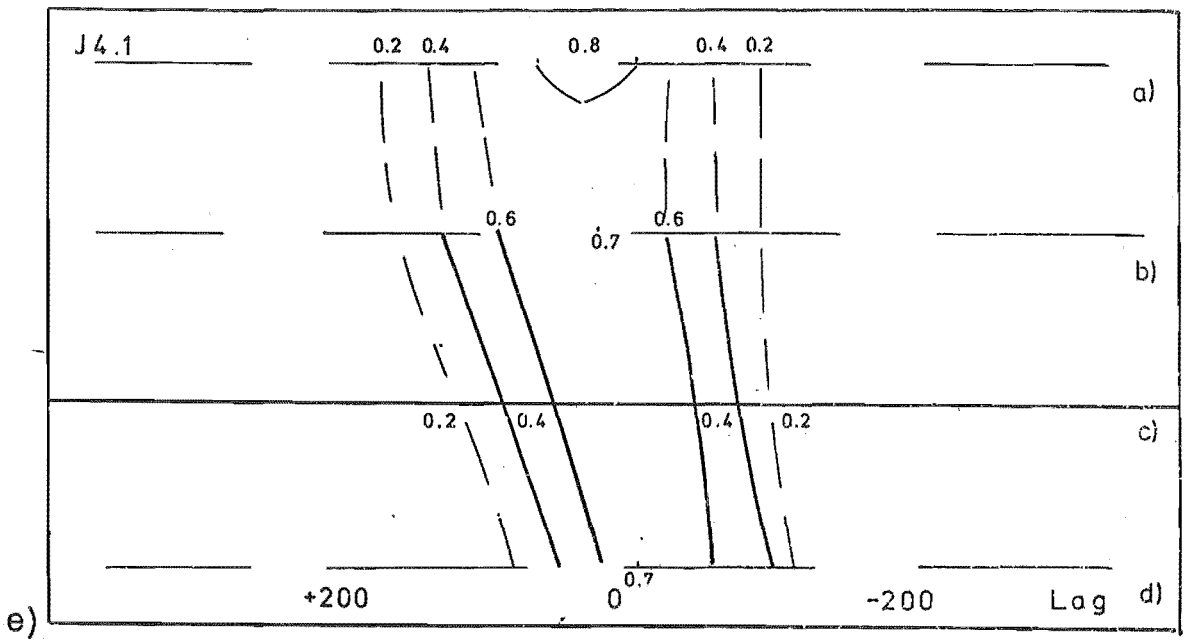
J4.1
0.2 0.4
0.8
0.4 0.2
a)
0.6
0.6
0.7
b)
0.2
0.4
0.4
0.2
c)
0.7
+200
0
-200
Lag
d)

e)

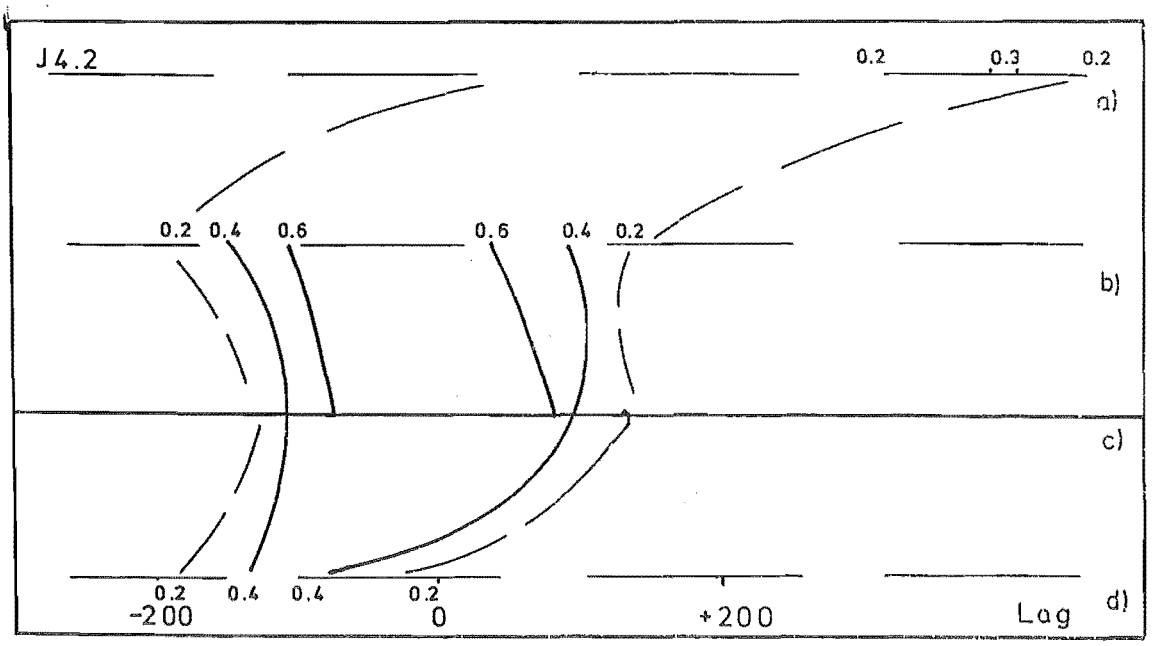
J4.2
0.2
0.3
0.2
a)
0.2 0.4 0.6
0.6 0.4 0.2
b)
c)
0.2
0.4
0.4
0.2
-200
0
+200
Lag
d)

f)

Stratification

The principal stratification types observed in the upper foreshore of NMB are illustrated in Plate 4.1 and Figure 4.8. Their characteristics are summarized in Table 4.6 and described below.

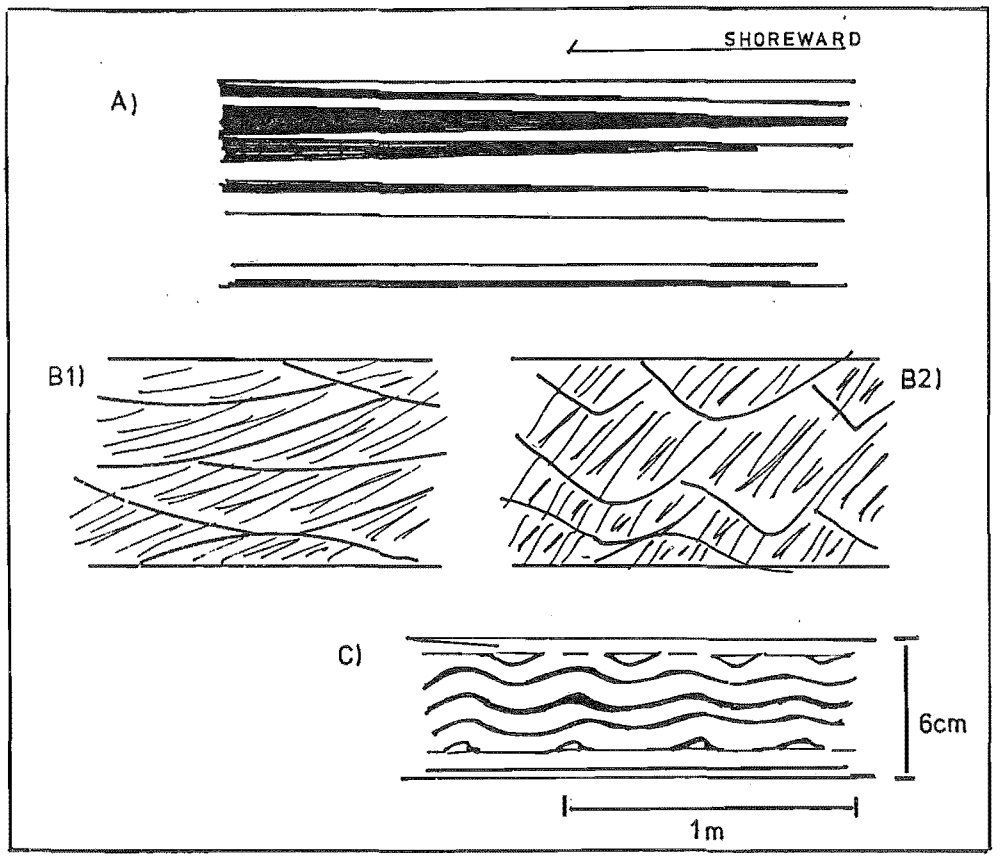

Figure 4.8. Illustrations of the principal stratification types observed in the upper foreshore of NMB (See also Plate 4.1 and Table 4.6).

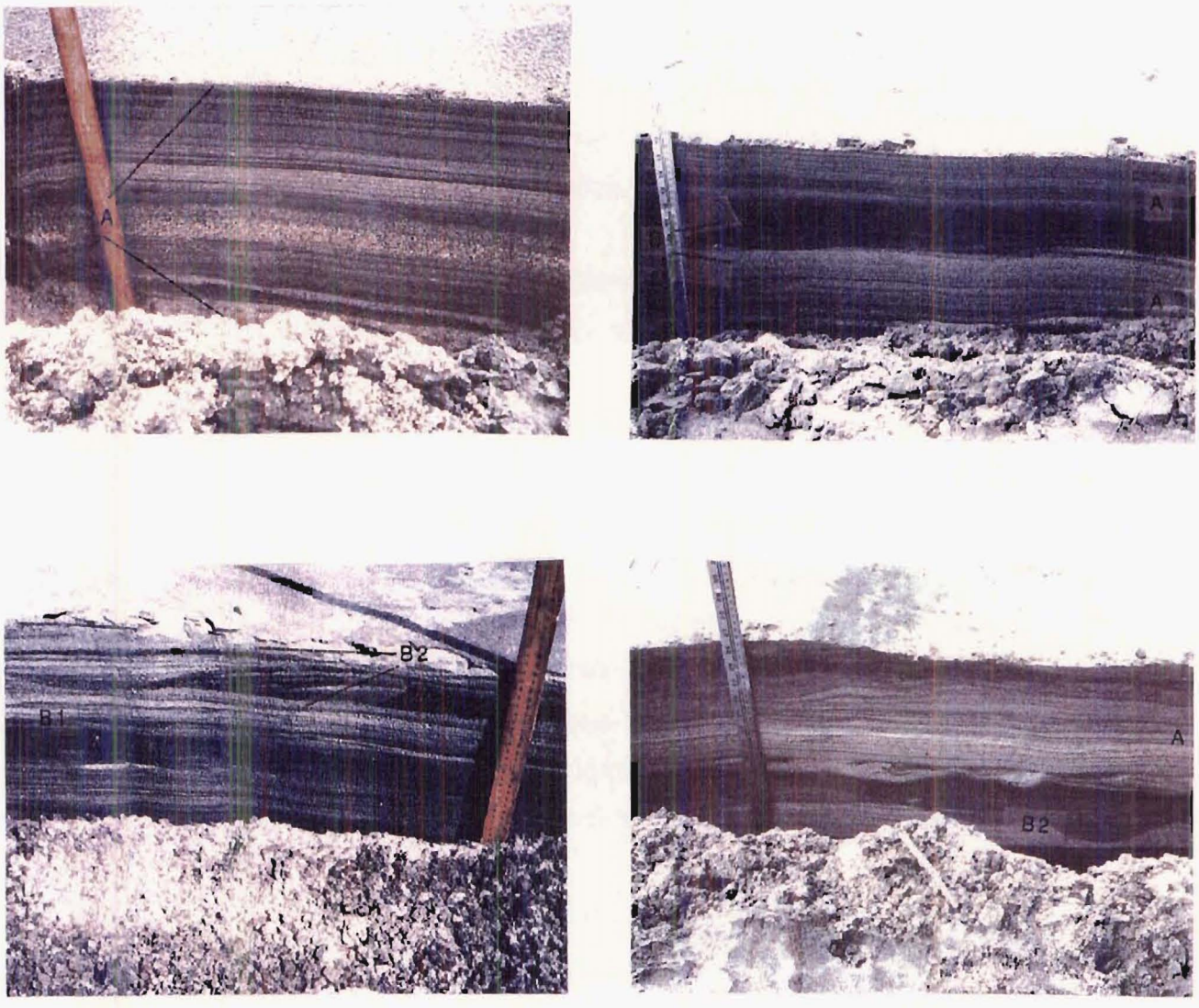

Plates 4.1. Stratification observed in upper foreshore trenches at NMB (see also Table 4.6 and Figure 4.8). Letters indicate: A) Near-horizontal lamination, B1) Low angle 'Foreset' cross-bedding, B2) High angle 'Backset' cross-bedding , C) Parallel wavy bedding.

TABLE 4.6 GEOMETRIC CHARACTERISTICS OF STRATIFICATION

A) NEAR-HORIZONTAL LAMINATION

Horizontal to low angle (2-3^{0}), seaward dipping.

THICKNESS -Thin bedded to thinly laminated; most 0.1-2.0cm, but ranging from 0.1-10.0cm. Contrasting thinner (0.1-0.5cm) finer grained, better sorted and/or heavy mineral-rich layers: thicker (0.5-2.0cm) coarser grained, poorer sorted, quartz-rich laminae.

LENGTH -Most in the 1-2m range; parallel, tabular to wedge shaped laminae (1-5m) predominant. Subtle, low angle bounding surfaces.

B) CROSS-BEDDING

B1) FORESET Low angle (5-6^{0}), shoreward dipping.

THICKNESS -Very thinly cross bedded to cross laminated; generally 2.0cm, but ranging from 1.0-4.0cm thick.

LENGTH -Generally 1m; tabular to lenticular with low angle truncation/reactivation surfaces.
*Commonly in sets, but also occurs as isolated concave and convex lenses 10cm-1m in length, 0.5-2cm thick

B2) BACKSET High angle (12-25^{0}), shoreward dipping.

THICKNESS -Very thinly cross bedded; generally 5cm, but range from (3-6cm).

LENGTH -Generally 50cm, but range from 35-70cm; lenticular with high angle truncation/reactivation surfaces.

C) PARALLEL WAVY (Drape) LAMINATION

~20cm wavelength, 1-4cm thick

The principal stratification type observed in the trenches was near-horizontal lamination (Type A). The lamination was defined by the alternation of thinner, better sorted, darker-colored, finer-grained layers, and thicker, poorer sorted, lighter-colored, coarser-grained layers. Individual layers were horizontal to low angle (2-3°) seaward dipping. Layer thicknesses ranged from thinly laminated (<0.3cm) to thin bedded (3-10cm); most were in the 1mm-2cm thickness range. Individual layers were traced cross shore for distances up to 5m, but most were 1-2m in length. The layers were tabular (plane parallel) to wedge-shaped (plane nonparallel). Close inspection of layers revealed subtle, low angle concave and convex discordances along bounding surfaces. Thus many layers were actually slightly curved, and resembled long, extremely low amplitude wave forms in shape.

Two principal forms of cross-bedding were distinguished (Figure 4.8, Table 4.6) The most common consisted of low angle (~5-6°), shoreward dipping, long (~1 m), tabular or wedge- shaped to wavy, very thinly cross-bedded (~2cm thick), fine-medium sands (Type B1-foreset). Internally the cross strata commonly exhibited a progressive decrease in slope and became sub-horizontal towards the upper boundary. Low angle reactivation surfaces were also common. Although this stratification type usually occurred in sets, occasionally it appeared as an isolated lens of fine or coarse sand within a matrix of near horizontal lamination.

High angle (~12-25°), shoreward-dipping, trough-shaped (~50cm long), very thinly cross-bedded (~3-6cm thick), fine-medium sands were observed less frequently (Type B2-backset). These trough cross strata tended to occur in the uppermost portion of the upper foreshore as sets with intersecting scour surfaces. Internal layers were commonly sub-parallel with the basal scour surface and progressively steepened towards the upper portion where they were truncated. High angle reactivation surfaces were common internally.

Finally, although rare, parallel wavy beds (Type C) 1-4 cm thick and ~20cm in wavelength were also observed in the upper foreshore trenches.

4.2.2 SEDIMENT TEXTURES

Based on the systematic variation of textural parameters that occurred within and between grain layers in the sediment peels (see Chapter 2), two lamination types were recognized in the upper foreshore of NMB (Table 4.7). Heavy and light minerals within grain layers of **Type 1** lamination are inferred to be in a standard form of dynamic equivalence. In contrast, heavy and light minerals in grain layers of **Type 2** lamination are inferred to be in a modified form of dynamic equivalence. Grain layers in Type 1 lamination are finer-grained, better sorted and more heavy mineral-rich than grain layers in Type 2 lamination. Finally, uniform to weakly inverse grading characterizes Type 1 lamination: Type 2 lamination has more complex grading patterns, exhibiting both inverse and normal grading.

The two lamination types are described in greater detail below. The basis for the segregation of the two lamination types is also considered below.

Dynamic Equivalence

Vertical plots of the mean grain size of the individual quartz, garnet, and ilmenite populations are given in Figures 4.9a-e (see also Plates 4.2). These plots show relatively little variation between grain layers in the mean size of either of the two heavy mineral species. The uniformity of the two heavy mineral populations is also demonstrated by the low standard deviation of the garnet (0.015) and ilmenite (0.017) populations between grain layers (Table 4.8a). Thus, from grain layer to grain layer garnet and ilmenite populations exhibit an almost constant size ratio. These observations suggest the existence of settling and/or dispersive equivalence between the two heavy mineral species.

When the grain layer mean grain size values are used to calculate the mean grain settling velocities and grain dispersive pressures (see Chapter 2) of garnet (2.81cm/s; 0.001568 g/cm) and ilmenite (2.79 cm/s; 0.001437 g/cm) populations, the two heavy

TABLE 4.7 LAMINATION TEXTURAL CHARACTERISTICS

	TYPE 1	TYPE 2
INTRAGRAIN-LAYER PATTERNS		
-Quartz population		
Grain size and sorting	FINER, BETTER Mean Size 0.24mm Mean S.D. 0.06	COARSER, POORER Mean Size 0.35mm Mean S.D. 0.13
Distribution Shape	NORMAL	FINE SKEWED
-Composition	HEAVY-RICH Mean 69% heavy	QUARTZ-RICH Mean 53% quartz
-Dynamic Equivalence	STANDARD (dispersive)	MODIFIED (hindered settling)
INTERGRAIN-LAYER PATTERNS		
-Grading	UNIFORM to weakly INVERSE	INVERSE and NORMAL

mineral species exhibit a less than 1% difference in settling velocity, and an 8% difference in grain dispersive pressure (Table 4.8b). The close correspondence between garnet and ilmenite settling velocities is also observed in the plot of grain layer mean garnet versus ilmenite settling velocities given in Figure (4.10a). In this figure, points can be seen to cluster around a central location about the line corresponding to settling equivalence.

In comparison to the uniformity in mean size of the heavy mineral populations between grain layers , the mean size of the quartz populations vary widely from grain layer to grain layer. The wide range in mean quartz grain size between grain layers is evident in Figures 4.9a-e, where the line corresponding to the mean quartz grain sizes

FOLLOWING PAGES

Figures 4.9 (a-e). Schematic columns through the sediment peels and vertical plots of: 1) the mean grain size of the individual quartz, garnet, and ilmenite populations (darkest line is garnet, lightest line is ilmenite: sloid black lines denote settling and dispersive equivalent diameters), 2) the mean grain size of the total sample population, 3) the quartz content in each grain layer.

Plates 4.2. Grain layers in sediment peels. These photographs accompany the schematic columns shown in Figure 4.9a-e. Each photograph is numbered. This number is used in Figure 4.9a-e to indicate the date and the portion of the column that the photograph depicts.

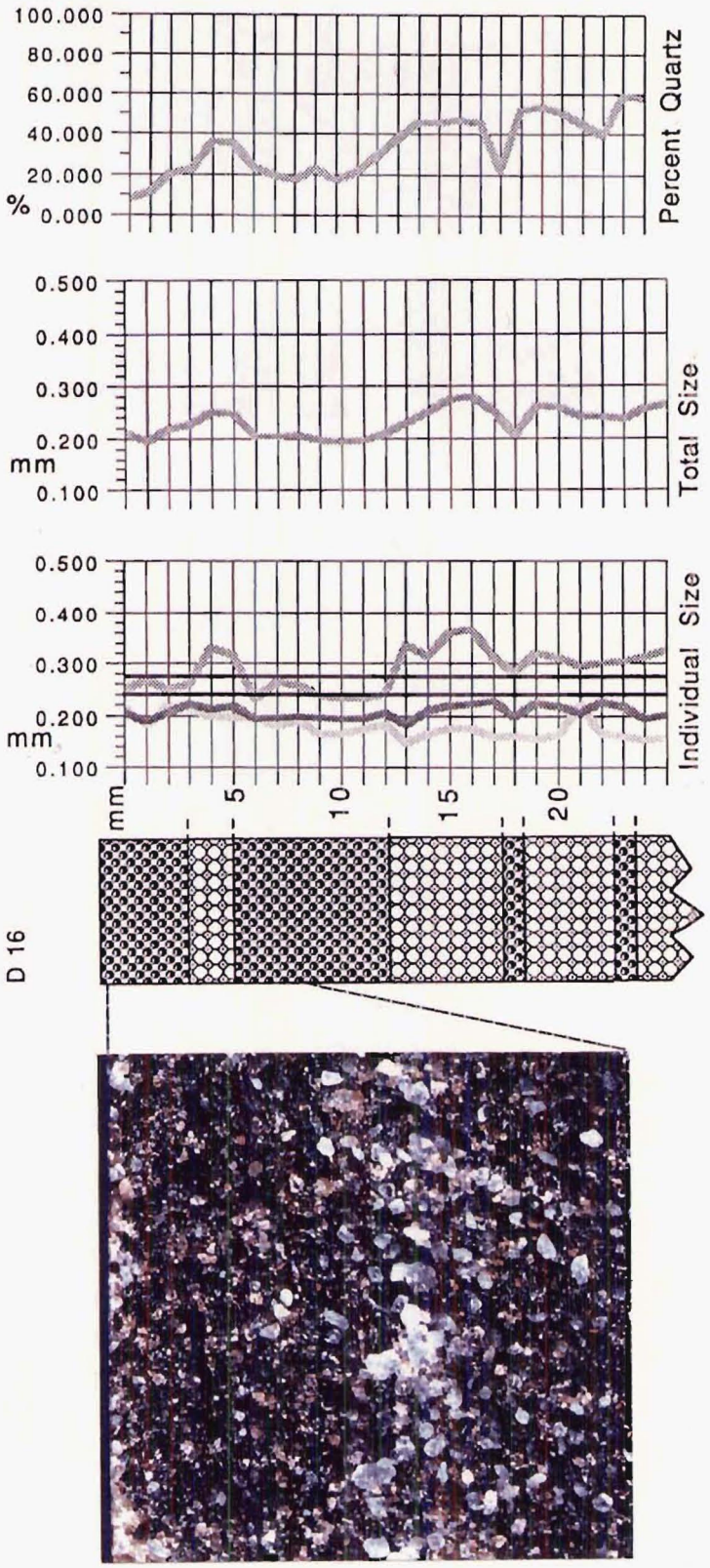
100.000
80.000
60.000
40.000
20.000
% 0.000
Percent Quartz
0.500
0.400
0.300
0.200
mm
0.100
Total Size
0.500
0.400
0.300
0.200
mm
0.100
Individual Size
mm
5
10
15
20
D 16

D 18
5
mm
Individual Size
0.100
0.200
0.300
0.400
0.500
mm
Total Size
0.100
0.200
0.300
0.400
0.500
mm
Percent Quartz
0.000
20.000
40.000
60.000
80.000
100.000
%

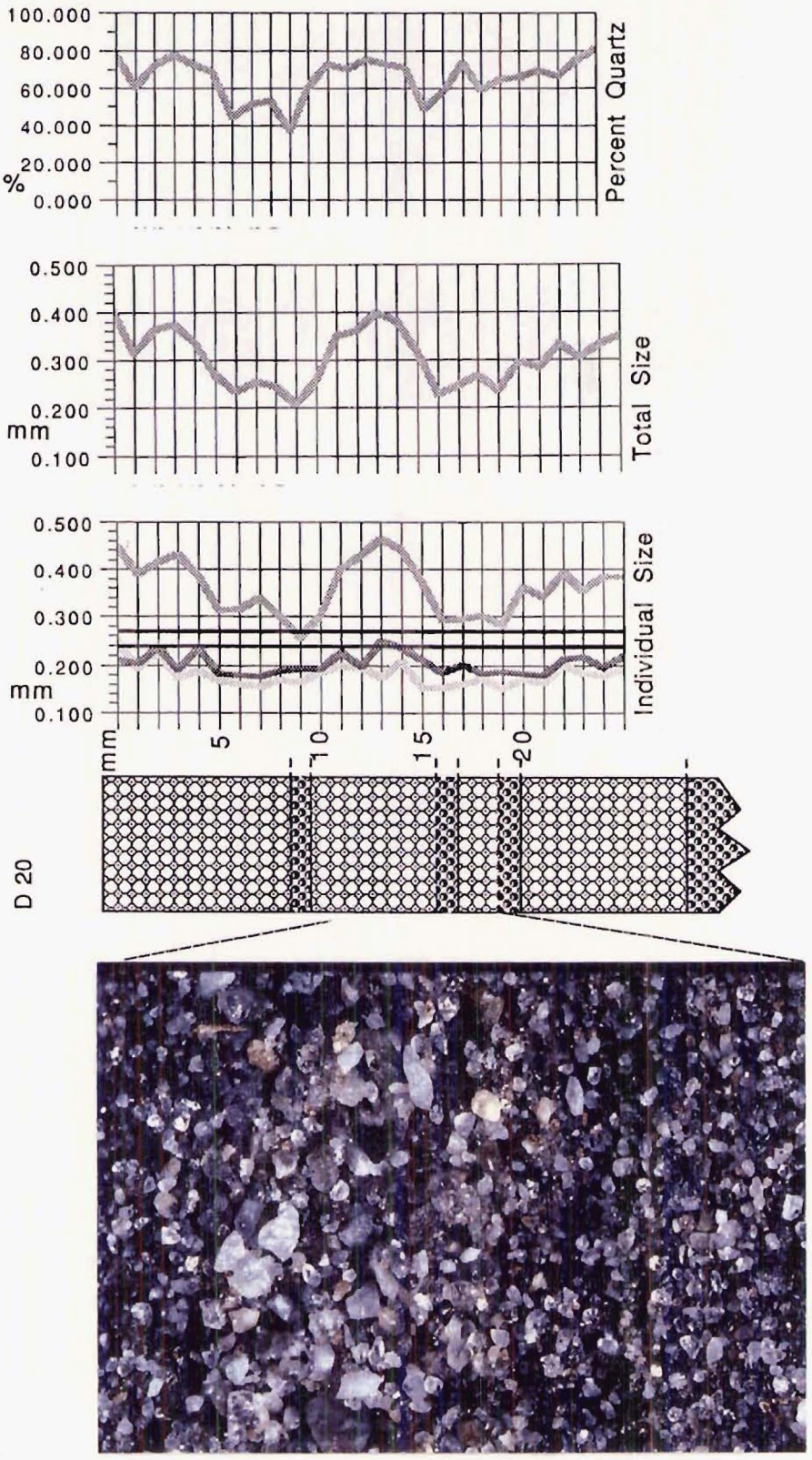
100.000
80.000
60.000
40.000
20.000
0.000
%
Percent Quartz
0.500
0.400
0.300
0.200
0.100
mm
Total Size
0.500
0.400
0.300
0.200
0.100
mm
Individual Size
mm
5
10
15
20
D 20

D 31
mm
20
15
10
5
Individual Size
Total Size
Percent Quartz
0.100
0.200
0.300
0.400
0.500
0.00
20.00
40.00
60.00
80.00
100.00
%

100.00
80.00
60.00
40.00
%
20.00
0.00
Percent Quartz
0.500
0.400
0.300
mm
0.200
0.100
Total Size
0.500
0.400
0.300
mm
0.200
0.100
Individual Size
mm
30
D 31

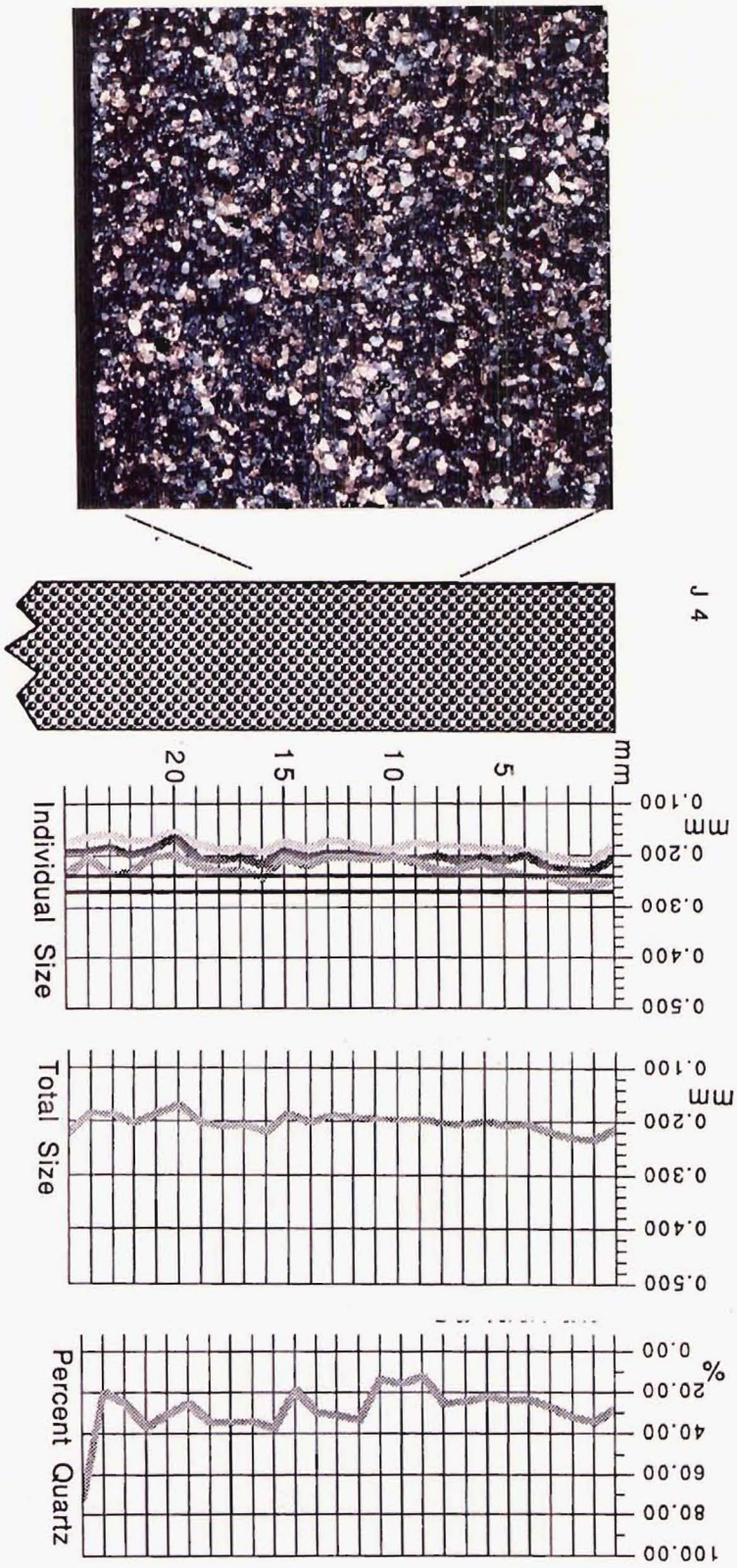
J 4
mm
20
15
10
5
Individual Size
Total Size
Percent Quartz
0.100
0.200
0.300
0.400
0.500
0.00
20.00
40.00
60.00
80.00
100.00
%

TABLE 4.8a MINERAL SPECIES POPULATION SUMMARY STATISTICS

	QUARTZ	GARNET	ILMENITE
MEAN SIZE (D(mm))	0.292	0.198	0.173
S.D.	0.066	0.015	0.017
MAXIMUM	0.721	0.248	0.251
MINIMUM	0.194	0.164	0.141
MEAN STANDARD DEVIATION	0.090	0.045	0.041
S.D.	0.046	0.010	0.016
MAXIMUM	0.374	0.083	0.161
MINIMUM	0.029	0.026	0.018

TABLE 4.8b QUARTZ AND HEAVY MINERAL EQUIVALENCE

	QUARTZ	GARNET	ILMENITE
Mean SIZE (D(mm))	0.292	0.198	0.173
DENSITY (r_s(g/cm^3))	2.65	4.0	4.8
Mean SETTLING VELOCITY (W_s (cm/s))	3.14	2.81	2.79
Equivalent Quartz Diameter (mm)	0.266		
Mean DISPERSIVE PRESSURE (g/cm)	0.002259	0.001568	0.001437
Equivalent Quartz Diameter(mm)	0.238		

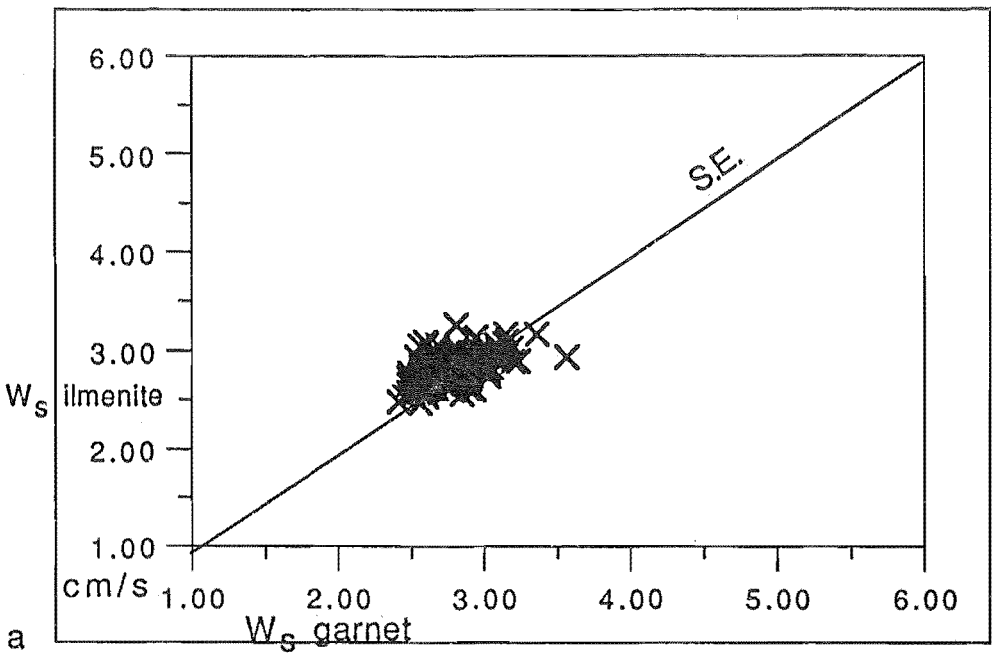

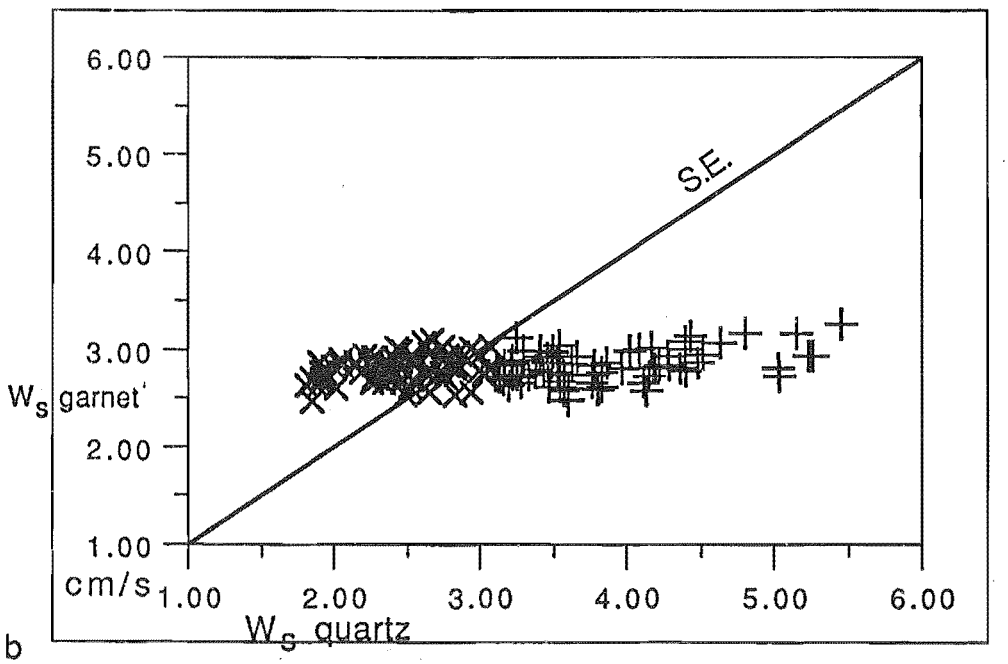

Figure 4.10. a) Plot of mean settling velocity of ilmenite versus mean settling velocity of garnet in grain layers; b) Plot of mean settling velocity of garnet versus mean settling velocity of quartz in grain layers. In both figures, the line labeled S.E. indicates settling equivalence. In b) x = Type 1 and + = Type 2 grain layers.

can be seen to vary widely with respect to the two heavy mineral lines. It is also evident in the high standard deviation of the mean of the quartz grain size given in Table 4.8a.

Using the quartz population mean grain sizes to calculate the mean grain settling velocity and grain dispersive pressure of the quartz population (3.14 cm/s; 0.002259 g/cm), and comparing it to the average values of the heavy mineral populations, gives differences of 11% and 34% respectively (Table 4.8b). Although the difference in mean grain settling velocities between the quartz and heavy mineral populations is not particularly large on average, it is evident form the plot of garnet versus quartz grain layer mean settling velocities given in Figure (4.10b), that points are widely scattered about the central location. Thus some quartz populations may be in settling equivalence while others are not.

In Figures 4.9a-e. values of settling and dispersive equivalent quartz diameters predicted from the mean values of the heavy mineral populations (Table 4.8b) are shown as lines in the vertical plots of ilmenite, garnet and quartz grain layer mean sizes. Again, the mean quartz diameters within some grain layers fall within the bounds, while others do not. Correspondingly, these observations suggest that some grain layer quartz populations exist in a standard form of dynamic equivalence with the two heavy mineral species, while others do not. A quartz grain diameter of 0.285mm is proposed as a reasonable upper boundary (7.5% of settling equivalent quartz diameter) for standard dynamic equivalence between the quartz and heavy mineral populations.

Intra-layer Patterns

The equivalence relationships described above, when combined with intra-layer quartz population grain size distribution characteristics, provide the basis for segregation of Type 1 and Type 2 grain layers.

The 0.285mm dynamic equivalence boundary noted above corresponds closely to a threshold diameter recognized in the plot of grain layer mean quartz size against standard deviation (Figure 4.11). In this figure sorting can be seen to vary linearly with

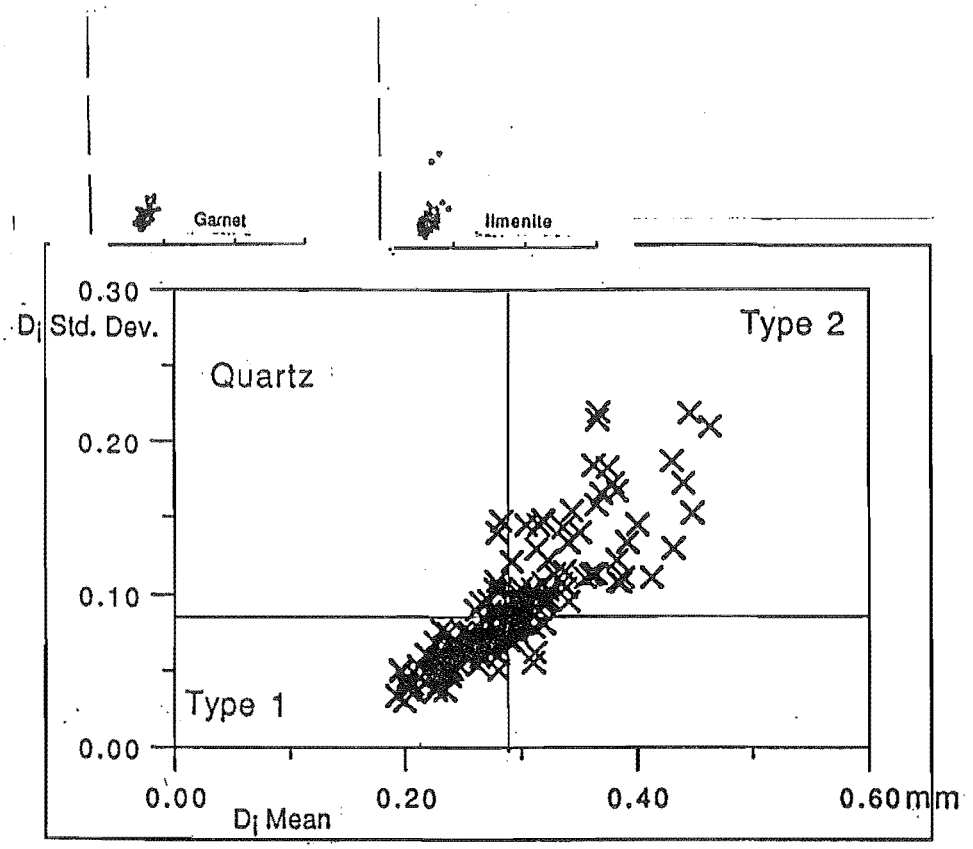

Figure 4.11. Plot of standard deviation versus mean grain size of quartz population in grain layers. The lines in this figure mark the threshold values referred to in the text and used to delineate Type 1 and Type 2 grain layers. (INSET (top): Plots of standard deviation versus mean grain size of garnet and ilmenite population in grain layers. Note, in contrast to the quartz population, how constant in size the two heavy mineral species are both within and between grain layers.)

mean grain size (increasing standard deviation with increasing grain size). While the linear relationship is well developed for the smaller grain sizes, beyond a mean size of ~0.3 mm it is less distinct. Above this threshold value standard deviation values are widely scattered, and tend to be high irrespective of the mean grain size.

Using the mean quartz grain size of 0.285mm and a corresponding standard deviation of 0.08 extrapolated from Figure 4.11, grain layer quartz populations were divided into two groups comprising 86.4% of all grain layers (Table 4.9a) Following from this segregation, it is noted that the standard dynamic equivalent quartz populations in **Type 1** grain layers are finer-grained and better sorted than the non standard dynamic equivalent quartz populations in **Type 2** grain layers (mean quartz grain size 0.241mm versus 0.346; mean std. dev. 0.057 versus 0.125 respectively [Table 4.9b]). Additional

TABLE 4.9a QUARTZ POPULATION CLASS FREQUENCY

SIZE	≤ .285mm	> .285mm
STANDARD DEVIATION		
	TYPE 1	
<0.08	43.5%	6.5%
		TYPE 2
≥0.08	7.1%	42.9%

TABLE 4.9b CLASS GRAIN SIZE SUMMARY STATISTICS

	TYPE 1	TYPE 2
MEAN SIZE (mm)	0.241 S.D.0.03	0.346 S.D.0.06
MEAN STANDARD DEVIATION	0.057	0.125
MEAN MAXIMUM SIZE (mm)	0.0397	0.801
MAXIMUM SIZE (mm)	0.598	1.605

summary statistics for the two grain layer quartz populations are given in Table 4.9b.

Besides the contrasts in grain size and sorting between Type 1 and Type 2 grain layer quartz populations, the grain layer quartz populations also exhibit differences in distribution shape (skewness and kurtosis). These differences are illustrated in Figures 4.12a and b, where grain layer quartz grain size distributions selected at random were classified on the basis of the criteria given above. In these figures, Type 1 quartz populations show more normal shaped distributions, while Type 2 quartz populations are

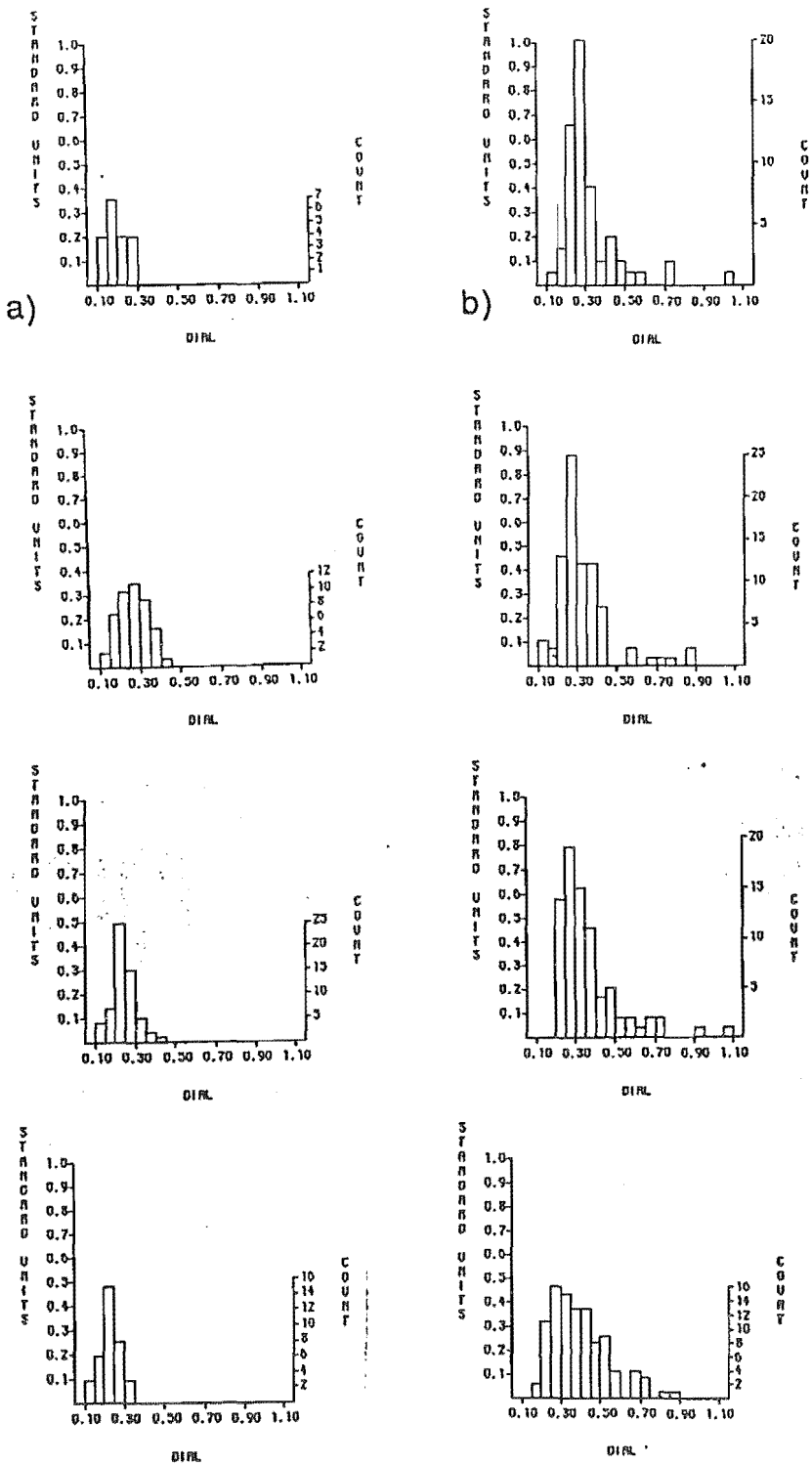

Figure 4.12. Grain size distributions of randomly selected grain layer quartz populations (a) Type 1 grain layers, b) Type 2 grain layers).

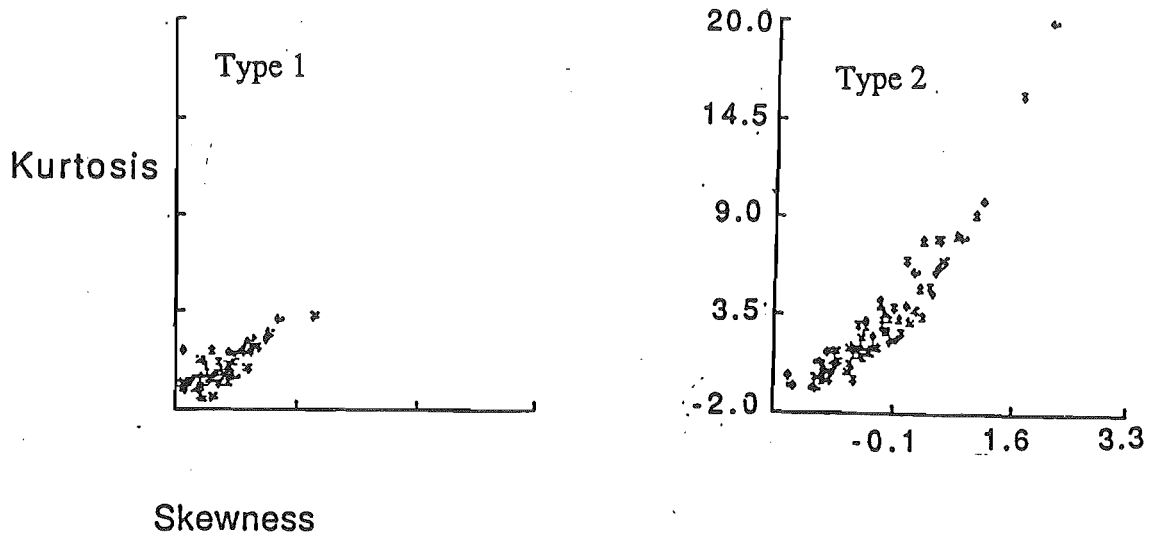

Figure 4.13. Plots of skewness versus kurtosis of quartz population in grain layers.

more fine skewed (ie. they have a fine grained peak and a well defined coarse tail). This visual observation was quantified by plotting distribution skewness against kurtosis for the two quartz populations (Figure 4.13). In this figure the two quartz populations can be seen to define two differently shaped distribution fields that correspond to the differences in distribution shape noted above.

Using the criteria described above to segregate them into Type 1 or Type 2 grain layers, the vertical sequence of grain layers observed in the peels were classified. The results of this classification are shown schematically in Figure 4.9a-e, where the vertical sequence of grain layer types are depicted in stratigraphic columns. In this figure groups of the same type grain layer define a lamination. That these classified laminae correspond to those observed visually can be seen in the photographs of representative sections of peel that accompany the stratigraphic columns (Plates 4.2). This agreement between prediction and observation supports the basic segregation of grain layer types outlined in this section.

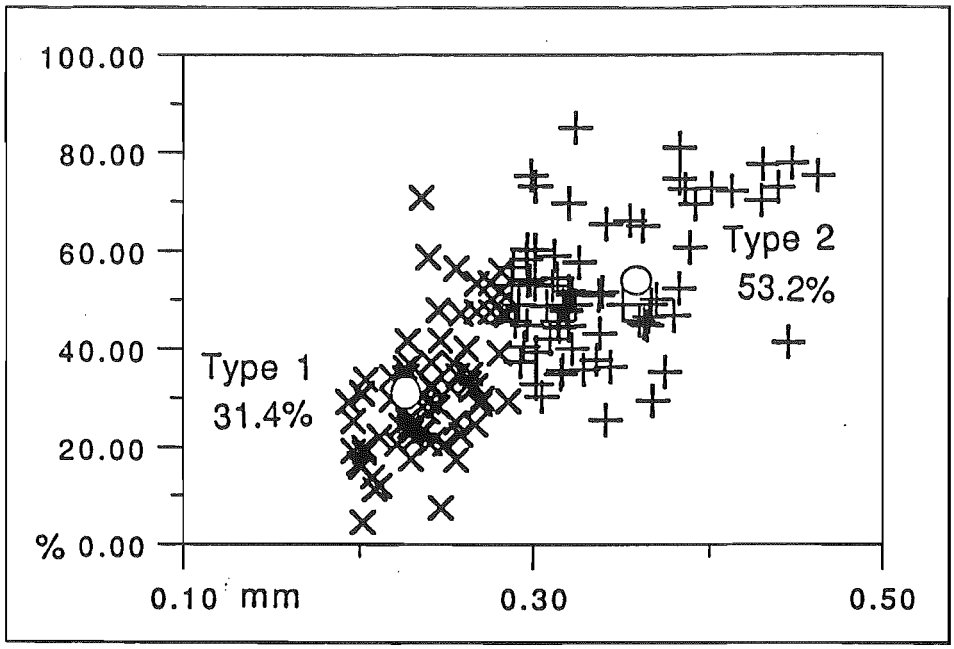

Figure 4.14. Plot of percent quartz versus mean grain size of quartz population in grain layers. (x = Type 1 and + = Type 2 grain layers; small circles indicate mean values for the two grain layer types).

Grain Layer Composition

Together with differences in dynamic equivalence and grain layer quartz population grain size distribution characteristics, differences in the quartz content also exist between the two lamination types. These differences are evident in Figure 4.14, where grain layer quartz content is plotted against mean quartz grain size. Examination of this figure shows a general trend of increasing quartz content in the grain layers with increasing mean quartz grain size. As a result, the finer-grained Type 1 grain layers are heavy mineral-rich, and the coarser-grained Type 2 grain layers are quartz-rich: Type 1 grain layers have a quartz content of 31%, and Type 2 grain layers a quartz content of 53% on average. These differences in composition are also evident in the vertical plot of the percent quartz within grain layers given in Figures 4.9a-e, where again the Type 1 grain layers show a lower quartz content than the Type 2 grain layers.

Inter-layer Patterns

A plot of the vertical sequence of mean grain size through the peels is shown in Figures 4.9a-e. Three types of grading are recognizable in these plots - normal, inverse, and uniform. Closer inspection of these plots in conjunction with the stratigraphic columns referred to earlier suggests that groups of Type 1 grain layers/Type 1 laminae tend to show uniform to weakly inverse grading. In contrast, groups of Type 2 grain layers/Type 2 laminae tend to have more complex grading patterns, showing both normal and inverse grading. Ideally, Type 2 lamination is characterized by a lower coarsening-upwards sequence that is followed by an upper fining-upwards sequence. In addition to the contrast in inter-layer grading, note that the finer, heavy mineral-rich Type 1 lamination is generally thinner than the coarser, quartz-rich Type 2 lamination.

4.2.3 FLOW CHARACTERISTICS

Swash and backwash flow characteristics obtained from the runup video recordings (see Chapter 2) are summarized in Table 4.10. The principal difference between swash and backwash is that the swash is a decelerating flow and the backwash is an accelerating flow. Also, as noted in the background section, the swash has a sediment laden, turbulent leading edge, whereas the backwash is relatively uniform along the entire length of the flow. Both swash and backwash are shallow, high velocity flows that posses a wavy free surface. However, surface flow velocities and bottom shear velocities in the swash are higher than those observed in backwash. This difference is offset by the backwash being a shallower flow than the swash. As a result Froude numbers in the backwash are higher than those in the swash.

Statistics of surface flow velocity, flow depth, bottom shear velocity, and Froude number observed in the swash and backwash are summarized in Table 4.11. They are used below to consider swash and backwash flow characteristics in greater detail. Results from December 18, when only five swash/backwash events were recorded, are excluded from the description.

TABLE 4.10 COMPARISON OF SWASH AND BACKWASH FLOWS

SIMILARITIES

Shallow, high velocity, transitional, supercritical 'sheetflows'

DIFFERENCES	SWASH	BACKWASH	
	Decelerating flow	Accelerating flow	
	Turbulent leading edge	Uniform	
Mean 85-100 cm/s Maximum 625 cm/s	Higher velocity	Lower veolicty	Mean 60-75cm/s Maximum 330cm/s
Mean ~7.5cm	Deeper	Shallower	Mean ~2.5cm
Mean 4.2_r-2.6_t cm/s Avg. Max. 8.5cm/s Absol. Max. 28cm/s	Higher bottom shear	Lower bottom shear	Mean 3.5_r-2.0_t cm/s Avg. Max. 6.5cm/s Absol. Max. 15cm/s
	Lower Froude number	Higher Froude number	

r=rough:t=transitional

TABLE 4.11 SWASH AND BACKWASH FLOW PARAMETERS

		$\overline{\text{Velocity}}$ (cm/s) (S.D.)	Max	$\overline{\text{Depth}}$ (cm) (S.D.)	Max	$\overline{\text{Froude \#}}$	$\overline{\text{max}}$	$\overline{U_*}$ rough (cm/s)	$\overline{\text{max}}$	$\overline{U_*}$ transitional (cm/s)
D16 n=91	SW	101.4 (46.4)	206.0	7.5 (5.4)	9.4	1.32	2.93	4.4	9.1	2.8
	BW	75.7 (38.0)	142.5	3.4 (2.4)	8.0	1.53	3.42	3.7	7.0	2.2
D18 n=5	SW	27.9 (8.4)	56.0	1.3 (0)	1.3	0.78	1.60	1.5	3.0	0.9
	BW	21.1 (11.6)	52.5	1.3 (0.2)	1.3	0.6	1.50	1.1	2.8	0.7
D20 n=42	SW	86.4 (51.2)	171.7	4.7 (4.2)	6.0	1.45	3.19	4.0	8.0	2.4
	BW	64.4 (39.8)	114.1	2.2 (1.3)	5.4	1.51	3.22	3.2	6.1	1.9
D31 n=72	SW	96.4 (44.6)	185.6	7.5 (7.1)	9.4	1.30	2.87	4.2	8.4	2.6
	BW	65.1 (34.6)	125.3	2.8 (2.5)	8.0	1.47	3.19	3.2	6.3	1.9
J4 n=31	SW	94.9 (36.4)	179.9	5.5 (3.6)	6.2	1.44	2.95	4.3	8.2	2.7
	BW	62.7 (33.2)	120.8	2.2 (1.0)	6.0	1.48	3.10	3.2	6.2	1.9

Velocity (U) and Depth (d)

Velocity and depth values obtained during the four data collection runs were similar. Mean time-averaged surface velocities of swash flows ranged from 86-101 cm/s; backwash flows from 63-78 cm/s (Standard Error of the Mean ± 6%). Average maximum velocities observed ranged from 172-206 cm/s and 114-143 cm/s for swash and backwash respectively. The maximum velocity measured was 625cm/s for a swash flow and 333 cm/s for a backwash flow. Significant surface velocities ($U_{1/3}$) ranged from 134 -153 cm/s and 96-116 cm/s for swash and backwash flows respectively.

Mean time-averaged swash depths in the upper foreshore ranged from 5-8 cm; backwash depths from 2-3 cm (S.E.M. ±12%). Average depth maxima ranged from 6-9 cm and 5-8 cm for swash and backwash respectively. The maximum water depth measured was 50cm.

On average, backwash flow velocities were on the order of 50-67% that of swash flow velocities. Backwash flow depths were on the order of 50-80% that of swash flow depths.

Shear Velocity (U*)

Shear velocity values were calculated from equation (4.2) for fully rough velocity profiles. For the given set of conditions, flow velocities on the order of 600 cm/s are required to develop fully rough flows. (In contrast, flow velocities of ~20 cm/s correspond to smooth flows.) The fully rough shear values can be regarded as an upper boundary, as based on observed swash and backwash velocity, NMB swash zone flows were transitional.

Mean bottom shear velocities ranged from 4.0-4.4 cm/s in swash flows and from 3.2-3.7 cm/s in backwash flows (S.E.M. ± 6%) Average U* maxima ranged from 8.0-9.1 cm/s in swash flows and from 6.1-7.0 cm/s in backwash flows. Absolute shear velocity maxima of 28 cm/s and 15 cm/s were calculated for swash and backwash flows respectively. Significant mean shear velocities ($U^*_{1/3}$) ranged from 5.8-6.4 cm/s for swash flows and from 4.8-5.4 cm/s for backwash flows. Significant U* maxima ranged

from 11.6-14.5 cm/s and 9.2-10.1 cm/s for swash and backwash flows respectively.

In order to place a lower boundary on the shear velocity values, transitional values were calculated using the empirical correction given in Komar (1976). Based on these calculations, mean bottom shear velocities in swash ranged from 2.44-2.77 cm/s and mean bottom shear velocities in backwash range from 1.87-2.18 cm/s. These transitional values are significantly lower (60%) than the shear velocity values for fully rough conditions given above. 'True' values of bottom shear velocity could be expected to fall within the bounds given; values towards the lower end of the range are probably more realistic.

With respect to the applicability of the equations for velocity profiles and the resulting accuracy of bottom shear velocity values given here, (irrespective of the assumption of clear, uniform, steady flow), it is unclear to what extent they still apply in extremely shallow flows (2.5cm) that are common in the swash zone. Additionally, it is unclear to what extent the highly turbulent, bore-like leading swash edge, in contrast to the more uniform sheet that characterizes the remainder of swash, effects the bottom shear velocities given above.

Given these considerations, relative differences in values are probably of more consequence than absolute values. In this regard, and following from velocities and depths already given, swash shear velocities were consistently higher than backwash shear velocities. The average shear velocity in backwash was on the order of 80% that of the average in swash. This apparent asymmetry in swash versus backwash forces on the foreshore is considered in greater detail in Chapter 5.

Froude Number (Fr)

In both swash and backwash flows Froude numbers were consistently high, being above 1.0 about 80% of the time. Mean Froude numbers for swash and backwash flows ranged from 1.30-1.45 for swash and from 1.47-1.53 for backwash (S.E.M. ± 4%). Average Froude maxima ranged from 2.93-3.19 and 3.10-3.42 in swash and backwash

respectively. Absolute maxima of 8.94 in swash and 7.10 in backwash were recorded. These supercritical Froude numbers correspond with the presence of a variety of water surface features that were observed in both swash and backwash on NMB. These features include stationary wave forms, breaking wave forms, and migratory wave forms moving both with and in opposition to the flow.

While Froude numbers are high in both swash and backwash, on average the backwash was associated with higher Froude numbers than the swash. The backwash, for example, exhibited mean Froude numbers greater than 2.0 about three to four times more frequently than did the swash. Froude numbers above this value are associated with the occurrence of breaking waves on the surface (Broome and Komar, 1979), thus the backwash has a correspondingly greater likelihood of exhibiting these features.

4.3 INTERPRETATION AND DISCUSSION: NMB SWASH ZONE BED DYNAMICS

4.3.1 THE NMB MICRODYNAMIC MODEL

Following from the concepts outlined within the microdynamic framework, the deposit characteristics observed on the upper foreshore of NMB, and described above, are explained in terms of the superposition of processes operating near the bed and throughout the flow within upper flow regime/upper stage flows. Specifically, external deposit characteristics (bedforms and stratification) observed on NMB are associated with the stationary and migratory surface wave forms that are characteristic of upper flow regime flows: Internal deposit characteristics (intra and inter-layer textures) observed on NMB are associated with the two-layer near bed flow structure that is characteristic of upper stage transport. Within this general upper flow regime bedform/upper stage transport dynamics framework, a further distinction is made between deposit characteristics attributed to swash and backwash flows.

TABLE 4.12 THE NMB MICRODYNAMIC MODEL

DEPOSIT CHARACTERISTICS		PROCESSES
	BEDFORM DYNAMICS	
BEDFORMS	STRATIFICATION	
		BACKWASH
-Antidunes	-Backset cross-laminae	-Upstream migrating and breaking water surface waves
		SWASH
-Bedwaves	-Near-horizontal lamination and Foreset cross-laminae	-Downstream migrating water surface waves
	-Drape laminae	-Stationary water surface waves
	TRANSPORT DYNAMICS	
LAMINATION		
		BACKWASH
TYPE 1 -Uniform sized heavy and light grains -Standard dynamic equivalence -Heavy mineral-rich -Uniform grading		-'Viscous' traction carpet layer deposited instantaneously in areas of local deceleration within an accelerating flow -Dominant support mechanism Dispersive pressure -Additional support mechanisms Excess pore pressure and fluid trubulence -Maximum entrainment selectivity
		SWASH
TYPE 2 -Large light and small heavy grains -Non standard equivalence -Light mineral-rich -Lower inverse and upper normal grading		-'Turbulent' traction carpet and suspension cloud layers deposited sequentially within decelerating flow -Dominant support mechanism Fluid turbulence, hindered settling, and buoyancy effects in upper layer Dispersive pressure in lower layer -Minimun entrainment selectivity

Backwash Bedform and Transport Dynamics. Breaking and upstream-migrating water surface waves in the accelerating, seaward-flowing backwash are associated with the antidune and other shorter, higher amplitude in-phase bedforms that develop on the uppermost foreshore surface. Shoreward-dipping, high angle, trough cross-(backset)-bedding is the principal stratification type associated with these bedforms. The formation of Type 1 lamination, which is predominant in these deposits, is also interpreted in the context of backwash processes. The better sorted, finer-grained, heavy mineral-rich textures, with uniform to weakly inverse grading, and that exhibit dynamic equivalence between heavy and light minerals, are interpreted as traction carpet layers deposited instantaneously in areas of local deceleration within an accelerating flow.

Swash Bedform and Transport Dynamics. Stationary and downstream-migrating water surface waves in the decelerating, shoreward-flowing swash are associated with the longer, lower amplitude in-phase bedwave forms that develop on the upper foreshore surface. Near-horizontal lamination and shoreward-dipping, low angle trough cross-(foreset)-bedding are the principal stratification types associated with these bedforms. The formation of Type 2 lamination, which is predominant in these deposits, is also interpreted in the context of swash processes. The poorer sorted, coarser-grained, quartz-rich textures, with both normal and inverse grading, and that do not show dynamic equivalence between heavy and light minerals, are interpreted as mixed traction carpet and suspension cloud layers deposited sequentially within a decelerating flow.

These two groups of swash and backwash process-form/texture associations, which constitute the NMB microdynamic model, are summarized in Table 4.12 and are detailed below.

SWASH ZONE BEDFORM DYNAMICS

Several lines of evidence suggest that upper flow regime conditions prevail in swash zone flows on NMB.

Swash zone flow parameters described on NMB are comparable to swash zone flow

TABLE 4.13 SUMMARY OF SIMILAR FLOW DATA FROM PREVIOUS STUDIES

WORKERS	SLOPE (tan ß)	GRAIN SIZE D (mm)	DEPTH h (cm)	VELOCITY U (cm/s)	FROUDE NUMBER	SHEAR VELOCITY U_* (cm/s)
NATURAL BEACH						
Sand						
This Study						
(n=462)	0.049	0.19	s5.0-7.5	86-101†,l	1.30-1.45	4.0-4.4[w]
	(0.041-0.058)		b2.5-5.0	63-76	1.47-1.53	3.2-3.7
Miller &Zeigler, (1958), (n=2)	0.11,0.23	??	b6.0	164,189	2.14,2.46	
Wright, (1976) (n=6)	0.035	–	0.5-6.0	40-80	0.52-3.61	
Broome &Komar, (1979), (n=??)	0.01	0.18	~5.0-10.0	~100-200[e]	~1.0-2.0	
Bradshaw,(1982)r (n=1)	0.03	??	5.0-15.0	200-300[l]	1.65-4.89	
Violante &Tanner, (1985) (n=5)	0.082 -0.12	??	s2.0-8.0	72-125†	0.82-1.98	
			b1.0-5.0	60-89	1.07-2.85	
Gravel						
Kirk, (1970) (n=??)	0.087-0.213	??	s??	~180[im]	??	
			b??	~125	??	
LABORATORY						
Wave Tank						
Nelson & Miller, (1974), (n=~150)	0.035-0.052	~0.55	s2.6-15.8	18-370†	0.08-2.71	1.2-106[w]
			b1.7-12.3	12-203	0.13-2.42	0.2-35
Flume						
Kennedy,(1961) (n=27)	0.0017 -0.016	0.23	4.5-11.0	42-106	0.70-1.49	3.6-12.2
Broome &Komar, (1979), (n=??)	0.005	??	5.0-7.0	60-100[mm]	~1.4-1.9	
Langford&Bracken, (1987),(n=??)	0.015	0.15	10	~90-170	0.99-1.70	
Bridge & Best, (1988),(n=??)	0.0071-0.0083	0.30	10	60-98[mm]	0.61-0.98	4.4-5.2[w]
Paola etal., (1989),(n=??)	–	0.40	9.0-10.5	100-128	1.12	

s=swash
b=backwash
w= wall law
l=leading edge velocity
e=estimated
Im=instrumented, maximum
mm=instrumented, mean at mid-depth
† = surface velocity from 'float'
* = $U_{1/3}$

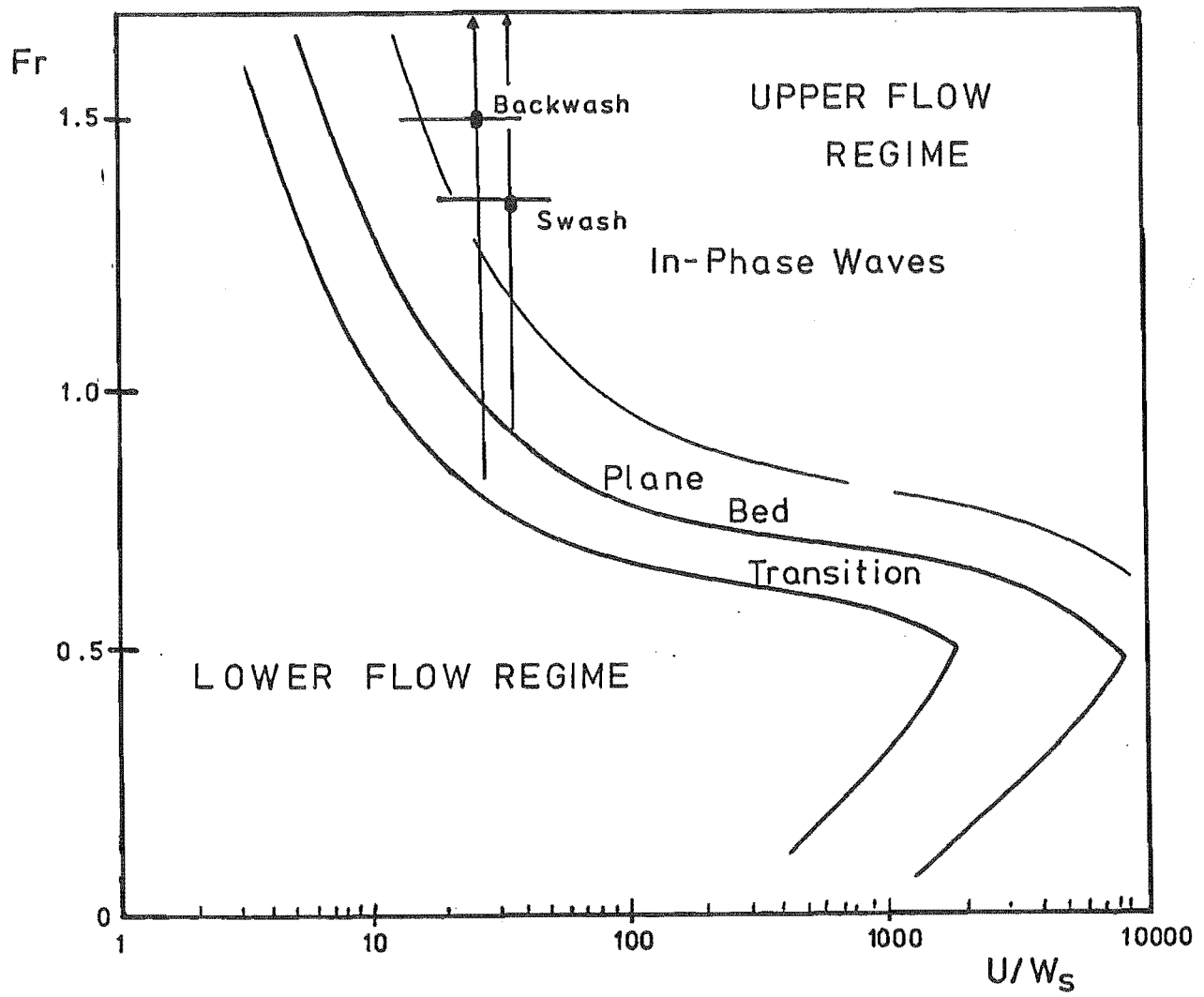

Figure 4.15. Plot of NMB swash zone flows on a bedform stability field diagram modified after Znamenskaya (1969). The mean and range of mean Froude number - flow velocity / settling velocity combinations for both swash and backwash are indicated separately in this figure.

parameters described elsewhere (Table 4.13). These flow parameters inturn compare favorably with flow parameters described for unidirectional flows in flumes during upper flow regime conditions (Table 4.13). These observations are in agreement with those made by Wright (1976) and Tanner (1977) and noted earlier.

Although NMB flow conditions plot in areas not normally depicted in bedform stability field diagrams, it is apparent in Figure 4.15, a bedform stability field diagram

from Znamenskaya (1969), that both swash and backwash flow parameters plot within the in-phase wave portion of the upper flow regime. Even for the more extreme conditions, swash zone flows do not plot any lower than the transitional area in this diagram. These observations are in agreement with those made by Nelson and Miller (1974), who also plotted swash zone flows on bedform stability field diagrams and found them to plot primarily within the upper flow regime.

Bedforms and stratification types observed on NMB (i.e antidunes, near-horizontal lamination, and backset bedding) are analogous to those described on sandy foreshores by a number of workers. Again, as noted in the background section, these bedforms and stratification types are the same as those developed during upper flow regime conditions as described by Cheel (1990) among others.

Finally, correspondence between flow and both form and stratification length scales is generally as predicted by Kennedy's (1961) relationship. In Table 4.14 the scale of bedforms, stratification, and predicted wave forms in the flow are compared to swash and backwash flow velocity values using equation (4.1). In this table it can bee seen that antidune and other bedwave length scales give predicted velocity values well within the range of observed flow velocity values. Similarly, the length scales of stratification give predicted velocity values that are within the average range of swash and backwash flow velocities. Thus, at NMB swash zone bedforms appear to be coupled to the form of the free surface.

Both swash and backwash are upper regime flows. However, if Kennedy's relationship is used to predict form length from observed velocities (the opposite of above), and if it is principally significant flow events that determine bedforms and stratification, then the differences in swash and backwash velocities suggest that specific bedform and stratification types are developed in each of these flows (Table 4.14). The shorter wavelength antidune forms and associated backset cross-bedding correspond to the lower end of the flow velocity range, and thus to the backwash which has the lower maximum velocities; the longer wavelength bedwaves and associated horizontal lamination correspond to the higher end of the flow velocity range, and thus to the swash

TABLE 4.14 PREDICTED AND OBSERVED FORM LENGHTS AND FLOW VELOCITIES USING KENNEDY'S (1961) RELATIONSHIP $U^2 = g\ L_b / 2\pi$

OBSERVED LENGTH (cm)	PREDICTED VELOCITY (cm/s)	OBSERVED VELOCITY (cm/s)		PREDICTED LENGTH (cm)	
		SWASH	BACKWASH	SWASH	BACKWASH
BEDWAVES					
1000-2000	400-560	Abs.Max. 625	333	2500	710
ANTIDUNES					
Max. 210	181	Sig.Max. 332	212	706	288
Mn Max. 102	126	266	182	453	212
Mean 81	112				
Mn Min. 67	102	Avg. Max 206	143	272	131
Min. 32	71	172	114	189	83
STRATIFICATION					
Cross-Bedding		Sig. 153	116	150	86
70	105	134	96	115	59
50	88				
35	74	Mean 101	76	65	37
Near-horizontal Lamination		86	63	47	25
100	125				
200	176				
500	279				
Wavy Bedding					
20	56				

which has the higher maximum velocities. (The tendency for horizontal lamination to exhibit smaller length scales than associated bedwaves could be accounted for by truncation of laminae, as is observed in cross-cutting relationships within the trenches.)

Cheel's (1990) upper flow regime bed phase model supports this interpretation based on Kennedy's relationship. The succession of bed phases that Cheel gives (with increasing flow velocity for a constant depth) may also be considered as a succession of bed phases that would be expected to occur with increasing Froude number (which would allow for different flow velocity and depth combinations). It was noted in the results section that it was the the backwash that had higher Froude numbers and therefore had a greater likelihood of exhibiting upstream-migrating and breaking water surface waves. Thus, the corresponding bed phase (i.e. antidune bedforms and backset bedding) would be expected to be the prominent backwash bed phase: The lower bed phases (i.e. downstream-migrating bedwaves and associated near-horizontal lamination and foreset cross-bedding) would be expected to be the prominent swash bed phases.

The cross-shore zonation of bedforms and stratification types (considered at length in Chapter 5) provides additional support for distinctive swash and backwash bedform/stratification type associations. Antidunes and backset bedding occur primarily in the uppermost foreshore at NMB. It is this area of the foreshore that is dominated by the backwash. Conversely, antidunes and high angle cross lamination are rare lower on the foreshore, where horizontal lamination is prevalent and the swash dominates.

Finally, the occurrence of seaward (i.e. backwash-induced) form migration on the uppermost foreshore and shoreward (i.e. swash-induced) form migration lower on the foreshore, reported earlier, also supports the distinction made above. In this respect, according to the interpretation made here, the contrasting observations on the directions and causes of swash zone bedwave migration reported by Waddell (1973, 1976), Sallenger and Richmond (1984), and Howd and Holman (1984a, b) are viewed as further evidence for the existence of separate, but genetically related swash and backwash bedform types and the more general distinction between swash and backwash bedform

dynamics.

SWASH ZONE TRANSPORT DYNAMICS

In the preceding section, the swash and backwash were established as upper flow regime flows. Based upon the connection between upper stage transport and upper flow regime conditions, it can be inferred that upper stage transport prevails in swash zone flows. In support of this suggestion, transport stage parameter values for NMB swash zone flows, based on mean shear and critical entrainment velocities, range from about 1.2-2.1. Although transport values around 1.2 may be somewhat low, in general these values are taken to be indicative of upper stage transport of fine-grained sands.

Process inferences based on the sediment textural patterns observed in the peels also suggest that NMB swash zone flows are upper stage flows, as they point towards the existence of a mixed traction carpet/suspension cloud near-bed flow structure. These process inferences are considered below. As was the case for swash zone bed dynamics, a distinction is made between swash and backwash transport dynamics. This distinction is based on differences between Type 1 and Type 2 lamination characteristics.

Models for Lamination Genesis in Swash and Backwash

Type 1 Lamination. In an accelerating upper stage flow, areas of deceleration exist locally (e.g. flow expansion over the trough of a bedwave). Thus, although the bed is being eroded, locally it experiences deposition. In this instance, it is only the lower traction carpet layer that is deposited on the bed, as it is this dispersive pressure-supported portion of the granular dispersion that is most sensitive to a change in flow strength (Lowe, 1982): The upper suspension cloud layer continues its movement over the bed. This scenario, of the local deposition of a traction carpet layer during conditions of net acceleration, is envisioned to take place in the backwash and to result in the formation of Type 1 lamination on NMB.

Earlier it was suggested that quartz and heavy mineral populations exist in settling

and/or dispersive equivalence within Type 1 lamination. Settling velocity values (W_s), values of critical shear velocity (U^*_e), and values of the shear velocity required to maintain a concentrated granular dispersion (U^*_d) are given in Table 4.15 for grain size and density combinations characteristic of Type 1 lamination. The close agreement between the 'critical dispersive shear velocity' of the coarser grains in the quartz population and those of the two heavy mineral species argues for the existence of dispersive equivalence between the quartz and heavy mineral populations in Type 1 lamination. Dispersive equivalence has been taken to be indicative of transport in a traction carpet layer supported by grain collision-generated dispersive pressure (Sallenger, 1979; Komar and Wang, 1984). The inverse grading exhibited in Type 1 lamination has also been suggested to be characteristic of dispersive pressure-supported traction carpet deposits (Clifton, 1969; Sallenger, 1979).

When compared to shear velocity values given in Table 4.15, the calculated swash and backwash shear velocity values (U^*) reported earlier are found to be insufficient to maintain the dispersion. Thus, although dispersive pressure may be the dominant support mechanism, contributing roles are probably played by other support mechanisms.

From the dynamic equivalence relationships reported earlier, and on the basis of the correspondence between mean quartz and heavy mineral settling velocities shown in Table 4.15, it could be argued that suspension sedimentation processes are important in the formation of Type 1 lamination. The lack of normal grading in Type 1 lamination, however, argues against this. Nonetheless, the role of fluid turbulence cannot be ruled out, and fluid turbulence probably does play a role in the maintenance of the dispersion (Lowe, 1982).

A more likely candidate as a significant support mechanism is excess pore pressure associated with the saturation of the foreshore. Excess pore pressure, through its effective reduction of the friction angle, would act to lower the the stress required for maintenance of a dispersion (Middleton and Southard, 1984). In the case of backwash, escaping pore fluid may slightly augment the flow itself (Emery and Foster, 1948), and

TABLE 4.15 HYDRAULIC GRAIN PARAMETERS OF LAMINATION TYPES

GRAIN PROPERTIES	U^*_e	W_s	U^*_d
TYPE 1 k_s = 0.020mm			
ILMENITE	1.96	2.79	5.16
Mean D_i = 0.018mm			
r_s = 4.8 g/cm^3			
GARNET			
Mean D_i = 0.020mm	1.71	2.81	4.89
r_s = 4.0 g/cm^3			
QUARTZ			
Mean D_i = 0.024mm	1.24	2.50	3.96
r_s = 2.65 g/cm^3			
Mean Max. D_i = 0.040mm	1.24	4.60	5.12
TYPE 2 k_s = 0.035mm			
ILMENITE			
Mean D_i = 0.018mm	2.71	2.79	5.16
r_s = 4.8 g/cm^3			
GARNET			
Mean D_i = 0.020mm	2.26	2.81	4.89
r_s = 4.0 g/cm^3			
QUARTZ			
Mean D_i = 0.035mm	1.48	4.00	4.78
r_s = 2.65 g/cm^3			
Mean Max. D_i = 0.080mm	1.45	9.50	7.24

U^*_e was calculated from equation (4.3). Equation (4.4) was used to calculate U^*_d (C_o was taken to be 0.65 and tan ϕ taken to be 32^o [Bagnold, 1966; Middleton and Hampton, 1976; Allen and Leeder, 1980; Komar and Wang, 1984; Hanes and Bowen, 1985; Hicks et al., 1988]).

work in combination with this support mechanism.

Heavy mineral-enrichment occurs during the Type 1 lamination formation process. Along the lines of the selective entrainment models proposed by Slingerland (1977) and Komar and Wang (1984), the high effective viscosity that exists in the traction carpet layer minimizes the effect of turbulence on entrainment, and maximizes entrainment selectivity. As a result only the most easily entrained (coarser, lighter) grains are removed from the bed, pushed up towards the top of the shear layer, and potentially moved out into the upper layer of flow. The (fine, heavy) grains (or lights that are equal to or smaller in size than the heavies) that are most difficult to entrain remain on the bed or within the basal shear layer. Through this selection process the 'clean' (well sorted - uniform sized heavy and light mineral), heavy-enriched Type 1 textures are developed.

Type 2 Lamination. A scenario similar to that outlined by Lowe (1982, 1988), for deposition of a combined traction carpet /suspension cloud in a decelerating fine-grained turbidity current, is envisioned to take place in the swash and to result in the formation of Type 2 lamination on NMB.

This scenario involves the sequential deposition of both the lower traction carpet layer and upper suspension cloud layer and therefore results in the preservation of the entire near-bed flow structure. The complex grading patterns of Type 2 lamination, characterized by an inverse graded lower portion that passes up to a normally graded upper portion, is suggestive of such a deposition process.

In this scenario, fluid turbulence is important throughout the flow, and is the dominant support mechanism in the upper suspension cloud layer. As was the case described above with respect to Type 1 lamination, dispersive pressure is the dominant support mechanism in the basal traction carpet layer. Evidence for dispersive pressure as a support mechanism is given in Table 4.15, where for Type 2 lamination, the critical dispersive shear velocity for mean-sized quartz approximates that of the two heavy minerals. The high dispersive shear velocities associated with the large quartz grains found in Type 2 lamination, however, suggests that other support mechanisms may also

be operating to maintain the dispersion.

Table 4.15 shows that the quartz grains associated with Type 2 quartz lamination possess high free settling velocities in comparison to those of the accompanying heavy mineral grains. This difference is particularly marked for the large quartz grains defining the coarse tail of the Type 2 quartz populations. Based on these latter observations, free settling is unlikely to have played a role in deposition of Type 2 lamination. However, if concentration-induced hindered settling and buoyancy effects are invoked, the apparently anomalous occurrence of the large quartz grains in Type 2 lamination can be accounted for. As noted by Kuenen (1951) and Lowe (1979), these processes act to reduce the effective single-particle settling velocities of the coarser grains and would allow for grains with different free settling velocities to be deposited together. Thus, although quartz and heavy mineral grains in Type 2 lamination do not represent a standard form of dynamic equivalence, they may be in dynamic equivalence nonetheless, as a modified form of settling equivalence.

Grain selection processes operating in the Type 2 scenario lead to the development of the 'dirty' (poorly sorted/coarse lights and small heavies) quartz-rich Type 2 textures. In contrast to the the selection process outlined for Type 1 lamination, fluid entrainment selectivity is at a minimum. Because of fluid turbulence almost any grain can be removed from the bed. Only the largest light and smallest heavy mineral grains remain on the bed The small heavy mineral grains remain because they are able to hide from the turbulence by sheltering between the large, light grains. The rapid rates of sedimentation associated with the deceleration of the swash flow further minimize the opportunity for any entrainment selection to occur.

Slope Effects

Consideration of slope effects, on bedform development and on entrainment, support the above distinctions between swash and backwash bedforms, stratification, and sediment textures.

Specifically, scour and fill is more efficient in downslope flows such as the backwash.

As a result bedform heights are amplified (Allen, 1983, 1985) and shorter, and thicker forms develop. Conversely, scour and fill is less efficient in up-slope flows, such as the swash. This tends to dampen bedform heights (Allen, 1983, 1985), and thus longer, thinner forms develop.

Also, the difference in swash and backwash slope should enforce flow acceleration/deceleration effects upon sediment transport: Greater stresses are required to transport sediment up-slope than downslope because in up-slope transport the sediment has to be carried up the slope as well as maintained off the bed (Bagnold, 1940; Allen, 1985).

The magnitude of this slope effect on entrainment was evaluated with a critical entrainment relationship given in Allen (1985) for quartz grains of varying sizes. Taking the mean beach face slope of 2.8° as representative, and using roughness diameters of 0.20 and 0.38mm, individual grain diameters of 0.20, 0.24, and 0.38mm, the increase in critical entrainment stresses required to move a grain upslope versus downslope ranged from about 1-15%. With lower roughness values this effect is accentuated. Thus, the fully developed traction carpet associated with Type 1 lamination is more likely to exist in downslope (backwash) flow than it is in up-slope (swash) flow.

4.3.2 IMPLICATIONS OF THE NMB MICRODYNAMIC MODEL TO MODELS FOR THE ORIGIN OF HORIZONTAL LAMINATION IN THE SWASH ZONE

Essentially two different models have been proposed specifically for the formation of horizontal lamination in the swash zone. One is a 'single process' model, the other a 'dual process' model.

Clifton (1969) recognized an inversely graded (in this case increasing in quartz content as well as coarsening upward) "two-fold sedimentation unit" as characteristic of lamination in the upper foreshore. He suggested that this light and dark couplet results from shearing of a high concentration bedload layer in the accelerating backwash and invoked dispersive pressure as the specific sorting mechanism. The work of Sallenger

(1979) supports Clifton's hypothesis. Sallenger (1979) measured grain sizes and densities in individual grain layers within beach lamination. In addition to observing inverse grading, he determined that the individual grain layers were in dispersive equivalence. Most workers accept this single process model as an explanation for the formation of horizontal lamination in the swash zone (Komar, 1989).

Thompson (1937) also observed alternating light and dark laminations in the upper foreshore. He suggested that the light layers resulted from suspension sedimentation in the decelerating swash. Thompson envisioned the dark layers as resulting from the combined effects of erosion of all but the heavy mineral-rich basal portion of the light layer in the ensuing backwash, and the addition of new heavy mineral grains deposited at the base of the light layer in the subsequent swash.

Besides Thompson, several other workers have also suggested that both swash and backwash play a role in lamination genesis (Sonu, 1972; Waddell 1973, 1976; Nelson and Miller, 1974; Slingerland, 1977, 1984). Slingerland's (1984) work is particularly noteworthy in this respect. Slingerland collected samples several grain layers thick from the upper foreshore surface following individual swash and backwash flow events and observed two contrasting textural types. He found that heavy versus light mineral settling velocity ratios of quartz-rich swash samples consistently approached unity, and suggested they were in settling equivalence. In contrast, the settling velocity ratios of heavy mineral-rich backwash samples were consistently greater than unity. Slingerland suggested that this deviation from standard hydraulic equivalence resulted from selective entrainment. Although not directly addressing the question of lamination genesis, and without reference to Thompson's (1937) work, Slingerland thus proposed essentially the same hypothesis of alternating settling in the swash and selective entrainment in the backwash as an explanation for his observations.

The interpretations made in this study, with respect to lamination genesis in the NMB swash zone, exhibit affinities to both the single and dual process models described above. However, the NMB model is more closely allied with the dual process model

suggested by Thompson (1937) and supported by the work of Slingerland (1984). The contrasts observed in bedforms, stratification, and sediment textures, taken together with a consideration of the differences in the nature of swash versus backwash flows, suggest that both backwash and swash play a role in lamination genesis on NMB.

This NMB model for swash zone lamination genesis does not preclude the single process model suggested by Clifton (1969) and supported by the work of Sallenger (1979), rather it incorporates it. The model for development of Type 1 lamination on NMB is analogous to the single process model. Furthermore, the possibility of a single process developing two different types of lamination is not ruled out by the present interpretation. To some extent this idea is applied in the case of Type 2 lamination genesis where, within the lamination, two layers are recognized to have been developed from what is essentially a single process. A single process model may also be valid in other situations, such as in lower stage transport, or aeolian transport, where internal lamination develops from grain avalanching. Internal cross-lamination observed on NMB may result from such a process.

Finally, according to the microdynamic framework, laminae observed in the swash zone of NMB are determined by flow-thickness scale processes as well as near-bed processes. This interpretation is in marked contrast to either of the two models for the formation of horizontal lamination in the swash zone described above. These models are limited to the consideration of smaller near-bed scale processes and do not consider the influence of the larger flow-thickness scale processes in lamination genesis.

4.4 CONCLUSIONS

In this Chapter the network of interactions that take place between grains, fluid, and bed within the swash zone of NMB were examined in the context of a microdynamic framework. According to this framework, deposit characteristics are inferred to result from the superposition of smaller scale near-bed processes, which control grain-size and sorting within the deposit, and larger scale processes that operate throughout the flow to

control bedform and stratification geometries. These two scales of interaction are referred to as *transport dynamics* and *bedform dynamics* respectively.

A secondary distinction between *lower stage/lower flow regime* and *upper stage/upper flow regime* dynamics is also made within the microdynamic framework. This distinction represents differences in the nature of interaction, as opposed to scales of interaction. Conceptually it is analogous to the distinction made in the previous chapter between different morphodynamic states.

Bedforms, stratification, sediment textures, and flow characteristics observed in the upper foreshore of NMB suggest that swash zone flows are upper stage/upper flow regime flows. Bedform dynamics within these shallow, high velocity flows is characterized by the occurrence of water-surface waves, and in-phase bedforms and associated stratification types. Bedform and stratification length scales, including near-horizontal lamination, were found to scale with those of the water surface waves as predicted by Kennedy's (1961) relationship. Similar to Lowe's (1982, 1988) and Hanes and Bowen's (1985) models, transport dynamics in the swash zone is characterized by the occurrence of a two-layer flow structure. Concentration effects are most important in the lower, *traction carpet layer* and least important in the upper, *suspension cloud layer* of the concentrated granular dispersion.

While swash and backwash were both classified as upper stage/upper flow regime flows, distinct microscale process-form assemblages were recognized for each flow type.

The existence of antidunes and associated backset cross-bedding in the upper most foreshore correspond with the occurrence of upstream-migratory and breaking water surface waves in the backwash. The finer grain sizes, better sorting, uniform to inverse grading, heavy and light mineral dynamic equivalence, and heavy mineral enrichment of Type1 lamination represents local deposition of a traction carpet layer within the accelerating backwash.

The existence of near-horizontal lamination and foreset cross-bedding lower on the foreshore corresponds with the occurrence of downstream-migratory and stationary water surface waves in the swash. The coarser grain sizes, poorer sorting, inverse and

normal grading, heavy and light mineral dynamic inequivalence, and quartz enrichment of Type 2 lamination represents deposition of combined traction carpet/suspension cloud layers within the decelerating swash.

Finally, the central theme of this work - the enmeshed nature of process-response interactions in sandy coastal systems - is well illustrated by the nature of microscale interactions described in this chapter. Here, it was shown that deposit characteristics represent a response to a variety of influences operating simultaneously at different scales.

CHAPTER 5 FORESHORE DYNAMICS: MESOSCALE

" Wave after wave, each mightier than the last
Til last, a ninth one, gathering half the deep
And full of voices, slowly rose and plunged
Roaring, and all the waves was in a flame"
Tenneyson, 'The Coming of Arthur'

This chapter describes concurrent variations in foreshore morphologic, stratigraphic, runup, and water table characteristics through storm/recovery cycles. Mesoscale storm and swell morphostratigraphies, and corresponding dissipative and reflective runup regimes, are recognized. These two process-form associations are considered in the context of a conceptual model for swash zone dynamics that focuses on inferred variations in the distribution and relative dominance of swash versus backwash forces on the foreshore.

5.1 BACKGROUND: SWASH ASYMMETRY AND RUNUP-WATER TABLE-MORPHOLOGY INTERACTIONS

Eliot and Clarke (1988) among others, have suggested that storm/recovery cycle profile changes exhibit affinities to tidal cycle profile changes, both in terms of the patterns of change and the processes governing change. Expanding upon this suggestion, the framework of a conceptual model for two-dimensional foreshore

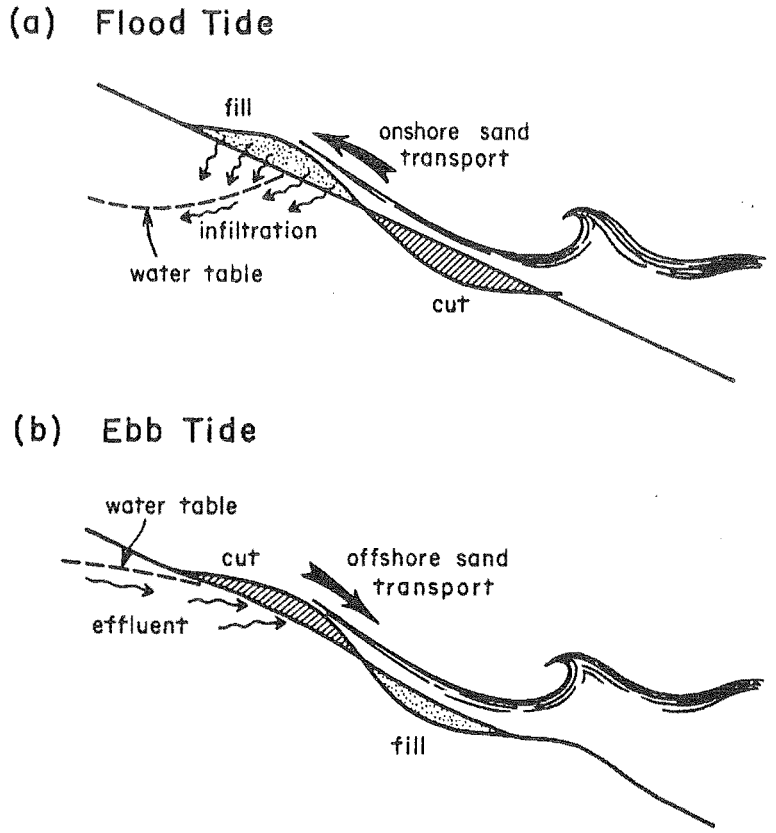

Figure 5.1. Duncan's (1964) model for profile change during the tidal cycle (*from* Komar, 1976a).

morphostratigraphic change through storm/recovery cycles is outlined below using Duncan's (1964) model for profile change through the tidal cycle as an analog.

SWASH ASYMMETRY AND THE CROSS-SHORE ZONATION OF SWASH AND BACKWASH FORCES

Duncan (1964) observed that during the flood tide deposition occurred on the upper foreshore and erosion occurred on the lower foreshore (Figure 5.1). During the ebb tide this pattern was reversed. Duncan suggested that these contrasting patterns of cut and fill resulted from differences in the relative forces of swash and backwash that existed during flood and ebb stages of the tidal cycle. During the flood tide, the swash is able to surge past the water table-saturated portion of the foreshore. As a result, a considerable amount of the runup volume is lost to percolation, and a weak backwash is generated: During the ebb tide, the swash is unable to surge over the saturated

portion of the foreshore. As a result, little runup volume is lost to percolation, and a strong backwash is generated.

In Duncan's model, the fundamental mechanism controlling profile change is the balance of onshore versus offshore forces. Within the swash zone this balance is asymmetric: The swash has greater energy than the backwash because of frictional and turbulent energy losses, as well as mass losses, that occur during the runup process (Bagnold, 1940). Thus, rather than the 'absolute value' of *swash asymmetry*, it is the changes that occur in the relative dominance of swash as opposed to backwash forces that are important.

Additionally, consideration of an ideal runup event, where a single swash runs up the foreshore and the ensuing backwash runs down the foreshore, suggests that swash asymmetry is distributed differentially across the foreshore (Bagnold, 1940; Kirk, 1970: Figure 5.2). At the uppermost portion of the swash zone, near the location of maximum swash excursion, is an area where swash forces are dominant relative to backwash forces. Due to thinning and percolation of the swash mass into the foreshore, there is negligible backwash generation in this *upper swash-dominated or deceleration zone*. There is also an area in the lowermost portion of the swash zone, near to where the outgoing backwash meets the incoming swash, where swash forces are dominant relative to backwash forces. In this *lower swash-dominated or deceleration zone* the outgoing backwash is in a state of decay, whereas the incoming swash, having experienced minimal frictional/turbulent and mass losses, is yet to decay. In between these two swash-dominated zones is an area where backwash forces are most dominant relative to swash forces. In this *middle backwash-dominated or acceleration zone* the swash mass has experienced significant decay, yet retains sufficient mass to generate a strong backwash.

The cross-shore distribution of swash asymmetry is described above in the context of a single swash cycle. However, through consideration of a net swash cycle, and in turn a resultant cross-shore distribution of swash asymmetry, this concept can be applied across a range of time scales.

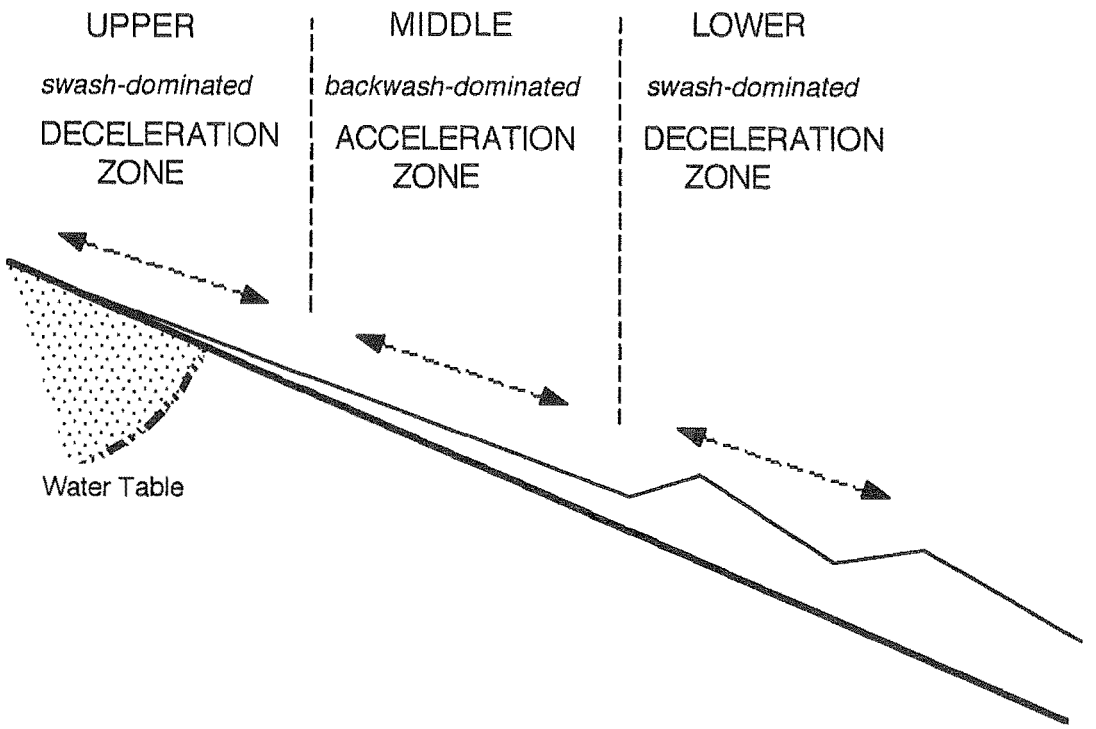

Figure 5.2. The cross-shore distribution of swash asymmetry.

Observations made previously by Sonu (1972) and Sonu (et. al., 1973), together with those presented later in this work, suggest that variations in the cross-shore distribution of swash asymmetry occur through storm/recovery cycles: The upper and lower swash-dominated zones expand or contract in extent relative to the extent of the backwash-dominated zone. Since the swash dominated zones tend to be areas of deposition and the backwash dominated zone an area of erosion, the changes in the relative extent of these zones result in changes in the pattern of erosion and deposition on the foreshore. Changes in the material properties of the foreshore occur in conjunction with these asymmetry-induced changes in foreshore morphology.

TABLE 5.1 FACTORS INFLUENCING SWASH ASYMMETRY

		Swash Dominance	Backwash Dominance
Incident Wave	Height	lower	higher
	Period	shorter	longer
	Angle of Incidence	low	high
Runup	Volume	smaller	larger
	Excursion Width	wider	narrower
	Period	shorter	longer
Water Table	Saturation	dry	wet
Beach	Slope	steep	gentle
	Grain Size	coarse	fine

COMPONENTS OF THE MODEL AND THEIR INFLUENCE UPON SWASH ASYMMETRY

The principal factors influencing both the relative dominance and the distribution of swash versus backwash forces on the foreshore include beach form and material properties, the beach water table, runup characteristics, and ultimately incident wave characteristics (Table 5.1). Although the influence of each of these factors on swash asymmetry is considered independently in the following paragraphs, it is in combination that these factors act to reinforce or cancel each others individual effects.

Runup Height/Swash Excursion Width

Intuitively, runup height (and thus runup volume) is expected to increase with

increasing wave height. This has been shown to be the case by a number of workers including Kirk (1970), Guza and Thornton (1982), and Holman and Sallenger (1985). The increased runup volumes that accompany increases in runup height move swash asymmetry towards conditions of relative backwash dominance: The swash mass experiences proportionately less mass loss and therefore more of it is available to contribute to the backwash. The converse is true when incident wave and runup heights are low: The swash mass experiences proportionately greater mass loss and therefore less of it is available to contribute to the backwash. In this situation swash asymmetry moves towards conditions of relative swash dominance (Table 5.1).

Less obvious is the influence that changes in swash excursion width (the horizontal component of runup) have upon the swash zone energy balance. Although absolute runup height increases with increasing wave heights, it was observed by Guza and Thornton (1982), Holman and Sallenger (1985), and Holman (1986), among others, that dimensionless runup height decreases with increasing wave height. This relationship is illustrated in Holman's (1986) plot of dimensionless runup height (R_V/H_b) against the Iribarren number, ξ , (Figure 5.3a), where

$$\xi = \tan \beta / (H_o / L_o)^{1/2} = (\pi / \varepsilon)^{1/2} \qquad (5.1)$$

(after Holman and Sallenger, 1985) and H_o and L_o are deepwater wave height and wavelength (taken here to be H_b and $gT^2/2\pi$ respectively).

What this relationship suggests is that the swash zone becomes proportionately smaller during storms. This favors relative backwash dominance during storms: The smaller the total area of foreshore the runup mass traverses, the smaller the area of dry foreshore it is exposed to, and therefore, the less mass loss its experiences. The opposing scenario applies during swell conditions: The swash mass is exposed to a larger area of dry foreshore and therefore experiences greater mass loss. As a result, swash asymmetry moves towards relative swash dominance (Table 5.1).

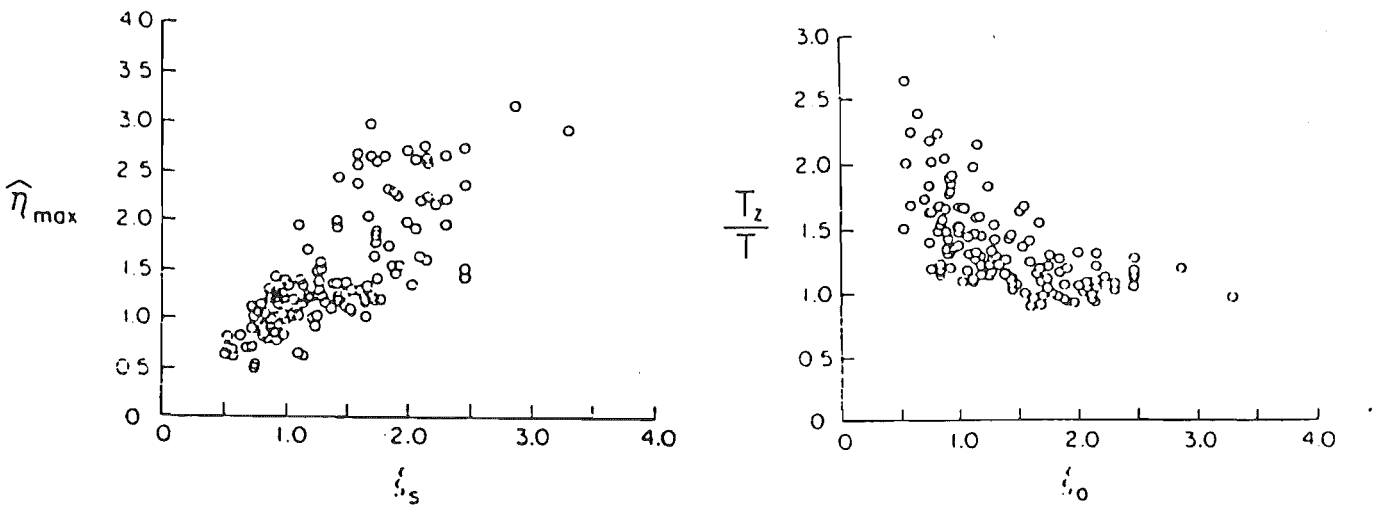

Figure 5.3. a) Holman's (1986) plot of dimensionless runup height ($\hat{\eta}_{max} \simeq R_h/H_{b,}$) against the Iribarren number, ξ ; b) Holman's (1986) plot of dimensionless runup period ($T_Z/T \simeq T_r/T_i$) against Iribarren number ξ.

Runup Period

Numerous workers have observed that runup period increases with increasing incident wave height and period, and decreasing beach slope (Emery and Gale, 1951; Kemp, 1961; Kirk, 1970; Battjes, 1974; Sonu, 1974; Huntley and Bowen, 1975; Sutherland et al., 1976; Waddell, 1976; Wright et al., 1979; Bradshaw, 1982; Guza and Thornton, 1982; Holman and Bowen, 1984; Holman and Sallenger, 1985; Holman, 1986). This low frequency shift that occurs during storms is commonly illustrated in terms of runup spectra. However, Holman's (1986) plot of dimensionless runup period (T_r/T_i) against Iribarren number also serves to illustrate this relationship (Figure 5.3b).

The low frequency shift is manifest as an increase in swash/backwash interaction and a change in swash asymmetry towards relative backwash dominance: The longer lasting swash is unable to move up and back down the slope without either merging

with the previous swash and/or colliding with the outgoing backwash (Kemp, 1961; Kirk 1970; Waddell 1973, 1976; Bradshaw, 1982). An increase in backwash relative to swash duration is the result (Kirk 1970; Waddell 1973, 1976; Marra, 1988). The converse holds true for swell conditions: The high frequency swashes move up and back down the foreshore without interruption, their duration is increased relative to that of the backwash, and as a result the relative influence of swash forces are enhanced (Table 5.1).

Beach Water Table

Beach water table characteristics have been considered by Bagnold (1940), Grant (1948), Emery and Foster (1948), Longuet-Higgins and Parkins (1962), Duncan (1964), Harrison (1969), Ericksen (1970), Pollock and Hummon (1971), Waddell (1973, 1976), Lanyon et al. (1982), and Eliot and Clarke (1988), among others. Referred to indirectly above, the influence of the beach water table on foreshore sedimentation was clearly demonstrated in similar experiments carried out by Bagnold (1940) and Longuet-Higgins and Parkins (1962). In both experiments, when an impermeable plate was inserted into the sand surface, to simulate a saturated foreshore, the sand layer above the plate was quickly eroded away. When the plate was removed, to allow percolation to occur, sand accumulated.

Thus, with respect to water table effects and swash asymmetry, two situations can be identified. At one extreme is a *dry* foreshore or swash zone, where runup mass loss is maximized due to percolation of the runup into the foreshore, and the relative dominance of swash over backwash is enhanced. At the other extreme is a *wet* foreshore or swash zone. In this situation runup mass loss due to percolation is minimized and the relative dominance of backwash over swash is enhanced (Table 5.1). Although only slightly, backwash dominance may be further enhanced by a contribution of water table outflow to the backwash mass (Emery and Foster, 1948; Ericksen, 1970).

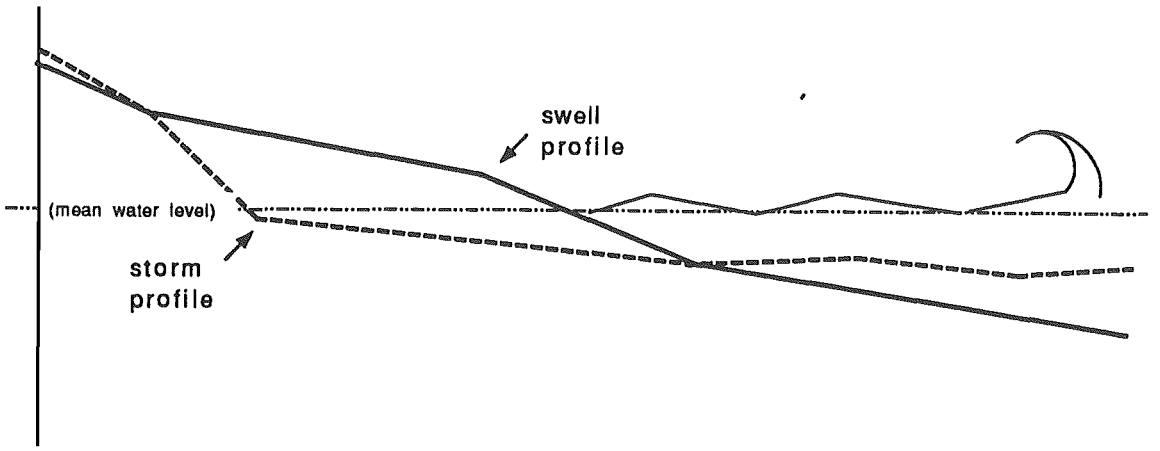

Figure 5.4. Storm and swell profiles.

Beach Form and Material Properties

Steep slopes decrease swash/backwash interactions and coarser grain sizes increase runup percolation (Bagnold, 1940; King, 1972; Bradshaw, 1982). Therefore, steep slopes and coarse grain sizes are associated with relative swash dominance. The converse is true for gentle slopes and fine grain sizes (Table 5.1).

Although beach form and material properties do influence swash asymmetry, as discussed briefly below, it is their role as response elements that is of primary interest in this study.

MORPHOSTRATIGRAPHIC COUPLING

The development of storm and swell profiles during contrasting phases of storm/recovery cycles is well recognized within the coastal literature (Figure 5.4: see also Chapter 3). Foreshore deposits have been described by numerous workers including Thompson (1937), Clifton et al. (1971), Sonu (1972, 1973), Clifton (1976), Hine (1979), Hunter et al., (1979), Reinson (1984), McCubbin (1982), Komar and

Wang, (1984), Short (1984), Terwindt et al. (1984), Thomas and Baba (1986).

Although much work has been done on the description of foreshore morphologies and foreshore deposits, a systematic examination of beach form and deposit characteristics through complete storm/recovery cycles is lacking (Komar, 1989). The study of Sonu (1972) is noteworthy in this respect. Sonu (1972) observed, an association between the accumulation of coarse grain sizes and the development of convex profiles during post-storm recovery, and the accumulation of fine grain sizes and the development of concave profiles during storms. Sonu's observations suggest that changes in foreshore deposit characteristics are coupled with the changes in beach profile form that occur during storm/recovery cycles.

5.2 RESULTS: NINE MILE BEACH FORESHORE MORPHOSTRATIGRAPHIES AND PROCESS REGIMES

Having outlined the framework of a conceptual model for mesoscale foreshore dynamics in the preceding section, this section describes concurrent observations of foreshore morphostratigraphies and runup processes observed through NMB storm/recovery cycles. Much of this section is based upon results obtained from storm/recovery cycles that occurred at bay and horn locations over the periods of December 13 -December 23 and December 28 - January 8 respectively. A time series of wave steepness through these storm recovery cycles is given in Figure 5.5 to provide a basis for future reference. (See also Chapter 2 for details on data collection and methodology relevant to results presented in this Chapter.)

5.2.1 NMB STORM AND SWELL FORESHORE MORPHOSTRATIGRAPHIES

Two-dimensional *storm* and *swell morphostratigraphies* are identified for the

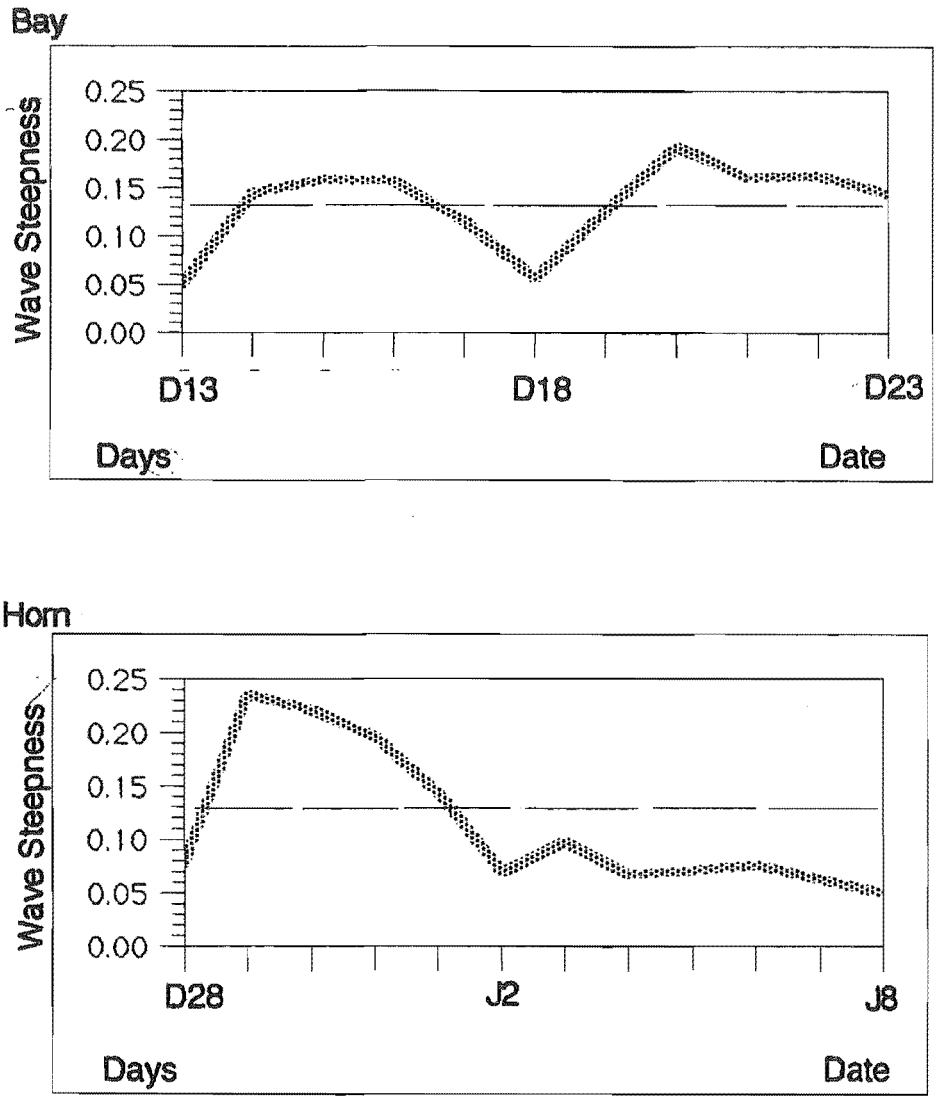

Figure 5.5. Time series of wave steepness through storm recovery cycles. Wave steepness is plotted as H_b/gT^2 x 100. The dashed line running through both figures indicates the mean wave steepness observed during the study period at Nine Mile Beach.

NMB foreshore (Table 5.2). Similar to the morphologic states described in Chapter 3, each morphostratigraphy is defined by an assemblage of morphologic and stratigraphic characteristics. Specifically, more concave-shaped foreshore profiles are associated with the storm morphostratigraphy: More convex-shaped profiles are associated with the swell morphostratigraphy. Correspondingly, mid-profile cut and a net loss of sediment from the foreshore accompanies the development of the storm

TABLE 5.2 Nine Mile Beach Foreshore
STORM AND SWELL MOPRHOSTRATIGRAPHIES

	STORM	SWELL
FORM		
Profile Shape	More CONCAVE	More CONVEX
Volume Flux	CUT (loss)	FILL (gain)
STRATIGRAPHY & SEDIMENTOLOGY		
Cross Section & Structures	Thick Tablular set with trough cross bedding of LITHOFACIES 1 at a maximum	Thin Wedge set with horizontal lamination of LITHOFACIES 2a & 2b at a maximum
Textures & Composition	Fine-grained, heavy mineral-rich TYPE 1 textures at a maximum	Coarse-grained, quartz-rich TYPE 2 textures at a maximum

morphostratigraphy: Profile fill and a net gain of sediment to the foreshore accompanies the development of the swell morphostratigraphy. Finally, with the storm morphostratigraphy, the occurrence of cross-laminated, heavy mineral-rich, fine-grained sands is at maximum in foreshore cross sections: With the swell morphostratigraphy the occurrence of horizontally laminated, quartz-rich, coarse-grained sands is at a maximum in foreshore cross sections.

These contrasts in profile shape, volume flux, stratigraphy, and sedimentology are described in greater detail below.

FORESHORE MORPHOLOGY

Figure 5.6 shows a sequence of profiles taken at a bay location prior to, through, and following a storm event. Of principal import here is the difference in shape between the December 14 profile, taken prior to the storm, and the December 16 profile, taken during the storm. Specifically, the December 16 storm profile has a more concave form; the December 14 swell profile a more convex form. Developed during contrasting phases of foreshore evolution, these storm and swell profiles are characteristic of their respective morphostratigraphy.

In Figure 5.7a and b the development of storm and swell profiles during respective phases of foreshore evolution are recognizable as opposing trends in the time series of profile shape indices RBS and RBW (see Chapters 2 and 3). Evident in these figures is a general tendency for RBS and RBW to increase (i.e. increasing concavity) during the storm phase, and for RBS and RBW to decrease (i.e. increasing convexity) during the recovery phase of the cycle

In Figure 5.7a for example, bay RBS values increase from approximately 1 to 1.5 and RBW values from approximately 1.5 to 1.7, with the occurrence of storm conditions over the period of December 14 -16. Over the period December 18 - 20 values of RBS then drop, from approximately 1.5 to 1.25 and RBW from approximately 2.0-1.75 with the the occurrence of swell conditions during this time. The profile shape indices again increase after December 20, with the return of storm conditions after this date

Similarly, in Figure 5.7b the profile shape indices indicate that the horn profiles became more concave (increasing RBS and RBW) when storm conditions prevailed over the period of December 28-January 3. After January 3, when swell conditions existed for an extended period, the profile gradually became more convex in shape (decreasing RBS and RBW).

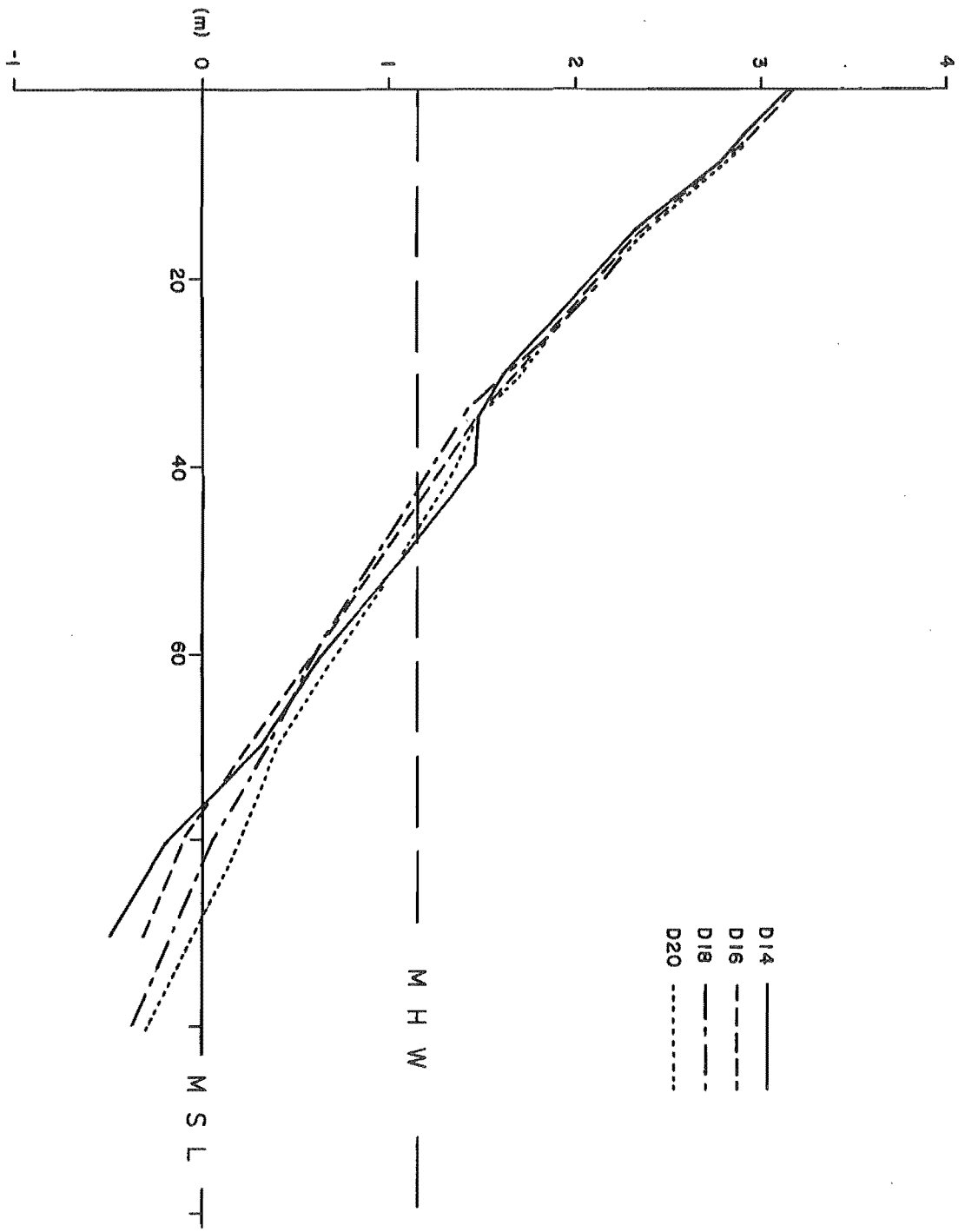

Figure 5.6. Representative sequence of Nine Mile Beach foreshore profiles.

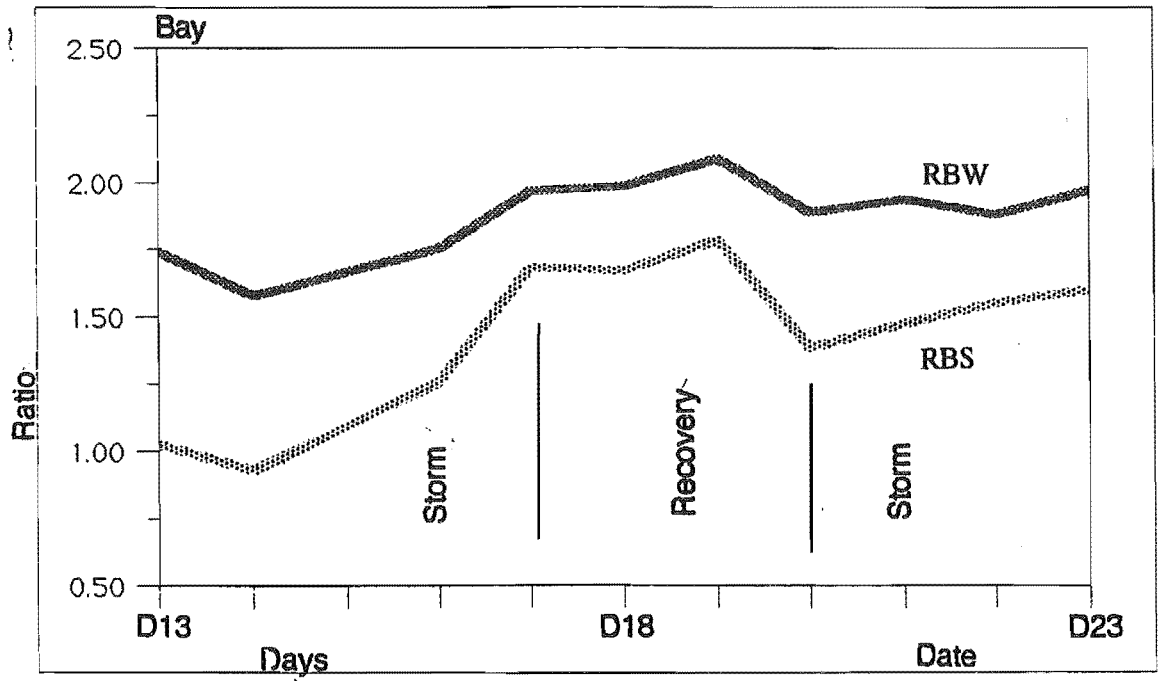

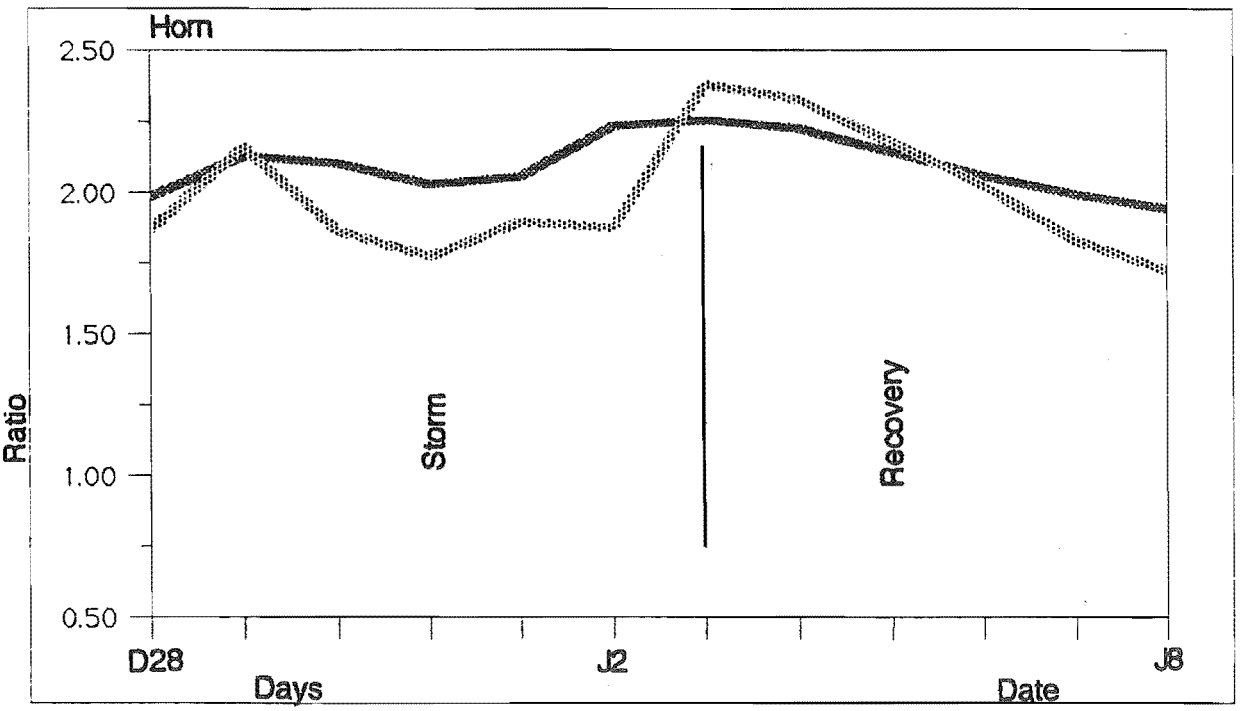

Figure 5.7. Time series of profile shape indices.

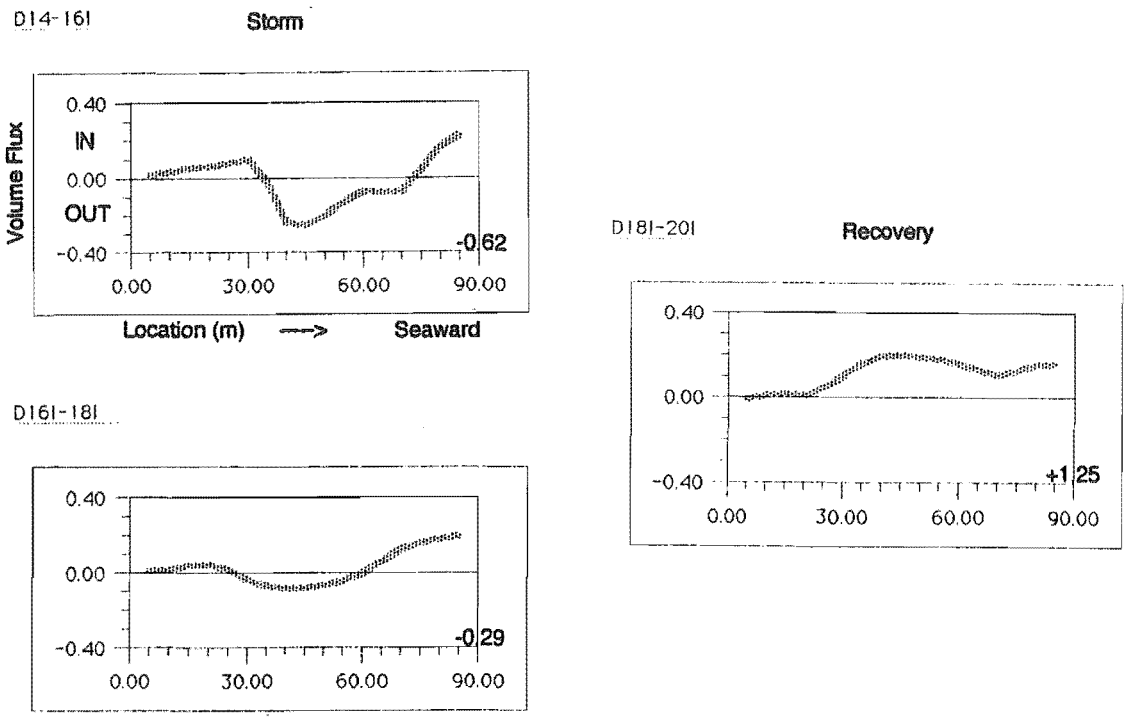

Figure 5.8a. Net volume flux per tidal cycle in the high tide swash zone - Bay. Values in right bottom corners indicate the total net cross-volume flux over the given period (+ = IN: - = OUT).

FORESHORE VOLUME FLUX

Distinct patterns of erosion and deposition accompany the profile changes described above and are characteristic of storm and swell morphostratigraphies.

For storm and swell phases of foreshore evolution, the net volume flux per tidal cycle is plotted in Figure 5.8 at five meter cross-shore increments. The storm volume flux patterns of Figure 5.8a show erosion occurring in the middle portion of the profile and deposition occurring on the upper and lower portions of the profile. The swell volume flux pattern of Figure 5.8a shows deposition occurring along the entire length of the profile. The storm and swell volume flux patterns of Figure 5.8b exhibit patterns of cut and fill that are comparable to those of Figure 5.8a. In both instances,

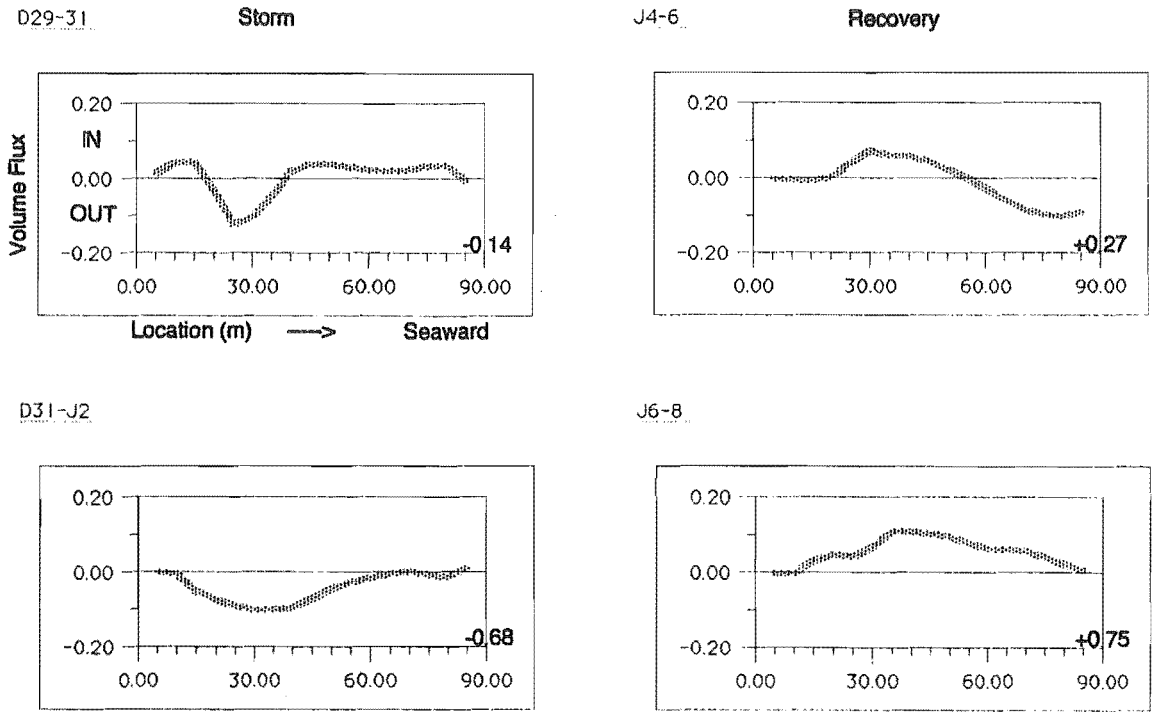

Figure 5.8b. Net volume flux per tidal cycle in the high tide swash zone - Horn. Values in right bottom corners indicate the total net cross-volume flux over the given period (+ = IN: - = OUT).

the storm volume flux pattern, like the corresponding storm profile, tends to be concave in shape; the swell volume flux pattern, like the corresponding swell profile, tends to be convex in shape.

Values of the the total net cross-shore volume flux in to or out of the high tide swash zone are included in Figure 5.8. These values show a good correspondence to the cross shore patterns of volume flux described above, with storm volume flux patterns consistently showing a net loss of sediment from the swash zone and swell volume flux patterns consistently showing a net gain of sediment to the swash zone. Specifically, over the period D14-D16 the profile showed at net loss of 0.62 m3/m/tidal cycle, D16-18 a net loss of 0.29 m3/m/tidal cycle, D29-31, a net loss of

TABLE 5.3 Nine Mile Beach UPPER FORESHORE LITHOFACIES

CHARACTERISTICS	PROCESSES	ENVIRONMENT
LITHOFACIES 1		
GEOMETRY	BACKWASH	ANTIDUNE
Size - 2-10cm:15-25m (H:L)	DOMINATED	FIELD
Shape - tabular, tapers seaward		
SEDIMENTOLOGY		
Structure		
-high, low angle, shoreward dipping trough cross beds		
-near-horizontal lamination to thin bedding		
Texture (Type 1)		
-fine grained, very well sorted, subangular-rounded		
-uniform to weak inverse grading		
Composition		
-Ilmenite, garnet-rich		
LITHOFACIES 2		
subfacies 2a		
GEOMETRY	SWASH	SWASH BAR
Size - 2-8+cm:15m+ (H:L)	DOMINATED	
Shape - wedge, tapers shoreward		
SEDIMENTOLOGY		
Structure		
-near horizontal-seaward dipping, thin bedding		
Texture (Type 2)		
-coarse-fine grained, moderately sorted, subangular-rounded		
-normal and inverse grading		
Composition		
-quartz-rich		

0.14 m3/m/tidal cycle, and D31-J3 a net loss of 0.68 m3/m/tidal cycle. Conversely, over the period D18-20 the profile showed a net gain of 1.25 m3/m/tidal cycle, J4-6 a net gain of 0.27 m3/m/tidal cycle, and J6-8 a net gain of 0.75 m3/m/tidal cycle.

LITHOFACIES 2		
subfacies 2b		
GEOMETRY	SWASH	BERM
Size - <2cm:5-10m (H:L)	DOMINATED	(swash mark)
Shape - lenticular		
SEDIMENTOLOGY		
Structures		
- thinly laminated		
- wind ripple cross lamination		
Texture (Type 2)		
-fine grained, well sorted,subangular-rounded		
-normal grading		
Composition		
-quartz-rich (± shells, organics)		
LITHOFACIES 3		
GEOMETRY	ALTERNATING	TERRACE
Size -1-6cm:15-40m (H:L)	SWASH AND BACKWASH	(sweep zone)
Shape - lenticular, tapers shoreward and seaward		
SEDIMENTOLOGY		
Structures		
- near-horizontal lamination-thin bedding		
Texture (Type 1 & 2)		
- interbedded fine and coarse sands		
Composition		
-alternating heavy and quartz-rich		

NMB STRATIGRAPHY AND SEDIMENTOLOGY

NMB Swash Zone Lithofacies

Three swash zone lithofacies were distinguished within the upper foreshore trenches

(see Chapter 2) of NMB. Each lithofacies comprises a distinctive set geometry with typical internal sedimentary structures and textures. The characteristics of the three NMB foreshore lithofacies are summarized in Table 5.3 and are described briefly below.

LITHOFACIES 1 occurs as a set that generally occupies the upper to middle portion of the upper foreshore, although thin heavy-mineral rich lenses (1cm:10m) located in the middle to lower portion of the upper foreshore are also included with this lithofacies. Usually being shorter and thicker than Lithofacies 2 sets, Lithofacies 1 sets also tend to be more tabular/less wedge-shaped than Lithofacies 2 sets.

With Lithofacies 1 the lower bounding surface of the set is erosional and truncates the foreshore surface at a low angle. The shoreward boundary of this surface however, may may be relatively steep. The upper bounding surface of the set is gradational; it gradually tapers seaward and merges with the other foreshore lithofacies. High angle shoreward-dipping trough cross-bedding is a characteristic feature of the set internally. Low angle shoreward-dipping trough cross-bedding and near-horizontal lamination to very thin bedding are also common however. Fine-grained, very well sorted, heavy mineral-rich sands (Type 1 textures of Chapter 4) are synonymous with Lithofacies 1.

LITHOFACIES 2 is subdivided into Subfacies 2a and 2b. Subfacies 2a is a set that generally occupies the lower to middle portion of the upper foreshore. Its lower boundary is erosional and truncates the foreshore surface at a high angle. Its upper bounding surface is gradational, and gradually tapers shoreward to merge with the other foreshore lithofacies. Internally, Subfacies 2a is characterized by near-horizontally-laminated to thin-bedded layers of coarse-grained, moderately sorted, quartz-rich sands (Type 2 textures of Chapter 4).

Subfacies 2b occurs as a thin, fine-grained, quartz-rich lens located in the uppermost portion of the upper foreshore. Concentrations of shells and organic matter may be present within the lens. Wind-ripple cross-lamination may also be evident.

LITHOFACIES 3 occurs as a variably sized, lenticular-shaped set that commonly occupies only the middle, but occasionally occupies the entire upper foreshore. Set boundaries are not distinct; they taper seaward and shoreward, and grade into the other NMB lithofacies. Near-horizontal lamination, composed of alternating dark and light layers (Type 1 and Type 2 lamination of Chapter 4), is characteristic of the set internally. However, shoreward-dipping high and low angle trough cross-bedding, wavy bedding, and lenticular bedding may also occur.

NMB Storm and Swell Cross Sections

Based on the distribution and character of the NMB swash zone lithofacies described above, two NMB upper foreshore cross-section types specific to storm and swell morphostratigraphic states are recognized (Figure 5.9).

The STORM CROSS SECTION (Figure 5.9a) is identified by the preeminence of Lithofacies 1 in the upper foreshore. The heavy mineral-rich, trough cross-bedded sands of Lithofacies 1 exhibit their maximum lateral extent relative to the quartz-rich, horizontally laminated sands of Lithofacies 2. In contrast, the SWELL CROSS SECTION (Figure 5.9b) is distinguished by the preeminence of Lithofacies 2 and/or 3 in the upper foreshore, as Lithofacies 1 exhibits its minimum lateral extent relative to to that of the other two lithofacies.

Aside from content, form also differs between the two cross-section types. The storm cross section is thick and tabular in shape, whereas as the swell cross section is thin and wedge-like in shape. These contrasts in form represent the maximization of the zone of active sedimentation during the development of the storm profile, and the minimization of the zone of active sedimentation during the development of the swell profile.

Differences in form and content between the idealized storm and swell cross-sections described above, are evident in the sequence of upper foreshore cross sections observed during the study period at NMB and presented in Figures 5.10 (a-f). In the bay cross section sequence (Figure 5.10 a-c), note how Lithofacies 2a, 2b, and 3

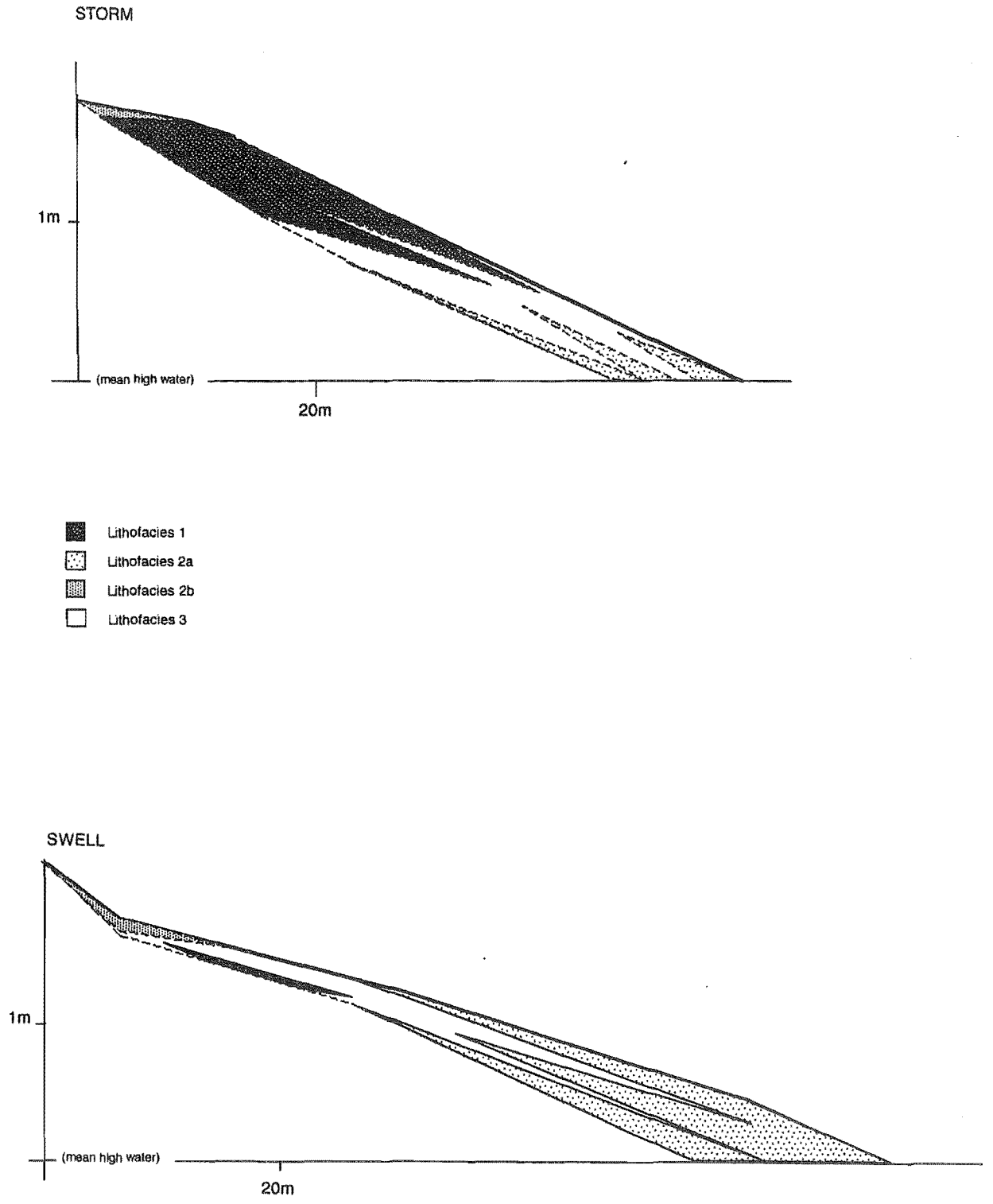

Figure 5.9. Idealized NMB Storm and Swell upper Foreshore Cross-sections.

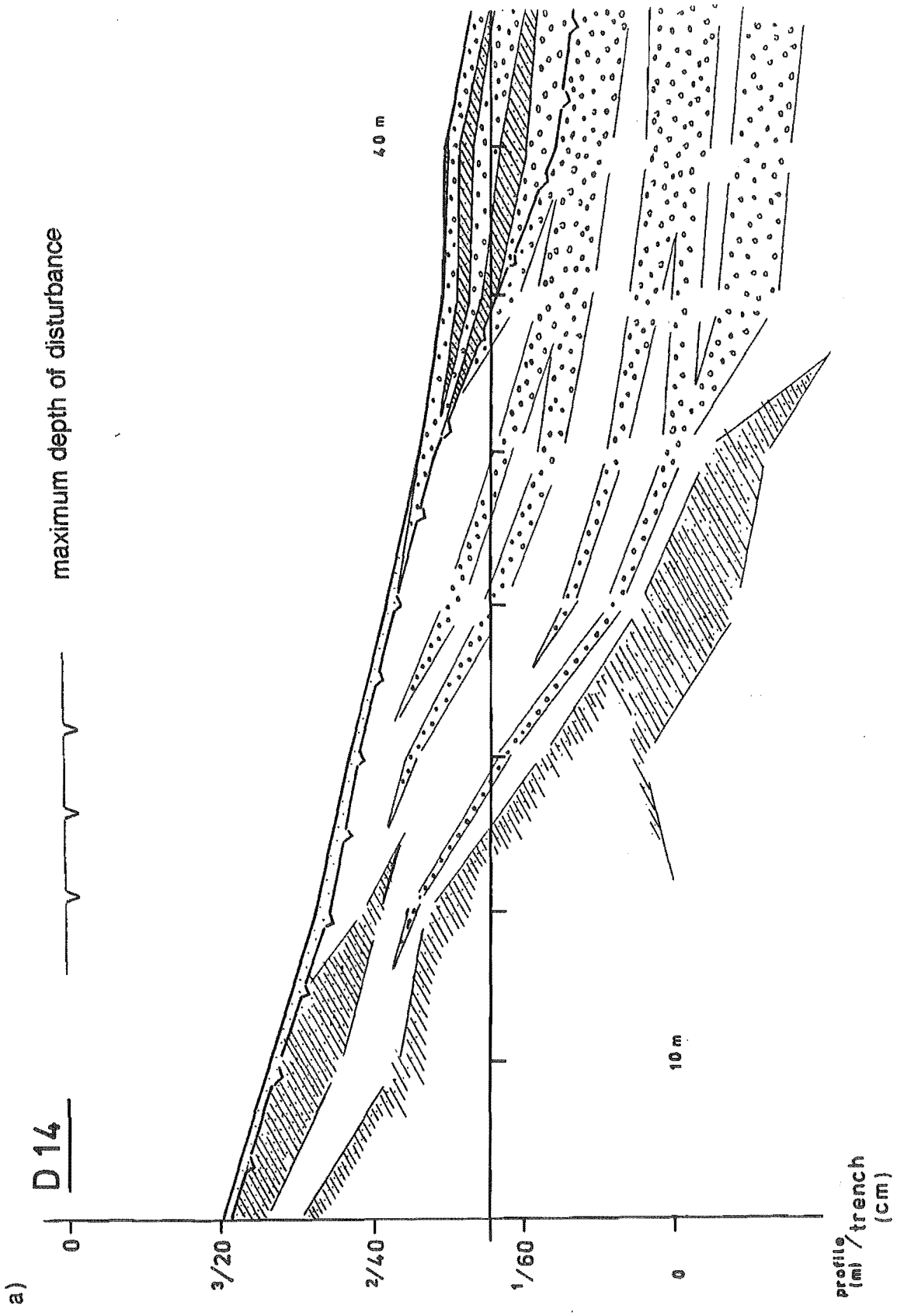

Figure 5.10 (a-f). Sequence of upper foreshore cross-sections observed during the study period at NMB.

b)

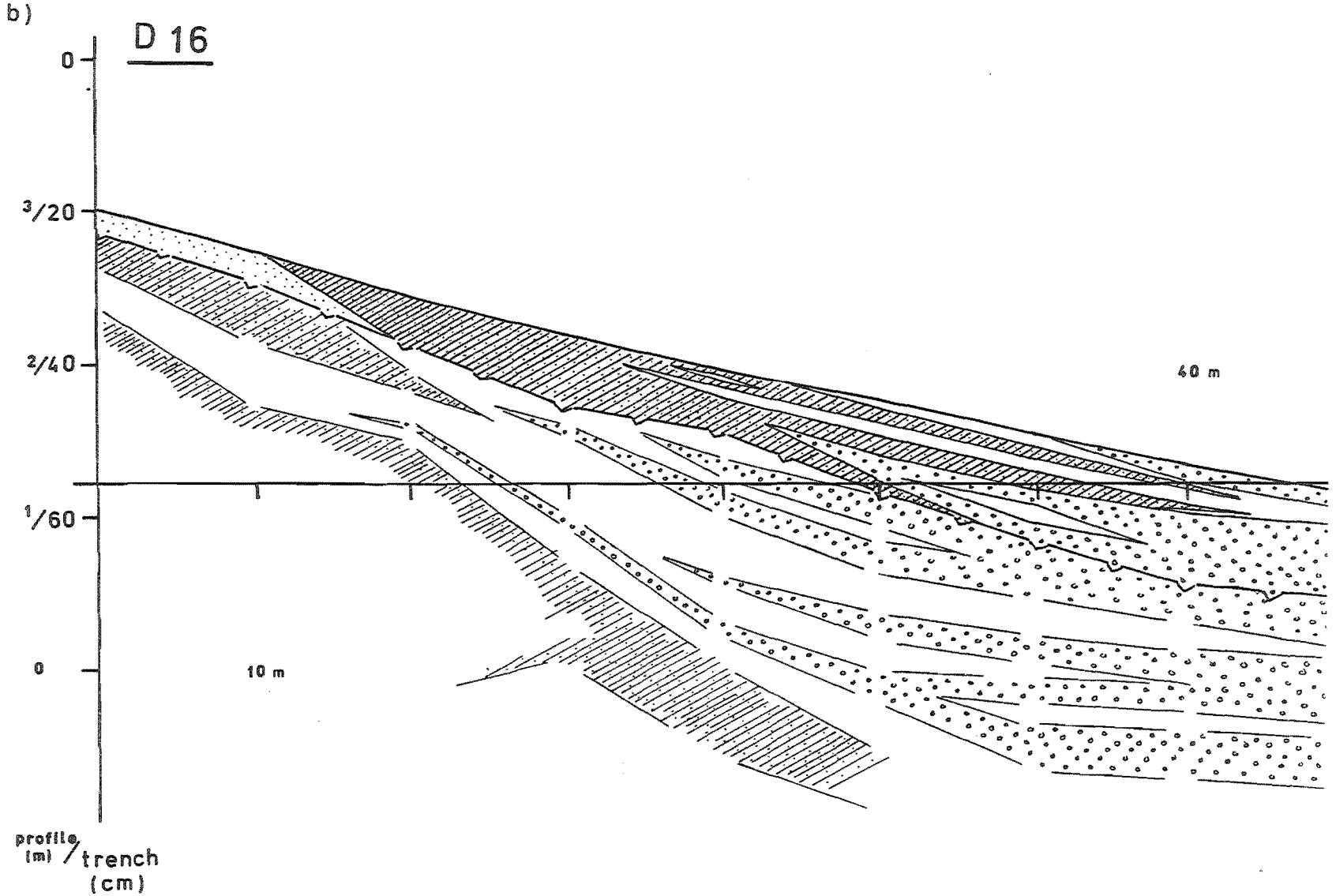

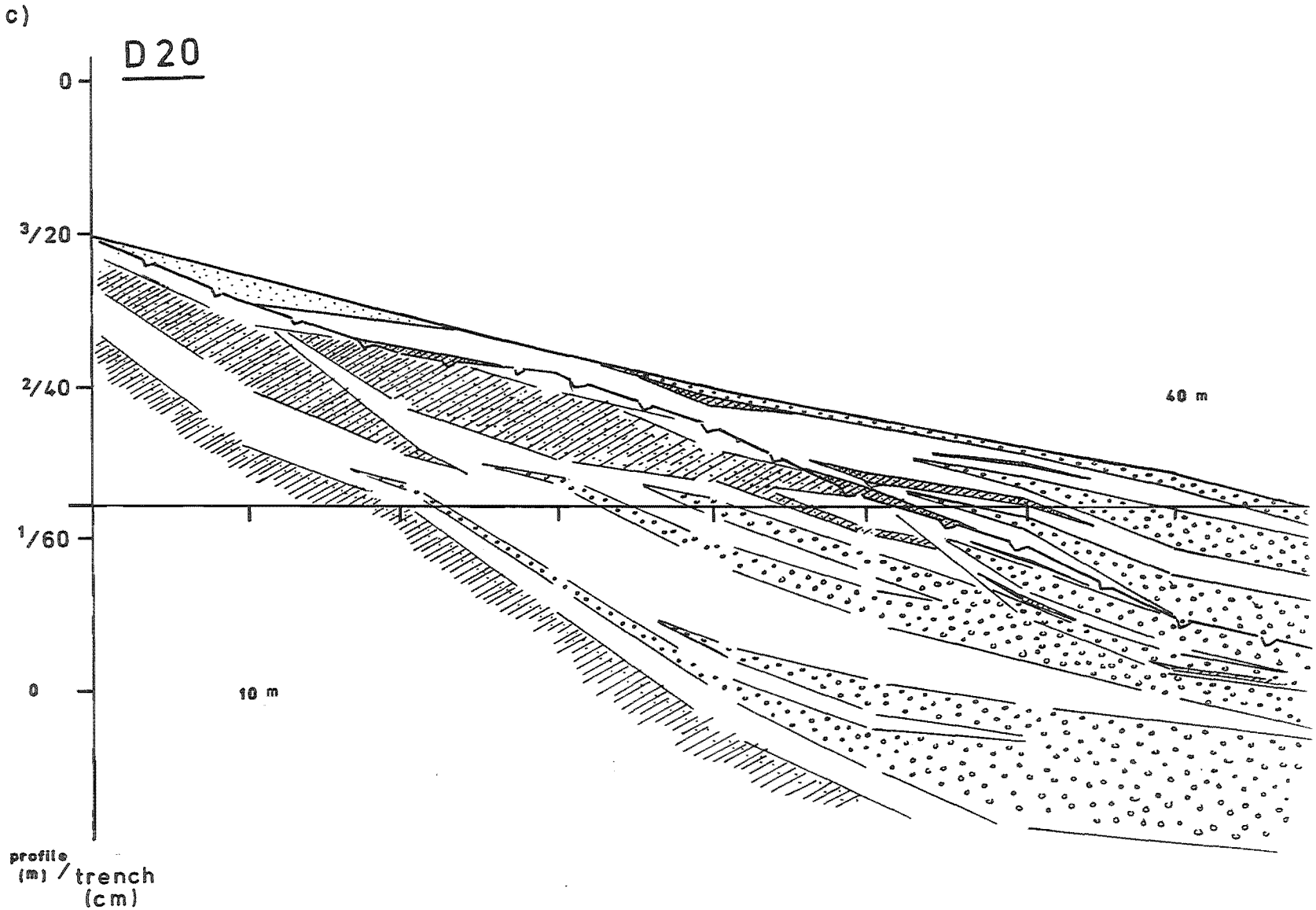
c)
D 20
0
3/20
2/40
1/60
0
10 m
40 m
profile (m) / trench (cm)

d)

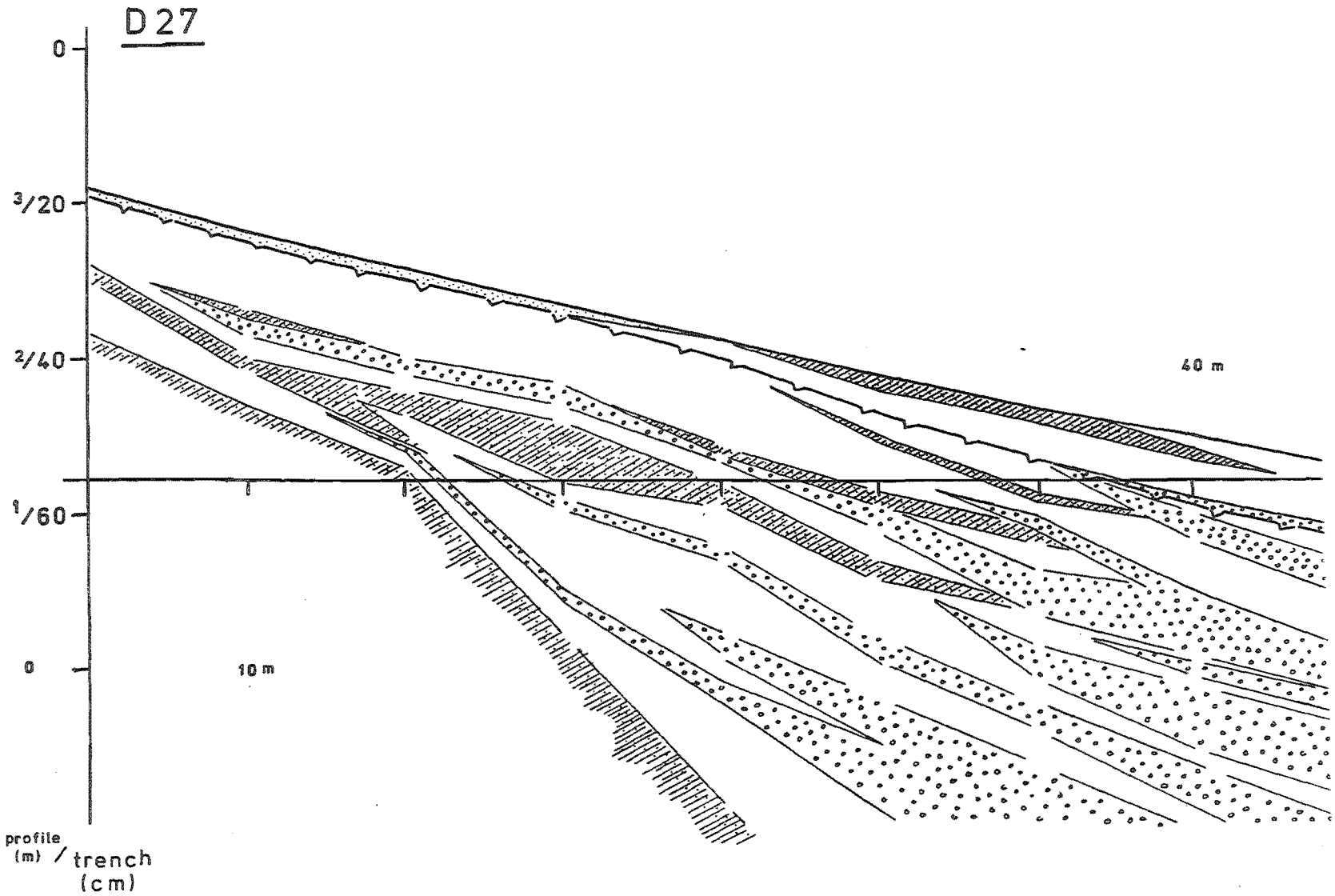

e)

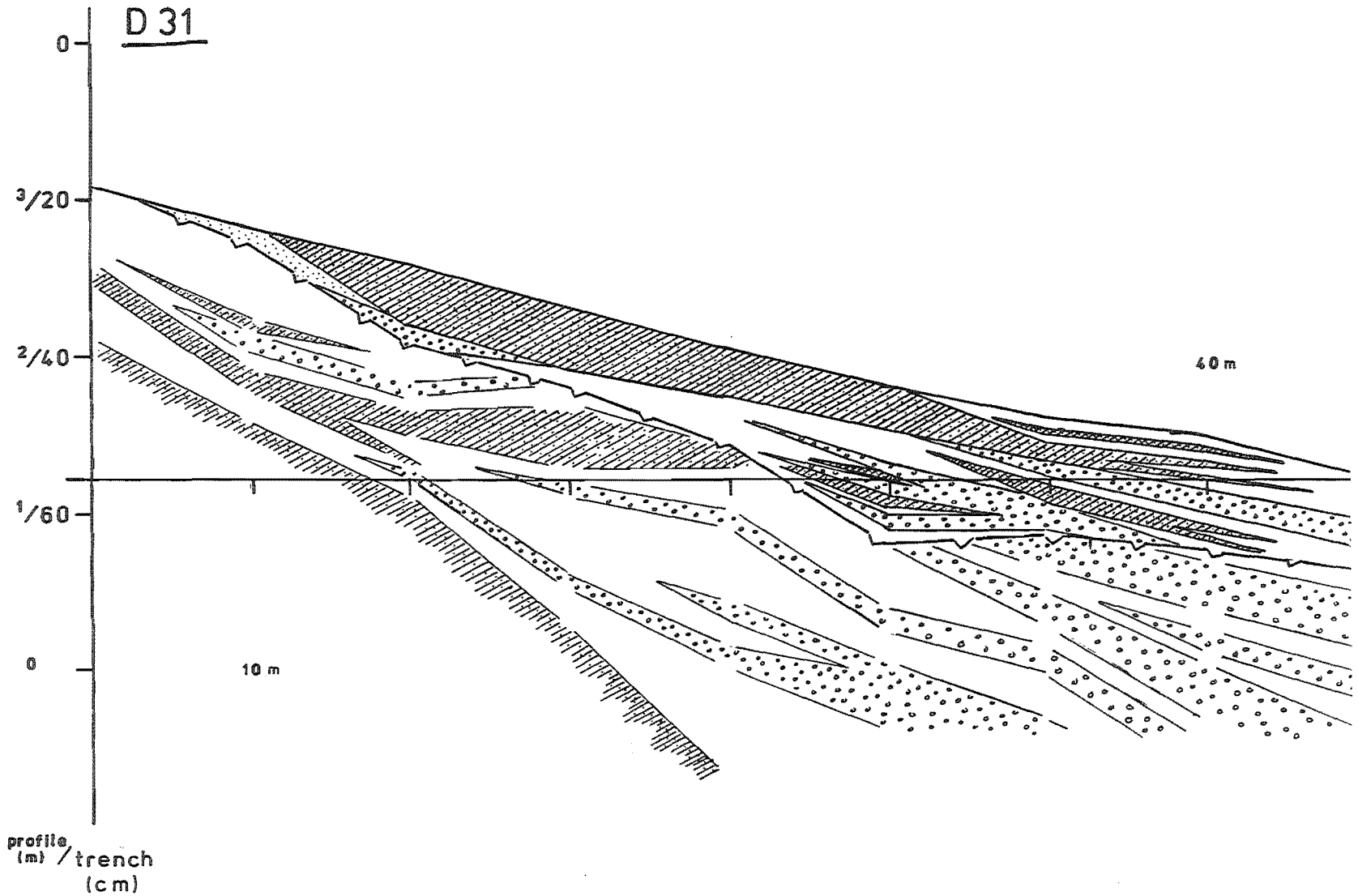

f)

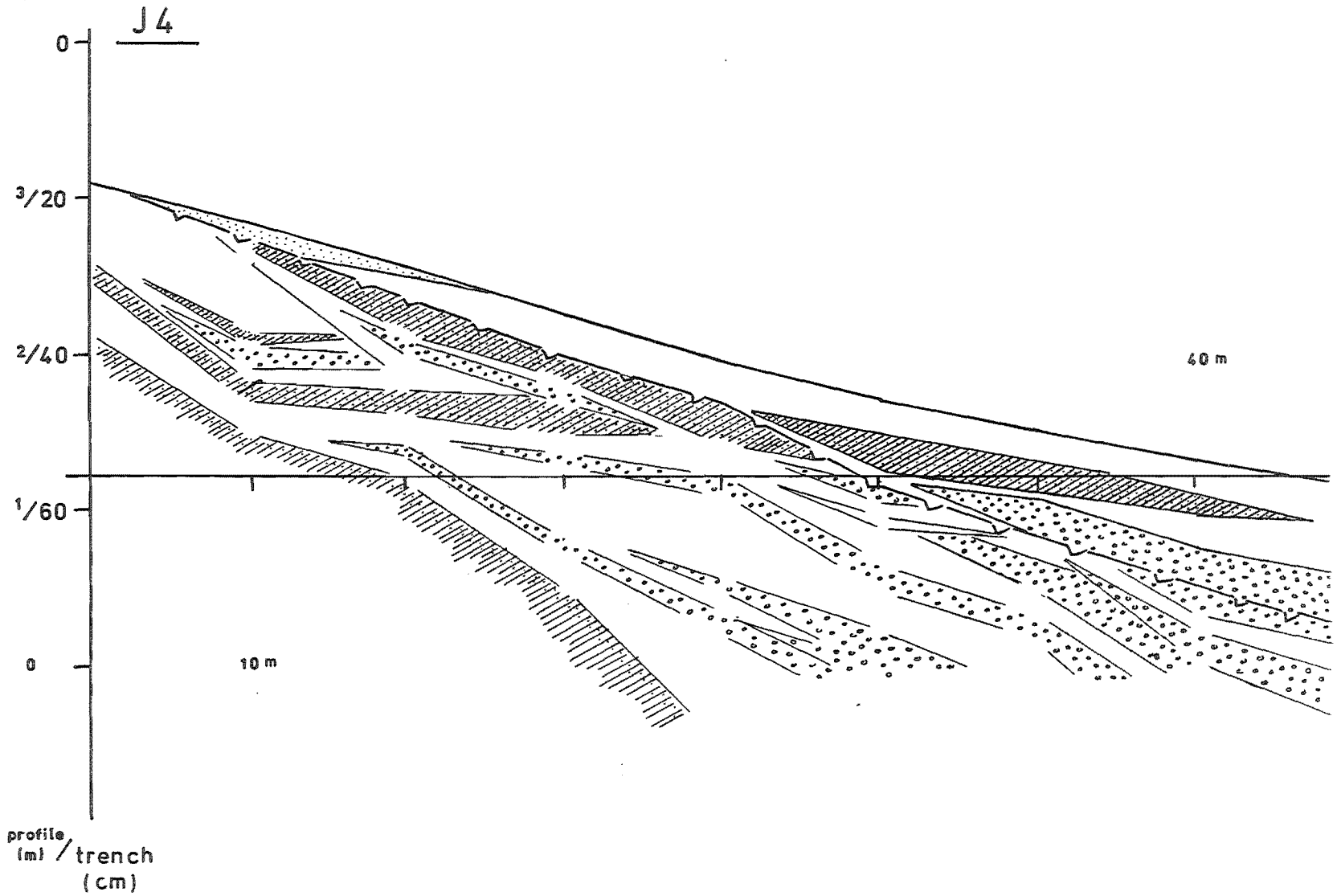

define a shoreward-thinning wedge of active sedimentation in the December 14 swell cross section (Figure 5.10a). Also, the occurrence of Lithofacies 1 is limited to only a small area in the lee of the swash bar/berm in this cross section. In contrast, the December 16 storm cross section (Figure 5.10b) shows a much thicker zone of active sedimentation. In the December 16 cross section, lithofacies 2 is now the dominant lithofacies; Lithofacies 2a and 2b have contracted towards the lower and upper extremes of the upper foreshore respectively. A reoccurrence of the dominance of Lithofacies 2a, 2b, and 3 is shown in the December 20 swell cross-section (Figure 5.10c).

A similar pattern is exhibited in the horn sequence of cross-sections given in Figures 5.10 d-f. In the December 31 storm cross section (Figure 5.10e), Lithofacies 1 can be seen to have its maximum thickness and lateral extent. In comparison, the December 27 and January 4 swell cross sections (Figures 5.10d and 5.10f respectively) show this lithofacies to be at a minimum in thickness and extent. Also note how the overall cross-sectional form is much thinner and more wedge-shaped in these two cross sections than in the December 31 cross section.

5.2.2 NMB DISSIPATIVE AND REFLECTIVE RUNUP REGIMES

Dissipative and reflective runup regimes are identified for the NMB foreshore (Table 5.4). In comparison to the reflective regime, the dissipative regime is characterized by higher incident waves, lower frequency and proportionately lower amplitude runup, and a lesser amount of runup percolation. Conversely, the reflective regime is characterized by lower waves, higher frequency and proportionately higher amplitude runup, and a greater amount of runup percolation than the dissipative regime.

Corresponding trends in relationships between incident wave conditions and runup height/excursion, runup period, and water table excursion, form the basis for the

TABLE 5.4 Nine Mile Beach
DISSIPATIVE and REFLECTIVE RUNUP REGIMES

	DISSIPATIVE (lower ξ)	**REFLECTIVE** (higher ξ)
Incident Waves	H_b higher	H_b lower
Runup		
Absolute Height (a) VOLUME	R_V higher LARGER	R_V lower SMALLER
Dimensionless Height / WIDTH	R_V/H_b lower NARROWER	R_V/H_b higher WIDER
Absolute Period	T_r longer	T_r shorter
Dimensionless Period / DURATION	T_r/T_i larger LONGER	T_r/T_i smaller SHORTER
Water Table		
Dimensionless Width / SATURATION	WT_h/R_h larger MORE	WT_h/R_h smaller LESS

identification of the two runup regimes. These relationships are examined below.

NMB Runup Height / Excursion Width

In Figure 5.11 runup height (R_V) is plotted against breaker height (H_b). In this figure, runup height can be seen to increase from approximately 1.0 to 2.5 meters as

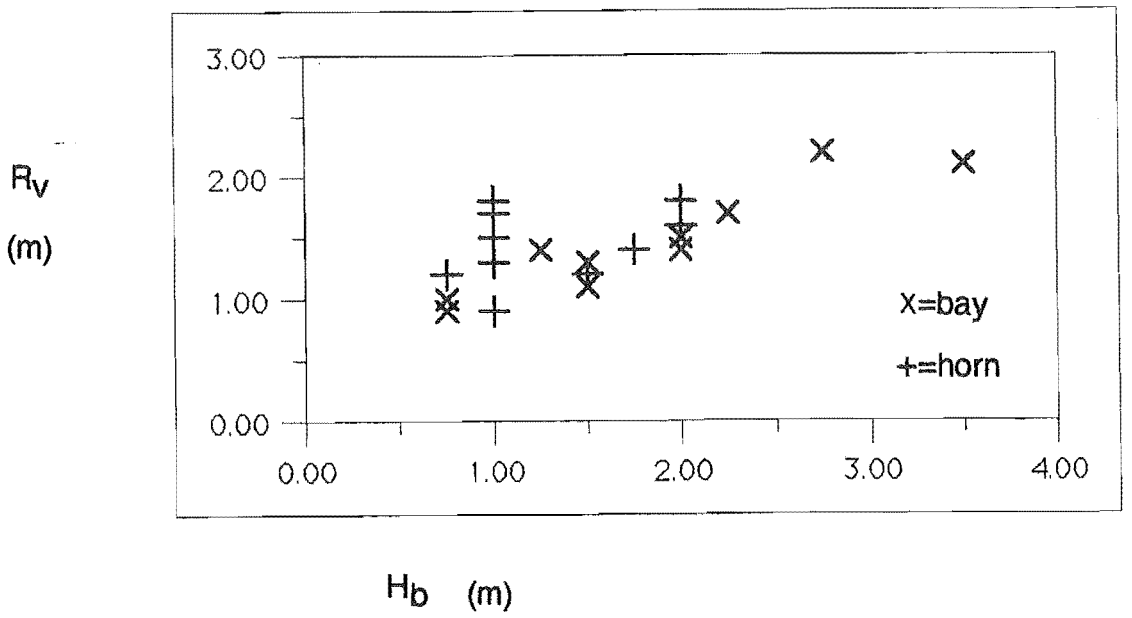

Figure 5.11. Plot of runup height against breaker height at NMB.

breaker height increases from approximately 1.0 to 4.0 meters.

In Figure 5.12a dimensionless runup height (R_V/H_b) is plotted against the Iribarren number (ξ) at a scale comparable to that in Figure 5.3a. Although the NMB data set of Figure 5.12a extends over a much narrower range of ξ values than does the larger data set of Holman (1986), both data sets exhibit a similar trend of increasing dimensionless runup height with increasing Iribarren number. For the NMB data set, this trend is more clearly illustrated in Figure 5.12b, where (following from considerations noted in Chapter 3) dimensionless runup height is plotted against the inverse of the Dean parameter (Ω) at a finer scaling. In this figure, dimensionless runup height can be seen to increase from approximately 0.5 to 2.0 as the inverse of the Dean parameter increases from approximately 0.1 to 0.5.

Thus, in agreement with observations made in the background section, although absolute runup volumes ($\propto R_V$) are larger in the dissipative regime, swash zone widths ($\simeq R_V/H_b$) are relatively narrower. The converse is true for the reflective regime

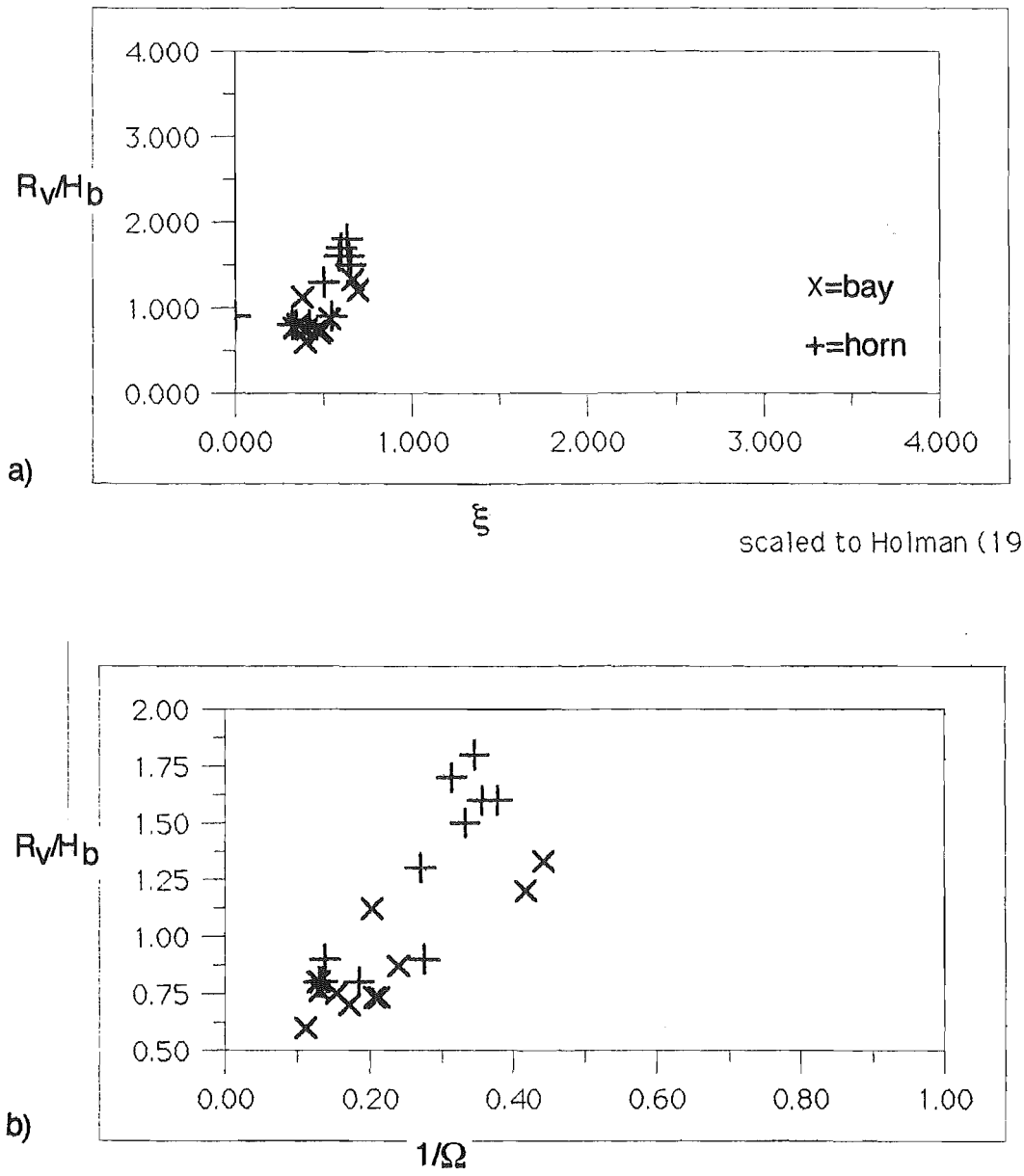

Figure 5.12. (a) Dimensionless runup height (R_V/H_b) plotted against the Iribarren number (ξ): (b) Dimensionless runup height plotted against the inverse of the Dean parameter (Ω).

(Table 5.4).

NMB Runup Period

Log plots of runup height power spectra are given in Figure 5.13 a and b [5.1]. The

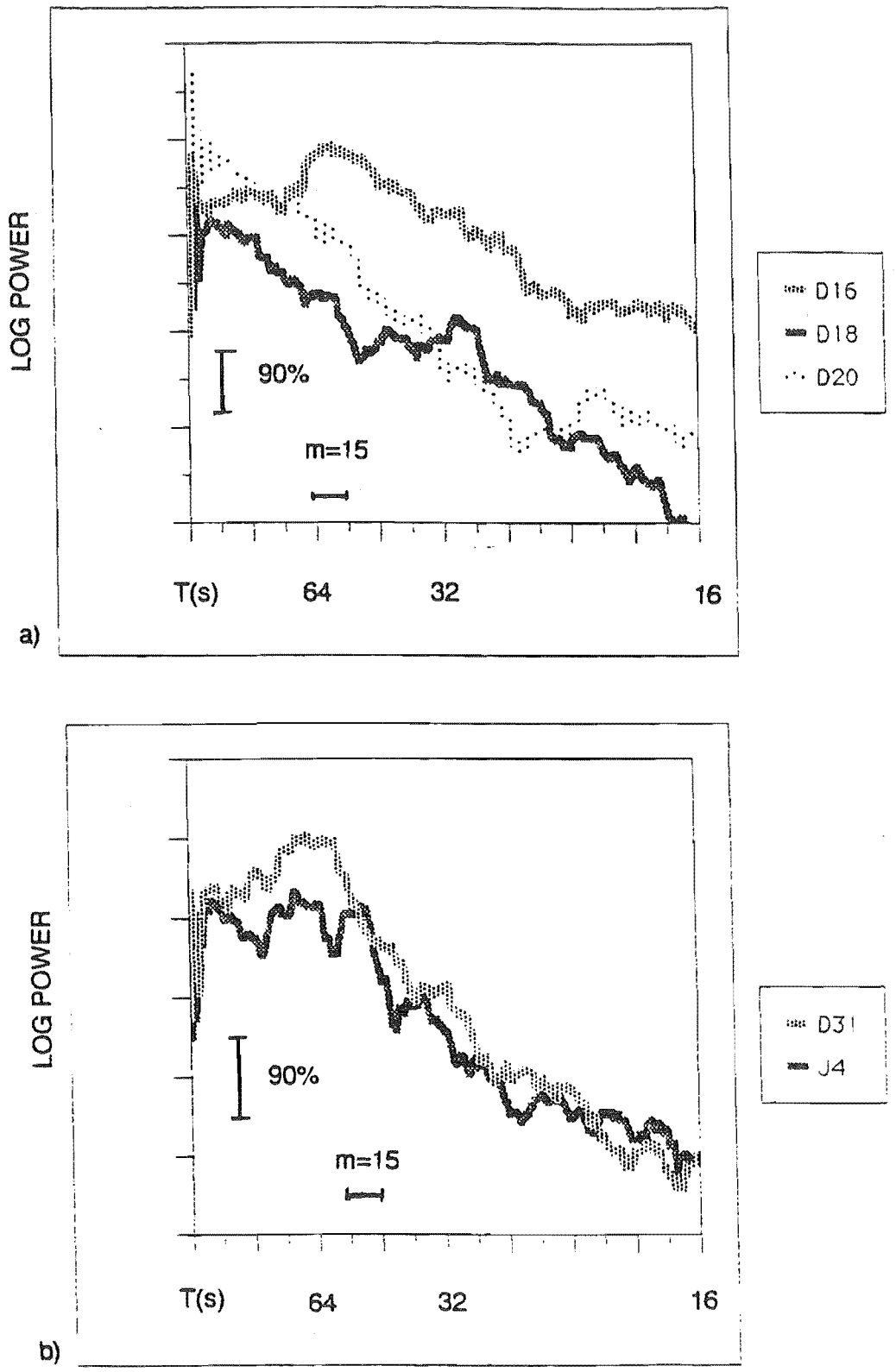

Figure 5.13. Log plots of runup height power spectra (a) bay: b) horn). Note the two spectra of 5.13 b are averages of pairs of spectra measured during a three hour period across the high tide.

bay power spectra of December 16 (ξ = 0. 403) shows a broad peak centered around a frequency that corresponds to a runup period of approximately 52 seconds. The peak is spread across a frequency band that corresponds to runup periods of approximately 64 to 42 seconds. (Figure 5.13a). In contrast to the well developed infragravity band exhibited on December 16, the December 18 spectrum shows more energy at higher (subharmonic) frequencies. On December 18 (ξ = 0.690) the peak in the spectrum is centered around a frequency that corresponds to a runup period of approximately 28 seconds. The peak is spread across a frequency band that corresponds to runup periods of approximately 32 to 26 seconds. On December 20 (ξ = 0.334) a greater amount of spectral energy is again concentrated at lower frequencies (runup periods > 52 seconds).

The horn spectral pairs presented in Figure 5.13b exhibit characteristics similar to those described above. On December 31 (ξ = 0.368) energy in the spectrum is spread across the infragravity band (runup periods of approximately 86-52 seconds). The spectral peak occurs at a frequency that corresponds to a runup period of approximately 64 seconds. On January 4 (ξ = 0.650) spectral energy tends to be concentrated at frequency bands corresponding to runup periods of 64-32 seconds. Although these peaks occur at somewhat lower frequencies than might be expected, they do occur at higher frequencies than those in the December 31 spectra.

In Figures 5.14 a and b dimensionless runup period (T_r/T_i) is plotted against the Iribarren number. The data in Figure 5.14a exhibit a distribution that is comparable to that of Figure 5.3b. However, the anticipated trend of increasing dimensionless runup period with decreasing Iribarren number is not readily discernible in Figure 5.14a. In addition to differences in scaling between the two figures and too few data points in Figure 5.14a, the lack of a discernible trend in the data may be due to the occurrence of NMB T_r/T_i values within a range of ξ values that naturally tend to exhibit large scatter. Even with the small amount of data, the finer scaling of Figure 5.14b makes the anticipated trend discernible. In this plot, dimensionless runup period shows an

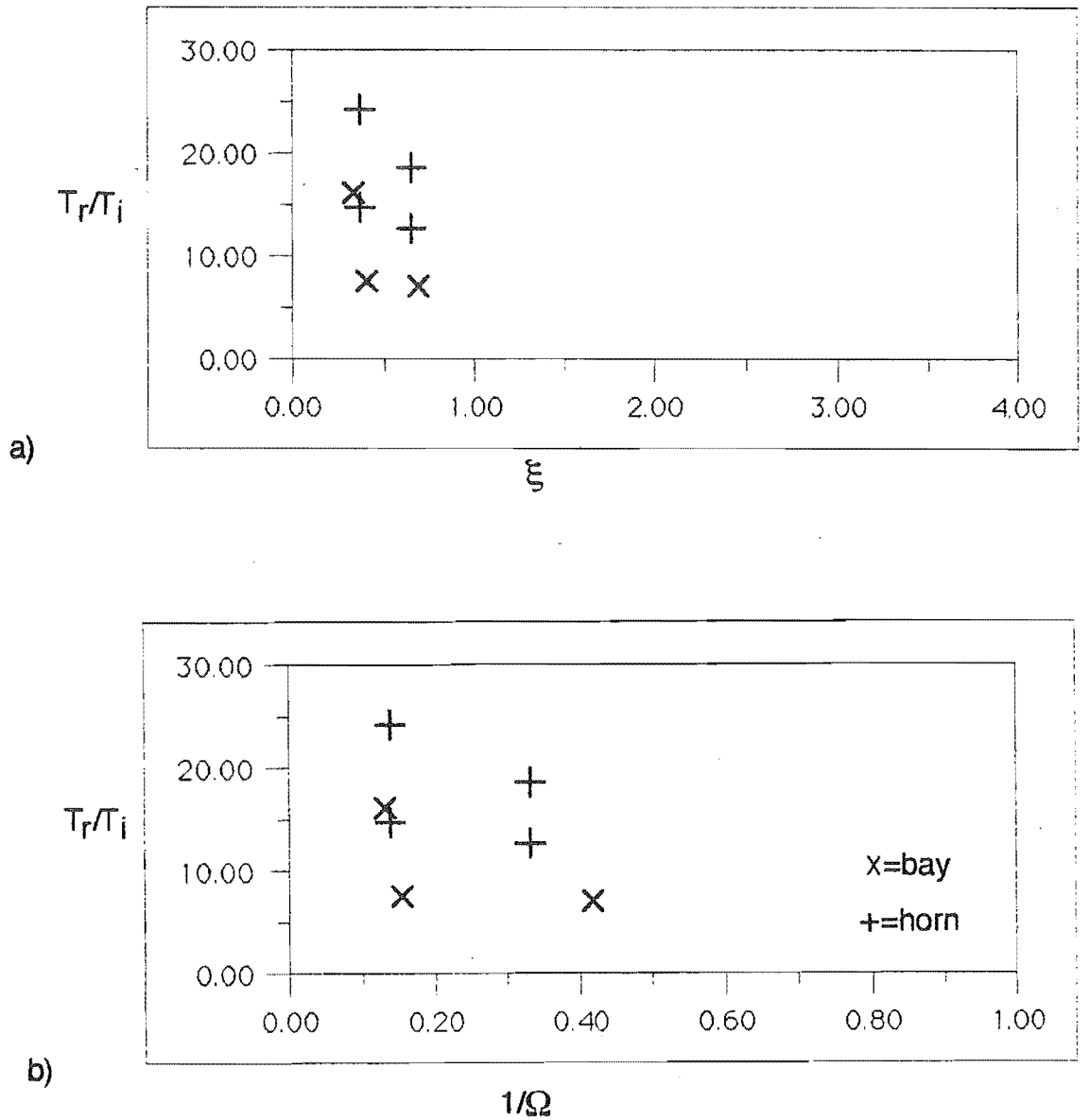

Figure 5.14. (a) Dimensionless runup period (Tr/Ti) plotted against the Iribarren number (ξ): (b) Dimensionless runup period plotted against the inverse of the Dean parameter (Ω).

increase in values from approximately 10 to 20 as the values of the inverse Dean parameter decrease from approximately 0.5 to 0.1.

Thus, in agreement with observations reported in the background section, longer runup periods are associated with more dissipative conditions (lower ξ) , and shorter runup periods are associated with more reflective conditions (higher ξ). As will be

shown later, these differences in runup period correspond to differences between the two runup regimes in the relative duration of swash versus backwash flows (Table 5.4)

NMB Water Table

Water table characteristics recorded at NMB (see Chapter 2) are summarized in Tables 5.5 a and b. In agreement with observations reported in the background section, at NMB the peak in water table elevation was found to lag behind the peak of high tide sea level elevation (5.5a). The amount of lag observed at NMB was variable, ranging from 45 minutes to 2 hours and 15 minutes.

Water table lag results in a systematic variation in the extent of foreshore saturation over the tidal cycle (Duncan, 1964, Harrison, 1969). The tendency for the greatest amount of swash zone saturation to occur during the falling half-tide is evident in the ratios of water table excursion width to swash excursion width (WT_h/R_h) given in Table 5.5b: The falling half-tide (@ t=3.0) values are consistently higher than the rising half-tide (@ t= 8.0) values.

Of greater import to this study is the possibility that systematic variations in the extent of foreshore saturation occur over storm/recovery, as well as tidal, cycles. Table 5.5 b shows that, as nearshore conditions became more reflective, the percent of swash zone saturation averaged over a tidal cycle decreased. The percent of saturation changed from 86% on December 16 to 75% on December 18, and from 67% on December 31 to 63% on January 4. A trend of increasing extent of swash zone saturation with increasing dissipativeness is also evident in Figure 5.15. Although limited in amount, the data obtained during this study does suggest that a variation in the extent of foreshore saturation, may also occur over storm/recovery cycles. Specifically, the dissipative runup regime is characterized by a greater amount of swash zone saturation than the reflective runup regime (Table 5.4).

TABLE 5.5a WATER TABLE LAG

DATE	TIME		
	HIGH WATER TABLE	HIGH TIDE	LAG
N16	12:15	11:30	0:45
N18	02:00	12:30	1:30
N20	02:45	01:45	1:00
D16	01:00	10:45	2:15
D18	02:15	01:00	1:15
D20	03:30	02:15	1:15
J3	03:30	02:15	1:15
J4	04:45	03:00	1:45

TABLE 5.5b VARIATION IN EXTENT OF SWASH ZONE SATURATION WITH STAGE OF TIDAL CYCLE

DATE	R_h(m)	TIME	WT_h (m)	WT_h/R_h	average % SATURATED through 1 tidal cycle
D16	35.00	@8.0	20.00	0.57	
		@3.0	40.00	1.14	86.00
D18	20.00	@8.0	10.00	0.50	
		@3.0	20.00	1.00	75.00
D20	40.00	@8.0	30.00	0.75	
		@3.0	32.50	0.81	78.00
D31	37.50	@8.0	17.50	0.47	
		@3.0	32.50	0.86	67.00
J1	22.50	@8.0	7.50	0.33	
		@3.0	17.50	0.77	55.00
J3	15.00	@8.0	5.00	0.33	
		@3.0	15.00	1.00	67.00
J4	30.00	@8.0	15.00	0.50	
		@3.0	22.50	0.75	63.00

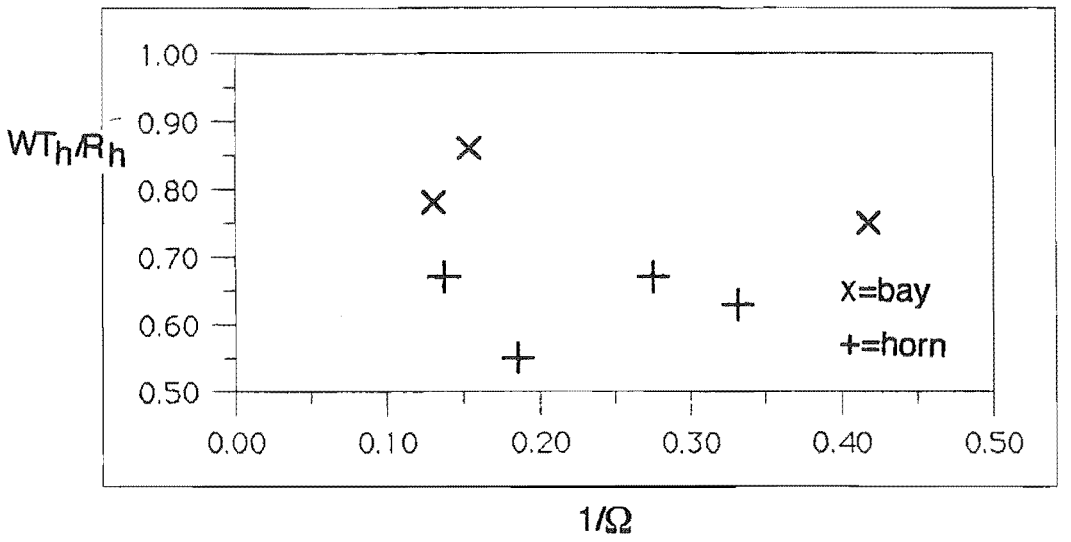

Figure 5.15 Percent swash zone saturation (WT_h/R_h) plotted against the inverse of the Dean parameter (Ω).

LOCAL SWASH ASYMMETRY

The resultant effect of the interactions described above is that the two runup regimes exhibit differences in the relative dominance and distribution of swash versus backwash forces on the foreshore (i.e. runup is 'swash dominated' in the reflective regime and 'backwash dominated' in the dissipative regime). In Table 5.6, local differences in the relative dominance of swash versus backwash forces on the NMB foreshore are quantified.

Local swash asymmetry is evident from the data presented in Table 5.6[5.2]. Swash shear velocities are seen to be consistently higher than backwash shear velocities. Conversely, backwash durations are consistently longer than swash durations. Specifically, on all occasions the local average U* was approximately 4 cm/s for a swash and approximately 3 cm/s for a backwash; the local average duration was approximately 4 seconds for a swash and approximately 7 seconds for a backwash.

TABLE 5.6 LOCAL SWASH ASYMMETRY*

DATE			ENERGY	RELATIVE ASYMMETRY	ELEVATION CHANGE
D16	SW U*(cm/s)	4.41	SW		
	SW Duration (s)	4.21	81.9		
				BACKWASH	LOSS
	BW U*	3.49	BW		(0.4cm)
	BW Duration	7.17	87.3		
	SW/BW U*	1.26	SW/BW		
	SW/BW Dur.	0.59	0.94		
D20	Sw U*	3.97	SW		
	SW Duration	4.26	67.1		
				SWASH	GAIN
	BW U*	2.86	BW		(1.4cm)
	BW Duration	7.51	61.4		
	SW/BW U*	1.39	SW/BW		
	SW/BW Dur.	0.57	1.09		
D31	Sw U*	4.22	SW		
	SW Duration	4.02	71.6		
				BACKWASH	LOSS
	BW U*	3.07	BW		(4.3cm)
	BW Duration	7.68	72.4		
	SW/BW U*	1.37	SW/BW		
	SW/BW Dur.	0.52	0.99		
J4	Sw U*	4.28	SW		
	SW Duration	3.74	68.5		
				SWASH	GAIN
	BW U*	2.77	BW		(0.2cm)
	BW Duration	6.65	51.0		
	SW/BW U*	1.55	SW/BW		
	SW/BW Dur.	0.56	1.34		

In addition to swash asymmetry, the constancy of the values given above suggest that a condition of dynamic equilibrium may exist locally on the foreshore. It is within this narrow range of values that subtle, but significant shifts in the degree of local swash asymmetry occur. These subtle shifts in the relative dominance of swash versus backwash forces are represented as changes in the relative magnitude and duration of swash versus backwash forces (Table 5.6). For example, on December 31 the ratio of swash to backwash U* has a value of 1.37 and on January 4 the same ratio has a value of 1.55: The ratio of swash to backwash duration has a value of 0.52 and on January 4 a value of 0.56. Similarly, on December 31 the swash is 0.99 times as energetic as the backwash: On January 4 the swash is 1.34 times as energetic as the backwash. Thus, backwash domination occurred locally within the dissipative runup regime that existed during the storm conditions of December 31. Swash domination occurred locally within the reflective runup regime that existed during the swell conditions of January 4. With respect to relative differences in swash versus backwash forces, results similar to those presented above were also obtained for the the dissipative runup regime that existed during the storm conditions of December 16 and the reflective runup regime that existed during the swell conditions of December 20 (Table 5.6).

Changes in bed elevation occurred in conjunction with the changes in swash asymmetry described above (Table 5.6). On December 31, at the location where relative backwash dominance occurred, a net loss of 4.3cm in elevation was observed. On January 4, at the location where relative swash dominance occurred, a net gain of 0.2cm in elevation was observed. On December 16 and December 20 similar results were obtained. The correspondence between swash asymmetry and bed elevation change that was observed observed locally at NMB agrees with those predicted by the conceptual model considered throughout this chapter and sets the stage for the process-form associations discussed in the following section.

5.3 INTERPRETATION AND DISCUSSION: NMB FORESHORE DYNAMICS

NMB LITHOFACIES - PROCESS ZONE ASSOCIATIONS

Lithofacies 1: Middle Acceleration Zone (antidune field)

In Chapter 4, the sedimentary structures and sediment textures that make up Lithofacies 1 were attributed to sedimentation processes that occur in backwash: High angle, shoreward-dipping trough cross-stratification composed of fine-grained, heavy mineral-rich sands was associated with upstream-migrating in phase waves and antidune bedform migration in the seaward flowing, accelerating backwash. The tapering-seaward shape of Lithofacies 1 also suggests the role of backwash in its formation. Further, the location of Lithofacies 1 in the middle portions of NMB cross sections also suggests that backwash plays a prominent role in its development. It is in this area of the foreshore, associated with swash velocity decay but swash mass retention, that the backwash is best developed. As a result it is in this area of the foreshore that the transport dynamics responsible for heavy mineral concentration and bed dynamics associated with antidune formation are most likely to occur. Thus, in the context of the cross-shore distribution of swash asymmetry, Lithofacies 1 is indicative of the middle backwash-dominated acceleration zone. Its depositional environment is the 'antidune field' that is best developed within this zone during storms (Table 5.3).

Although Lithofacies 1 is best developed during dissipative conditions that occur in association with the storm morphostratigraphy its occurrence is not limited to these conditions. Lithofacies 1 may also occur in conjunction with the swell morphostratigraphy that develops during reflective conditions. However, under reflective conditions the heavy mineral accumulations are more localized, occurring in areas of backwash dominated/accelerating flow that exist in the lee of swash bar/berm deposits . Such occurrences of Lithofacies 1 are evident in Figures 5.10a and c. Similar occurrences in swash bar deposits on lake shores in Kenya have been reported

by Reid and Frostick (1985).

Lithofacies 2: Upper and Lower Deceleration Zones (swash bar/berm)

In Chapter 4, the sedimentary structures and sediment textures that make up Lithofacies 2a were attributed to sedimentation processes that occur in swash: Near-horizontal to seaward-dipping lamination composed of coarse-grained, quartz-rich sands was associated with stationary and downstream-migrating in phase waves and bedwaves in the shoreward flowing, decelerating swash. The tapering-shoreward wedge shape of Lithofacies 2a also suggests the role of swash in its formation. Further, the location of Lithofacies 2a in the lower portion of NMB cross sections also suggests that swash plays a prominent role in its development. It is within the lower portion of the foreshore, where the swash mass first forms following bore collapse and then decelerates as it climbs the foreshore slope, that the swash exhibits a primary influence upon foreshore sedimentation. As a result it is in this area of the foreshore that the transport dynamics responsible for the accumulation of coarse-grained quartz-rich laminae and bed dynamics associated with near-horizontal lamination formation are most likely to occur. Thus, in the context of the cross-shore distribution of swash asymmetry, Lithofacies 2a is indicative of the lower swash-dominated deceleration zone. Its depositional setting is the 'swash bar' that develops in this zone (Table 5.3). Specifically, Lithofacies 2a is characteristic of the deposit found on the stoss side of the swash bar that develops in the lower foreshore and migrates shoreward during post-storm recovery.

Similarities between Lithofacies 2a and 2b sediment textures suggest that swash processes are also important in the development of Lithofacies 2b. The location of Lithofacies 2b in the upper most foreshore suggests that swash mass deceleration and and the accompanying percolation of the swash mass into the foreshore are the dominant processes controlling its formation. Correspondingly, it is in this area of the foreshore that the suspension sedimentation resulting in the accumulation of

Lithofacies 2b is most likely to occur. Subaerial processes are also likely to have an influence upon this intermittently wetted portion of the foreshore. The wind ripple cross-lamination associated with Lithofacies 2b is indicative of such subaerial processes. Thus, in the context of the cross-shore distribution of swash asymmetry, Lithofacies 2b correlates with the upper swash-dominated deceleration zone. Its depositional setting is the 'berm' that develops in this zone (Table 5.3). Specifically, Lithofacies 2b, with its accumulation of organic debris, represents a swash mark deposit found on the lee side of the berm that develops in the upper foreshore during post-storm recovery.

The swash bar/berm distinction made above is conceptually attractive. However , at NMB such a distinction is not always realized. In contrast to the simple model considered here, which treats the factors controlling swash asymmetry in terms of a resultant response over storm /recovery cycles, the superposition of lower order effects may have a prominent influence upon foreshore morphostratigraphy. The common occurrence of combined swash bar/berm deposits represents such influences. Combined swash bar/berm deposits, evident in Figure 5.10a, are inferred to be the result of the superposition of tidal or other higher frequencies oscillations of the simple pattern of asymmetry-induced zonation through the lower frequency storm/recovery cycle. That is, although the berm eventually ends up at the upper most portion of the foreshore, it may begin to develop at lower position in the foreshore during the neap tide and gradually migrate shoreward with the spring tide (Hine, 1979). Occurring simultaneously is the effect of the diurnal tidal cycle on foreshore sedimentation. At low tide berm-forming processes deposit sand in a particular foreshore location. At high tide swash bar-forming process deposit sand at this same location. The result is that combined swash bar/berm deposits may be formed at various times during storm recovery.

Lithofacies 3: Mixed Acceleration/Deceleration Zones (terrace)

The characteristics of Lithofacies 3 - alternating Type 1 and Type 2 lamination-

suggest that both swash and backwash processes are responsible for its formation. Its geometry both shorewards and seawards-pinching and its gradational relationship with the other NMB lithofacies also suggests that Lithofacies 3 is transitional facies which represents the influence of both swash and backwash processes. Lithofacies 3, which corresponds to the classic foreshore deposits described in the geologic literature, is interpreted as a 'terrace' deposit that develops in an area of the foreshore that exhibits a relatively equal distribution of swash and backwash forces. In the context of the cross-shore distribution of swash asymmetry these sweep zone deposits areas of foreshore equilibrium, where neither swash or backwash forces are particularly dominant.

THE NINE MILE BEACH MESODYNAMIC MODEL

Based upon the spatial distribution of the NMB lithofacies in the foreshore cross sections and their process implications discussed above, together with accompanying profile shape and volume changes, as well as runup/water table characteristics, two upper foreshore states are distinguished at NMB (Table 5.7: Figure 5.16: see also Table 5.2 and Table 5.4). These idealized foreshore states represent process-form/texture combinations that exist at the culmination of contrasting phases of profile evolution. The process-response relationships associated with these two foreshore states constitute the framework of the NMB mesodynamic model.

On *backwash dominated foreshores*, low frequency, relatively low amplitude runup over a saturated foreshore leads to the relative expansion of the middle backwash dominated zone. This facilitates the loss of sediment from the middle portion of the foreshore, the accumulation of tabular shaped set of heavy mineral-rich, fine-grained trough cross-bedded sands at this location, and the development of a concave foreshore profile. Thus, the storm morphostratigraphy and dissipative runup regime are associated with backwash dominated foreshores.

On *swash dominated foreshores,* high frequency, relatively high amplitude runup

TABLE 5.7 Nine Mile Beach FORESHORE STATES

STORM MORPHOSTRATIGRAPHY	**BACKWASH DOMINATED**	DISSIPATIVE RUNUP REGIME
Concave profile with tabular-shaped set composed of fine grained, heavy mineral-rich, trough cross-bedded sands	Erosion -SCARPING- in response to expansion of middle acceleration zone/ contraction of deceleration zones	Low frequency, relatively low amplitude runup over a saturated foreshore
SWELL MORPHOSTRATIGRAPHY	**SWASH DOMINATED**	REFLECTIVE RUNUP REGIME
Convex profile with wedge-shaped set composed of coarse grained, quartz-rich, near-horizontally laminated sands	Deposition -WELDING- in response to expansion of upper and lower deceleration zones/contraction of acceleration zone	High frequency, relatively high amplitude runup over an unsaturated foreshore

over a dry foreshore surface leads to the relative expansion of the upper and lower swash dominated zones. This facilitates a gain of sediment to the foreshore, the accumulation of quartz-rich, coarse-grained near-horizontally laminated sands, and the development of a convex foreshore profile. Thus, the swell morphostratigraphy and reflective runup regime are associated with swash dominated foreshores.

The two NMB upper foreshore states are considered further below.

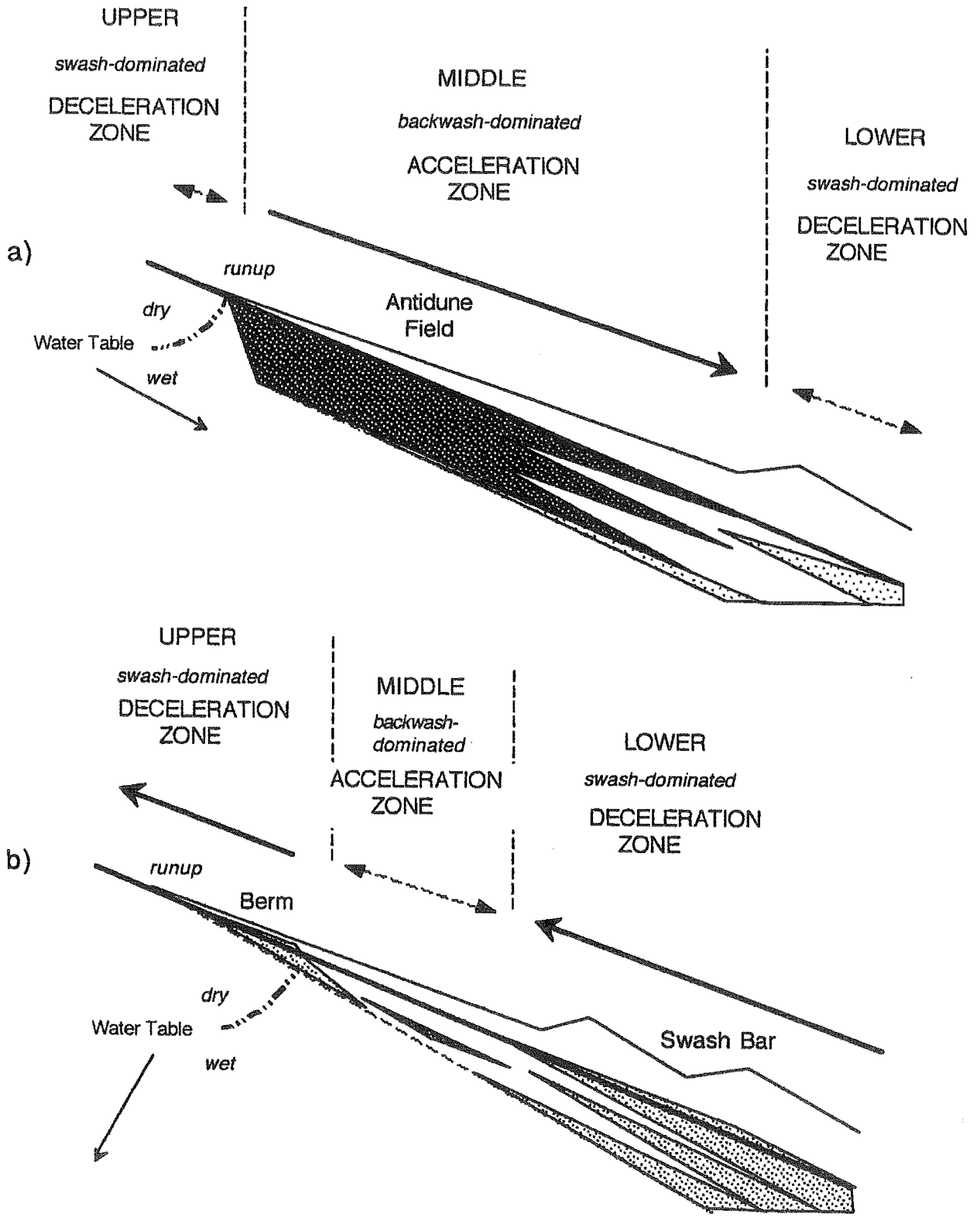

Figure 5.16. a) The Backwash Dominated Foreshore; b) The Swash Dominated Foreshore

The Backwash Dominated Foreshore

The predominance of Lithofacies 1 in the storm cross section, together with other characteristics of the storm morphostratigraphy, suggest that not only does backwash control the development of Lithofacies 1, but it is also central to the development of the storm morphostratigraphy. The tabular-shaped set of the storm cross section, with its abrupt shoreward boundary and gradually thinning seaward boundary, suggests that backwash processes control foreshore sedimentation. Similarly, the net flux of sediment out of the swash zone, the maximization of foreshore scour in the middle portion of the foreshore, and the accompanying changes in slope which lead to the development of the concave-shaped storm profile, suggest the role of backwash in the development of profile form as well as storm cross-sectional form and content.

Low frequency, backwash-induced 'scarping' is the term given here to describe these processes. Scarping occurs as the overall balance of forces on the foreshore abruptly shift from relative swash dominance to the relative dominance of backwash through a change in the distribution of backwash versus swash forces in the swash zone. Specifically, the middle -backwash dominated- acceleration zone expands, the upper and lower -swash dominated- deceleration zones contract. As a result backwash forces dominate swash zone sedimentation. The increase in the shoreward and seaward extent of Lithofacies 1 in the storm cross section relative to its occurrence in the swell cross section is a manifestation of the expansion/contraction of the backwash/swash dominated process zones that occurs during storm conditions.

Changes in the nature of runup-water table-morphology interactions that accompany the change toward dissipative conditions force scarping. Under dissipative conditions runup is higher than it is under reflective conditions. However, the swash zone is relatively narrower and therefore a greater proportion of the foreshore it passes over is saturated. Thus the larger swash mass experiences minimal mass loss. The finer grain sizes associated with the storm foreshore contribute to this effect. The result is that during dissipative conditions the mass of swash available to generate backwash is

maximized.

The maximization of backwash duration accompanies this effect. Under dissipative conditions, lower frequency motions dominate runup. Incoming swash experience strong interaction in the form of bore to bore merging and swash backwash collision. As a result, swashes are rarely able to complete their journey up the foreshore. Correspondingly the stronger backwashes occur less frequently but are longer in duration.

The net result of these interactions is that under dissipative conditions the proportion of the swash zone/area of the foreshore dominated by the backwash is at a maximum.

The Swash Dominated Foreshore

The predominance of Lithofacies 2 in the storm cross section, together with other characteristics of the storm morphostratigraphy, suggest that not only does swash control the development of Lithofacies 2, but it is also central to the development of the swell morphostratigraphy. The wedge-shaped set, with a gradational shoreward boundary and gradually thickening seaward boundary suggests that swash processes control foreshore sedimentation. Similarly, the net flux of sediment into the swash zone, the maximization of foreshore fill, particularly in the lower portion of the foreshore, and the accompanying changes in slope which lead to the development of the convex-shaped swell profile, suggest the role of swash in the development of profile form as well as storm cross-sectional form and content.

High frequency, swash-induced 'welding' is the term given here to describe these processes. Welding occurs as the overall balance of forces on the foreshore gradually shift from relative backwash dominance to the relative dominance of swash through a change in the distribution of backwash versus swash forces in the swash zone. Specifically, the upper and lower -swash dominated- deceleration zones expand, the the middle acceleration zone contracts. As a result swash forces dominate swash zone sedimentation. The increase in the shoreward extent of lithofacies 2a and seaward

extent of lithofacies 2b in the swell cross section relative to their occurrence in the storm cross section is a manifestation of the expansion/contraction phenomena of the swash/backwash dominated process zones that occurs during swell conditions.

Changes in the nature of runup-water table-morphology interactions that accompany the change toward reflective conditions force welding. Under reflective conditions runup is lower than it is under dissipative conditions. However, the swash zone is relatively wider and therefore a greater proportion of the foreshore it passes over is unsaturated. Thus the smaller swash mass experiences maximum mass loss. The coarser grain sizes associated with the swell foreshore contribute to this effect. The result is that during reflective conditions the mass of swash available to generate backwash is minimized.

The minimization of backwash duration accompanies this effect. Under reflective conditions, higher frequency motions dominate runup. Incoming swashes experience little or no interaction and are generally able to complete their journey up the foreshore. Correspondingly the weaker backwashes occur more frequently but are shorter in duration.

The net result of these interactions is that under reflective conditions the proportion of the swash zone/area of the foreshore dominated by the swash is at a maximum .

LONGSHORE VARIABILITY

In Chapter 3 spatial (longshore) as well as temporal variations in beach form and processes were shown to be important in the rhythmic NMB beach and surf zone system. Through analogies between dissipative/reflective and horn/bay runup regime contrasts the spatial variability in foreshore morphostratigraphy that exists at NMB can be assimilated into the NMB mesodynamic model. Specifically, more reflective runup regimes exist at horns, and as a result so to do more swell-like morphostratigraphies (i.e. both are swash dominated foreshores): More dissipative runup regimes exist at bays, and as a result so to do more storm-like

morphostratigraphies (i.e. both are backwash dominated foreshores). Such spatial storm/swell-like contrasts between bays and horns, although generally less distinct than the temporal storm/swell contrast of which they are superimposed upon, are nonetheless, an important aspect of NMB foreshore dynamics. Spatial variations in NMB foreshore dynamics are considered further below.

Although not discussed with respect to characteristics of runup regimes in the results section, differences in horn versus bay runup regimes were observed at NMB. Figure 5.12b, the plot of dimensionless runup height against the inverse of the Dean parameter, shows that horns are generally more reflective than bays. In this figure bay values of dimensionless runup height exhibit a tendency to be lower than horn values of dimensionless runup height (~1.25 vs. 1.75 respectively) at more reflective values of the inverse Dean parameter (~0.40) in particular. Thus, at least under reflective nearshore conditions, runup on the horns is relatively higher than it is in the bays. This would favor relative swash dominance on horns and relative backwash dominance in bays.

Although Figures 5.13 a and b give bay and horn spectra, due to non-synchronous observations the spectra are unfortunately not comparable. Differences between bay and horn spectra were, however, discussed in Chapter 3 in terms of process signatures. There it was noted that resonant motions at higher (subharmonic) frequencies are prominent on horns and lower (infragravity) frequencies are prominent in bays (Wright, 1982; Wright and Short, 1983, 1984). Thus although not evident in NMB data, it can be inferred form the results of previous workers that runup periods are shorter on horns than in bays. This would favor relative swash dominance on horns and relative backwash dominance in bays.

In Table 5.5b bay values of the percentage of foreshore saturation are consistently higher than horn values. For example, the average percentage of foreshore saturation in the bay is 80%, on the horn 63%. Such differences in the extent of foreshore saturation (water table elevation) between horns and bays have also been reported by

Eliott and Clarke (1988). Such tendencies would also favor relative swash dominance on horns and relative backwash dominance in bays.

Thus, runup regimes at horns and bays exhibit similar contrasts spatially in terms of resultant runup-water table-morphology interactions as those exhibited temporally under storm and swell conditions. As a result, similar contrasts in relative swash versus backwash dominance and associated patterns of asymmetry induced process zonation should exist. Such contrasts are represented in the NMB horn and bay morphostratigraphies.

Differences in NMB horn and bay profile form were considered at length in Chapter 3. They are comparable to those exhibited between storm and swell profiles as illustrated in Figure 5..4 and 5.6. Specifically, horns exhibit more steeply sloping, convex-shaped, swell-like foreshore profiles. Bays, on the other hand, exhibit more gently sloping, concave-shaped, storm-like profiles. Such contrasts between horn and bay profile form are well established (Zenkovich, 1967; Sonu, 1973). Similarly, with respect to volume flux the general tendency for accretion on horns and erosion in bays is well documented (Wright et al., 1979; Short, 1981). This spatial pattern mirrors the temporal pattern of profile accretion during swell conditions and profile erosion during storms.

In addition to profile form, horns and bays exhibit similar contrasts in stratigraphy and sedimentology. At NMB the coarse-grained, quartz-rich Lithofacies 2 a and b tend to be more prominent on the horns; fine-grained, heavy mineral-rich, Lithofacies 1 more prominent in the bays. Similarly cross sections are more wedge-shaped on the horns and horns and more tabular-shaped in the bays. Thus, horns exhibit more swell-like morphostratigraphies and bays exhibit more storm-like morphostratigraphies.

As was the case for horn and bay spectra, the foreshore cross-sections given in Figure 5.10 a-f are not directly comparable due to non-synchronicity of the observations. Comparisons of the bay cross-sections in a-c with the horn cross-sections in d-f do not reveal a well -developed pattern of spatial variation. Temporal patterns dominate morphostratigraphic variation in these cross-sections.

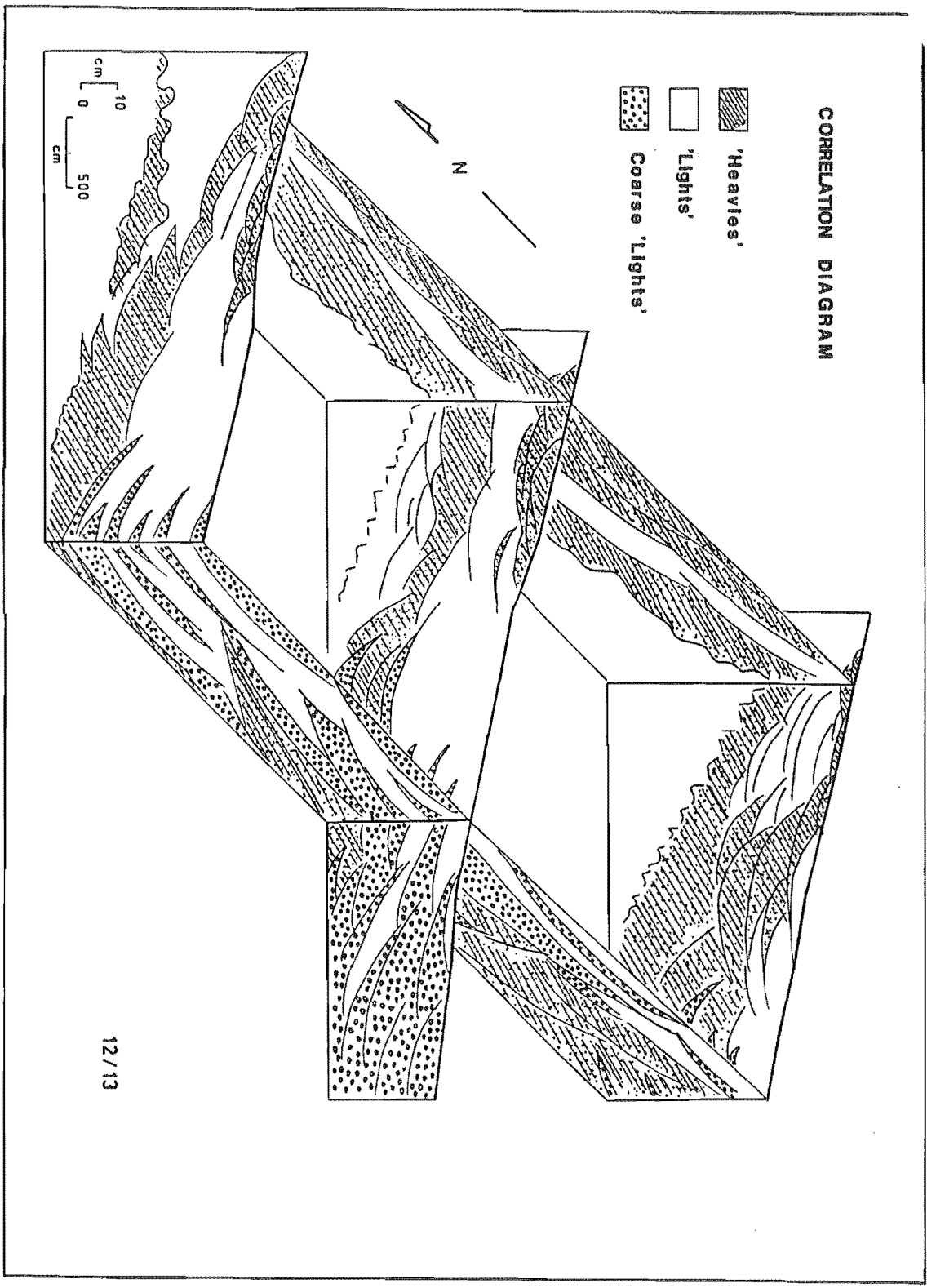

Figure 5.17. Correlation Diagram (from Marra, 1988). In this figure 'Heavies', 'Lights', and 'Coarse Lights' correspond to Lithofacies 1, Lithofacies 3, and Lithofacies 2 of this text respectively. Longshore distance between cross-sections is 100 meters.

Horn and bay morphostratigraphic contrasts are clearly evident in Figure 5.17 however. The correlation diagram in this figure is centered on a concave-shaped bay profile; more convex-shaped horn profiles are located 100 meters to the north and south. Three different depositional units are evident in this diagram. Each illustrates horn and bay stratigraphic contrasts. The first unit, a thin upper heavy mineral layer, is thickest in the center bay cross-section and thins both north and south towards the horn cross-sections. The second unit, a middle light mineral layer, is also thickest in the center bay cross section. This unit remains thick in the northern cross-section, but thins dramatically towards the south. In contrast, the the third unit, a basal heavy mineral layer, is thickest in the southern cross-section and thins dramatically towards the north.

Reviewing the sequence of events leading up to the formation of these units supports the applicability of the mesodynamic model to spatial variability in foreshore dynamics, as observed conditions conform closely to those predicted by the model. The initial event leading to the formation of these three units involved the occurrence of a high energy storm that scoured out a bay larger in scale than the one captured in the diagram. All three profiles experienced relative backwash dominated, dissipative conditions at this time. The basal heavy mineral layer formed in association with this event. An extended period of recovery followed the major storm event. During this recovery period, the center and northern profiles initially continued to act as bays, experiencing more dissipative conditions than the southern profile. This is represented by the removal and truncation of the basal heavy layer in the center and northern section and the maintenance of the basal layer in the southern section. As recovery continued, conditions across the entire section of shore became swash dominated. During this period of reflective runup the large bay was filled with lights. The recovery period was halted by the occurrence of a moderate energy storm event. This most recent event resulted in the formation of the existing central bay with the greatest amount of heavy mineral accumulation and the flanking horns with lesser amounts of

heavy mineral accumulation. The distribution of this upper heavy mineral unit in the correlation diagram conforms most closely to that predicted by the model: Dissipative runup in the bay resulting in relative backwash dominance and the development of a more storm-like morphostratigraphy - Reflective runup on the horns resulting in relative swash dominance and the development of a more swell-like morphostratigraphy.

5.4 CONCLUSIONS

In this chapter, systematic changes in foreshore sedimentology and stratigraphy were found to accompany the well recognized patterns of storm/recovery cycle morphologic variation. Specifically, the accumulation of finer-grained, heavy mineral-rich, seaward-dipping trough cross stratified sands in the upper to middle foreshore (NMB Lithofacies 1) are associated with the occurrence of concave-shaped 'storm' profiles: The accumulation of coarser-grained, quartz- rich, near-horizontally laminated sands across the entire upper foreshore (NMB Lithofacies 2) are associated with the occurrence of convex-shaped 'swell' profiles. The term *storm* and *swell morphostratigraphy*, respectively, was applied to these assemblages of morphologic and stratigraphic characteristics.

Dissipative and *reflective runup regimes* were also identified. The runup regimes encompass idealized sets of resultant runup and water table characteristics observed at culminating phases of storm/recovery cycles. Specifically, the dissipative runup regime is characterized by relatively low amplitude, low frequency runup over a wet foreshore. The reflective runup regime is characterized by relatively high amplitude, high frequency runup over a dry foreshore.

The occurrence of the storm morphostratigraphy was found to correspond with that of the dissipative runup regime. Conversely, correspondence was observed between the swell morphostratigraphy and the reflective runup regime.

A conceptual model for swash zone dynamics that focuses on inferred variations in

the distribution and relative dominance of swash versus backwash forces on the foreshore is used to explain the observed mesoscale process-form coupling. In this model, the relative dominance of swash forces on the foreshore results from increased swash mass loss and decreased backwash duration. These conditions accompany reflective runup. Similarly, the relative dominance of backwash forces on the foreshore results from decreased swash mass loss and increased backwash duration. These conditions accompany dissipative runup.

Associated with the simple shift in swash asymmetry towards relative swash or backwash dominance over the entire foreshore, is a corresponding shift in asymmetry-induced process zonation. On *swash dominated foreshores* the extent of upper and lower -swash dominated- deceleration zones is maximized relative to that of the middle -backwash dominated- acceleration zone. As a result swash-induced welding leads to the development of the swell morphostratigraphy, with its swash bar and/or berm. On *backwash dominated foreshores* the extent of the middle -backwash dominated- acceleration zone is maximized relative to that of the upper and lower -swash dominated- deceleration zones. As a result backwash-induced *scarping* leads to the a development of the storm morphostratigraphy, with its antidune field.

The simple two-dimensional model for storm/recovery cycle foreshore dynamics, which exhibits affinities to Duncan's (1964) tidal cycle model, is also used to explain spatial variations in foreshore morphostratigraphy that are prominent on NMB. Specifically, more reflective runup regime exists on horns and as a result so do more swell-like morphostratigraphies; more dissipative runup regime exists in bays and as a result so do more storm-like morphostratigraphies.

Although complicated by local variations induced by the superposition of other scales of unsteadiness, the simple model for mesoscale foreshore dynamics described in this chapter provides a useful conceptual framework for the further exploration of variations in foreshore morphologic, stratigraphic, runup, and water table characteristics through storm/recovery cycles.

Finally, the central theme of this work - the enmeshed nature of process-response

interactions in sandy coastal systems- is well illustrated by the nature of mesoscale process-response interactions described in this chapter. Here it was shown that foreshore morphostratigraphies represent a response to a variety of influences operating simultaneously across a range of temporal and spatial scales.

5.1 The following procedure was used to derive the log plots of runup height power spectra given in figure 5.13 a and b. A 'synthetic' time series was generated from the video recordings of runup (described in Chapter 2). The original time series consisted of a series of runup height maxima. (As only runup that entered the camera view could be recorded, all runup maxima below a particular cross-shore location were filtered out of the time series.) All points located halfway between each pair of runup maxima within the time series were determined. The same value of minimum runup height was inserted at each of these positions in the time series. A linear interpolation was preformed on these time series to yield the synthetic time series of equally spaced values that were then used in further analyses. Each synthetic time series was demeaned, detrended, and tapered prior to fourier analysis. The resulting time series was then smoothed (with a moving average) and logged prior to plotting.

It is suggested that the methodology employed here to generate runup height spectra tended to truncate both the highest and lowest frequency components of the 'true' spectrum, while providing a good approximation of the bulk of the spectrum. Aside from intuitive reasoning, this statement is based upon an analysis that was carried out on the coherency of 'true' and 'synthetic' spectra. (T. Lippman provided the runup height time series used for this analysis. It was of identical length to that obtained during this study and came from a runup record obtained at a beach on the Oregon coast that is similar to NMB.) The results of this analysis showed that, at a 90% level of significance, 95% of the spectrum was coherent at a frequency range corresponding to runup periods of 205 to 16 seconds and 100% was coherent between the range corresponding to periods of 42 to 16 seconds. Thus, although the methodology described above may not provide a representation of 'true' runup spectra, it does provide spectra that are suitable for the types of intercomparisons made in this study.

5.2 Local swash and backwash energy was calculated as U^{*2} integrated over the duration of the swash or backwash event. These values are proportional to transport rates (Allen, 1985). They are 'local' values in that they are derived from surface flow velocities and durations observed at a single cross shore location (see Chapter 2 and Chapter 4). Similar determinations have been made by Schiffman (1965) and Kirk (1970) among others.

CHAPTER 6 SUMMARY

"The world thus appears as a complicated tissue of events, in which connections of different kinds alternate or overlap or combine and thereby determine the texture of the whole."

W. Heisenberg

6.1 ISOLATED PARTS AND INTERCONNECTED WHOLES

Each of the three principal chapters in this study examined a network of process-response interactions that operate at a particular range of scales to determine resultant morphologies and/or material properties (Table 6.1). Chapter 3 described nearshore morphologies and processes at spatial scales of meters to kilometers and temporal scales of days to weeks. Chapter 4 described bedforms, stratification, sediment textures, and transport processes at spatial scales of millimeters to centimeters and temporal scales of seconds to minutes. Chapter 5 described foreshore morphology, stratigraphy, and runup processes at spatial scales of centimeters to meters and temporal scales of hours.

The three chapters collectively constitute a larger network of process-response interactions that define swash zone dynamics. The mesoscale foreshore dynamics of Chapter 5 encompass all aspects of the microscale transport and bedform dynamics of Chapter 4, yet are themselves encompassed within the macroscale beach and surf zone dynamics of Chapter 3.

Thus, each chapter is both a collection of isolated parts that together makeup interconnected wholes and an isolated part in a larger interconnected whole. As such, each chapter and the work as a whole demonstrate the enmeshed nature of swash zone dynamics.

The identification of a mosaic of interlocking models developed and/or applied during this study is the means by which the connection of isolated parts is achieved. Specifically, the bootstrap approach successfully established a linkage from incident wave condition-morphologic interactions occurring at the macroscale to flow-grain-bed interactions operating at the microscale, through their mutual relationship to the temporal and saptial variations in the relative dominance of swash versus backwash forces operating at the mesoscale, or *swash asymmetry*. The result is a broader, more unified understanding of swash zone dynamics in a rhythmic 'black sand' beach system. The implication, that the bootstrap approach should be applied elsewhere as an approach to problem solving.

Findings and conclusions specific to each chapter are summarized below.

6.2 METHODOLOGY

With the above ideas in mind and with respect to the methodology employed during this study, two separate but integrated data collection plans facilitated concurrent measurement of process-response parameters across a range of spatial and temporal scales. Despite limitations relating to record length and quality, this 'separate but integrated' methodology in and of itself enables the aims of this study to be accomplished.

Large Scale Data Collection and Analysis

Large scale data collection involved the concurrent observation of nearshore conditions, plan and profile form, and foreshore stratigraphy on a daily basis. Large scale data collection was carried out through four storm/recovery cycles and totaled 43

Figure 6.1 SPATIOTEMPORAL NETWORK OF PROCESS/RESPONSE INTERACTIONS OPERATING IN THE NINE MILE BEACH SWASH ZONE

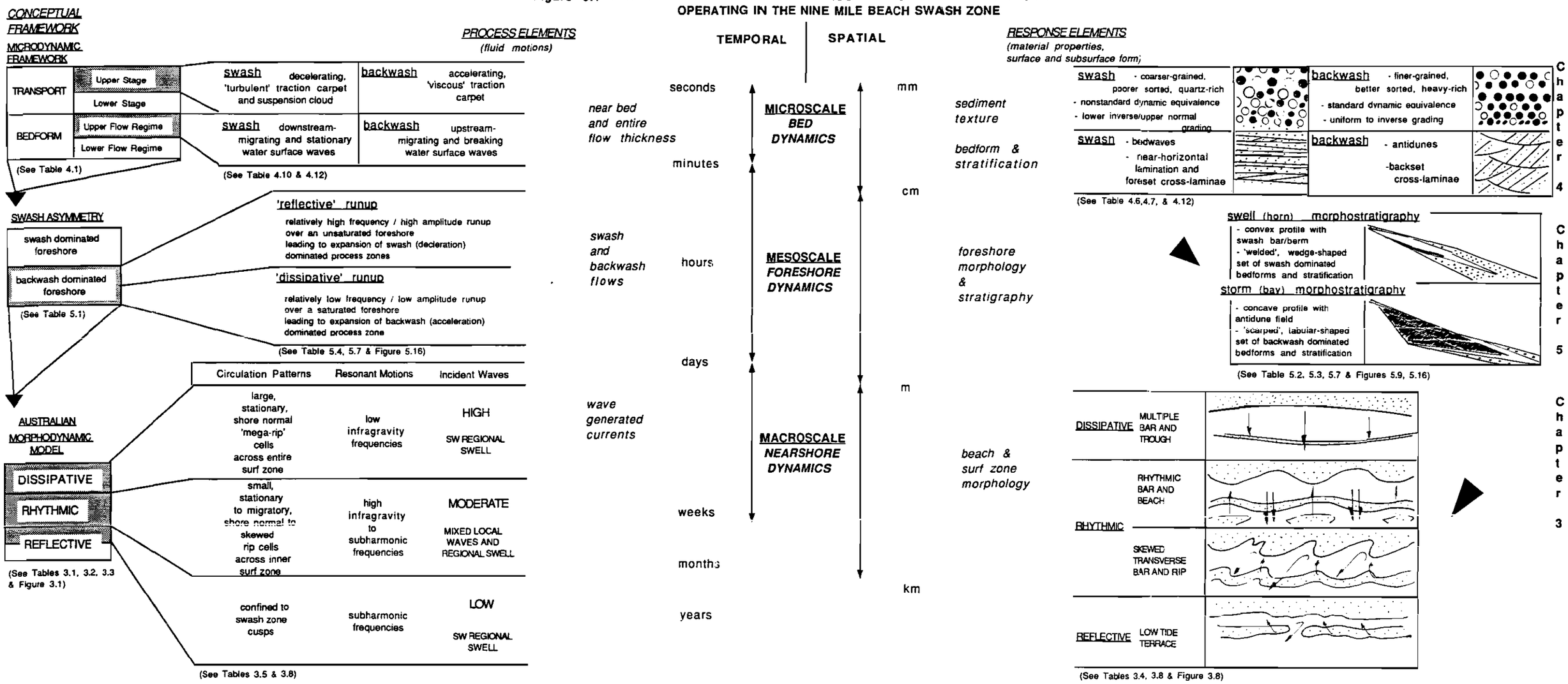

days of observations.

Simple techniques were used to obtain measurements of nearshore conditions at NMB (e.g. visual observations for wave height and period; compass and hand-held anemometer for local surface wind direction and magnitude; dye for littoral current surface velocity). Simple procedures were also used to collect data on plan and profile morphology at NMB (e.g. profile surveys; plan sketches and photographs of plan morphology). These simple techniques are easily employed by a single worker and involve minimal expenditure. However, data are only adequate in comparison to that which is obtainable using instrumented data collection techniques.

During this study, additional evidence on the nature of subaqueous beach morphology was obtained from an experimental photographic technique carried out on a limited basis. The technique is a powerful morphologic data collection tool. It is particularly well suited to high energy surf zones.

As part of this study, a classification scheme for rhythmic topographies was developed for use as a data analysis tool. Unlike existing classification schemes for rhythmic topographies, which are based solely on the longshore length of the rhythmic features, the classification scheme is morphogenetic. The inclusion of form genesis in the classification scheme eliminates much of the awkwardness and confusion associated with existing classification schemes.

Two additional profile parameters were also defined for use as a data analysis tool. The beach profile shape indices, defined here as the ratio of high-tide beach slope to mid-tide beach slope (RBS) and the ratio of mid-tide beach width to high-tide beach width (RBW), express profile form in terms of the degree of profile concavity or convexity. As higher sensitivity form indicators, the profile shape indices complement the standard profile parameters of volume exchange, beach mobility, and backshore mobility.

An integral part of this study involved the descriptions of sedimentary structures and textures from closely spaced trenches excavated in the NMB foreshore. Here taken in conjunction with the recording of nearshore process and beach form

parameters on a daily basis, the descriptions of foreshore stratigraphy yield a wealth of process-sensitive information that is rarely, but should be regularly, incorporated into studies of modern beach processes.

Small Scale Data Collection and Analysis

Small scale data collection involved the concurrent observation of swash zone flow characteristics, foreshore bed form, and foreshore material properties through the tidal cycle. Small scale data collection was carried out on 10 occasions, the results from five of which were examined in this study.

Video recording techniques were successfully employed during this study to measure runup excursions, depths, and surface velocities on the upper foreshore. A total of 241 individual swash/backwash events were sampled, approximately every 1.5 seconds on average, using this methodology. These video recording techniques have advantages over conventional current meters. They work well in the periodic, shallow, rapid, sediment-laden flows of the swash zone. They are inexpensive and their deployment logistics simple. They provide a visual record of what are often complex flow events. They even have a use as oral data recorders of field notes. However, in comparison to current meter-based techniques, the nature of the data has limitations. Leading edge and surface velocities are adequate but not ideal flow parameters. Also, data acquisition is time consuming. The application of improved video manipulation technology would reduce this disadvantage. Still, and at the very least, video recording techniques have a role to play in a larger data collection network.

During this study detailed sediment sampling techniques were employed. Grain counts of individual grain layers were obtained from color slides of sediment peels taken from box cores. A total of 170 individual grain layers with an average sample size of 168 grains were sampled. Textural parameters obtained from the peels show close correspondence to those obtained using standard techniques (e.g. mean grain size of 0.238mm from the peels versus mean grain size of 0.19mm and 0.22mm from

standard sieving and settling tube analyses respectively / mean settling velocity of 2.97cm/s calculated from the peels versus a mean settling velocity of 2.70 cm/s measured from settling tube analysis of bulk samples). The fine scale sampling technique employed in this study is very time consuming. However, the use of more sophisticated 'frame-grabbing' video recording techniques would greatly reduce this limitation. Sampling at this fine scale, and the conversion of this data to hydraulic grain parameters and equivalence relationships, yields valuable process-sensitive information generally lost in standard grain sampling and size analysis procedures. This suggests that greater success in relating sediment textures to formative processes can be achieved through the application of the sorts of detailed sediment sampling techniques employed during this study. With respect to the study of nearshore processes in particular, detailed sediment sampling has received little attention. Yet, as a component in a data collection network, it too has a role to play.

6.3 MACROSCALE DYNAMICS

The "Australian model" for coastal morphodynamics was introduced in Chapter 3. This model provides a framework for the investigation of NMB beach and surf zone dynamics. In it, nearshore morphologies represent the resultant response to a combination of standing wave motions and nearshore circulation patterns that coexist with the nearshore. Particular beach and surf zone morphologies, or "beach states", are associated with particular combinations of standing wave motions and nearshore circulation patterns, or "process signatures". Morphologies change as variations in wave energy level at seasonal, storm, tidal, and wave group time scales force changes in the relative dominance of the various types of fluid motions.

Based on a comparison to Australian model morphologies, four beach states were identified at NMB: Low Tide Terrace, Multiple Bar and Trough, Rhythmic Bar and Beach, and Skewed Transverse Bar and Rip. Having persisted for 70% of the study

period, the Rhythmic Bar and Beach and Skewed Transverse Bar and Rip states are modal states within the NMB system. Associated with these two beach states is a range of rhythmic topographies that are characterized by the presence of a crescentic inner bar and rhythmic shoreline.

Regional southwesterly swell is the dominant component (60%) in a NMB wave climate that is characterized by the regular (every 4-5 days on average) occurrence of waves greater than 2 meters in height and 10-13 seconds in period. Superimposed upon these high frequency variations in wave height is a regularly northerly-flowing longshore current and an approximately 3 meter semi-diurnal tide.

Obtained through the application of similarity parameters, correspondence between NMB beach state morphologies and wave climate components suggest that the two rhythmic states exist in conjunction with all wave climate components (ie. southwesterly regional and local swell, and local storm waves). In contrast, the broad surf zones and multiple bars of the Multiple Bar and Trough state only develop at the onset of high energy (H_b>2.25m) southwesterly swell: The narrow surf zones and irregular shoals of the Low Tide Terrace state only develop after extended periods of low energy (H_b<1.0m) southwesterly swell.

The characteristic pattern of morphologic evolution observed at NMB consists of an alternation between abrupt (1-2 days) offshore movement of the inner bar during storms and gradual (7+ days) onshore and alongshore migration and welding of the inner bar during post-storm recovery. The predominance of this pattern of morphologic evolution corresponds with the prevalence of rhythmic topographies at NMB. Both are attributed to the combined effects of response asymmetry and high frequency temporal energy variability. That is, rhythmic morphologies prevail at NMB primarily because there is insufficient time between storms for reflective morphologies to develop.

A decrease in rhythm spacings also occurs as part of the the NMB pattern of morphologic evolution. Following from the Australian model, this is taken to represent a downward shift in the dominant period of nearshore resonance. Large surf

cusps (500-1000m wavelength) of the Multiple Bar and Trough state correspond to resonant motions at low infragravity frequencies (100-200 seconds). Small surf cusps (500-100m wavelength) of the two rhythmic states correspond to resonant motions at high infragravity to subharmonic frequencies (50-100 seconds). Small surf cusps (<100m wavelength) of the Low Tide Terrace state correspond to resonant motions at subharmonic frequencies (25-50 seconds).

Although generally comparable to the pattern of morphologic evolution described in the Australian model, the NMB pattern of morphologic evolution differs in that the sequential decrease in rhythmic shoreline spacings culminates in the development of skewed, migratory shoreline rhythms. This difference between NMB Australian model morphologies at the later stages of post-storm recovery is attributed to the greater influence of longshore currents/littoral drift in the NMB nearshore system than in those used to develop the Australian model.

Another difference between NMB and Australian model morphologies occurs with respect to morphologic expression. At NMB the beach and surf zone morphologies tend to be more subtly expressed than the Australian model morphologies (i.e. barforms exhibit lower elevations and longer wavelengths). This difference in morphologic expression is attributed to a greater influence of tidally-induced variations in surf zone width and breaker position at NMB.

The observations and interpretations of Chapter 3 suggest that the Australian model provides a useful framework for the study of sand beach morphodynamics. Its appeal lies in its ability to incorporate the diversity of forms and processes in sandy coastal systems into a comprehensive framework for the investigation of sand beach dynamics. However, modifications are required. This study points towards a particular need to focus greater attention on sandy coastal systems where longshore currents are a prominent process component. In a more general sense, this study highlights the need to examine morphologic expression and patterns of morphologic change in sandy coastal systems with different combinations of process components.

In this regard, long-term monitoring of concurrent process and form measurements could be readily facilitated through use of computer-enhanced wide-angle video recording techniques such as those recently employed by Lippman and Holman (1989:1990) to monitor bar field dynamics, Holman et al. (1991) to monitor profile changes, and these same workers to monitor nearshore fluid motions (Lippman and Holman, 1991).

6.4 MICROSCALE DYNAMICS

The 'microdynamic framework' was outlined in Chapter 4. It was developed as part of this study to provide a basis for the description and analysis of bedform and transport dynamics within swash zone flows. In it, deposit characteristics represent the resultant response to a combination of fluid-bed-grain interactions that occur simultaneously both near the bed and throughout the entire thickness of the flow. Central to the microdynamic framework is a conceptual distinction in deposit characteristics between internal textural properties (attributed to smaller near-bed scale processes) and external bedform and stratification geometries (attributed to larger entire flow-thickness scale processes). In the microdynamic framework particular assemblages of deposit characteristics are associated with particular combinations of near-bed and flow -thickness scale processes.

Long wavelength, low relief 'bedwave' and antidune forms were the characteristic surface features of the NMB upper foreshore. Bedwaves exhibited lengths on the order of 10-20 meters and heights in the 0.10-2.5 centimeter range. Antidunes averaged ~1 meter in length and 2 centimeters in height. Near-horizontal lamination is the prominent stratification type observed on NMB. Its dimensions are generally on the order of 1-2 meters in length and 0.1-2.0 centimeters in height. Low (5-6^{o}) and high (12-25^{o}) angle shoreward-dipping cross-stratification, generally ranging from 0.5-1 meters in length and 1-5 centimeters in height, was also common.

Two lamination types were identified in the upper foreshore of NMB. Type 1 grain

layers are finer-grained , better sorted, and more heavy mineral-rich than Type 2 grain layers (0.24mm versus 0.35mm mean size: 0.06 versus 0.13 mean standard deviation: 69% versus 53% heavy minerals respectively). In Type 1 lamination heavy and light minerals within grain layers are inferred to be in a standard form of dynamic equivalence (dispersive). In Type 2 lamination heavy and light minerals within grain layers are believed to be in a modified form of dynamic equivalence (hindered settling). Type 1 lamination is characterized by uniform to weakly inverse grading. Type 2 lamination is characterized by more complex combinations of inverse and normal grading.

Mean time-averaged surface flow velocities ranged from 86-101 cm/s for the swash and from 63-78 cm/s for the backwash. Average velocity maxima ranged from 172-206 cm/s and 114-143 cm/s in the swash and backwash respectively. Mean time-averaged flow depths ranged from 5-8 centimeters for the swash and 2-3 centimeters for the backwash. The maximum water depth measured was 50 centimeters. For both swash and backwash, mean bottom shear velocities were calculated to be on the order of 2.0-4.5 cm/s. Mean Froude numbers greater than 2.0 (breaking surface waves) were found occur about three to four times more frequently in the backwash than in the swash.

Viewed in the context of the microdynamic framework, deposit and flow characteristics suggest that swash zone flows are upper stage ($U^*/U^*_e > \sim 1.2$), upper flow regime flows. Bedform dynamics within these shallow, high velocity flows is characterized by the occurrence of water-surface waves, and in-phase bedforms and associated stratification types. Bedform and stratification length scales, including near-horizontal lamination, were found to scale with those of the water surface waves as predicted by Kennedy's (1961) relationship. Transport dynamics is characterized by the existence of a two-layer granular dispersion. After models of Lowe (1982, 1988) and Hanes and Bowen (1985), there is inferred to be a lower 'traction carpet' layer dominated by granular fluid mechanics and an upper 'suspension cloud' layer dominated by turbulent fluid mechanics. Sediment textures within and

between laminae exhibit characteristics that are indicative of the lower or upper flow layer.

Distinct microscale process-form assemblages were recognized for each flow type. Breaking and upstream-migrating water surface waves in the accelerating, seaward-flowing backwash are associated with the antidune and other shorter, higher amplitude in-phase bedforms that develop on the uppermost foreshore surface. Shoreward-dipping, high angle, trough cross-(backset)-bedding is the principal stratification type associated with these bedforms. The formation of Type 1 lamination, which is predominant in these deposits, is also interpreted in the context of backwash processes. The better sorted, finer-grained, heavy mineral-rich textures, with uniform to weakly inverse grading, and that exhibit dynamic equivalence between heavy and light minerals, are interpreted as traction carpet layers deposited instantaneously in areas of local deceleration within an accelerating flow.

Stationary and downstream-migrating water surface waves in the decelerating, shoreward-flowing swash are associated with the longer, lower amplitude in-phase bedwave forms that develop on the upper foreshore surface. Near-horizontal lamination and shoreward-dipping, low angle trough cross-(foreset)-bedding are the principal stratification types associated with these bedforms. The formation of Type 2 lamination, which is predominant in these deposits, is also interpreted in the context of swash processes. The poorer sorted, coarser-grained, quartz-rich textures, with both normal and inverse grading, and that do not show dynamic equivalence between heavy and light minerals, are interpreted as mixed traction carpet and suspension cloud layers deposited sequentially within a decelerating flow.

The observations and interpretations presented in Chapter 4 have implications to existing models for the the origin of horizontal lamination in the swash zone. Unlike the commonly accepted 'single process' model of Clifton (1969), this study suggests that both swash and backwash have a role to play in lamination genesis. Further, the results of this study suggest that flow-thickness scale as well as near-bed scale

processes influence lamination genesis.

The microdynamic framework was applied in this study as a basis for the description and analysis of bedform and transport dynamics within swash zone flows. However, it is wider ranging in applicability. It has the ability to do at the microscale what the Australian model does at the macroscale, namely, to encompass the diversity of material properties, bedforms, and processes in fluid flows. As such, it has the potential to function as a comprehensive framework for the investigation of transport and bedform dynamics. To explore this potential, attention should be directed towards the identification of systematic variations in bedform/stratification types and sediment textures for different combinations of flow depth, velocity, and sediment concentration under conditions of both flow acceleration and deceleration in general. With respect to the topics covered in Chapter 4, there is a particular need for further examination of transport and bedform dynamics in high velocity, high concentration flows, along the lines of the laboratory studies of Bridge and Best (1988), Paola et al. (1989), Arnott and Hand (1989), and Cheel (1990).

6.5 MESOSCALE DYNAMICS

Chapter 5 outlines the NMB mesodynamic model. Developed as part of this study, this conceptual model provides a basis for the consideration of two-dimensional storm/recovery cycle foreshore dynamics at NMB. In it, a particular foreshore morphostratigraphy and runup regime is associated with the contrasting phases of the storm/recovery cycle. In the NMB mesodynamic model, as in Duncan's (1964) tidal cycle model, the balance of onshore versus offshore forces, or swash asymmetry, is the fundamental mechanism controlling foreshore morphostratigraphic change. In the NMB mesodynamic model variations in swash asymmetry are manifest not only in terms of the overall relative swash or backwash dominance, but also in terms of the cross-shore distribution of swash versus backwash forces.

Three swash zone lithofacies were distinguished within the upper foreshore of

NMB. Lithofacies 1 occurs as a tabular-shaped set that generally occupies the upper to middle portion of the upper foreshore. High angle shoreward-dipping trough cross-bedding composed of fine-grained, very well sorted, heavy mineral-rich sands (Type 1 textures) are a characteristic feature of Lithofacies 1 internally. In the context of the cross-shore zonation of swash asymmetry, Lithofacies 1 is indicative of the middle backwash-dominated acceleration zone. Its depositional environment is the 'antidune field' that is best developed within this zone during storms.

Lithofacies 2 is composed of Subfacies 2a and 2b. Subfacies 2a is a wedge-shaped set that generally occupies the lower to middle portion of the upper foreshore. Internally, Subfacies 2a is characterized by near-horizontally-laminated to thin-bedded layers of coarse-grained, moderately sorted, quartz-rich sands (Type 2 textures). In the context of the cross-shore zonation of swash asymmetry, Subfacies 2a is indicative of the lower swash-dominated deceleration zone. Its depositional setting is the 'swash bar' that develops in the lower foreshore and migrates shoreward during post-storm recovery. Subfacies 2b occurs as a thin, fine-grained, quartz-rich lens located in the uppermost portion of the upper foreshore. Subfacies 2b correlates with the upper swash-dominated deceleration zone. Its depositional setting is the 'berm' that develops in the upper foreshore during post-storm recovery.

Lithofacies 3 occurs as a variably-sized, lenticular-shaped set that commonly occupies only the middle, but occasionally occupies the entire upper foreshore. Near-horizontal lamination, composed of alternating dark and light layers is characteristic of the set internally. In the context of the cross-shore zonation of swash asymmetry, Lithofacies 3 is interpreted as a 'terrace' deposit that develops in the sweep zone where neither swash or backwash forces are dominant.

Storm and swell morphostratigraphies were identified for the NMB foreshore. Each morphostratigraphy is defined by an assemblage of coupled morphologic and stratigraphic characteristics. The storm morphostratigraphy is distinguished by a thick, tabular-shaped cross-sectional form dominated by the occurrence of Lithofacies 1. Higher values of RBS (~1.5) and RBW (~2.0) are indicative of the more concave-

shaped storm foreshore profile. Storm foreshore volume flux is net negative and exhibits a pattern of mid-profile cut. The swell morphostratigraphy is distinguished by a thin, wedge-shaped cross-sectional form dominated by the occurrence of Lithofacies 2 and 3. Lower values of RBS (~1.0) and RBW (~1.5) are indicative of the more convex-shaped swell foreshore profile. Swell foreshore volume flux is net positive and exhibits a pattern of seaward-increasing profile fill.

Dissipative and reflective runup regimes were also identified for the NMB foreshore. The two runup regimes represent idealized sets of resultant runup and water table characteristics that exist at culminating phases of storm/recovery cycles. Although absolute runup volumes are larger in the dissipative regime, runup is proportionately lower in amplitude (R_V/H_b = 0.5 dissipative versus 2.0 reflective) and correspondingly the swash zone is relatively narrower in width. Lower frequency/ longer period runup is associated with the dissipative regime (T_r/T_i = 25 dissipative versus 5 reflective). The dissipative runup regime is also characterized by a greater extent of saturated swash zone than the reflective runup regime (WT_h/R_h = ~76% dissipative versus ~69% reflective).

The storm morphostratigraphy and dissipative runup regime are associated with the 'backwash dominated foreshore'. The swell morphostratigraphy and reflective runup regime are associated with the 'swash dominated foreshore'. On backwash dominated foreshores the relative dominance of backwash forces on the foreshore results from decreased swash mass loss and increased backwash duration - conditions which accompany dissipative runup. The converse is true for swash dominated foreshores. Associated with the simple shift in swash asymmetry towards relative swash or backwash dominance over the entire foreshore, is a corresponding shift in asymmetry-induced process zonation. On backwash dominated foreshores the extent of the middle -backwash dominated- acceleration zone is maximized relative to that of the upper and lower -swash dominated- deceleration zones. As a result backwash-induced scarping leads to the development of the storm morphostratigraphy, with its antidune

field. On swash dominated foreshores the extent of upper and lower -swash dominated- deceleration zones is maximized relative to that of the middle -backwash dominated- acceleration zone. As a result swash-induced welding leads to the development of the swell morphostratigraphy, with its swash bar and/or berm.

The NMB mesodynamic model of Chapter 5 provides a conceptual framework for further examination of mesoscale foreshore dynamics. Not only is it applicable to storm/recovery scale foreshore dynamics, but the concepts encompassed within it are applicable to other scales of unsteadiness as well. In this work for example, distinctions comparable to those made temporally between storm and recovery phases were found to exist spatially between bays and horns respectively. Specifically, bays are identified as backwash dominated foreshores. Their morphostratigraphy is more storm-like (i.e. more concave-shaped, lithofacies 1-filled profiles). Their runup regime is more dissipative (i.e. relatively lower amplitude, lower frequency runup over a more saturated foreshore). Horns are identified as swash dominated foreshores. Their morphostratigraphy is more swell-like (i.e. more convex-shaped, lithofacies 2 and 3-filled profiles). Their runup regime is more reflective (i.e. relatively higher amplitude, higher frequency runup over a less saturated foreshore). Generally less distinct than the storm/swell distinction upon which they are superimposed, and only well developed in association with particular beach states, the horn/bay distinction is nonetheless a fundamental component of NMB foreshore dynamics.

Before the complexities of process-form feedbacks in sandy coastal systems, and in particular rhythmic beaches, can be unraveled, further work is needed which addresses the intermediate scale of process-response interaction covered in Chapter 5, for it at this level that unification across the spatiotemporal scales covered in this work is achieved. Studies which combine detailed mapping of foreshore morphostratigraphies together with the collection of process measurements, including beach water table dynamics, would go along way towards addressing this need.

ACKNOWLEDGEMENTS

A number of people have helped me to complete this work - at different times and in different places. I will do my best to acknowledge them all.

In New Zealand, at University of Canterbury, Christchurch -

I wish to thank my supervisor Dr. D.W. Lewis (Geology), not only for his useful comments at all stages of this work, but for his patience and understanding in the long and drawn-out final stages of this work. I also wish to thank my advisors Dr. R.M. Kirk (Geography) and Dr. A.J. Sutherland (Civil Engineering) for their helpful comments at various stages of this work. It is Dr. Kirk I have to thank for getting me hooked on things coastal. I owe a special thanks to my friend Dr. Murray Hicks (DSIR). My queries on the road to Akaroa, and the numerous others I subjected him to, always proved insightful. I wish to thank Mr. Nick Clarke, formerly of the Audio Visual Center, and his staff. I am indebted to them for the use of their video recording equipment and facilities. I also wish to acknowledge technicians Mr. Davy Jones, Mr. Albert Downing, Mr. Arthur Alloway and secretary Ms. Wendy Nutthal. Their various efforts were greatly appreciated. Thanks also go out to Professor Jim Cole and Dr. Steve Weaver for their efforts on my behalf.

In Oregon, at Oregon State University, Corvallis -

In addition to thanking Dr. Paul Komar for review of my manuscript, I wish to extend a very special thank you to Dr. Komar for providing me with the opportunity to participate in all sorts of lectures, seminars, and discussions. In this last respect, I also wish to thank Dr. Rob Holman, Dr. Peter Howd, Dr. Tom Lippmann and the other members of the 'coastal crew'. The knowledge they all so freely disseminated, particularly on Thursdays, was invaluable to me.

Also I wish to thank Dr A.D. Short, whom I visited at the University of Sydney, and Dr. Tony Bowen, who was a visiting professor at O.S.U. while I was there, for their comments on particular portions of my work.

I wish to acknowledge my parents assistance throughout this endeavour. I feel extremely fortunate to have had their support.

Finally, Karla. Thank you does not begin to express my appreciation for her assistance, encouragement, and patience throughout this endeavour. Our time in this together will always be special to me.

REFERENCES

ALLEN, J.R.L., 1967. Notes on some fundamentals of paleocurrent analysis, with reference to preservation potential and sources of variance. Sedimentology 9:75-88.

-----, 1968. CURRENT RIPPLES: THEIR RELATION TO PATTERNS OF WATER AND SEDIMENT MOTION. North-Holland Publ. Co., Amsterdam, 433p.

-----, 1983. River bedforms: progress and problems. Spec. Pub. Int. Assoc. Sediment. 6:19-33.

-----, 1984. Parallel lamination developed from upper-stage plane beds: a model based on the larger coherent structures of the turbulent boundary layer. Sed. Geol. 39:227-242.

-----, 1985. PRINCIPLES OF PHYSICAL SEDIMENTOLOGY. Allen and Unwin, London, 272p.

ALLEN, J.R.L., AND LEEDER, M.R., 1980. Criteria for the instability of upper-stage plane beds. Sedimentology 27:209-217.

ANDREWS, P.B., AND VAN DER LINGEN, G.J., 1969. Environmentally significant sedimentologic characteristics of beach sands. N. Z. Jour. Geol. Geophys. 12: 119-137.

ANTIA, E.E., 1987. Preliminary observations on beach cusp formation and characteristics on tidally and morphodynamically distinct beaches on the Nigerian coast. Mar. Geol. 78:23-33.

ARNOTT, R.W.C. AND HAND, B.M., 1989. Bedforms, Primary Structures, and Grain Fabric in the Presence of Suspended Sediment Rain. Jour. Sed. Pet. 59:1062-1069.

BABA, J. AND KOMAR, P.D., 1981. Measurements and analysis of settling velocities of natural quartz sand grains. Jour. Sed. Pet. 51:631-640.

BAGNOLD, R.A., 1940. Beach formation by waves: Some model-experiments in a wave tank. Jour. Inst. Civil Eng. 15:27-52.

-----, 1954. Experiments on a gravity-free dispersion of large solid spheres in a Newtonian fluid under shear. Proc. Roy. Soc. (London), Ser. A 225:49-63.

BAGNOLD, R.A., 1956. The flow of cohesionless grains in fluids. Phil. Trans. Roy. Soc. Lond. A249:335-397.

-----, 1966. An approach to the sediment transport problem from general physics. U.S. G.S. Prof. Paper 422I, 37p.

BALSILLIE, J.H., AND CARTER, R.W.G., 1984. The visual estimation of shore-breaking wave heights. Coastal Eng. 8:367-385.

BARCILON, A.I. AND LAU, J.P., 1973. A model for formation of transverse bars. Jour. Geophys. Res. 78(15):2656-2664.

BASCOM, W.H., 1954. Characteristics of natural beaches. Proc. 4th Conf. Coastal Eng. 163-180.

BATTJES, J.A., 1974. Surf similarity. Proc. 14th Conf. Coastal Eng., ASCE, New York. 466-480.

BLATT, H., MIDDLETON, G., AND MURRAY, R., 1980. ORIGIN OF SEDIMENTARY ROCKS. 2nd ed., Prentice-Hall Inc., Engelwood N.J., 782p.

BOUMA, A. H., 1969. METHODS FOR THE STUDY OF SEDIMENTARY STRUCTURES. J. Wiley & Sons, 458p.

BOWEN, A.J., 1980. Simple models of nearshore sedimentation; beach profiles and longshore bars. In THE COASTLINE OF CANADA, McCANN, S.B. ed.; Geological Survey of Canada, Paper 80-10:1-11.

BOWEN, A.J. AND INMAN, D.L., 1971. Edge waves and crescentic bars. Jour. Geophys. Res. 76:8662-8671.

BOWMAN, D., 1979. Validity of visually estimated wave parameters. Israel Jour. Earth-Sciences 28:94-99.

BRADSHAW, M., 1982. Bores and swash on natural beaches. Coastal Studies Unit Tech. Rept. 82/4, Coastal Studies Unit, Dept. of Geography, Univ. of Sydney, Sydney, N.S.W. 107p.

BRIDGE, J.S., 1978. Origin of horizontal lamination under turbulent boundary layers. Sed. Geol. 20:1-16.

BRIDGE, J.S. AND BEST, J.L., 1988. Flow, sediment transport, and bedform dynamics over the transition from dunes to upper-stage plane beds: implications for the formation of planar laminae. Sedimentology 35:753-763.

BROOME, R. AND KOMAR, P.D., 1979. Undular hydraulic jumps and the formation of backwash ripples on beaches. Sedimentology

26:543-559.

BRUUN, P., 1954. Migrating sand waves or sand humps, with special reference to investigations carried out on the Danish North Sea coast. Proc. 5th Conf. Coastal Eng. ASCE, New York. 269-295.

CAPRA, F., 1982. THE TURNING POINT. Simon and Schuster, New York. 464p.

CARTER, L. 1975. Sedimentation on the Continental Terrace around New Zealand: A Review. Marine Geol. 19:209-237.

CARTER, R.W.G., 1988. COASTAL ENVIRONMENTS. Academic Press, San Diego, 617p.

CHAPELL, J. AND ELIOT, I.G., 1979. Surf-beach dynamics in time and space-An Australian case study, and elements of a predictive model. Marine Geol. 32:231-250.

CHEEL, R.J., 1984. Heavy mineral shadows, a new sedimentary structure formed under upper-flow-regime conditions: Its directional and hydraulic significance. Jour. Sed. Pet. 54:1175-1182.

-----, R.J., 1990. Horizontal lamination and the sequence of bed phases and stratification under upper-flow-regime conditions. Sedimentology 37:517-529.

CHEEL, R.J. AND MIDDLETON, G.V., 1986a. Measurement of small-scale laminae in sand-sized sediments. Jour. Sed. Pet. 56:547-548.

-----, 1986b. Horizontal laminae formed under upper flow regime plane bed conditions. Jour. of Geol. 94:489-504.

CLIFTON, H.E., 1969. Beach lamination: nature and origin. Marine Geol. 7:553-559.

-----, 1976. Wave-formed sedimentary structures- a conceptual model. In BEACHES AND NEARSHORE SEDIMENTATION, DAVIS, R.A. jr. AND ETHINGTON, R.L., ed. S.E.P.M. Spec. Pub. #24:126-148.

CLIFTON, H.E., HUNTER, R.E., AND PHILLIPS, R.L., 1971. Depositional structures and processes in the non-barred high-energy nearshore. Jour. Sed. Pet. 41:651-670.

CERC (COASTAL ENGINEERING RESEARCH CENTER), 1984. Shore Protection Manual. 4th ed. Dept. of Army, Waterways Experiment Station, Corps of Eng. 2Vol.

CULLEY, S.K., 1986. Standing edge waves on a pocket beach. unpub. M.Sc. Thesis, Oceanography, Oregon State Univ., Corvallis, OR. 77p.

DALRYMPLE, R.A. AND THOMPSON, W.W., 1977. Study of equilibrium beach profiles; Proc. 15th Int. Conf. Coastal Eng. ASCE, Honolulu. 1277-1296.

DAVIES, J.L., 1964. A morphogenic approach to world shorelines. Zeit. fur Geomorph. 8:127-142

-----, J.L., 1973. GEOGRAPHICAL VARIATION IN COASTAL DEVELOPMENT. Hafner, New York, 204p.

DAVIS, J.C., 1973. STATISTICS AND DATA ANALYSIS IN GEOLOGY. J. Wiley & Sons, 550p.

DEAN, R.G., 1973. Heuristic models of sand transport in the surf zone. Proc. Conf. on Engineering Dynamics in the Surf Zone, Sydney, N.S.W. 208-214.

DOLAN, R. AND FERM, J., 1968. Crescentic landforms along the Atlantic coast of the United States. Science 159:627-628.

DOLAN R., VINCENT, L., AND HAYDEN, B., 1974. Crescentic coastal landforms. Z. Geomorphol. 18:1-12.

DUNCAN, J.R., 1964. The effects of water table and tide cycle on swash-backwash sediment distribution and beach profile development. Mar. Geol. 2:186-197.

ELIOT, I.G. AND CLARKE, D.J., 1988. Semi-diurnal variation in beachface aggradation and degradation. Marine Geol. 79:1-22.

EMERY, K.O., 1978. Grain size in laminae of beach sand. Jour. Sed. Pet. 48:1203-1212.

EMERY, K.O. AND FOSTER, J.F., 1948. Water tables in marine beaches. Jour. Marine Res. 7:644-654.

EMERY, K.O. AND GALE, J.F., 1951. Swash and swash marks. Trans. Am. Geophys. Union 32(1):31-36.

ERICKSEN, N.J., 1970. Measurement of tide induced changes to water table profiles in coarse and fine sand beaches along Pegasus Bay, Canterbury. Earth Sci. Jour. 4-1:24-31.

EVANS, O.F., 1939. Mass transport of sediments on subaqueous terraces. Jour. Geol. 47:324-334.

FRANCIS, J.R.D., 1973. Experiments on the motion of solitary grains along the bed of a water stream. Proc. R. Soc. Lond. (A)332: 443-471.

FURKERT, F.W., 1947. Westport Harbour. Trans. R. Soc. N.Z. 76(3): 373-402.

GALVIN, C.J. jr., 1972. Wave breaking in shallow water. In WAVES ON BEACHES AND RESULTING SEDIMENT TRANSPORT. MEYER, R.E. ed.

Academic Press, p413-456.

GIBBS, R.J., MATHEWS, M.D., AND LINK, D.A., 1971. The relationship between sphere size and settling velocity. Jour. Sed. Pet. 41:7-18.

GLEICK, J., 1987. CHAOS- MAKING A NEW SCIENCE. Viking Penguin Inc., New York. 352p.

GRACE, J.T., GROTHAUS, B.T., AND EHRLICH, R., 1978. Size frequency distributions taken from within sand laminae. Jour. Sed. Pet. 48:1193-1202.

GRANT, U.S., 1948. Influence of the beach water table on beach aggradation and degradation. J. Marine Res. 7:655-660.

GREENWOOD, B. AND MITTLER, P.R., 1984. Sediment flux and equilibrium slopes in a barred nearshore. Marine Geol. 60:79-98.

GUZA, R.T. AND BOWEN, A.J., 1981. On the amplitude of beach cusps. Jour. Geophys. Res. 86:4125-4132.

GUZA, R.T. AND INMAN, D.L., 1975. Edge waves and beach cusps. Jour. Geophys. Res. 80:2997-3012.

GUZA, R.T. AND THORNTON, E.B., 1982. Swash oscillations on a natural beach. Jour. Geophys. Res. 87:C1:483-491.

HAMPTON, M.A., 1979. Buoyancy in debris flows. Jour. Sed. Pet. 49:753-758.

HANES, D.M. AND BOWEN, A.J., 1985. A granular-fluid model for steady intense bed-load transport. Jour. Geophys. Res. 90 (C5):9149-9158.

HARRISON, W., 1969. Empirical equations for foreshore changes over a tidal cycle. Marine Geol. 7:529-551.

HAWKING, S.W., 1988. A BRIEF HISTORY OF TIME. Bantam Books, New York. 198p.

HAYES, M.O., 1972. Forms of sediment accumulation in the beach zone. In WAVES ON BEACHES AND RESULTING SEDIMENT TRANSPORT. MEYER, R.E. ed. Academic Press, p297-356.

HAYES, M.O. AND BOOTHROYD, J.C., 1969. Storms as modifying agents in the coastal environment. In COASTAL ENVIRONMENTS: NE MASSACHUSETTS. HAYES, M.O., ed., Dept. of Geology, Univ. of Mass., Amherst., p290-315.

HICKS, D.M., INMAN, D.L., AND LEEDER, M.R., 1988. Bedload stresses and Bagnold's bedload transport theory-a reevaluation. unpub. ms.

HINE, A.C., 1979. Mechanisms of berm development and resulting beach growth along a barrier spit complex. Sedimentology 26:333-351.

HOLMAN, R.A., 1986. Extreme value statistics for wave run-up on a natural beach. Coastal Eng. 9:527-544.

HOLMAN, R.A. AND BOWEN, A.J., 1979. Edge waves on complex beach profiles. Jour. Geophys. Res. 84:6339-6346.

-----, 1982. Bars, bumps, and holes: Models for the generation of complex beach topography. Jour. Geophys. Res. 87(C1):457-468.

-----, 1984. Longshore structure of infragravity wave motions. Jour. Geophys. Res. 89(C4):6446-6452.

HOLMAN, R.A. AND GUZA, R.T., 1984. Measuring run-up on a natural beach. Coastal Eng. 8:129-140.

HOLMAN, R.A., LIPPMANN, T.C., O'NEILL, P.V., AND HATHAWAY, K., 1991. Video estimation of subaerial beach profiles. Marine Geol. 97:225-231.

HOLMAN, R.A. AND SALLENGER, A.H., Jr., 1985. Setup and swash on a natural beach. Jour. Geophys. Res. 90:C1:945-953.

HORIKAWA, K., 1980. Coastal Sediment Processes. In APPLICATION OF STOCHASTIC PROCESSES ON SEDIMENT TRANSPORT. SHEN, H.W. AND KIKKAWA, H. ed., Water Resources Publications 17:1-66.

HOWD, P. A. AND HOLMAN, R.A., 1984a. Beach foreshore response to long period waves. Proc. 19th Conf. Coastal Eng. ASCE, Houston 132: 1968-1982.

-----, 1987. A simple model of beach foreshore response to long period waves. Mar. Geol. 78:11-22.

HUNTER, R.E., CLIFTON, H.E., AND PHILLIPS, R.L., 1979. Depositional processes, sedimentary structures, and predicted vertical sequences in barred nearshore systems, Southern Oregon Coast. Jour. Sed. Pet. 49:711-726.

HUNTLEY, D.A. AND BOWEN, A.J., 1975. Comparison of the hydrodynamics of steep and shallow beaches. In NEARSHORE SEDIMENT DYNAMICS AND SEDIMENTATION: AN INTERDISCIPLINARY REVIEW. HAILS, J. AND CARR, A. ed., J. Wiley & Sons, London, p69-109.

IBBEKEN, H. AND SCHELEYER, R., 1986. Photo-sieving: a method for grain-size analysis of coarse-grained, unconsolidated bedding surfaces. Earth Surface Processes and Landforms 11:59-77.

INMAN, D.L., AND GUZA, R.T., 1982. The origin of swash cusps on beaches. Mar. Geol. 49:133-148.

JACKSON, R.G., 1975. Hierarchical attributes and a unifying model of bed forms composed of cohesionless material and produced by shearing flow. Geol. Soc. Am. Bull. 86:1523-1533.

JOHNSON, J.W., 1949. Scale effects in hydraulic models involving wave motion. Trans. Am Geophys. Union 30:517-525.

KEMP, P.H., 1961. The relationship between wave action and beach profile characteristics. Proc. 7th. Conf. Coastal Eng. ASCE, p262-277.

KENNEDY, J.F., 1961. Stationary waves and antidunes in alluvial channels. Rept. KH-R-2, U.S. Dept. of Agriculture. W.M. Keck Lab. of Hydraulics and Water Resources, Div. of Eng. C.I.T., Pasadena, California: 139p.

KING, C.A.M., 1972. BEACHES AND COASTS, 2nd ed. Edward Arnold Ltd., London, 570p.

KIRK, R.M., 1970. Swash zone processes. Unpub. Ph.D. Thesis, Dept. of Geography, Univ. of Canterbury, Christchurch, N.Z.

KOMAR, P.D., 1976a. BEACH PROCESSES AND SEDIMENTATION. Prentice-Hall Inc., Englewood Cliffs, New Jersey, 429p.

-----, 1976b. Boundary layer flow under steady unidirectional currents. In MARINE SEDIMENT TRANSPORT AND ENVIRONMENTAL MANAGEMENT. STANLEY, D.J. AND SWIFT, D.J.P. ed., J. Wiley & Sons, New York, p91-106.

-----, 1981. The application of the Gibbs equation for grain settling velocities to conditions other than quartz grains in water. Jour. Sed. Pet. 51:1125-1132.

-----, 1983a. Rhythmic shoreline features and their origins. In MEGA-GEOMORPHOLOGY. GARDNER, R. AND SCOGIG, H. ed.. Clarendon Press, Oxford, p92-112.

-----, 1983b. Beach processes and erosion-an introduction. In HANDBOOK OF COASTAL PROCESSES AND EROSION. P.D. KOMAR ed., CRC Press, Boca Raton, FL, p1-20.

-----, 1989. Physical processes of waves and currents and the formation of marine placers. Reviews in Aquatic Sciences V1-3:393-423.

KOMAR, P.D. AND ENFIELD, D.B., 1987. Short-term sea-level changes and coastal erosion. In SEA LEVEL FLUCTUATIONS AND COASTAL EVOLUTION, NUMMEDAL, D., PILKEY, O.H., AND HOWARD, J. ed., SEPM Spec. Pub. #41:17-27.

KOMAR, P.D. AND GAUGHAN, M.K., 1972. Airy wave theory and breaker height prediction. Proc. 13th Conf. Coastal Eng., p405-418.

KOMAR, P.D. AND WANG, C., 1984. Processes of selective grain transport and the formation of placers on beaches. Jour. Geol. 92:637-655.

KUENEN, P.H., 1951. Properties of turbidity currents of high density. S.E.P.M. Spec. Pub. #2:14-33.

LANGFORD, R. AND BRACKEN, B., 1987. Medano Creek, Colorado, a model for upper-flow-regime fluvial deposition. Jour. Sed. Pet. 57:863-870.

LANYON, J.A., ELIOT, I.G. AND CLARKE, D.J., 1982. Aust. Jour. Mar. Freshwater. Res. 33:377-400.

LEEDER, M.R., 1979. 'Bedload' dynamics: Grain-grain interactions in water flows. Earth Surf. Processes 4:229-240.

LEEDER, M.R., 1982. SEDIMENTOLOGY: PROCESS AND PRODUCT. Allen and Unwin Inc., 344p.

LEEDER, M.R., 1983. On the interactions between turbulent flow, sediment transport and bedform mechanics in channelized flows. Spec. Publs. Ass. Sediment. 6:5-18.

LEROY, S.D., 1981. Grain-size and moment measures: A new look at Karl Pearson's ideas on distributions. Jour. Sed. Pet. 51:625-630.

LEWIS, D.W., 1982. PRACTICAL SEDIMENTOLOGY. Apteryx Books.

LIPPMANN, T.C. AND HOLMAN, R.A., 1989. Quantification of sand bar morphology: A video technique based on wave dissipation. Jour. Geophys. Res. 94-C1:995-1011.

-----, 1990. The stability and spatial variability of sand bar morphology. Jour. Geophys. Res. 95(C7):11575-90.

-----, 1991. Phase speed and angle of breaking waves measured with video technique. Proc. Coastal Sediments 91', ASCE Special Conf. W.R. Div., Seattle., p542-556.

LONGUET-HIGGINS, M.S. AND PARKINS, D.W., 1962. Sea waves and beach cusps. Geographical Journal 128:194-201.

LOWE, D.R., 1979. Sediment gravity flows: Their classification and some problems of application to natural flows. S.E.P.M. Spec. Pub. #27:75-82.

LOWE, D.R., 1982. Sediment gravity flows: II. Depositional models with special reference to the deposits of high-density turbidity currents. Jour. Sed. Pet. 52:279-297.

-----, 1988. Suspended-load fallout rate as an independent variable in the analysis of current structures. Sedimentology 35:765-766.

LUMSDEN, J.L., KIRK, R.M., AND HASTIE, W.J., 1985. Westport Harbour study. unpub. report to M.O.T. Westport Harbour Adv. Comm. by R.W. Morris and Assoc. Consulting Eng. Ltd..

McBRIDE, E.F., SHEPHER, R.G., AND CRAWLEY, R.A., 1975. Origin of parallel, near-horizontal laminae by migration of bedforms in a small flume. Jour. Sed. Pet. 45:132-139.

McCUBBIN, D.G., 1982. Barrier-island and strand plain facies. In SANDSTONE DEPOSITIONAL ENVIRONMENTS. SCHOLLE, P.A. and SPEARING, D. ed., A.A.P.G. Memoir 31: 247-279.

MACPHERSON, R.I., 1978. GEOLOGY OF QUATERNARY ILMENITE-BEARING COASTAL DEPOSITS AT WESTPORT. N.Z. Geol. Survey Bull. 87.

MANGIN, C.M., 1973. Coastal processes and development in the southern Karamea Bight. Unpub. M.A. Thesis, Dept. of Geography, Univ. of Canterbury, Christchurch, N.Z.

MARRA, J.J., 1985. Heavy mineral content of Nine Mile Beach, West Coast, South Island. Unpub. Rept., Univ. of Canterbury, Christchurch, N.Z.

-----, 1988. Placer geometry and mechanisms of placer concentration on a rhythmic beach. Abs. USGS Annual Meeting, Denver, V20-7:A141

MEYER, R.E. AND TAYLOR, A.D., 1972. Run-up on beaches. In WAVES ON BEACHES AND RESULTING SEDIMENT TRANSPORT. MEYER, R.E. ed. p357-411.

MIDDLETON, G.V. AND HAMPTON, M.A., 1976. Subaqueous sediment transport and deposition by sediment gravity flow. In MARINE SEDIMENT TRANSPORT AND ENVIRONMENTAL MANAGEMENT. STANLEY, D.J. and SWIFT, D.J.P. ed., J.Wiley & Sons, New York, p197-218.

MIDDLETON, G.V. AND SOUTHARD, J.B., 1978. MECHANICS OF SEDIMENT MOVEMENT. S.E.P.M. Short Course #3, Tulsa, Oklahoma.

-----, 1984. MECHANICS OF SEDIMENT MOVEMENT. S.E.P.M. Short Course #3, 2nd ed., Providence, 401p.

MILLER, R.L., 1968. Experimental determination of run-up of undular and fully developed bores. Jour. of Geophys. Res. 73-14:4497-4510.

MILLER, R.L. AND ZEIGLER, J.M., 1958. A model relating dynamics and sediment pattern in equilibrium in the region of shoaling waves, breaker zone, and foreshore. Jour. Geol. 66:417-441.

MOSS, A.J., 1972. Bed-load sediments. Sedimentology 18:159-219.

MUNK, W.H., 1944. Proposed uniform procedure for observing waves and interpreting instrument records (declassified U.S. Govt. document). Scripps Institute of Oceanog., S.I.O. Report 26.

NELSON, C.L. AND MILLER, R.L. 1974. The interaction of fluid and sediment on the foreshore. Tech. Rept. #15, Fluid Dynamics and Sediment Transport Lab. Dept of Geophys. Sciences, Univ. of Chicago: 175p.

NIKURADSE, J., 1933. Laws of flow in rough pipes. Natl. Advisory Comm. Aeronautics Tech. Memo. 1292 (translation from German, 1950)

PANIN, N. AND PANIN, S., 1967. Regressive sand waves on the Black Sea shore. Marine Geol. 5:221-226.

PAOLA, C., WIELE, S.M., AND REINHART, M.A., 1989. Upper-regime parallel lamination as the result of turbulent sediment transport and low amplitude bedforms. Sedimentology 36:47-59.

PFAHLERT, J.J., 1984. Coastal dynamics and sedimentation at Point Elizabeth, West Coast, South Island, New Zealand. Unpub. M.Sc. Thesis, Univ. of Canterbury, Christchurch, N.Z.

PICKRILL, R.A. AND MITCHELL, J.S., 1979. Ocean wave characteristics around New Zealand. N.Z. Jour. Mar. Freshwater Res. 13:501-520.

PIERSON, W.J., NEWMANN, G., AND JAMES, R.W., 1955. Practical methods for observing and forecasting ocean waves by means of wave spectra and statistics. U.S. Naval Oceanographic Office. H.O. Publication 603.

POLLOCK, L.W. AND HUMMON, W.D., 1971. Cyclic changes in interstitial water content, atmospheric exposure, and temperature in a marine beach. Limnol. and Oceanography 16(3):522-535.

REID, I. AND FROSTICK, L.B., 1985. Beach orientation, bar morphology and the concentration of metalliferous deposits: a case study, Lake Turkana, N Kenya. Jour. Geol. Soc. London 142:837-848.

REID, S.J., AND COLLEN, B., 1983. Analyses of wave and wind reports from ships in the Tasman Sea and New Zealand areas. N.Z. Met S. Misc. Pub.182, 74p.

REINECK, H.E., AND SINGH, I.B., 1980. DEPOSITIONAL SEDIMENTARY ENVIRONMENTS. 2nd ed., Springer-Verlag, Heidelberg, 549p.

REINSON, G.E., 1984. Barrier-island and associated strand-plain systems. In FACIES MODELS, 2nd ed., R.G. WALKER ed., Geosciences Canada Reprint Series 1. 119-140.

RUBEY, W.W., 1933. The size distribution of heavy minerals within a sandstone. Jour. Sed. Pet. 3:3-29.

RUSSEL, R.J. AND McINTIRE, W.G., 1965. Beach cusps. Bull. Geol. Soc. Am. 76:17-45.

SALLENGER, A.H., Jr., 1979a. Beach-cusp formation. Mar. Geol. 29:23-37.

-----,1979b. Inverse grading and hydraulic equivalence in grain-flow deposits. Jour. Sed. Pet. 49:553-562.

SALLENGER, A.H., Jr. AND RICHMOND, B.M., 1984. High-frequency sediment-level oscillations in the swash zone. Marine Geol. 60:155-164.

SCHIFFMAN, A., 1965. Energy measurements in the swash-surf zone. Limnol. and Oceanography 10:255-260.

SEYMOUR, R.J. AND AUBREY, D.G., 1985. Rhythmic beach cusp formation: A conceptual synthesis. Marine Geol. 65:289-304.

SHEPARD, F.P., 1950. Beach cycles in southern California. U.S. Army Corp of Engrs., Beach Erosion Board Tech. Memo. 15, 31p.

SHORT, A.D., 1975. Multiple offshore bars and standing waves. Jour. Geophys. Res. 80:3838-40.

-----, 1979, Wave power and beach stages: A global model. Proc. 16th Conf. Coastal Eng., Hamburg, 1978, 1145-1162.

-----, 1981. Beach response to variations in breaker height. Proc. 17th Conf. Coastal Eng., Sydney, 1980, 1016-1035.

-----, 1984. Beach and nearshore facies: Southeast Australia. In HYDRODYNAMICS AND SEDIMENTATION IN WAVE-DOMINATED COASTAL ENVIRONMENTS, B. GREENWOOD and R.A. DAVIS, Jr. ed. Marine Geol. 60:261-282.

SIEMELINK, M.G., 1984. Morphodynamics of a mixed sand and gravel beach. Unpub. M.Sc. Thesis, Univ. of Canterbury, Christchurch.

N.Z.

SIMONS, D.B., RICHARDSON, E.V., AND NORDIN, C.F. jr., 1965. Sedimentary structures generated by flow in alluvial channels. In PRIMARY SEDIMENTARY STRUCTURES AND THEIR HYDRODYNAMIC INTERPRETATION MIDDLETON, G.V. ed., S.E.P.M. Spec. Pub. 12:34-52.

SLINGERLAND, R.L., 1977. The effects of entrainment on the hydraulic equivalence relationships of light and heavy minerals in sands. Jour. Sed. Pet. 47:753-770.

-----, 1984. Role of hydraulic sorting in the origin of fluvial placers. Jour. Sed. Pet. 54:137-150.

SLINGERLAND, R.L. AND SMITH, N.D., 1986. Occurrence and formation of water-laid placers. Ann. Rev. Earth and Planet. Sci. 14:113-147.

SMITH, N.D., 1971. Pseudo-planar stratification produced by very low amplitude sand waves. Jour. Sed. Pet. 41:69-73.

SONU, C.J., 1972. Bimodal composition and cyclic characteristics of beach sediment in continuously changing profiles. Jour. Sed. Pet. 42(4):852-857.

-----, 1973. Three dimensional beach changes. Jour. Geol. 81:42-64.

-----, 1974. Measurement of swash profile and orbital motion on the beach. In OCEAN WAVE MEASUREMENT AND ANALYSIS. A.S.C.E. 1:621-638.

SONU, C.J. AND JAMES, W.R., 1973. A Markov model for beach profile change. Jour. Geophys Res. 78(9):1462-1471.

SONU, C.J., MURRAY, S.P., HSU, S.A., SUHAYADA, J.N., AND WADDELL, E., 1973. Sea breeze and coastal processes. Trans. Am Geophys. 54(9):820-833.

SONU, C.J. AND RUSSEL, R.J., 1966. Topographic changes in the surf zone profile. Proc. 10th Conf. Coastal Eng., Council Wave Research. Tokyo, 502-524.

SONU, C.J. AND VAN BEEK, J.L., 1971. Systematic changes on the Outer Banks, North Carolina. Jour. Geol., 79:416-425.

SUTHERLAND, A.J., SHARMA, J.N., AND SHEMDIN, O.H., 1976. Wave run-up on a simulated beach. Proc. 15th Conf. Coastal Eng. ASCE, New York, 752-765.

TANNER, W.F., 1977. Froude regimes in the swash zone. In COASTAL SEDIMENTOLOGY. TANNER, W.F. ed., Geology Dept. Florida State Univ., Tallahassee, Florida:289-297.

TERWINDT, J.H.J., HULSBERGEN, C.H., AND KOHSIEK, L.H.M., 1984. Structures in deposits from beach recovery, after erosion by swell waves around the

southwestern coast of Aruba (Netherlands Antilles). In HYDRODYNAMICS AND SEDIMENTATION IN WAVE-DOMINATED COASTAL ENVIRONMENTS. B. GREENWOOD AND R.A. DAVIS, Jr. ed., Marine Geol. 60:283-311.

THOMAS, K.V. AND BABA, M., 1986. Berm development on a monsoon-influenced microtidal beach. Sedimentology 33:537-546.

THOMPSON, W.C., 1972. Period by the wave-group method. Proc. 13th Conf. Coastal Eng., 197-214.

THOMPSON, W.O., 1937. Original structures of beaches bars and dunes. G.S.A. Bull. 48:723-752.

VALENTINE, E.M., AND MACKY, G.H., 1984, Sea wave climate at Ngkawau, Westport, and Carters Beach. MOWD Central Lab. Report #3-84/4; 2vols.

VINCENT, L., 1973. Quantification of shoreline meandering. Office of Naval Res. Geography prog. Tech. Report #7, 93p.

VIOLANTE, R.A. AND TANNER, W.F., 1985. Rain waves vs swash-zone ripple marks: Why are they mutually exclusive?. Jour. Coastal Res. 1-4:375-381.

WADDELL, E., 1973. Dynamics of swash and implication to beach response. Tech. Rept. #139, Coastal Studies Unit, Louisiana State Univ., Baton Rouge, Louisiana: 49p.

-----, 1976. Swash-groundwater-beach profile interactions. In BEACHES AND NEARSHORE SEDIMENTATION, DAVIS, R.A. jr. AND ETHINGTON, R.L., ed. S.E.P.M. Spec. Pub. #24:115-125.

WALKER, R.G., 1978. Deep-water sandstone facies and ancient submarine fans: models for stratigraphic traps. AAPG Bull., 62:932-66

-----, 1979. Shallow marine sands. In FACIES MODELS. WALKER, R.G. ed., GeoSciences Canada Reprint Series 1: 75-91.

-----, 1984. General introduction: Facies, facies sequences and facies models. in FACIES MODELS, 2nd ed., R.G. WALKER ed., Geosciences Canada Reprint Series 1: 1-13.

WINKELMOLEN, A.M., 1982. Critical remarks on grain parameters, with special emphasis on shape. Sedimentology 29:255-265.

WRIGHT, L.D., 1981. Beach cut in relation to surf zone morphodynamics. Proc.17th Conf. Coastal Eng., Sydney, 1980, 978-996.

WRIGHT, L.D., 1982. Field observations of long-period, surf zone standing waves in relation to contrasting beach morphologies. Aust. J. Marine Freshwater Res. 33:181-201.

WRIGHT, L.D., CHAPPEL, J., THOM, B.G., BRADSHAW, M.P., AND COWELL, P., 1979. Morphodynamics of reflective and dissipative beach and inshore systems:Southeastern Australia. Marine Geol. 32:105-140.

WRIGHT, L.D., GUZA, R.T., AND SHORT, A. D., 1982. Dynamics of a highly dissipative surf zone. Marine Geol. 45:41-62.

WRIGHT, L.D., NIELSEN, P., SHI, N. C., AND LIST, J.H., 1986. Morphodynamics of a bar-trough surf zone. Marine Geol. 70:251-286.

WRIGHT, L.D. AND SHORT, A. D., 1983. Morphodynamics of beaches and surfzones in Australia. In HANDBOOK OF COASTAL PROCESSES AND EROSION. P.D. KOMAR ed., CRC Press, Boca Raton, FL, 35-64.

-----, 1984. Morphodynamic variability of surf zones and beaches: A synthesis. Marine Geol. 56: 93-118.

WRIGHT, L.D., SHORT, A.D., AND GREEN, M.O., 1985. Short-terms changes in the morphodynamic states of beaches and surfzones: An empirical predictive model. Marine Geol. 62:339-364.

WRIGHT, L.D., SHORT, A.D., BOON J.D., HAYDEN B., KIMBALL S., AND LIST, J.H., 1987. The morphodynamic effects of incident wave groupiness and tide range on an energetic beach. Marine Geol. 74:1-20.

WRIGHT, L.D. AND THOM, B. G., 1977. Coastal depositional landforms: a morphodynamic approach. ?Progress in Physical Geography 1:412-459?

WRIGHT, P., 1976. A cine-camera technique for process measurement on a ridge and runnel beach. Sedimentology 23:705-712.

YALIN, M.S., 1972. MECHANICS OF SEDIMENT TRANSPORT. Pergamon Press; 290p.

YASSO, W.E., AND HARTMAN, E.M. jr., 1972. Rapid field technique using spray adhesive to obtain peels of unconsolidated sediment. Sedimentology 19:295-298.

ZENKOVICH, V.P., 1967, Processes of Coastal Development. STEERS, J.A. ed., Oliver and Boyd Pub.

ZNAMENSKAYA, N.S., 1969. Morphological principles of modeling of river-bed process. Proc. 13th Congr. Intl. Assoc. Hydr. Res., Kyoto, Japan, 5:195-200.

PLACER GEOMETRY AND MECHANISMS OF PLACER CONCENTRATION ON A RHYTHMIC BEACH.

MARRA, J. J. Department of Geology, University of Canterbury, Christchurch.

The 'heavy-mineral rich' Nine Mile Beach on the west coast of the South Island, New Zealand, is characterized by a variable moderate-high energy wave climate and rhythmic foreshore topography. Visual observation of nearshore wave conditions, measurement of beach profiles, and trenching of the upper-foreshore over a series of storm/post-storm recovery cycles shows that there is a marked 'local' variation in placer concentration. Differential entrainment and transport of 'heavy' versus 'light' minerals associated with low-frequency pulsing of seaward return flows in rip bays, and subsequent formation of lag deposits at the uppermost portion of rip bays is proposed as a model to explain the observed local variation in placer concentration. It is suggested here that, along with the more commonly recognized regional patterns, local variation in beach placer geometry must be considered in minerals exploration programs.

MARRA, J.J., 1988. Placer geometry and mechanisms of placer concentration on a rhythmic beach. Abs. USGS Annual Meeting, Denver, V20-7:A141